

Extracellular Vesicles for Therapeutic RNA Delivery

Daniel E. Murphy

ISBN: 978-94-6458-115-7
Cover art: Evie Murphy
Lay-out: Publiss | www.publiss.nl
Print: Ridderprint | www.ridderprint.nl

© Copyright 2022: Daniel E. Murphy

All rights reserved. No part of this publication may be reproduced, stored in a retrieval system, or transmitted in any form or by any means, electronic, mechanical, by photocopying, recording, or otherwise, without the prior written permission of the author.

Extracellular Vesicles for Therapeutic RNA Delivery

**Extracellulaire Membraanblaasjes voor de Afgifte van RNA
Medicijnen**
(met een samenvatting in het Nederlands)

Proefschrift

ter verkrijging van de
graad van doctor aan de
Universiteit Utrecht
op gezag van de
rector magnificus, prof.dr.
H.R.B.M. Kummeling, ingevolge
het besluit van het college voor
promoties in het openbaar te
verdedigen op

dinsdag 5 april 2022
des middags te 12.15 uur

door

Daniel Edwin Murphy

geboren op 26 mei 1992
te Bristol, Verenigd Koninkrijk

Promotor:

Prof. dr. R.M. Schiffelers

Copromotoren:

Dr. P. Vader

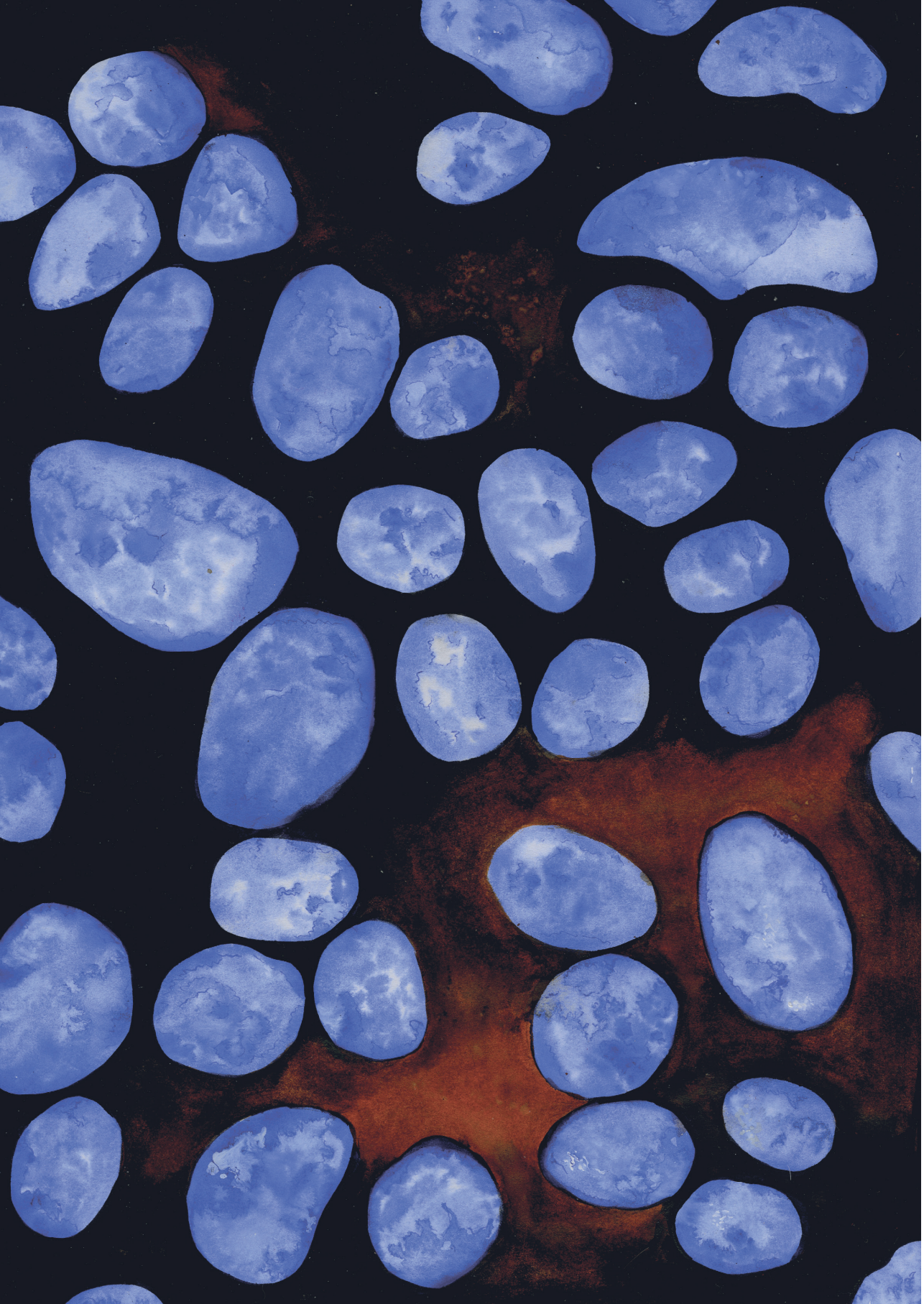
Dr. O.G. de Jong

Dit proefschrift werd (mede) mogelijk gemaakt met financiële steun van European Union's Horizon 2020 Research and Innovation program project B-SMART No. 721058.

For my Grandfather,
Prof. Paul Murphy
1930 - 2020

Table of Contents

Chapter 1:	Introduction	9
Chapter 2:	Extracellular vesicle-based therapeutics: natural versus engineered targeting and trafficking	17
Chapter 3:	A CRISPR-Cas9-based reporter system for single-cell detection of extracellular vesicle-mediated functional transfer of RNA	45
Chapter 4:	Natural or Synthetic RNA Delivery: A Stoichiometric Comparison of Extracellular Vesicles and Synthetic Nanoparticles	95
Chapter 5:	A comparison of extracellular vesicle and lipid nanoparticle cellular uptake and intracellular trafficking	123
Chapter 6:	Development and Optimisation of a Cell Membrane Sheet-Based RNA Release Assay to Assess Extracellular Vesicle Content Release	147
Chapter 7:	Summary and Perspectives	165
Appendices		177



INTRODUCTION

CHAPTER 1

INTRODUCTION

In recent years, RNA therapeutics have emerged as a class of drugs with the potential to treat diseases which were previously thought 'undruggable'. In contrast to conventional therapeutics which aim to alter pathological mechanisms once they have developed, RNA therapeutics possess the ability to treat genetic sources of disease at the post-transcriptional level.

For example, pathological gene expression can be halted by miRNA or siRNA mediated knockdown. This could be used to halt plaque formation in Alzheimer's by preventing expression of plaque protein precursors¹. In contrast to siRNA and miRNAs, rather than preventing gene expression, mRNA therapeutics could introduce the expression of a therapeutic protein. This approach will be utilised by future mRNA vaccines which encode protein antigens of infectious microbes, thereby stimulating the immune system to develop immunity to these pathogens upon mRNA expression². Furthermore, RNA therapeutics possess the ability to treat more complex sources of genetic disease. For instance, transthyretin amyloidosis has recently been successfully treated using the dual delivery of mRNA for the Cas9 endonuclease and an sgRNA targeting the misfolded transthyretin source of disease³.

Despite the existence of many promising disease targets, RNA therapeutics are far from reaching their full potential. This is mainly due to the fact that the delivery of RNA is opposed by obstacles which are not faced by conventional small molecule therapeutics. To reach its site of function in the cytosol of a target cell, a therapeutic RNA must first bypass several layers of defence which have evolved to prevent exogenous RNA from entering cells. Firstly, RNA therapeutics are large polar molecules which will not passively diffuse across cell membranes. Furthermore, free RNA is subject to rapid degradation in the circulation by RNases, renal clearance and scavenger receptor-mediated removal by hepatocytes⁴. It is clear that if RNA therapeutics are to achieve their promise, a suitably efficient method to bypass these barriers is crucial.

Currently, most RNA delivery strategies involve the encapsulation of RNA within a synthetic nanoparticle which protects the delicate cargo and facilitates uptake into target cells. For example, RNA can be contained within a liposome composed of a lipid bilayer sphere with an aqueous core, loaded within a polymeric micelle or can be mixed with lipid to form a multi lamellar lipid nanoparticle (LNP). The latter option is furthest in terms of clinical development as the first clinically approved RNA therapeutic was an LNP encapsulated siRNA for the treatment of hereditary transthyretin-mediated amyloidosis, Onpatro.

The successful clinical development of Onpatro is an extremely important milestone for RNA therapeutics, however delivery of RNA drugs is currently limited to the liver. This is due to the fact that for most types of NP the majority of intravenous injected particles will be taken up and removed from the circulation by hepatic Kupffer cells. Furthermore, synthetic NPs can be immunogenic and are often too toxic to tolerate at doses required for therapeutic effects. In addition, even if a synthetic NP is able to reach its target cell and enter it through a process of endocytosis, it is most likely destined for trafficking to the lysosome for degradation. It has been estimated that as little as 1-2% of RNA molecules contained within synthetic NPs taken up by a cell will eventually reach the cytosol where they function⁵. It is therefore clear that for RNA therapeutics to achieve their full potential improved delivery systems must be developed.

Extracellular vesicles (EVs) have emerged as a potential solution to the delivery obstacles faced by RNA therapeutics. These are lipid bound nanoparticles of natural rather than synthetic origin. They are between 30-2000nm in size and are released from all cell types⁶. They can be divided into microvesicles which are produced by budding from the cell surface or exosomes which are released from cells following the fusion of a multivesicular body with the cell surface⁷. These natural particles are capable of functionally transferring RNA amongst other macromolecules to recipient cells, thereby facilitating intercellular communication. This process has been reported to affect numerous (patho)physiological processes. For instance, neurons have been shown to produce EVs containing miRNA-124a, the transfer of which regulates the expression of glutamate transporters in recipient astroglia⁸. Furthermore, in breast cancer the transfer of miRNA-19 via EVs has been demonstrated to inhibit the expression of the miRNA-19 target tumour suppressor PTEN which subsequently primes the tumour microenvironment for metastatic outgrowth *in vivo*⁹. These examples demonstrate that EVs are a natural mechanism for intercellular RNA transfer and for this reason they have gained attention as a potential vehicle for therapeutic RNA delivery.

EVs possess several potential advantages over synthetic NPs. Firstly, as they are of natural origin and are already present in the circulation, they are less toxic and immunogenic than synthetic NPs meaning higher doses can be tolerated¹⁰. In addition, EVs of autologous origin could avoid problems associated with immunogenicity. Certain EVs also possess an endogenous cell targeting ability. For example, the integrin composition of tumour-secreted EVs has been shown to influence their targeting *in vivo*¹¹. This natural targeting ability of EVs could be utilised to specifically deliver RNA to target cells. As well as being less toxic and immunogenic while also possessing an endogenous targeting ability, there

is some evidence that EVs are capable of crossing hard to penetrate biological barriers such as the blood-brain barrier¹². These features make EVs an attractive candidate for a vehicle for therapeutic RNA delivery.

In addition to the aforementioned attractive features of EVs, evidence is emerging that suggests that EVs deliver RNA to its cytosolic site of action with high efficiency. Firstly, the functional intercellular transfer of RNA plays a role in numerous biological processes^{8,9,13,14} despite the presence of an extremely low amount of these RNAs in EVs¹⁵. A good example is that of the oncogenic miRNA-21 which is relatively abundant in cancer-derived EVs. The EV-mediated transfer of this RNA has been shown to promote tumour progression and growth^{13,16,17}. Interestingly, despite the well characterised ability of this miRNA to promote cancer progression via EV-mediated transfer, it is present at far fewer than one copy per particle¹⁷. There is also evidence that mRNA can be functionally transferred by EVs¹⁸. This is of interest as mRNA makes up a very small proportion of the total RNA contained within EVs with even the most abundant mRNA being found in only 1 out of 1000 particles after an analysis of glioma-derived EVs¹⁹. Taken together, the fact that these examples of functional transfer occur despite the extremely low loading of RNA is indirect evidence of highly efficient transfer.

However, direct evidence of highly efficient EV-mediated RNA transfer is lacking. This is largely due to the absence of suitable tools to directly study this transfer. One method for studying EV-mediated RNA transfer is to use fluorescently labelled RNA²⁰. This can be visualised within recipient cells but provides no information as to whether this labelled RNA is functional within recipient cells. Other studies have made use of siRNA or miRNA-mediated knockdown of target genes as a readout for functional RNA delivery²¹. However, due to the low RNA loading of EVs, the siRNA or miRNA mediated influence on gene expression is likely to be undetectable in a bulk measurement of cells. mRNA based reporter systems have been developed which address this need and are theoretically capable of detecting EV-mediated RNA transfer at the single cell level²². These systems rely on the expression of mRNA to protein as a readout in recipient cells. However, a major drawback is the fact that results can be confounded by EV-mediated transfer of protein derived from the expression of reporter mRNA in the EV-producing donor cell²³. Therefore, to effectively study EV-mediated RNA transfer, a highly sensitive single-cell reporter system capable of specific activation by RNA only is required.

We therefore set out to provide the field with a suitable tool for the study of EV-mediated RNA transfer which lead to the development of the highly sensitive CROSS-FIRE reporter

system. This system was then used to provide direct evidence that EVs indeed deliver RNA with extremely high efficiency and outperform 'state-of-the-art' DLin-DMA-MC3-LNPs. The remainder of the thesis investigated whether this high delivery efficiency could be explained by intracellular trafficking routes of EVs post-uptake or potential fusogenic properties of EVs in acidic compartments.

SUMMARY OF THESIS

In **Chapter 2** we review the ways in which EVs could be utilised in a therapeutic context. We discuss uptake and post-uptake trafficking routes by which EVs deliver their cargo to recipient cells and how these routes may influence cargo delivery. The biodistribution and endogenous cell targeting features which may be relevant to the development of EV therapeutics are also discussed along with ways in which EVs can be modified to improve their therapeutic characteristics.

In **Chapter 3** we describe the development and validation of the CROSS-FIRE system, a novel CRISPR/Cas9 based reporter system for the study of EV-mediated RNA transfer. We use this system to identify genes involved in EV biogenesis, endocytosis and internal membrane trafficking which are involved in EV-mediated RNA delivery.

In **Chapter 4** we studied and compared the delivery efficiency of EVs to the state-of-the-art DLin-DMA-MC3-LNP formulation. We used the CROSS-FIRE reporter system to demonstrate that EVs deliver RNA with an efficiency orders of magnitude higher than that of the tested LNPs.

In an attempt to elucidate how EVs deliver RNA with higher efficiency, **Chapter 5** describes a comparative analysis of post-uptake trafficking of EVs and LNPs. EVs and LNPs were shown to follow similar routes post-uptake which suggests that the high RNA delivery efficiency of EVs is conferred by other features.

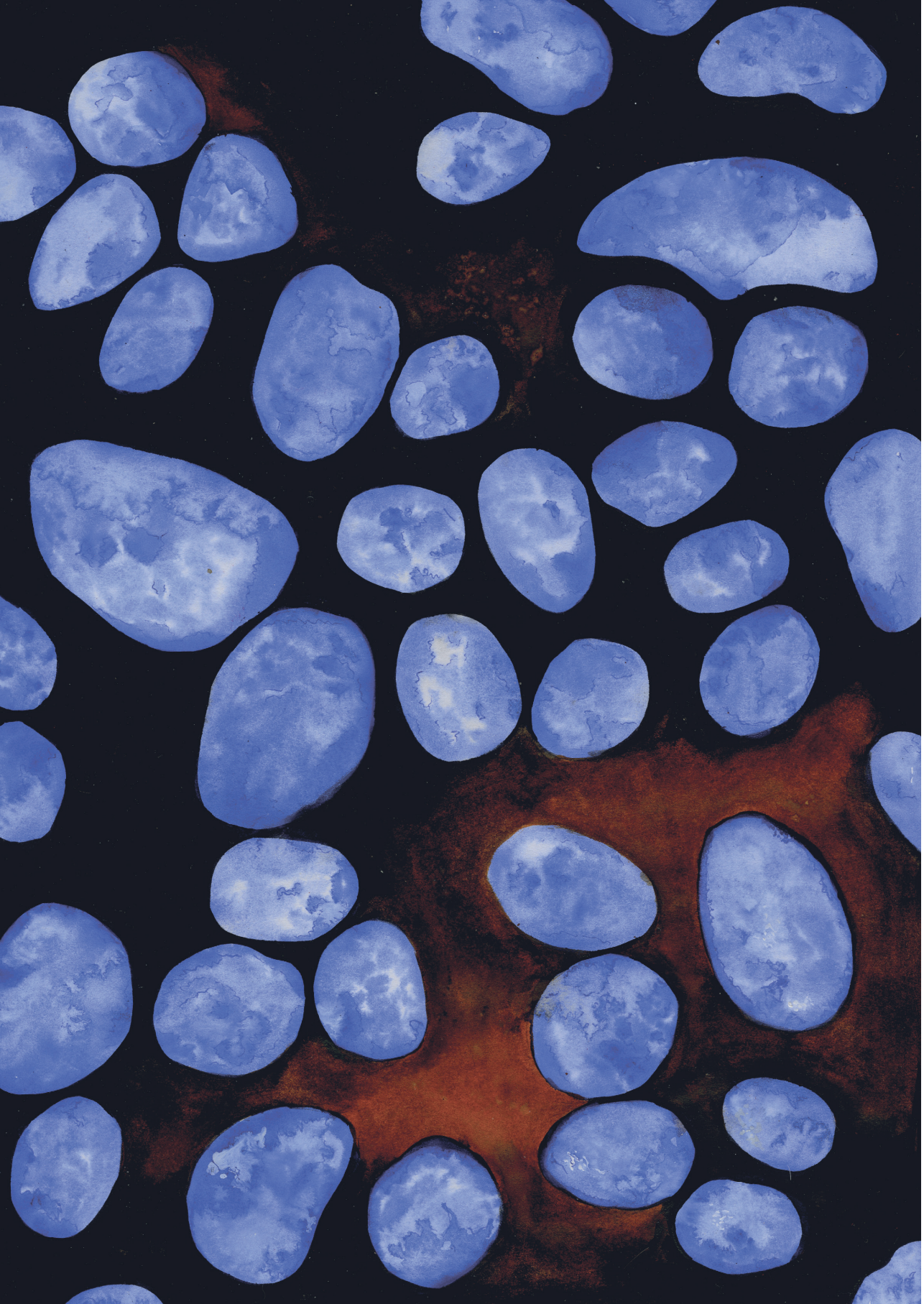
One such potential feature is pH dependent content release. In **Chapter 6** we describe the development of an assay to demonstrate fusion and release of RNA cargo from EVs at acidic pH.

Finally, in **Chapter 7** we provide a summary of the research contained in this thesis and suggest perspectives for future work which could further the development of EVs as a potential therapeutic delivery vehicle.

REFERENCES

1. Chen S, Ge X, Chen Y, Lv N, Liu Z, Yuan W. Advances with RNA interference in Alzheimer's disease research. *Drug Des Devel Ther.* 2013;7:117-125. doi:10.2147/DDDT.S40229
2. Chahal JS, Fang T, Woodham AW, et al. An RNA nanoparticle vaccine against Zika virus elicits antibody and CD8+ T cell responses in a mouse model. *Sci Rep.* 2017;7(1):252. doi:10.1038/s41598-017-00193-w
3. Gillmore JD, Gane E, Taubel J, et al. CRISPR-Cas9 In Vivo Gene Editing for Transthyretin Amyloidosis. *N Engl J Med.* June 2021. doi:10.1056/NEJMoa2107454
4. Dowdy SF. Overcoming cellular barriers for RNA therapeutics. *Nat Biotechnol.* 2017;35(3):222-229. doi:10.1038/nbt.3802
5. Gilleron J, Querbes W, Zeigerer A, et al. Image-based analysis of lipid nanoparticle-mediated siRNA delivery, intracellular trafficking and endosomal escape. *Nat Biotechnol.* 2013;31(7):638-646. doi:10.1038/nbt.2612
6. El Andaloussi S, Mäger I, Breakefield XO, Wood MJA. Extracellular vesicles: Biology and emerging therapeutic opportunities. *Nat Rev Drug Discov.* 2013;12(5):347-357. doi:10.1038/nrd3978
7. Van Niel G, D'Angelo G, Raposo G. Shedding light on the cell biology of extracellular vesicles. *Nat Rev Mol Cell Biol.* 2018;19(4):213-228. doi:10.1038/nrm.2017.125
8. Morel L, Regan M, Higashimori H, et al. Neuronal Exosomal miRNA-dependent Translational Regulation of Astroglial Glutamate Transporter GLT1 * \square . 2013;288(10):7105-7116. doi:10.1074/jbc.M112.410944
9. Zhang L, Zhang S, Yao J, et al. Microenvironment-induced PTEN loss by exosomal microRNA primes brain metastasis outgrowth. *Nature.* 2015;527(7576):100-104. doi:10.1038/nature15376
10. Zhu X, Badawi M, Pomeroy S, Sutaria DS, Xie Z, Baek A. Comprehensive toxicity and immunogenicity studies reveal minimal effects in mice following sustained dosing of extracellular vesicles derived from HEK293T cells. *J Extracell Vesicles.* 2017;6(00). doi:10.1080/2013078.2017.1324730
11. Hoshino A, Costa-Silva B, Shen TL, et al. Tumour exosome integrins determine organotropic metastasis. *Nature.* 2015;527(7578):329-335. doi:10.1038/nature15756
12. Alvarez-Erviti L, Seow Y, Yin H, Betts C, Lakhai S, Wood MJA. Delivery of siRNA to the mouse brain by systemic injection of targeted exosomes. *Nat Biotechnol.* 2011;29(4):341-345. doi:10.1038/nbt.1807
13. Abels ER, Maas SLN, Nieland L, et al. Glioblastoma-Associated Microglia Reprogramming Is Mediated by Functional Transfer of Extracellular Article Glioblastoma-Associated Microglia Reprogramming Is Mediated by Functional Transfer of Extracellular miR-21. *CellReports.* 2019;28(12):3105-3119.e7. doi:10.1016/j.celrep.2019.08.036
14. Pegtel DM, Cosmopoulos K, Thorley-Lawson DA, et al. Functional delivery of viral miRNAs via exosomes. *Proc Natl Acad Sci.* 2010;107(14):6328-6333. doi:10.1073/pnas.0914843107
15. Chevillet JR, Kang Q, Ruf IK, et al. Quantitative and stoichiometric analysis of the microRNA content of exosomes. *PNAS.* 2014;111(41):14888-14893. doi:10.1073/pnas.1408301111
16. Liao J, Liu RAN, Shi Y, Yin L, Pu Y. Exosome-shuttling microRNA-21 promotes cell migration and invasion-targeting PDCD4 in esophageal cancer. *Int J Oncol.* 2016;(87):2567-2579. doi:10.3892/ijo.2016.3453

17. He D, Wang H, Ho S, et al. Total internal reflection-based single-vesicle in situ quantitative and stoichiometric analysis of tumor-derived exosomal microRNAs for diagnosis and treatment monitoring. *Theranostics*. 2019;9(15):4494-4507. doi:10.7150/thno.33683
18. Skog J, Würdinger T, Rijn S Van, et al. Glioblastoma microvesicles transport RNA and proteins that promote tumour growth and provide diagnostic biomarkers. 2008;10(12). doi:10.1038/ncb1800
19. Wei Z, Batagov AO, Schinelli S, et al. Coding and noncoding landscape of extracellular RNA released by human glioma stem cells. doi:10.1038/s41467-017-01196-x
20. Mighty J, Zhou J, Benito-martin A, et al. Analysis of Adult Neural Retina Extracellular Vesicle Release , RNA Transport and Proteomic Cargo. :1-10.
21. Albanese M, Chen Y-FA, Hüls C, et al. Micro RNAs are minor constituents of extracellular vesicles and are hardly delivered to target cells. 2020. doi:10.1101/2020.05.20.106393
22. Zomer A, Maynard C, Verweij FJ, et al. In vivo imaging reveals extracellular vesicle-mediated phenocopying of metastatic behavior. *Cell*. 2015;161(5):1046-1057. doi:10.1016/j.cell.2015.04.042
23. Somiya M. Where does the cargo go?: Solutions to provide experimental support for the "extracellular vesicle cargo transfer hypothesis." *J Cell Commun Signal*. 2020;14(2):135-146. doi:10.1007/s12079-020-00552-9



EXTRACELLULAR VESICLE-BASED THERAPEUTICS: NATURAL VERSUS ENGINEERED TARGETING AND TRAFFICKING

Daniel E. Murphy^a, Olivier G. de Jong^a, Maarten Brouwer^a,
Matthew J. Wood^c, Grégory Lavieu^d, Raymond M. Schiffelers^a
& Pieter Vader^{a,b}

a: CDL Research, University Medical Center Utrecht, Utrecht,
the Netherlands

b: Department of Experimental Cardiology, University Medical
Center Utrecht, Utrecht, the Netherlands

C: Department of Physiology, Anatomy and Genetics, University of
Oxford, Oxford, UK

D: Institut Curie, PSL Research University, INSERM U932,
Paris, France

**Experimental & Molecular Medicine,
Volume 51, pages 1–12, (2019)**

CHAPTER 2

ABSTRACT

Extracellular vesicles (EVs) are increasingly being recognized as mediators of intercellular signaling via the delivery of effector molecules. Interestingly, certain types of EVs are also capable of inducing therapeutic responses. For these reasons, the therapeutic potential of EVs is a topic of intense research, both in the context of drug delivery and regenerative medicine. However, to fully utilize EVs for therapeutic purposes, an improved understanding of the mechanisms by which they function would be highly advantageous. Here, the current state of knowledge regarding the cellular uptake and trafficking of EVs is reviewed, along with a consideration of how these pathways potentially influence the functions of therapeutic EVs. Furthermore, the natural cell-targeting abilities, biodistribution profiles, and pharmacokinetics of exogenously administered EVs, along with the components responsible for these features are discussed. An overview of the potential clinical applications and preclinical examples of their successful use is also provided. Finally, examples of EV modifications that have successfully been employed to improve their therapeutic characteristics receive a particular focus. We suggest that, in addition to investigation of EV cell targeting and routes of uptake, future research into the routes of intracellular trafficking in recipient cells is required to optimally utilize EVs for therapeutic purposes.

INTRODUCTION

A major limiting factor in the development and application of biologicals is an appropriate method for the delivery of these molecules to their sites of action. For example, RNA therapeutics possess great potential due to their ability to alter gene expression; however, the large polar RNA molecule is unable to cross the cell membrane and is subject to rapid digestion by extracellular RNases. Current conventional strategies designed to overcome these barriers involve enveloping therapeutic RNA within synthetic nanoparticles¹ or conjugating RNA to specific ligands designed to promote uptake². More recently, the FDA has approved lipid nanoparticles (LNPs) developed by Alnylam for the delivery of siRNAs to treat hereditary transthyretin amyloidosis, representing the first-ever approved drug based on RNA interference. LNPs protect their delicate cargo from degradation and facilitate entry into cells. Despite overcoming these obstacles, LNPs can display (dose-limiting) toxicity and LNP-mediated RNA delivery is largely limited to the liver³. Thus, ineffective delivery to other tissues continues to delay the development of effective therapeutic strategies.

A solution to this drug delivery problem is urgently needed, and for this reason, the therapeutic potential of extracellular vesicles (EVs) has become a topic of intense research. These lipid-bound particles with a diameter of 30–1000 nm facilitate intercellular communication following their release from donor cells and subsequent internalization into surrounding or distant recipient cells. This process results in the transfer of their protein, lipid, and RNA cargo, thereby eliciting a response in recipient cells⁴. Due to this ability to function as an endogenous intercellular cargo transfer system, EVs have been studied for use as potential vehicles for drug delivery. In addition to their ability to deliver exogenous therapeutic cargo, certain EVs also possess inherent therapeutic characteristics, most notably in the context of regenerative medicine⁵.

In order to understand how EVs can be optimally utilized for therapeutic purposes, it is important to understand the processes by which they are formed and how they function in health and disease. EVs are classed into two major subtypes based on their biogenesis—exosomes and microvesicles. Exosomes range from 30–100 nm in diameter and are derived from endosomal compartments⁶. In contrast, microvesicles are formed through a process of budding and pinching off from the cell membrane⁷. They are highly heterogeneous in size and vary from 50–1000 nm in diameter.

Exosomes are formed within multivesicular endosomes (MVEs) through a process of inward budding, resulting in the formation of intraluminal vesicles (ILVs). These

ILVs are released into the extracellular environment—at which point they are termed exosomes—upon the maturation of the MVE and subsequent fusion with the cell surface. This process depends on numerous pathways, many of which have not yet been fully elucidated; however, proteins with important roles in this process are the endosomal sorting complexes required for transport (ESCRT) protein family⁸. Various members of the ESCRT family are responsible for the organization of proteins on the MVE membrane and the eventual budding off into the MVE lumen, which is assisted by ESCRT-III⁹. ILVs are also generated through a process that does not require the ESCRT complex. An important factor required for ESCRT-independent ILV formation is the tetraspanin CD63¹⁰. CD63 is a typical EV protein marker, and its importance in EV biogenesis is highlighted by the observation that its knockout results in decreased EV release from human embryonic kidney 293 (HEK293) cells¹¹. Another important mediator of ESCRT-independent ILV formation is neutral sphingomyelinase 2. This enzyme is responsible for the synthesis of the lipid ceramide, which forms microdomains on the MVE membrane, a process that is crucial for ILV generation¹². The formation of these ceramide-rich lipid microdomains is followed by an inward invagination that may be promoted by the cone-like shape of the ceramide molecule¹³. Other proteins have recently been shown to be involved in exosome formation. Hsp90, a chaperone protein, appears to exhibit specific MVE-related activity that triggers the deformation of the MVE, fusion of the MVE with the plasma membrane and subsequent release of exosomes¹⁴. Further studies are needed to elucidate whether microvesicle formation is a completely Hsp90-independent process.

Similarly to exosomes, the secretion of microvesicles is also partially ESCRT dependent and requires the formation of lipid microdomains at the plasma membrane. The ESCRT-1 component tumor susceptibility gene 101 has been reported to interact with arrestin domain-containing protein 1 at the cell surface, which mediates the budding off of microvesicles¹⁵. In addition, the formation of ceramide-rich lipid microdomains is also involved in microvesicle formation¹⁶. In contrast to exosome formation, in which ESCRT-III is responsible for the scission of ILVs into the MVE lumen, a reorganization of the actin-myosin cytoskeletal network mediated by ADP-ribosylation factor 6 is the mechanism by which budding microvesicles are released from the plasma membrane¹⁷.

EVs are loaded with a diverse range of proteins, some of which are common to most EV subsets released from most cell types, such as the membrane-bound tetraspanins CD9, CD81, and CD63¹⁸. Others are detected in EVs derived from only a specific subset of cell types, such as the truncated form of epidermal growth factor receptor known as EGFRvIII, which has been identified on the surface of glioma-derived EVs¹⁹.

In addition to their protein contents, EVs are also loaded with nucleic acids. For example, there are examples of mRNA transcripts loaded within EVs which can be functionally transferred from producer to recipient cells^{20,21}. Noncoding RNAs (ncRNAs) such as microRNAs (miRNAs) are also loaded in EVs, some of which are enriched in comparison to their cells of origin²². The incorporation of ncRNAs is also influenced by the status of the producing cell. For example, immune activation has been shown to influence the ncRNA transcriptome of dendritic cell-derived EVs²³. These observations suggest that the ncRNA content of EVs plays a physiological role. Furthermore, various types of DNA, such as mitochondrial and genomic DNA have also been found within EVs^{24,25}.

The lipid composition of EVs is markedly different from the composition of the cell membrane. EVs can be enriched in phosphatidylserine (PS)²⁶, lipids that positively regulate the curvature of the outer membrane positive such as lysophosphatidylcholine and lipids that negatively regulate the curvature of the inner membrane such as cardiolipin²⁷. The lipids contained in EVs may exert a signaling function. For example, eicosanoids present in EVs, such as prostaglandins and leukotrienes, have been implicated in signaling processes²⁸.

In most cases, the precise mechanisms by which EVs exert their functions remain to be elucidated. However, some EVs transfer active cargo that has been specifically shown to induce a response in recipient cells. Functional transfer of chemokine receptor 5 (CCR5) by EVs from CCR5+ cells to CCR5- monocytes provided an important factor required for HIV infection and rendered previously resistant cells sensitive to infection²⁹. EGFRVIII was shown to be transferred from EGFRVIII-positive glioma cells to EGFRVIII-negative glioma cells via EVs. Interestingly, this transfer led to the activation of EGFRVIII-mediated oncogenic pathways in the recipient cells¹⁹.

In addition to functional protein transfer, EV-mediated RNA delivery has also been implicated in pathophysiological processes. For example, the transfer of miRNA-19 from astrocytes to breast cancer cells via EVs has been shown to inhibit the expression of its target, PTEN. This reduction in PTEN expression is associated with a priming of the tumor microenvironment for metastatic outgrowth *in vivo*³⁰. Furthermore, EV-mediated RNA transfer has also been shown to promote the induction of a metastatic phenotype *in vivo*. The transfer of EVs containing mRNA transcripts involved in metastasis and migration from highly metastatic MDA-MB-231 cells to less metastatic T47D cells induced a highly metastatic phenotype in cells that functionally took up MDA-MB-231-derived EVs³¹.

The fact that EVs have been shown to induce functional effects via the delivery of RNA and protein molecules provides great promise to the EV therapeutic field. To induce their functional influence, these EV-delivered molecules must reach their site of action within the cell in adequate quantities. Strikingly, the mechanisms responsible for EV-mediated delivery of these molecules have not yet been determined. Although some evidence that specific EV types are able to deliver their cargo via direct fusion with the plasma membrane is available^{32,33,34}, EVs most likely deliver their cargo through a route similar to viruses via escape of endosomal compartments. It is anticipated that by shedding light on the EV cargo delivery process, the drug delivery field may be able to improve the delivery of therapeutic molecules to their intracellular sites of action.

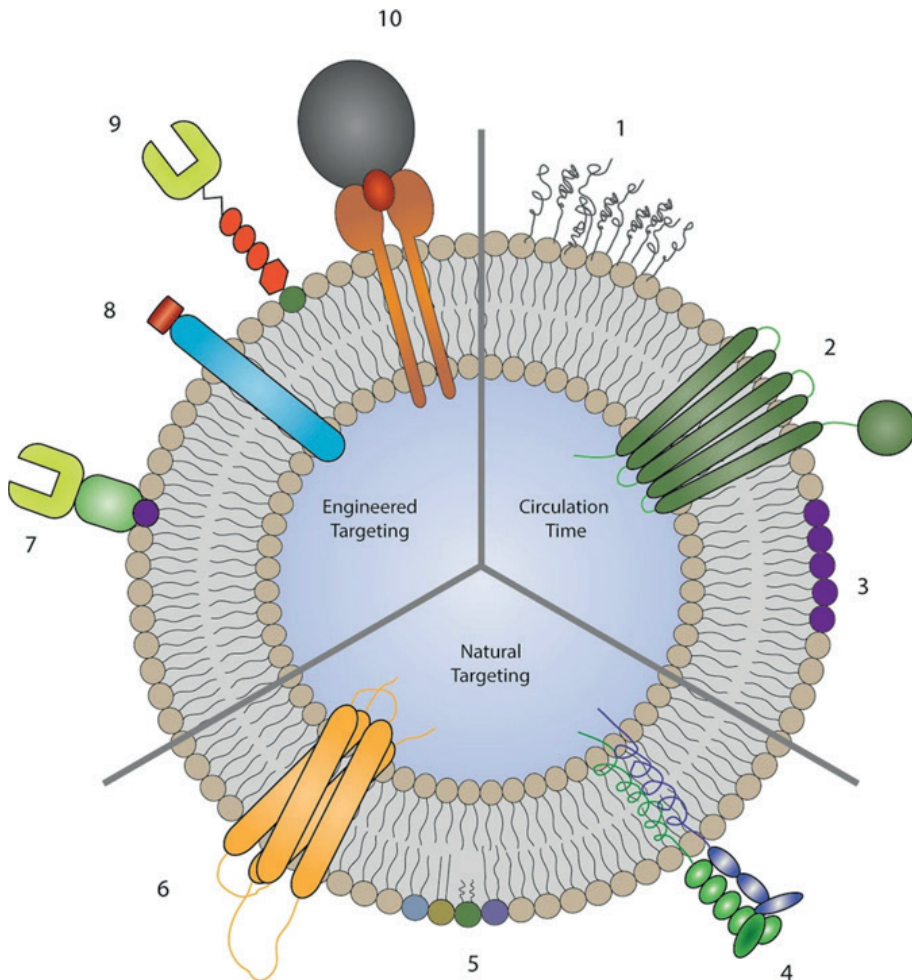
EV THERAPEUTICS

EVs can possess inherent tissue repair-promoting properties that may be exploited therapeutically. For example, researchers initially thought that the cardioprotective properties of mesenchymal stem cells (MSCs) resulted from their differentiation into healthy myocardium. However, the effects were later shown to be due to the paracrine effects of MSCs on the surrounding host tissues. Great interest in the therapeutic potential of EVs was generated when it was demonstrated that EVs are an important component of MSC-mediated cardioprotection⁵. Since this discovery, extensive preclinical research has revealed the utility of EVs as a therapeutic agent in liver³⁵ and cardiac³⁶ regenerative medicine.

EVs possess numerous advantages over cell-based therapies in the context of regenerative medicine. A major advantage is that EVs, depending on their source, may be less immunogenic than their parental cells, likely due to a lower abundance of transmembrane proteins such as MHC complexes on their surface³⁷. Unlike live cells, EVs have a long shelf life and may be transported and stored for long periods. Furthermore, EVs do not replicate after injection. Thus, EVs present less risk of tumor generation and the transfer of latent viral pathogens.

EVs also possess numerous advantageous features as drug delivery vehicles that may help them to outperform synthetic drug carriers. Notably, EVs seem to possess an intrinsic ability to cross tissue and cellular barriers³⁸. In addition, synthetic drug carriers, such as LNPs and polymeric micelles, suffer from high immunogenicity and toxicity³⁹. As therapeutic EVs are derived from either autologous or benign biological sources, they are less likely to induce these adverse effects. In fact, MSC-derived EVs have been shown

to exert inhibitory effects on immune responses⁴⁰. Furthermore, some EVs may possess inherent targeting characteristics and display tropism for a particular cell or tissue⁴¹. This feature could be exploited to selectively deliver drugs to their intended targets while avoiding off-target effects.



▲Fig. 1: Naturally occurring or artificial features of EVs that alter the circulation time and targeting. The addition of polyethylene glycol (1) increases the circulation time⁷⁹, the presence of CD47 (2) inhibits uptake and clearance from the circulation by macrophages, while PS58 (3) is recognized by macrophages, leading to increased clearance. The integrin (4), lipid (5), and tetraspanin (6) compositions of EVs influence their natural targeting properties. These targeting properties are altered by the addition of targeting moieties anchored via the phosphatidylserine-binding C1C2 domains of lactadherin82 (7), the expression of lysosome-associated membrane protein 2 fusion proteins³⁸ (8), glycosylphosphatidylinositol-anchored targeting moieties⁸¹ (9), and transferrin-conjugated magnetic particles bound to transferrin receptor expressed on EVs⁹³ (10)

EVs have been successfully utilized as a drug delivery system in preclinical settings. Recently, large quantities of MSC-derived EVs loaded with an anti-KRASG12D siRNA were produced by electroporation, which were capable of increasing survival in a mouse model of pancreatic cancer⁴². However, it should be noted that controversy exists regarding the effectiveness of electroporation for siRNA loading into EVs^{43,44}. EVs have also been successfully used in preclinical regenerative medicine. For instance, MSC-derived EVs were capable of inducing osteochondral regeneration in a rat model of joint damage after an intra-articular injection⁴⁵.

Numerous additional examples reveal the successful preclinical use of EVs, some of which are summarized later in this review. However, rather than focusing on these specific examples, a better understanding of their inherent general features, such as EV circulation kinetics, targeting, internalization, and intracellular trafficking routes, is needed to fully exploit these features of EVs for therapeutic purposes. In this review, we aim to summarize the current knowledge on these topics. We also aim to summarize methods for altering the characteristics of EVs to improve their therapeutic activity (Fig. 1).

CIRCULATION KINETICS AND BIODISTRIBUTION OF EVS

The surface protein components of EVs are in part responsible for the determination of their circulation kinetics and biodistribution profile. This was clearly demonstrated by the observation that protease treatment of EVs prior to administration via intravenous injection resulted in a delayed clearance of EVs. Protease treatment also significantly reduced accumulation of EVs in the lungs, but did not alter uptake by macrophages⁴⁶. However, according to other studies, EV surface proteins do indeed affect uptake by macrophages; for instance, CD47 has been found to inhibit EV uptake by macrophages⁴⁷.

The biodistribution of therapeutic EVs is a crucial aspect of their efficacy and safety. In order to successfully make use of EVs for therapeutic delivery, an improved understanding of the biodistribution profile of exogenously administered EVs is pivotal. Using EVs labeled with a lipophilic dye, it was found that EVs accumulated primarily in the liver, spleen, and gastrointestinal tract of mice but that the biodistribution could be influenced by route of administration. Interestingly, the cellular origin of EVs also influenced this profile, suggesting that EVs from different cell sources possess different targeting characteristics. EVs from HEK293T cells also accumulated in subcutaneous tumors, a property which could be harnessed by EV-based anti-cancer therapeutics⁴⁸. Another approach for labeling EVs

for biodistribution studies is tagging EVs with luciferase. Using this method, it was found that luciferase-labeled EVs accumulated mostly in the lungs, liver, spleen and kidney⁴⁹. Furthermore, *Gaussia princeps* luciferase-labeled EVs derived from a variety of mouse cell lines were used to demonstrate that intravenously administered EVs accumulated in the liver and were rapidly cleared from circulation in a partly macrophage-dependent manner⁵⁰. Despite differences in biodistribution being observed between studies which have made use of EVs of different origins and different labeling techniques, a common consensus is that a large proportion of EVs are destined to accumulate in the liver and spleen, which could be exploited for specific therapeutic targeting of these organs.

In addition to the effects of the cell source, EVs with different sizes have also been shown to possess differing biodistribution profiles. Asymmetric flow-field fractionation has been used to isolate three subsets of EVs based on size. These subsets possessed differing molecular compositions and biophysical properties. Consistent with other observations, the majority of all subsets accumulated in the liver. However, the levels of accumulation in the bone and lymph nodes were significantly higher for large EVs as compared to the smaller subsets⁵¹. This is an interesting observation, but it remains unclear whether this is a result of EV size per se rather than a result of their differing molecular compositions.

None of these studies identified a significant distribution of EVs to the brain. However, there is some evidence that this may change during conditions of ischemic stroke. In a mouse model, strong uptake of cardiosphere-derived EVs was observed in the stroke penumbra. This phenomenon could be exploited for therapeutic targeting of tissues that are damaged after stroke⁵².

Despite the knowledge provided by these studies, an improved understanding of the factors that affect biodistribution would be highly beneficial for improving targeted EV delivery.

TARGETING AND INTERNALIZATION—NATURAL TARGETING PROPERTIES OF EVS

For an EV to exert its function, it must first bind to its recipient cell, and it is known that different EVs are capable of preferentially binding to specific target cell types. This inherent targeting ability of EVs is a feature that could be used to target EV drug delivery vehicles to their desired sites of action. Some of the features that are known to influence EV targeting are summarized in Table 1.

Table 1 - An overview of natural EV features that influence targeting

EV Characteristic	Example	Reference
Protein Composition	<u>Integrin profile</u> The display of different integrin complexes directs EVs to either the liver and brain or lungs.	53
	<u>Tetraspanin profile</u> EVs containing the tetraspanin Tspan8 in complex with integrin $\alpha 4$ were shown to be selectively taken up by cells of the pancreas.	54
	CD63+ EVs were taken up by neurons and glial cells, while CD63- EVs bound only to the dendrites of neurons.	55
	<u>Fibronectin</u> Fibronectin on MVEC-derived EVs mediates binding to OPCs via HPSGs.	56
Lipid Composition	PS-coated beads are targeted and tethered to phagocytic cells via T-cell immunoglobulin mucin protein 4 receptor.	57
	PS-containing liposomes competitively inhibit EV uptake by murine macrophages.	58
Glycan Composition	Glycans on the EV surface direct EVs to CCR8-expressing GBM8 cells via a triple interaction with CCL18.	59
	Glycans enriched on MSC-derived EVs are involved in targeting EVs to HeLa cells via SIGLECs.	60
Negative Charge	Negatively charged PS- and phosphatidylglycerol-containing liposomes reduce EV uptake by murine macrophages, while neutral phosphatidylcholine liposomes did not.	58

As mentioned above, the protein contents of EVs alter targeting behaviors. For example, EVs displaying integrin $\alpha 6$ in complex with subunits $\beta 1$ and $\beta 4$ are directed to S100-A4-positive fibroblasts and surfactant protein C-positive epithelial cells in the lungs. EVs expressing subunits $\beta 5$ and $\beta 4$ are preferentially targeted to Kupffer cells in the liver and CD31-positive endothelial cells in the brain, respectively⁵³.

The tetraspanin class of proteins is abundant on the surface of many EV types¹⁸, and their roles in EV targeting have been investigated. This class of proteins forms a diverse range of complexes with other tetraspanins and integrins, and these complexes have

been shown to determine targeting behaviors. For instance, a complex of the tetraspanin Tspan8 with integrin $\alpha 4$ has been shown to selectively target EVs to cells in the pancreas⁵⁴. In addition, CD63-positive EVs have been shown to target neuronal and glial cells, while CD63-negative EVs bound only to the dendrites of neurons⁵⁵. Furthermore, fibronectin present on the EV surface has been implicated in targeting microvascular endothelial cell-derived EVs to oligodendrocyte precursor cells via an interaction with heparin sulfate proteoglycans⁵⁶.

The EV lipid composition also influences targeting behavior, the clearest example being the targeting of macrophages via recognition of PS on the EV surface. The importance of PS in this interaction is confirmed by the observation that PS-coated beads are targeted and taken up by phagocytic cells via tethering by T-cell immunoglobulin mucin protein 4 receptor⁵⁷. Furthermore, PS-containing liposomes have been shown to reduce EV uptake by competing with and thereby inhibiting their uptake by macrophages. This recognition of PS by macrophages is likely partially mediated by its negative charge, as the uptake of negatively charged phosphatidylglycerol-containing liposomes also inhibited uptake, while neutral phosphatidylcholine-containing liposomes did not⁵⁸.

In addition to lipid and protein determinants of EV targeting, glycans on the EV surface also play a role in cell targeting or uptake. Glycans have been shown to direct EV targeting towards CCR8-positive glioblastoma cells via a triple interaction with the CCR8 ligand CCL18⁵⁹, while glycans on MSC-derived EVs have been shown to direct EVs towards surface-bound sialic acid-binding immunoglobulins, such as lectin receptors, expressed on the surface of HeLa cells⁶⁰.

TARGETING AND INTERNALIZATION - MECHANISMS INVOLVED IN THE INTERNALIZATION OF EVS

It is important to study the ways in which EVs are internalized as this may be crucial for functional outcomes as the route of EV internalization dictates the functional response or efficiency of cargo delivery.

There are multiple routes through which EVs can be internalized by recipient cells, including phagocytosis, macropinocytosis, and receptor-mediated endocytosis. These routes result in the formation of intracellular vesicles containing the internalized material, which may then be further processed or sorted for degradation⁶¹. EVs may also fuse directly with the cell membrane; however, few examples of this process have been reported³². Extensive research has been conducted into the routes of EV uptake, some

of which is summarized in Table 2. Numerous uptake routes have been implicated in EV function, and the major route of uptake seems to depend on the cell type being studied.

Table 2 An overview of research into EV uptake routes

Cell types	Study Method Summary	Implicated uptake route(s)	Reference
PC12 cell donor to bone marrow-derived mesenchymal stromal cell recipient	K ⁺ depletion and siRNA-mediated knockdown to inhibit key proteins involved in specific uptake routes.	Clathrin-mediated endocytosis and macropinocytosis	⁶³
U87 glioblastoma cell donor to human umbilical vein endothelial cell, mouse embryonic fibroblast and U87 cell recipients	Chemical inhibition of cholesterol synthesis to inhibit lipid raft formation.	Lipid raft-dependent endocytosis	⁶⁶
Mutu -, Mutu I and Mutu III donors to various epithelial cell line recipients	Chemical inhibition of endocytosis, caveolin knockdown and determination of the co-localization of labeled EVs with tagged components of endocytosis.	Clathrin-independent endocytosis	⁶⁴
A431 cell donor to HeLa cell recipient	Chemical inhibition of cholesterol synthesis, tyrosine kinases, Na ⁺ /H ⁺ exchange and phosphoinositide 3-kinase. The siRNA-mediated knockdown of various key proteins involved in specific endocytosis pathways was also employed.	Clathrin-independent endocytosis and macropinocytosis	⁶⁵
HeLa cell donor to MIA PaCa-2, A431 and BxPC-3 cell recipients	Activation of macropinocytosis via stimulation of EGFR, CXCR4 and oncogenic Ras.	Macropinocytosis	⁶⁷
Oli-neu cell donor to primary mouse oligodendrocyte, cortical neuron, astrocyte and microglial recipients	Chemical inhibition of macropinocytosis.	Macropinocytosis	⁶⁸
DU145 cell donor to HeLa cell and primary lung fibroblast recipients	Chemical inhibitors of endocytosis and siRNA-mediated knockdown of key proteins involved in specific endocytosis pathways.	Macropinocytosis and fluid-phase endocytosis	⁶⁹
H4 neuroglioma cell donor to H4 neuroglioma and Chinese hamster ovary cell recipients	Chemical inhibition of macropinocytosis and clathrin- and caveolin-mediated endocytosis	None	⁷¹
K562 and MT4 cell donors to Raw264.7 and NIH 3T3 cell recipients	Chemical inhibition of phagocytosis and siRNA-mediated knockdown of key proteins involved in phagocytosis.	Phagocytosis	⁷²

Clathrin-mediated endocytosis is a well-understood route of uptake for extracellular material and involves the formation of clathrin-coated endocytic vesicles⁶². CME has been implicated in EV uptake, as its inhibition resulted in reduced uptake in bone marrow-derived mesenchymal stromal cells⁶³. Clathrin-independent endocytosis, which involves the formation of caveolin-coated invaginations on the cell membrane⁶¹, is another route of EV uptake^{64,65}. It should be noted that this caveolin-dependent endocytosis has also been identified as a negative regulator of EV uptake⁶⁶. In addition, a major route of EV uptake is macropinocytosis. This involves the uptake of large quantities of extracellular fluid into a macropinosome in a process that depends on actin polymerization⁶². Numerous examples of EV uptake through this pathway have been reported^{63,65,67,68,69}. Finally, phagocytic cells, such as macrophages, also take up EVs via phagocytosis⁵⁸.

The uptake of lipoproteins is often associated with the existence of a specific receptor. For instance, the uptake of LDL is now well characterized, and a receptor has long since been identified⁷⁰. Currently, researchers have not determined whether such a bona fide receptor exists for EVs in general, or at least for a particular EV subtype. All the aforementioned proteins are broadly involved in EV targeting and uptake but are neither sufficient nor absolutely required for EV uptake. The discovery of a putative uptake receptor for a specific type or subtype of EV would tremendously improve the design of engineered EV therapeutics.

The routes by which EVs are taken up are diverse and depend on the producer and recipient cell type. To successfully develop therapeutic EVs, it would be of great interest to determine which routes of uptake result in high levels of functional cargo delivery, so that therapeutic EVs could be steered towards this route.

INTRACELLULAR TRAFFICKING OF EVS

Following uptake, extracellular material is kept separate from the cytosol and enters the endosomal system in early endosomes (EEs). Most of the EE contents are destined for degradation in the acidic environment of the lysosomes, including internalized EVs⁷¹. However, for EVs to exert their function, their cargo must reach its intracellular site of action. The ability of EVs to at least partially avoid this degradative pathway was revealed by the observation that EVs follow a similar route to human immunodeficiency virus for dissemination after uptake in mature dendritic cells⁷². This observation is of great interest, as it indicates that EVs are capable of bypassing degradative uptake pathways, but this finding may be specific to dendritic cells. It should also be noted that protease treatment

did not alter this post-uptake trafficking, suggesting that this observation may not be the result of EV-specific features. Despite these concerns, a mechanism for EV escape from degradative pathways after uptake likely exists, as it has been observed in numerous cases that EVs are capable of exerting functional effects via the delivery of their cargo.

To investigate possible routes of degradative escape, EVs labeled with CD63-GFP/CD63-mCherry were produced and followed after internalization by human primary fibroblasts, Huh7 and HEK293 cells. Post-uptake, EVs were seen to be surrounded by larger vesicles which were then trafficked towards ER filaments, where interactions with the ER were observed, as demonstrated by microscopy. A potential exchange of content at these interaction sites between the vesicles and the ER was proposed⁷³. This hypothesis is strengthened by the fact that Rab5- and Rab7-positive endosomal vesicles are known to interact with the ER⁷⁴. The mechanisms underlying this potential process of functional content release, which requires content crossing the exosomal and endosomal membranes, remain unknown. In regards to miRNAs and siRNAs, if EV-mediated delivery to the ER is possible, this could be a pathway for functionally altering gene expression.

An analysis of internalized PC12 cell-derived EVs labeled with lipophilic dyes and amino-reactive fluorophores by live-cell fluorescence microscopy in PC12 cells revealed that EVs were first encapsulated in EEs, which then moved towards the perinuclear space, the location of endosomes as well as lysosomes. Here, it was observed that the labeled protein signal began to separate from the EV membrane signal within 3 h, indicating separation of transmembrane proteins and lipids in the EV membrane. Between 6 and 24 h, the signal of the lipid-labeled EVs was substantially reduced and not present in the perinuclear space, suggesting that the lipids were recycled and transported to other parts of the cell⁷⁵. In contrast, the signal of the transmembrane proteins could still be observed in the perinuclear space, suggesting that much of the protein remained in the lysosomes. This implies that a large amount of membrane-bound EV cargo is degraded in the lysosomes post-uptake.

It should be noted that research into the post-uptake routes of EV trafficking is hindered by the recent finding that commonly used lipophilic dyes used for EV labeling, such as PKH26, form particles which are hard to distinguish from labeled EVs and colocalize with them in subcellular compartments⁷⁶. In addition, EVs are often tracked with fluorescently labeled tetraspanin proteins⁷⁷, which remain associated with membranes even when EV content delivery occurs. It seems evident that assessment of EV content release must involve the use of cytosolic EV markers and the development of new assays to study EV cargo transfer.

The evidence suggesting that EVs are able to escape endosomal degradative pathways post-uptake is of great interest, as this feature could be exploited for therapeutic delivery. However, the mechanisms by which EVs are capable of avoiding degradation are currently poorly understood. In order to fully utilize EVs as therapeutics it is necessary to determine the intracellular routes and mechanisms by which their cargo is delivered.

ENGINEERING APPROACHES THAT IMPACT CIRCULATION KINETICS AND BIODISTRIBUTION

Altogether, EVs clearly possess many potential advantageous features compared to synthetic delivery systems in terms of their intrinsic therapeutic properties and ability to deliver functional cargo. However, unmodified EVs suffer from rapid clearance and low accumulation in target tissues and cells⁴⁸. Therefore, EVs have been modified in order to steer their delivery towards their target sites of action.

In order to increase circulation time and improve delivery to target tissues, EVs have been coated with polyethylene glycol (PEG) functionalised with anti-EGFR nanobodies. PEG is a hydrophilic polymer and is known to increase the circulation time of nanoparticles⁷⁸. It was found that PEGylation increased EV circulation time and reduced nonspecific interactions with cells, while enhancing the nanobody-mediated interaction with EGFR-expressing cells⁷⁹. Similarly, the effect of cloaking of the EV surface with streptavidin conjugated to PEG via its linkage to 1,2-bis(dimethylphosphino)ethane lipids has also been employed. The streptavidin component facilitated the conjugation of targeting components, which successfully altered EV biodistribution in mice⁸⁰. It should be noted however, that the addition of PEG to the surface of liposomes is known to hinder their escape from the endosome after uptake, which may also apply to PEGylated EVs⁷⁸.

Another approach used to increase circulation time is through the increased expression of CD47 on the EV surface. This protein has been shown to act in opposition to PS, which promotes the initiation of phagocytosis and subsequent removal from the circulation by macrophages⁵⁸. The CD47 protein has been found on EVs from specific cell types and has been demonstrated to increase circulation time following intraperitoneal injection⁴⁷. This feature could be exploited to prolong the circulation time of therapeutic EVs, and thus increase the window for targeted delivery to specific tissues.

ENGINEERING APPROACHES THAT IMPACT THE TARGETING OR INTERNALIZATION OF EVS

A major challenge hindering the utilization of EVs in a therapeutic context is the difficulty in ensuring delivery to their sites of therapeutic action while avoiding accumulation at off-target sites. Nonspecific delivery decreases efficacy and may induce off-target effects.

The targeting properties of EVs can be influenced by genetic modification of producer cells. The first example of EVs targeted in such a way involved the fusion of lysosome-associated membrane protein 2 (Lamp2b) with the rabies viral glycoprotein peptide. Lamp2b is abundant on the surface of EVs, while the rabies viral glycoprotein peptide binds specifically to the acetylcholine receptor. It was found that this fusion protein conferred EVs with the ability to target neurons, oligodendrocytes and microglia within the brain after systemic injection³⁸. EVs with engineered targeting abilities have also been produced by modification of producer cells to produce recombinant EGFR-specific nanobodies with glycosylphosphatidylinositol (GPI)-anchoring peptides. As EVs are enriched in GPI, nanobodies were highly enriched on the EV surface, which provided the EVs with targeting specificity for EGFR+cells⁸¹. While both of these methods successfully targeted EVs to their intended cells of action, the genetic modification of producer cells may be challenging to utilize for future production of therapeutic EVs, due to their time-consuming production and difficulties in applying them to cells derived from a patient's own body fluids⁴¹.

The application of targeting components post-EV production is an attractive option, as targeting ligands can be applied in a controllable manner at high densities⁴¹. There are numerous recent examples of targeting capabilities being conferred by the addition of nanobodies and antibodies post-EV production. For example, the high concentration of PS in EV membranes has been exploited by fusing targeting proteins to the C1C2 domain of lactadherin, which binds to PS with high affinity. An anti-EGFR nanobody fused to C1C2 self-associated onto EV membranes and promoted EV uptake by EGFR+cells in a dose-dependent manner. Nontargeted control nanobody fusion proteins did not alter interactions with cells, and the addition of the fusion protein did not alter EV size or integrity, demonstrating this method's suitability for therapeutic EV targeting⁸². A similar approach was exploited by fusing an anti-Her2 single-chain variable fragment to the C1C2 domain. This fusion protein was able to latch onto the surface of EVs and targeted the delivery of an mRNA encoding a prodrug converting enzyme to Her2+cells. Remarkably, when administered with the prodrug, these targeted EVs were capable of almost entirely halting the growth of orthotopic Her2+BT474 xenografts in vivo⁸³.

In addition to antibodies and nanobodies, EVs have also been functionalized with targeting peptides postproduction. For example, a multifunctional peptide was able to anchor itself to the EV membrane has been used. This peptide also contained a sequence directed to the low density lipoprotein receptor which is expressed on the BBB and glioma cells and an apoptosis-inducing sequence. The peptide contained an ApoA-I mimetic sequence that associated with phospholipids and allowed incorporation onto the EVs via simple incubation. This approach allowed accumulation of systemically injected EVs in the brain and a successful targeting of methotrexate-loaded EVs to glioma cells in mouse models, resulting in an increase in survival in mouse models of glioma⁸⁴.

Table 3 - Examples of engineering EV targeting by the addition of peptides

Targeting Peptide	Linkage Method	Result	Reference
RGERPPR – A specific peptide for the neuropilin-1 receptor expressed specifically on glioma and tumor vascular endothelial cells.	Click Chemistry (cycloaddition reaction of sulfonyl azide).	EVs cross the BBB and target glioma cells to deliver the therapeutic payload, resulting in the increased survival of a murine model of glioma.	⁹⁰
M12 – A muscle targeting peptide	Using phage display, the CP05 peptide, which binds to the extracellular loop of CD63 with high affinity, was identified. Fusion of the targeting peptides to CP05 facilitated the coating of the EV surface via the CP05-CD63 interaction.	Targeted EVs successfully delivered splice-correcting oligomers to muscle in a dystrophin-deficient mouse model of muscular dystrophy.	⁹¹
RGD – Specifically binds to integrin $\alpha v \beta 3$ expressed on the surface of angiogenic blood vessels.	RGD was anchored to the EV surface via linkage to PEG, a lipid that self-assembles into the EV membrane.	EVs were targeted to $\alpha v \beta 3$ cells in zebrafish and promoted angiogenesis.	⁹²
CTP – Cardiac targeting peptide	Recombinant CTP-Lamp2b expressed in donor cells.	A 15% increase in delivery to mouse hearts after an intravenous injection.	⁹³

Click-chemistry refers to a group of reactions which involve the conjugation of molecules in a modular fashion⁸⁵. One such reaction is bio-orthogonal copper-free azide alkyne cyclo-addition, which was used to couple a cyclo Arg-Gly-Asp-D-Tyr-Lys peptide to the surface of MSC-derived EVs. This peptide binds with high affinity to integrin $\alpha v \beta 3$, which is

expressed in ischemic reactive cerebral vascular endothelial cells. These engineered EVs targeted the ischemic regions of the brain in a murine artery occlusion model while EVs displaying a control peptide did not. In addition, the targeted EVs were able to reduce the inflammatory response via delivery of their loaded curcumin cargo. The approach used in these experiments was robust, rapid, and scalable and could be applied to many other targeting peptides⁸⁶. In addition to the two described here, there are numerous further examples of targeting peptides being linked to the EV surface, which are described in Table 3.

In addition to their use as mediators of cell targeting, peptides have also been used in order to promote the uptake of EVs into cells. For example, Nakase et al. decorated the surface of EVs with an arginine-rich micropinocytosis-inducing peptide via a sulfon- ϵ -maleimidocaproyl-oxysulfosuccinimide ester linkage. This modification substantially increased uptake into CHO-K1 cells. Interestingly, this increase in uptake was associated with an improved delivery of the loaded ribosome-inactivating cytotoxic saporin protein⁷⁷. The application of this cell-penetrating peptide may be a suitable method for improving the intracellular delivery of therapeutic EV cargo. Furthermore, the same group were also able to promote EV uptake by inducing the clustering and activation of EGFR. Activation of this receptor is known to induce EV uptake via the promotion of macropinocytosis⁶⁷. Recipient HeLa cells were engineered to express a modified form of EGFR which bound with high affinity to a stearylated peptide which could be anchored to the EV membrane with high affinity. These modified EVs were capable of inducing receptor clustering and promoting uptake via macropinocytosis and an associated increase in the activity of loaded saporin⁸⁷.

In addition to the use of targeting peptides, nanobodies, and antibodies, pseudotyping has also been used to promote EV uptake. Pseudotyping is a well-studied method commonly used in virology to alter the tropism of a viruses via the introduction of foreign protein tropism determinants from another distinct viral species⁸⁸. Meyer et al. utilized this method by expressing vesicular stomatitis virus glycoprotein in HEK293 cells. This protein was chosen because it is often used to increase the cell tropism and transduction efficiency of therapeutic retroviral vectors. The vesicular stomatitis virus glycoprotein was expressed in the membranes of EVs, and its ectodomain was responsible for inducing a large increase in uptake in several different cell types⁸⁹.

Most of the research aiming to alter EV tropism has relied on the addition of proteins or peptides. However, augmented targeting of specific liver cells and an increase in EV

uptake has been achieved by modifying the surface of EVs with cationized pullulan. This polysaccharide is known to bind an asialoglycoprotein receptor expressed specifically on hepatocytes. The modification of the surface of MSC-derived EVs with this molecule promoted an increase in uptake *in vitro*. Furthermore, in a rat model of liver damage, pullulan-modified EVs were targeted to the liver and significantly improved clinical parameters of liver function⁹⁰.

Another innovative approach to direct EV targeting, which does not rely on proteins or peptides, is through the addition of nucleic acid aptamers which are able to bind target molecules. This approach was recently utilized to direct HEK293T-derived EVs towards prostate cancer cells. In this study, the three-way-join (3WJ) of the bacteriophage phi29 motor packaging RNA was used as a building block to which cholesterol and a targeting aptamer specific for prostate-specific membrane antigen (PSMA) were fused. When cholesterol was bound to the “arrowhead”, the 3WJ was loaded inside of the EVs; however, when cholesterol bound to the “arrowtail”, the 3WJ was displayed on the EV surface. This observation was exploited to produce EVs which contained a therapeutic anti-survivin siRNA and displayed a PSMA-binding RNA aptamer on their surface. The addition of this aptamer increased uptake in PSMA+ cell lines and reduced tumor growth in mouse xenograft models⁹¹. In addition to RNA aptamers, DNA aptamers have also been used to direct EV targeting. The DNA aptamer AS1411 specific for nucleolin, was used to target the delivery of therapeutic siRNAs to cells positive for this protein expressed on the surface of breast cancer cells. The modification of EVs with this aptamer promoted the delivery to tumors *in vivo*, which was associated with an inhibition of tumor growth⁹².

EVs have also been targeted without the addition of targeting ligands, but instead by the addition of magnetic particles. In this way, the biodistribution of EVs decorated with magnetic particles can be controlled using directed magnetic fields. For example, the abundance of transferrin receptor on blood-derived EVs was exploited to coat their surface with transferrin-conjugated superparamagnetic nanoparticles. Post intravenous administration, the biodistribution of these particles was successfully controlled and targeted towards murine tumors using external magnets⁹³.

Although many examples of the targeting of EVs to specific cell types or tissues exist, relatively few examples of EVs being targeted towards specific uptake routes or subcellular locations have been reported. EVs have been shown to be directed towards specific uptake routes when decorated with anti-Her2 antibodies. Anti-Her2 directed EVs displayed different co-localization patterns to wild-type EVs and EVs coated with

a nonspecific antibody. Wild-type EVs mainly co-localized with a protein known to be taken up via caveolae-mediated endocytosis, while nonspecific antibody-coated EVs co-localized with most strongly with dextran, which is taken up by macropinocytosis. When anti-Her2-targeted EVs were analyzed, they co-localized with markers known to be taken up by macropinocytosis, caveolin-mediated, and clathrin-mediated endocytosis⁹⁴.

Altogether, these observations provide evidence that it is possible to tune EV routes of uptake and subsequent subcellular destination. This tuning may substantially increase the efficiency of RNA therapeutic delivery by avoiding degradative uptake routes.

CONCLUSIONS AND PERSPECTIVES

In recent years, the importance of EVs as mediators of intercellular communication has been reported, and it has been demonstrated that EVs possess several features which make them amenable to therapeutic use. For these reasons, the EV field is undergoing a period of rapid growth. This growth has been associated with discoveries which have elucidated some of the targeting abilities, uptake routes, and biodistribution profiles of EVs.

Despite these recent advances, many aspects of their fundamental biology remain to be elucidated. In order to effectively utilize EVs in a therapeutic context, it would be highly advantageous to first gain an improved understanding of aspects of their biology.

Although there have been many successful attempts to alter the biodistribution and cell-targeting properties of EVs, there has been relatively little work undertaken with the purpose of increasing the delivery of EV cargo to its intracellular site of action. It is possible that a large proportion of EVs taken up by a cell are destined for degradation. Therefore, the identification of features which would allow for improved cargo escape would be highly advantageous.

In addition, the routes of EV uptake are highly diverse and vary according to cell and EV types. It is possible that a particular uptake route may result in the delivery of a greater amount functional cargo to the recipient cell than other routes. If EVs were steered towards cellular uptake mechanisms that result in the increased functional delivery of cargo, the efficacy and efficiency of EV-mediated therapeutic strategies would be substantially improved.

It is also known that EV preparations contain a range of EV subtypes, which vary in terms of subcellular site of origin, size, and protein markers. At present it is

extremely challenging to separate these subtypes for functional analysis, and further characterization of the physical and functional properties of subpopulations found in the heterogeneous population of EVs is still ongoing. However, it is possible that the research of certain subtypes for therapeutic purposes could result in the discovery of additional advantageous modifications or strategies for EV-based therapeutics.

In conclusion, many aspects of the uptake, biodistribution, targeting, and trafficking of EVs have been elucidated. A large amount of successful research has also been undertaken into methods by which these features may be altered to produce effective therapeutic EVs. However, in order to translate these findings into clinically successful therapeutics, further research into the underlying biology of EV-mediated cargo transfer and processing is required.

ACKNOWLEDGEMENTS:

The work of DEM and RS is supported by the European Union's Horizon 2020 Research and Innovation Programme under grant agreement No. 721058. OGdj is supported by a Research Grant from the Biotechnology and Biological Sciences Research Council (BB/M024393/1). PV is supported by a VENI Fellowship (# 13667) from The Netherlands Organisation for Scientific Research (NWO). T. The work of GL is supported by Fondation ARC (PJA20171206453), Cancéropôle Île-de-France (Emergence 2018) and French National Research Agency (ANR-10-IDEX-0001-02 PSL, ANR-11-LABX-0043 and ANR-18-CE15-0008). Fondation ARC (PJS20171206453), Cancéropôle Île-de-France (Emergence 2018) and the French National Research Agency (ANR-EVUp).

COMPETING INTERESTS

MW is a co-founder and non-executive director of Evox Therapeutics.

REFERENCES

1. van der Meel R, Fens MHAM, Vader P, van Solinge WW, Eniola-Adefeso O, Schiffelers RM. Extracellular vesicles as drug delivery systems: Lessons from the liposome field. *J Control Release*. 2014;195:72-85. doi:<https://doi.org/10.1016/j.jconrel.2014.07.049>
2. Springer AD, Dowdy SF. GalNAc-siRNA Conjugates: Leading the Way for Delivery of RNAi Therapeutics. *Nucleic Acid Ther*. 2018;28(3):109-118. doi:10.1089/nat.2018.0736
3. Dowdy SF. Overcoming cellular barriers for RNA therapeutics. *Nat Biotechnol*. 2017;35(3):222-229. doi:10.1038/nbt.3802
4. El Andaloussi S, Mäger I, Breakefield XO, Wood MJA. Extracellular vesicles: Biology and emerging therapeutic opportunities. *Nat Rev Drug Discov*. 2013;12(5):347-357. doi:10.1038/nrd3978
5. Lai RC, Arslan F, Lee MM, et al. Exosome secreted by MSC reduces myocardial ischemia/reperfusion injury. *Stem Cell Res*. 2010;4(3):214-222. doi:10.1016/j.scr.2009.12.003
6. van der Pol E, Boing AN, Harrison P, Sturk A, Nieuwland R. Classification, Functions, and Clinical Relevance of Extracellular Vesicles. *Pharmacol Rev*. 2012;64(3):676-705. doi:10.1124/pr.112.005983
7. Van Niel G, D'Angelo G, Raposo G. Shedding light on the cell biology of extracellular vesicles. *Nat Rev Mol Cell Biol*. 2018;19(4):213-228. doi:10.1038/nrm.2017.125
8. Hurley JH. ESCRT complexes and the biogenesis of multivesicular bodies. *Curr Opin Cell Biol*. 2008;20(1):4-11. doi:10.1016/j.ceb.2007.12.002
9. Hurley JH, Hanson PI. Membrane budding and scission by the ESCRT machinery: It's all in the neck. *Nat Rev Mol Cell Biol*. 2010;11(8):556-566. doi:10.1038/nrm2937
10. Colombo M, Moita C, Niel G Van, Kowal J, Vigneron J. Analysis of ESCRT functions in exosome biogenesis , composition and secretion highlights the heterogeneity of extracellular vesicles. 2011. doi:10.1242/jcs.128868
11. Hurwitz SN, Conlon MM, Rider MA, Brownstein NC, Meckes DG. Nanoparticle analysis sheds budding insights into genetic drivers of extracellular vesicle biogenesis. *J Extracell Vesicles*. 2016;5(1):1-20. doi:10.3402/jev.v5.31295
12. Trajkovic K, Hsu C, Chiantia S, et al. Ceramide Triggers Budding of Exosome Vesicles into Multivesicular Endosomes. 2008;319(April).
13. Goñi FM, Alonso A. *Biochimica et Biophysica Acta* Effects of ceramide and other simple sphingolipids on membrane lateral structure. *BBA - Biomembr*. 2009;1788(1):169-177. doi:10.1016/j.bbamem.2008.09.002
14. Lauwers E, Wang Y-C, Gallardo R, et al. Hsp90 Mediates Membrane Deformation and Exosome Release. *Mol Cell*. 2018;71(5):689-702.e9. doi:10.1016/j.molcel.2018.07.016
15. Nabhan JF, Hu R, Oh RS, Cohen SN, Lu Q. Formation and release of arrestin domain-containing protein 1-mediated microvesicles (ARMMs) at plasma membrane by recruitment of TSG101 protein. 2012. doi:10.1073/pnas.1200448109/-/DCSupplemental.www.pnas.org/cgi/doi/10.1073/pnas.1200448109
16. Menck K, Sönmezer C, Worst TS, et al. Neutral sphingomyelinases control extracellular vesicles budding from the plasma membrane. *J Extracell Vesicles*. 2017;6(1). doi:10.1080/20013078.2017.1378056
17. Vandhana Muralidharan-Chari, James Clancy, Carolyn Plou, Maryse Romao, Philippe Chavrier, Graca Raposo CD-S. ARF6-Regulated Shedding of Tumor Cell-Derived Plasma Membrane Microvesicles. *Curr Biol*. 2009;19(22):1875-1885. doi:10.1016/j.cub.2009.09.059.ARF6-regulated

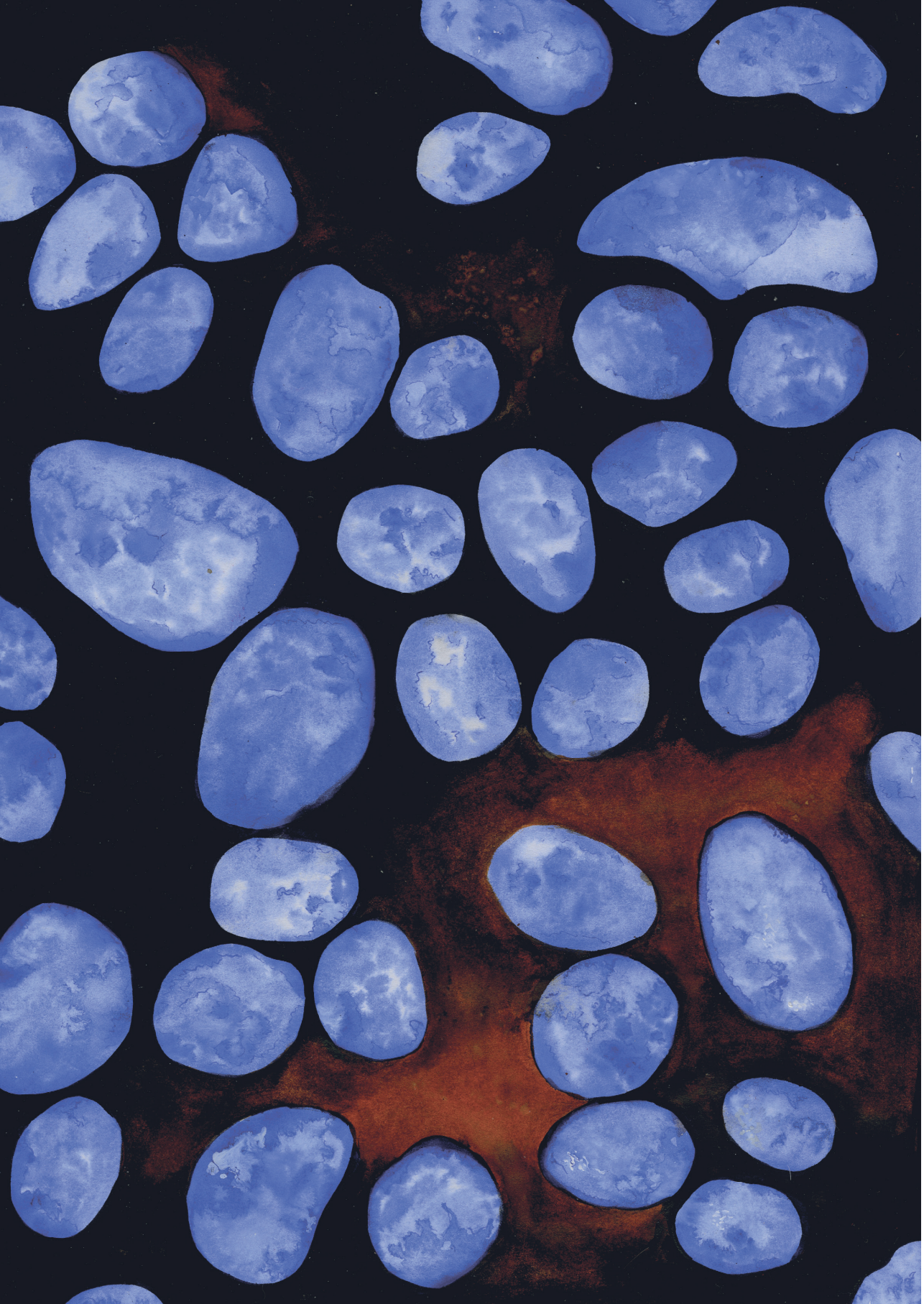
18. Lötvall J, Hill AF, Hochberg F, et al. Minimal experimental requirements for definition of extracellular vesicles and their functions: A position statement from the International Society for Extracellular Vesicles. *J Extracell Vesicles*. 2014;3(1). doi:10.3402/jev.v3.26913
19. Al-Nedawi K, Meehan B, Micallef J, et al. Intercellular transfer of the oncogenic receptor EGFRVIII by microvesicles derived from tumour cells. *Nat Cell Biol*. 2008;10(5):619-624. doi:10.1038/ncb1725
20. Hadi Valadi; Karin Ekström; Apostolos Bossios; Margareta Sjöstrand; James J Lee ; Jan Lotvall. Exosome-mediated transfer of mRNAs and microRNAs is a novel mechanism of genetic exchange between cells. *Nat Cell Biol*. 2007;9:654–659.
21. Skog J, Wurdinger T, Rijn S Van, et al. Glioblastoma microvesicles transport RNA and protein that promote tumor growth and provide diagnostic biomarkers. *Nat Cell Biol*. 2012;10(12):1470-1476. doi:10.1038/ncb1800.Glioblastoma
22. Hoen ENMN-, Buermans HPJ, Waasdorp M, Stoorvogel W, Wauben MHM, Hoen PAC. Deep sequencing of RNA from immune cell-derived vesicles uncovers the selective incorporation of small non-coding RNA biotypes with potential regulatory functions. 2012;40(18):9272-9285. doi:10.1093/nar/gks658
23. Driedonks TAP, van der Grein SG, Ariyurek Y, et al. Immune stimuli shape the small non-coding transcriptome of extracellular vesicles released by dendritic cells. *Cell Mol Life Sci*. 2018;75(20):3857-3875. doi:10.1007/s00018-018-2842-8
24. Guescini M, Genedani S, Agnati LF, Institutet K. Astrocytes and Glioblastoma cells release exosomes carrying mtDNA Astrocytes and Glioblastoma cells release exosomes carrying mtDNA. 2010;(May 2014). doi:10.1007/s00702-009-0288-8
25. Thakur BK, Zhang H, Becker A, et al. Double-stranded DNA in exosomes: a novel biomarker in cancer detection. *Cell Res*. 2014;24(6):766-769. doi:10.1038/cr.2014.44
26. Llorente A, Skotland T, Sylväne T, et al. Biochimica et Biophysica Acta Molecular lipidomics of exosomes released by PC-3 prostate cancer cells. 2013;1831:1302-1309. doi:10.1016/j.bbali.2013.04.011
27. Haraszi RA, Didiot M, Sapp E, et al. High-resolution proteomic and lipidomic analysis of exosomes and microvesicles from different cell sources. 2016;1:1-14.
28. Boilard E. Extracellular vesicles and their content in bioactive lipid mediators: more than a sack of microRNA. *J Lipid Res*. 2018:1-25.
29. Mack M, Kleinschmidt A, Brühl H, et al. Transfer of the chemokine receptor CCR5 between cells by membrane- derived microparticles: A mechanism for cellular human immunodeficiency virus 1 infection. *Nat Med*. 2000;6(7):769-775. doi:10.1038/77498
30. Zhang L, Zhang S, Yao J, et al. Microenvironment-induced PTEN loss by exosomal microRNA primes brain metastasis outgrowth. *Nature*. 2015;527(7576):100-104. doi:10.1038/nature15376
31. Zomer A, Maynard C, Verweij FJ, et al. In vivo imaging reveals extracellular vesicle-mediated phenocopying of metastatic behavior. *Cell*. 2015;161(5):1046-1057. doi:10.1016/j.cell.2015.04.042
32. Montecalvo A, Larregina AT, Shufesky WJ, et al. Mechanism of transfer of functional microRNAs between mouse dendritic cells via exosomes. *Blood*. 2012;119(3):756-766. doi:10.1182/blood-2011-02-338004
33. Del Conde I, Shrimpton CN, Thiagarajan P, Lopez JA. Tissue-factor-bearing microvesicles arise from lipid rafts and fuse with activated platelets to initiate coagulation. *Blood*. 2005;106(5):1604-1611. doi:10.1182/blood-2004-03-1095

34. Parolini I, Federici C, Raggi C, et al. Microenvironmental pH is a key factor for exosome traffic in tumor cells. *J Biol Chem*. 2009;284(49):34211-34222. doi:10.1074/jbc.M109.041152
35. Lou G, Chen Z, Zheng M, Liu Y. Mesenchymal stem cell-derived exosomes as a new therapeutic strategy for liver diseases. *Exp Mol Med*. 2017;49(6):e346. doi:10.1038/emm.2017.63
36. Adamiak M, Sahoo S. Exosomes in Myocardial Repair: Advances and Challenges in the Development of Next-Generation Therapeutics. *Mol Ther*. 2018;26(7):1635-1643. doi:10.1016/j.ymthe.2018.04.024
37. Ong S-G, Wu JC. Exosomes as potential alternatives to stem cell therapy in mediating cardiac regeneration. *Circ Res*. 2015;117(1):7-9. doi:10.1161/CIRCRESAHA.115.306593
38. Alvarez-Erviti L, Seow Y, Yin H, Betts C, Lakhali S, Wood MJA. Delivery of siRNA to the mouse brain by systemic injection of targeted exosomes. *Nat Biotechnol*. 2011;29(4):341-345. doi:10.1038/nbt.1807
39. Ha D, Yang N, Nadithe V. Exosomes as therapeutic drug carriers and delivery vehicles across biological membranes: current perspectives and future challenges. *Acta Pharm Sin B*. 2016;6(4):287-296. doi:10.1016/j.apsb.2016.02.001
40. Shigemoto-Kuroda T, Oh JY, Kim D-K, et al. MSC-derived Extracellular Vesicles Attenuate Immune Responses in Two Autoimmune Murine Models: Type 1 Diabetes and Uveoretinitis. *Stem cell reports*. 2017;8(5):1214-1225. doi:10.1016/j.stemcr.2017.04.008
41. Kooijmans SAA, Schiffelers RM, Zarovni N, Vago R. Modulation of tissue tropism and biological activity of exosomes and other extracellular vesicles: New nanotools for cancer treatment. *Pharmacol Res*. 2016;111:487-500. doi:10.1016/j.phrs.2016.07.006
42. Mendt M, Kamerkar S, Sugimoto H, et al. Generation and testing of clinical-grade exosomes for pancreatic cancer. *JCI Insight*. 2018;3(8):1-22. doi:10.1172/jci.insight.99263
43. Kooijmans SAA, Stremersch S, Braeckmans K, et al. Electroporation-induced siRNA precipitation obscures the efficiency of siRNA loading into extracellular vesicles. *J Control Release*. 2013;172(1):229-238. doi:10.1016/j.jconrel.2013.08.014
44. Kooijmans SAA, Vader P, Schiffelers RM. Tumour-bound RNA-laden exosomes. *Nat Biomed Eng*. 2017;1(8):634-636. doi:10.1038/s41551-017-0119-4
45. Zhang S, Chu WC, Lai RC, Lim SK, Hui JHP, Toh WS. Exosomes derived from human embryonic mesenchymal stem cells promote osteochondral regeneration. *Osteoarthritis Cartil*. 2016;24(12):2135-2140. doi:10.1016/j.joca.2016.06.022
46. Charoenviriyakul C, Takahashi Y, Morishita M, Nishikawa M, Takakura Y. Role of Extracellular Vesicle Surface Proteins in the Pharmacokinetics of Extracellular Vesicles. *Mol Pharm*. 2018;15(3):1073-1080. doi:10.1021/acs.molpharmaceut.7b00950
47. Kamerkar S, Lebleu VS, Sugimoto H, et al. Exosomes facilitate therapeutic targeting of oncogenic KRAS in pancreatic cancer. *Nature*. 2017;546(7659):498-503. doi:10.1038/nature22341
48. Wiklander OPB, Nordin JZ, O'Loughlin A, et al. Extracellular vesicle in vivo biodistribution is determined by cell source, route of administration and targeting. *J Extracell Vesicles*. 2015;4(2015):1-13. doi:10.3402/jev.v4.26316
49. Gangadaran P, Li XJ, Lee HW, et al. A new bioluminescent reporter system to study the biodistribution of systematically injected tumor-derived bioluminescent extracellular vesicles in mice. *Oncotarget*. 2017;8(66):109894-109914. doi:10.18632/oncotarget.22493
50. Charoenviriyakul C, Takahashi Y, Morishita M, Matsumoto A, Nishikawa M, Takakura Y. Cell type-specific and common characteristics of exosomes derived from mouse cell lines: Yield, physicochemical properties, and pharmacokinetics. *Eur J Pharm Sci*. 2017;96:316-322. doi:10.1016/j.ejps.2016.10.009

51. Zhang H, Freitas D, Kim HS, et al. Identification of distinct nanoparticles and subsets of extracellular vesicles by asymmetric flow field-flow fractionation. *Nat Cell Biol.* 2018;20(3):332-343. doi:10.1038/s41556-018-0040-4
52. Lapchak PA, Boitano PD, de Couto G, Marbán E. Intravenous xenogeneic human cardiosphere-derived cell extracellular vesicles (exosomes) improves behavioral function in small-clot embolized rabbits. *Exp Neurol.* 2018;307(April):109-117. doi:10.1016/j.expneurol.2018.06.007
53. Hoshino A, Costa-Silva B, Shen TL, et al. Tumour exosome integrins determine organotropic metastasis. *Nature.* 2015;527(7578):329-335. doi:10.1038/nature15756
54. Rana S, Yue S, Stadel D, Zöller M. Toward tailored exosomes: The exosomal tetraspanin web contributes to target cell selection. *Int J Biochem Cell Biol.* 2012;44(9):1574-1584. doi:10.1016/j.biocel.2012.06.018
55. Laulagnier K, Javalet C, Hemming FJ, et al. Amyloid precursor protein products concentrate in a subset of exosomes specifically endocytosed by neurons. *Cell Mol Life Sci.* 2018;75(4):757-773. doi:10.1007/s00018-017-2664-0
56. Osawa S, Kurachi M, Yamamoto H, Yoshimoto Y, Ishizaki Y. Fibronectin on extracellular vesicles from microvascular endothelial cells is involved in the vesicle uptake into oligodendrocyte precursor cells. *Biochem Biophys Res Commun.* 2017;488(1):232-238. doi:10.1016/j.bbrc.2017.05.049
57. Flannagan RS, Canton J, Furuya W, Glogauer M, Grinstein S. The phosphatidylserine receptor TIM4 utilizes integrins as coreceptors to effect phagocytosis. *Mol Biol Cell.* 2014;25(9):1511-1522. doi:10.1091/mbc.E13-04-0212
58. Matsumoto A, Takahashi Y, Nishikawa M, et al. Role of Phosphatidylserine-Derived Negative Surface Charges in the Recognition and Uptake of Intravenously Injected B16BL6-Derived Exosomes by Macrophages. *J Pharm Sci.* 2017;106(1):168-175. doi:10.1016/j.xphs.2016.07.022
59. Berenguer J, Lagerweij T, Zhao XW, et al. Glycosylated extracellular vesicles released by glioblastoma cells are decorated by CCL18 allowing for cellular uptake via chemokine receptor CCR8. *J Extracell Vesicles.* 2018;7(1). doi:10.1080/20013078.2018.1446660
60. Shimoda A, Tahara Y, Sawada S, Sasaki Y, Akiyoshi K. Glycan profiling analysis using evanescent-field fluorescence-assisted lectin array: Importance of sugar recognition for cellular uptake of exosomes from mesenchymal stem cells. *Biochem Biophys Res Commun.* 2017;491(3):701-707. doi:10.1016/j.bbrc.2017.07.126
61. Mulcahy LA, Pink RC, Carter DRF. Routes and mechanisms of extracellular vesicle uptake. *J Extracell Vesicles.* 2014;3(1). doi:10.3402/jev.v3.24641
62. Conner SD, Schmid SL. Regulated portals of entry into the cell. *Nature.* 2003;422:37-44.
63. Tian T, Zhu YL, Zhou YY, et al. Exosome uptake through clathrin-mediated endocytosis and macropinocytosis and mediating miR-21 delivery. *J Biol Chem.* 2014;289(32):22258-22267. doi:10.1074/jbc.M114.588046
64. Nanbo A, Kawanishi E, Yoshida R, Yoshiyama H. Exosomes Derived from Epstein-Barr Virus-Infected Cells Are Internalized via Caveola-Dependent Endocytosis and Promote Phenotypic Modulation in Target Cells. *J Virol.* 2013;87(18):10334-10347. doi:10.1128/JVI.01310-13
65. Costa Verdera H, Gitz-Francois JJ, Schiffelers RM, Vader P. Cellular uptake of extracellular vesicles is mediated by clathrin-independent endocytosis and macropinocytosis. *J Control Release.* 2017;266(July):100-108. doi:10.1016/j.jconrel.2017.09.019
66. Svensson KJ, Christianson HC, Wittrup A, et al. Exosome uptake depends on ERK1/2-heat shock protein 27 signaling and lipid raft-mediated endocytosis negatively regulated by caveolin-1. *J Biol Chem.* 2013;288(24):17713-17724. doi:10.1074/jbc.M112.445403

67. Nakase I, Kobayashi NB, Takatani-Nakase T, Yoshida T. Active macropinocytosis induction by stimulation of epidermal growth factor receptor and oncogenic Ras expression potentiates cellular uptake efficacy of exosomes. *Sci Rep.* 2015;5(January):1-14. doi:10.1038/srep10300
68. Fitzner D, Schnaars M, van Rossum D, et al. Selective transfer of exosomes from oligodendrocytes to microglia by macropinocytosis. *J Cell Sci.* 2011;124(3):447-458. doi:10.1242/jcs.074088
69. Roberts-Dalton HD, Cocks A, Falcon-Perez JM, et al. Fluorescence labelling of extracellular vesicles using a novel thiol-based strategy for quantitative analysis of cellular delivery and intracellular traffic. *Nanoscale.* 2017;9(36):13693-13706. doi:10.1039/c7nr04128d
70. Brown MS, Goldstein JL. Familial hypercholesterolemia: defective binding of lipoproteins to cultured fibroblasts associated with impaired regulation of 3-hydroxy-3-methylglutaryl coenzyme A reductase activity. *Proc Natl Acad Sci U S A.* 1974;71(3):788-792. <https://www.ncbi.nlm.nih.gov/pubmed/4362634>.
71. Delenclos M, Trendafilova T, Mahesh D, et al. Investigation of endocytic pathways for the internalization of exosome-associated oligomeric alpha-synuclein. *Front Neurosci.* 2017;11(MAR):1-10. doi:10.3389/fnins.2017.00172
72. Feng D, Zhao WL, Ye YY, et al. Cellular internalization of exosomes occurs through phagocytosis. *Traffic.* 2010;11(5):675-687. doi:10.1111/j.1600-0854.2010.01041.x
73. Kooijmans SAA, Fliervoet LAL, Van Der Meel R, et al. PEGylated and targeted extracellular vesicles display enhanced cell specificity and circulation time. *J Control Release.* 2016;224:77-85. doi:10.1016/j.jconrel.2016.01.009
74. Kooijmans SAA, Gitz-Francois JJM, Schiffelers RM, Vader P. Recombinant phosphatidylserine-binding nanobodies for targeting of extracellular vesicles to tumor cells: a plug-and-play approach. *Nanoscale.* 2018;2413-2426. doi:10.1039/C7NR06966A
75. Kooijmans SAA, Aleza CG, Roffler SR, van Solinge WW, Vader P, Schiffelers RM. Display of GPI-anchored anti-EGFR nanobodies on extracellular vesicles promotes tumour cell targeting. *J Extracell Vesicles.* 2016;5(1):31053. doi:10.3402/jev.v5.31053
76. Qi H, Liu C, Long L, et al. Blood Exosomes Endowed with Magnetic and Targeting Properties for Cancer Therapy. *ACS Nano.* 2016;10(3):3323-3333. doi:10.1021/acsnano.5b06939
77. Yuyama K, Sun H, Mitsutake S, Igarashi Y. Sphingolipid-modulated exosome secretion promotes clearance of amyloid- β by microglia. *J Biol Chem.* 2012;287(14):10977-10989. doi:10.1074/jbc.M111.324616
78. Izquierdo-Useros N, Naranjo-Gómez M, Archer J, et al. Capture and transfer of HIV-1 particles by mature dendritic cells converges with the exosome-dissemination pathway. *Blood.* 2009;113(12):2732 LP-2741. <http://www.bloodjournal.org/content/113/12/2732.abstract>.
79. Heusermann W, Hean J, Trojer D, et al. Exosomes surf on filopodia to enter cells at endocytic hot spots, traffic within endosomes, and are targeted to the ER. *J Cell Biol.* 2016;213(2):173-184. doi:10.1083/jcb.201506084
80. Friedman, JR., Dibenedetto JR, West M, Rowland AA VG. Endoplasmic reticulum-endosome contact increases as endosomes traffic and mature. *Mol Biol Cell.* 2013;24:1030-1040.
81. Tian T, Wang Y, Wang H, Zhu Z, Xiao Z. Visualizing of the cellular uptake and intracellular trafficking of exosomes by live-cell microscopy. *J Cell Biochem.* 2010;111(2):488-496. doi:10.1002/jcb.22733
82. Pužar Dominkuš P, Stenovec M, Sitar S, et al. PKH26 labeling of extracellular vesicles: Characterization and cellular internalization of contaminating PKH26 nanoparticles. *Biochim Biophys Acta - Biomembr.* 2018;1860(6):1350-1361. doi:10.1016/j.bbmem.2018.03.013
83. Nakase I, Noguchi K, Aoki A, Takatani-Nakase T, Fujii I, Futaki S. Arginine-rich cell-penetrating peptide-modified extracellular vesicles for active macropinocytosis induction and efficient intracellular delivery. *Sci Rep.* 2017;7(1):1-12. doi:10.1038/s41598-017-02014-6

84. Suk JS, Xu Q, Kim N, Hanes J, Ensign LM. PEGylation as a strategy for improving nanoparticle-based drug and gene delivery. *Adv Drug Deliv Rev.* 2016;99:28-51. doi:10.1016/j.addr.2015.09.012
85. Antes TJ, Middleton RC, Luther KM, et al. Targeting extracellular vesicles to injured tissue using membrane cloaking and surface display. *J Nanobiotechnology.* 2018;16(1):61. doi:10.1186/s12951-018-0388-4
86. Wang J-H, Forterre A V., Zhao J, et al. Anti-HER2 scFv-directed extracellular vesicle-mediated mRNA-based gene delivery inhibits growth of HER2-positive human breast tumor xenografts by prodrug activation. *Mol Cancer Ther.* 2018;molcanther.0827.2017. doi:10.1158/1535-7163.MCT-17-0827
87. Ye Z, Zhang T, He W, et al. Methotrexate-Loaded Extracellular Vesicles Functionalized with Therapeutic and Targeted Peptides for the Treatment of Glioblastoma Multiforme. *ACS Appl Mater Interfaces.* 2018;10(15):12341-12350. doi:10.1021/acsami.7b18135
88. Hein CD, Liu X-M, Wang D. Click Chemistry, A Powerful Tool for Pharmaceutical Sciences. *Pharm Res.* 2008;25(10):2216-2230. doi:10.1007/s11095-008-9616-1
89. Tian T, Zhang HX, He CP, et al. Surface functionalized exosomes as targeted drug delivery vehicles for cerebral ischemia therapy. *Biomaterials.* 2018;150:137-149. doi:10.1016/j.biomaterials.2017.10.012
90. Jia G, Han Y, An Y, et al. NRP-1 targeted and cargo-loaded exosomes facilitate simultaneous imaging and therapy of glioma in vitro and in vivo. *Biomaterials.* 2018;178:302-316. doi:10.1016/j.biomaterials.2018.06.029
91. Gao X, Ran N, Dong X, et al. Anchor peptide captures, targets, and loads exosomes of diverse origins for diagnostics and therapy. *Sci Transl Med.* 2018;10(444). doi:10.1126/scitranslmed.aat0195
92. Wang J, Li W, Lu Z, et al. The use of RGD-engineered exosomes for enhanced targeting ability and synergistic therapy toward angiogenesis. *Nanoscale.* 2017;9(40):15598-15605. doi:10.1039/c7nr04425a
93. Kim H, Yun N, Mun D, et al. Cardiac-specific delivery by cardiac tissue-targeting peptide-expressing exosomes. *Biochem Biophys Res Commun.* 2018;499(4):803-808. doi:10.1016/j.bbrc.2018.03.227
94. Nakase I, Ueno N, Katayama M, et al. Receptor clustering and activation by multivalent interaction through recognition peptides presented on exosomes. *Chem Commun.* 2017;53(2):317-320. doi:10.1039/C6CC06719K
95. Cronin J, Zhang X-Y, Reiser J. Altering the Tropism of Lentiviral Vectors through Pseudotyping. *Curr Gene Ther.* 2005;5(4):387-398. doi:10.2174/1566523054546224
96. Meyer C, Losacco J, Stickney Z, Li L, Marriott G, Lu B. Pseudotyping exosomes for enhanced protein delivery in mammalian cells. *Int J Nanomedicine.* 2017;12:3153-3170. doi:10.2147/IJN.S133430
97. Tamura R, Uemoto S, Tabata Y. Augmented liver targeting of exosomes by surface modification with cationized pullulan. *Acta Biomater.* 2017;57:274-284. doi:10.1016/j.actbio.2017.05.013
98. Pi F, Binzel DW, Lee TJ, et al. Nanoparticle orientation to control RNA loading and ligand display on extracellular vesicles for cancer regression. *Nat Nanotechnol.* 2018;13(1):82-89. doi:10.1038/s41565-017-0012-z
99. Wang Y, Chen X, Tian B, et al. Nucleolin-targeted extracellular vesicles as a versatile platform for biologics delivery to breast cancer. *Theranostics.* 2017;7(5):1360-1372. doi:10.7150/thno.16532
100. Longatti A, Schindler C, Collinson A, et al. High affinity single-chain variable fragments are specific and versatile targeting motifs for extracellular vesicles. *Nanoscale.* 2018;10(29):14230-14244. doi:10.1039/c8nr03970d



A CRISPR-CAS9-BASED REPORTER SYSTEM FOR SINGLE-CELL DETECTION OF EXTRACELLULAR VESICLE-MEDIATED FUNCTIONAL TRANSFER OF RNA

Olivier G. de Jong^{1,2}, Daniel E. Murphy¹, Imre Mäger², Eduard Willms^{2,3}, Antonio Garcia Guerra^{2,4}, Jerney J. Gitz-Francois¹, Juliet Lefferts⁵, Dhanu Gupta⁶, Sander C. Steenbeek⁷, Jacco van Rheenen⁷, Samir El Andaloussi⁶, Raymond M. Schiffelers¹, Matthew J.A. Wood², Pieter Vader^{1,8}.

1: Laboratory of Clinical Chemistry and Hematology, University Medical Center Utrecht, The Netherlands.

2: Department of Paediatrics, University of Oxford, United Kingdom.

3: Department of Physiology, Anatomy and Genetics. University of Oxford, United Kingdom.

4: Department of Physics. University of Oxford, United Kingdom.

5: Pediatric Pulmonology and Regenerative Medicine Center, University Medical Center Utrecht, The Netherlands.

6: Department of Laboratory Medicine, Clinical Research Center, Karolinska Institutet, Sweden.

7: Department of Molecular Pathology, Oncode Institute, Netherlands Cancer Institute, The Netherlands.

8: Department of Experimental Cardiology, University Medical Center Utrecht, The Netherlands.

**Nature Communications volume 11,
Article number: 1113 (2020)**

ABSTRACT

Extracellular vesicles (EVs) form an endogenous transport system for intercellular transfer of biological cargo, including RNA, that plays a pivotal role in physiological and pathological processes. Unfortunately, whereas biological effects of EV-mediated RNA transfer are abundantly studied, regulatory pathways and mechanisms remain poorly defined due to a lack of suitable readout systems. Here, we describe a highly-sensitive CRISPR/Cas9-based reporter system that allows direct functional study of EV-mediated transfer of small non-coding RNA molecules at single-cell resolution. Using this CCRISPR Operated Stoplight System for Functional Intercellular RNA Exchange (CROSS-FIRE) we uncover various genes involved in EV subtype biogenesis that play a regulatory role in RNA transfer. Moreover we identify multiple genes involved in endocytosis and intracellular membrane trafficking that strongly regulate EV-mediated functional RNA delivery. Altogether, this approach allows the elucidation of regulatory mechanisms in EV-mediated RNA transfer at the level of EV biogenesis, endocytosis, intracellular trafficking, and RNA delivery.

INTRODUCTION

Extracellular vesicles (EVs) are a heterogeneous population of small lipid membrane vesicles¹, which play a role in intercellular communication through the transfer of biological macromolecules, consisting of both soluble and (trans)membrane proteins, lipids, and RNA molecules²⁻⁵. EVs are conventionally classified into two major subtypes based on their biogenesis: exosomes and microvesicles^{1,5}. Exosomes are formed in the endosomal pathway, when intraluminal vesicle formation in the late endosome results in the formation of multivesicular bodies (MVBs)^{1,6}. These MVBs may fuse with the plasma membrane resulting in the release of the intraluminal vesicles, upon which these vesicles are termed exosomes. Alternatively, microvesicles are released directly from the plasma membrane. Together these EV populations form an endogenous transport system through which numerous molecules, including various RNA species, are transferred between cells⁵. Over the last decade it has become clear that EV-mediated RNA transfer plays a critical role in the regulation of numerous physiological and pathological processes including immunomodulation, angiogenesis, cell proliferation, neurodegenerative pathologies, cardiovascular events, and tumor metastasis^{4,7-11}. This has resulted in a vast increase in studies on EVs in the context of cell biology, homeostasis, novel targets for therapeutic intervention in pathologies, as well as a potential new source for biomarkers in diagnostics. Moreover, due to their endogenous capability of RNA transfer, EVs have sparked major interest as a potential therapeutic strategy for drug delivery, as well as regenerative medicine applications¹².

Despite the high number of studies focusing on EV-mediated RNA transfer in health and disease, fundamental studies on RNA uptake and processing mechanisms are currently lacking, mainly due to the absence of suitable readout systems to study RNA transfer^{13,14}. Current studies on EV uptake generally measure the uptake of fluorescently labelled EVs, either by use of fluorescent (membrane)dyes or by use of fluorescently labelled proteins that are enriched in EVs^{12,15}. Such studies have provided valuable information regarding general EV uptake mechanisms and dynamics, but are not necessarily representative of EV cargo delivery. To address these issues, reporter systems based on mRNA transfer, such as the Cre-LoxP reporter system, have been employed^{8,16}. However, EV-mediated transfer of large mRNA molecules such as Cre recombinase mRNA, a molecule of >350 kDa (over 1000nt, excluding post-transcriptional modifications) may differ from loading, transfer, and processing of small RNAs. This is underlined by multiple studies that have shown that EVs from various sources contain mainly small (~100nt) RNA molecules and only trace amounts of full length mRNA¹⁷⁻²³, and that the majority of mRNA in EVs is not

present as intact mRNAs^{24,25}. Moreover, a major drawback of mRNA-based systems is that it is inherently impossible to phenotypically distinguish between reporter activation as a result of the delivery of translated protein or the mRNA itself²⁶, which reduces the applicability of such systems to study RNA transfer specifically.

To overcome these challenges, we aimed to design a novel approach to study functional RNA delivery, capable of activating high expression of a fluorescent reporter protein, independent of translation of the RNA molecule. To this end, we explored the suitability of the CRISPR/Cas9 genome editing system. The CRISPR/Cas9 system is a gene-editing technique where the Cas9 protein is guided to a specific genomic sequence by a ~100 nucleotide, 35 kD, single guide RNA (sgRNA), resulting in a specific double-stranded break in the genomic DNA²⁷. Due to inaccuracies in the non-homologous end joining (NHEJ) repair mechanism, frameshifts may occur around the targeted genomic region²⁸. sgRNA molecules are highly suitable candidates to study functional intercellular RNA exchange, as the functionality of sgRNAs in this system is not based on RNA translation but rather on its secondary structure.

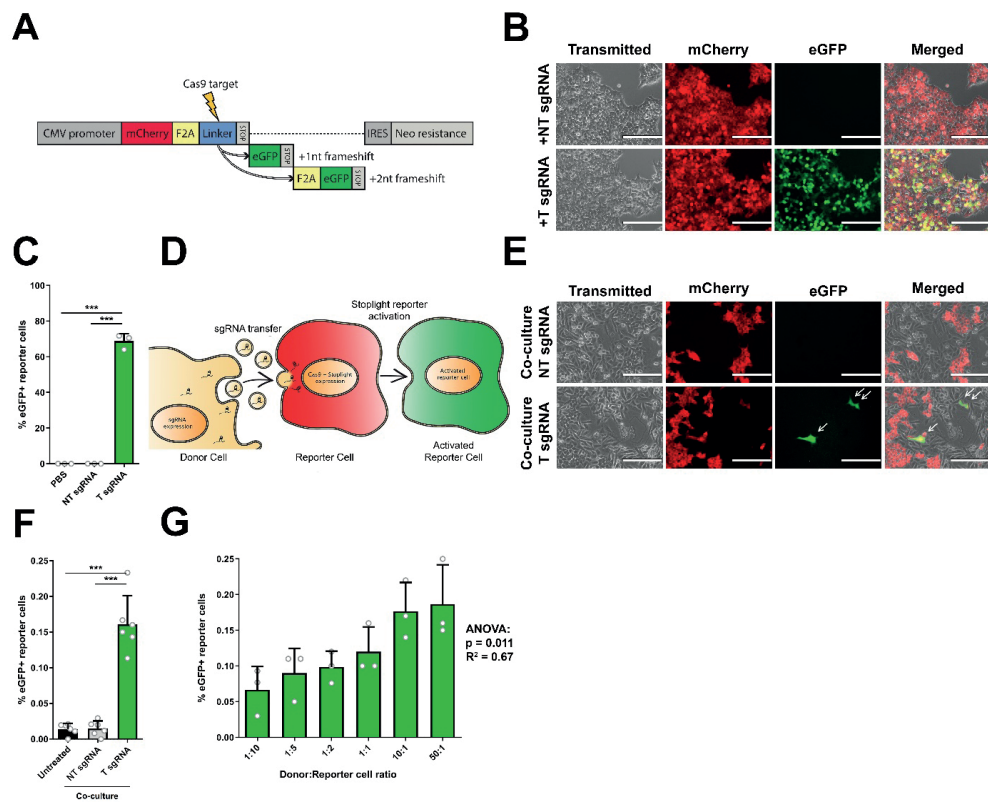
To visualize the transfer of sgRNAs, we designed a fluorescent “Stoplight” reporter system which is permanently activated in EV-acceptor cells upon functional transfer of a specific targeting sgRNA, expressed in EV-donor cells. Using this approach, we demonstrate functional intercellular sgRNA transfer using direct co-culture, transwell, and direct EV-addition experiments at single-cell resolution. Moreover, we establish protocols to study the effects of siRNA-mediated knockdown (KD) of single targets in both EV-acceptor and donor cells, as well as inhibitory compounds, on EV-mediated functional RNA transfer. First, we confirm the suitability of this system to study the role of specific genetic targets that we and other have previously shown to be pivotal for EV endocytosis and intracellular membrane trafficking. Then, using these protocols, we uncover several novel genes involved in the regulation of specific EV subtype biogenesis, as well as endocytosis and intracellular membrane trafficking that play a regulatory role in EV-mediated functional RNA delivery.

Altogether, we demonstrate a CRISPR/Cas9-based reporter system that allows the study of functional delivery of small non-coding RNAs with single-cell resolution. This novel approach allows the study of EV cargo processing in the context of functional RNA delivery, and may help to increase our understanding of the regulatory pathways that dictate the underlying processes. We term this approach the Crispr Operated Stoplight System for Functional Intercellular RNA Exchange (CROSS-FIRE).

RESULTS

Generation of a fluorescent CRISPR/Cas9 Stoplight reporter

To evaluate the intercellular transfer of RNAs, we designed a fluorescent “Stoplight” reporter system that constitutively expresses mCherry, followed by a “linker” region between mCherry and its stop codon which can be targeted by Cas9. Upon sgRNA delivery and subsequent NHEJ-mediated frameshift generation in this linker region of either +1nt or +2nt, the original stop codon will be bypassed, eliciting a permanently expressed eGFP signal (Fig. 1A). First, the Stoplight reporter construct was stably incorporated into HEK293T cells to confirm its functionality. As expected, Stoplight⁺ HEK293T cells showed high expression of mCherry, but only showed eGFP expression after transfection of both *Streptococcus pyogenes* Cas9 (spCas9) and a targeting sgRNA (Supplementary Fig. 1A). In order to generate a reporter exclusively for sgRNA delivery/transfer, stable Stoplight⁺spCas9⁺ HEK293T cells were generated, and subsequently transfected with plasmids encoding either a targeting sgRNA (T sgRNA), or a non-targeting sgRNA (NT sgRNA) control. As confirmed by fluorescence microscopy (Fig. 1B), flow cytometry (Fig. 1C, Supplementary Fig. 2), and *in silico* image-based analysis of confocal microscopy images (Supplementary Fig. 3A-C), Stoplight⁺spCas9⁺ cells expressing T sgRNA showed high levels of eGFP expression, whereas reporter cells expressing NT sgRNA, or left untreated, did not. Observed levels of activation of eGFP expression were in line with inDelphi *in silico* indel and frameshift predictions (Supplementary Fig. 1B, C) which, based on the target sequence, predicted a frameshift frequency of +1nt or +2nt of approx. 80%²⁹.



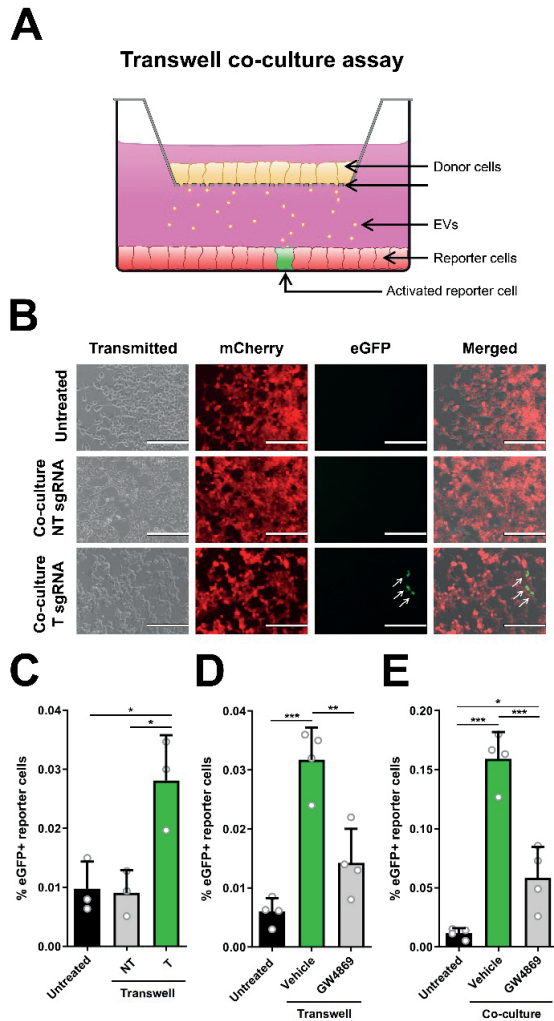
▲Figure 1 | Establishment of a CRISPR/Cas9-activated fluorescence reporter platform to study EV-mediated RNA transfer. a, Schematic showing the CRISPR/Cas9-activated fluorescence stoplight reporter system. mCherry is expressed under a CMV promoter, followed by a Cas9-targeted linker region and a stop codon. Two eGFP open reading frames are placed after the stop codon, one or two nucleotides (nt) out of frame, respectively. Upon a Cas9-mediated frameshift in the linker region, either one of these eGFP open reading frames will be permanently expressed alongside mCherry. F2A self-cleaving peptide domains are placed between each fluorescent protein. **b**, Fluorescent microscopy images of stable HEK293T Stoplight*spCas9⁺ cells after transfection of a plasmid encoding a sgRNA targeting the linker region of the Stoplight construct (+T sgRNA, bottom row), or a non-targeting sgRNA (+NT sgRNA, top row). Scale bar represents 200 nm. Representative images as observed in 3 independent experiments. **c**, Flow cytometry analysis of stable HEK293T Stoplight*spCas9⁺ cells after addition of PBS, transfection of a non-targeting sgRNA (NT sgRNA), or a sgRNA targeting the Stoplight construct (T sgRNA). Means + SD, n = 3 independent experiments, Student's t-test. **d**, Cartoon explaining the CROSS-FIRE system. Donor cells (yellow cell, left) express sgRNAs targeting a stoplight construct, which is expressed alongside Cas9 in reporter cells (red cell, middle). Upon functional transfer of sgRNAs from the donor cells to the reporter cell, Cas9 and sgRNA will together activate the stoplight construct in the reporter cell, resulting in permanent eGFP expression (green cell, right), which may then be quantified by fluorescence microscopy or flow cytometry. **e, f**, A five day co-culture of HEK293T Stoplight*spCas9⁺ reporter cells with MDA-MB-231 sgRNA⁺ donor cells expressing a targeting sgRNA (T sgRNA), and a non-targeting sgRNA (NT sgRNA), analyzed by fluorescence microscopy (**e**) and flow cytometry (**f**). Scale bar represents 200 nm. Representative images as observed in 6 independent experiments. Means + SD, n = 6 independent experiments, Tukey's multiple comparison test. **g**, Quantification of a five day co-culture of HEK293T Stoplight*spCas9⁺ reporter cells with MDA-MB-231 sgRNA⁺ donor cells in varying donor cell : reporter cell ratios by flow cytometry. Means + SD, n = 3 independent experiments, ANOVA. *** = p < 0.001.

Intercellular transfer of sgRNAs

Having validated the Stoplight reporter construct, we assessed whether “donor” cells expressing sgRNAs were capable of activating the Stoplight reporter system via transfer of sgRNAs to “reporter” cells (illustrated in Fig. 1D), an approach which we term the C RISPR Operated Stoplight System for Functional Intercellular RNA Exchange (CROSS-FIRE). To this end, stable sgRNA⁺ MDA-MB-231 donor lines were generated, expressing either T sgRNAs or NT sgRNAs, and co-cultured with a Stoplight⁺spCas9⁺ HEK293T reporter line. Co-culture of reporter cells with T sgRNA expressing donor cells resulted in significant reporter activation within five days, whereas co-culture with donor cells expressing NT sgRNAs did not (Fig. 1E-F, Supplementary Fig. 3D). Moreover, employing different donor:reporter cell ratios demonstrated reporter activation in a dose-dependent manner (Fig. 1G). Overall, the percentages of reporter activation in five days were found to be low (up to 0.2%). However, the observed low percentages of reporter activation do not necessarily reflect a low level of EV-mediated communication, but rather are the result of the low levels of sgRNA in EVs as we opted not to employ additional strategies for targeted loading of EVs with sgRNAs, such as RNA-binding proteins fused to EV-associated proteins, in order to study RNA loading and transfer in an unbiased manner.

To confirm that these observations were not due to reporter cell-line specific characteristics we generated five additional stable Stoplight⁺spCas9⁺ reporter cell lines using HeLa, HMEC-1, MCF-7, MDA-MB-231, and T47D cells. Similar to HEK293T reporter cells, all five cell lines showed a dose-dependent Stoplight reporter activation after co-culture with sgRNA⁺ MDA-MB-231 donor cells (Supplementary Fig. 4). Concordantly, various additional sgRNA⁺ donor cell lines commonly used for functional EV studies were generated: HEK293T, HMEC-1, and hTERT-MSK cells. Interestingly, co-culture of HEK293T Stoplight⁺spCas9⁺ reporter cells with sgRNA⁺ HMEC-1 and hTERT-MSK resulted in significant reporter activation within five days, whereas co-culture with sgRNA⁺ HEK293T did not (Supplementary Fig. 5).

Having demonstrated functional sgRNA transfer between multiple cell types in a co-culture setting, we deemed it important to rule out sgRNA transfer via cell-cell fusion. Therefore, we generated Gaussia luciferase (G.Luc)⁺sgRNA⁺ donor cells, which were co-cultured with Stoplight⁺spCas9⁺ reporter cells. After co-culture, cells were separated based on eGFP and mCherry expression by fluorescence activated cell sorting (FACS), and after recovery were subjected to a luciferase activity assay (as illustrated in Supplementary Fig. 6A). In case of cell-cell fusion, eGFP⁺ reporter cells should also show luciferase activity. After having confirmed luciferase activity in the stable sgRNA⁺G.Luc⁺ donor cells (Supplementary Fig. 6B),



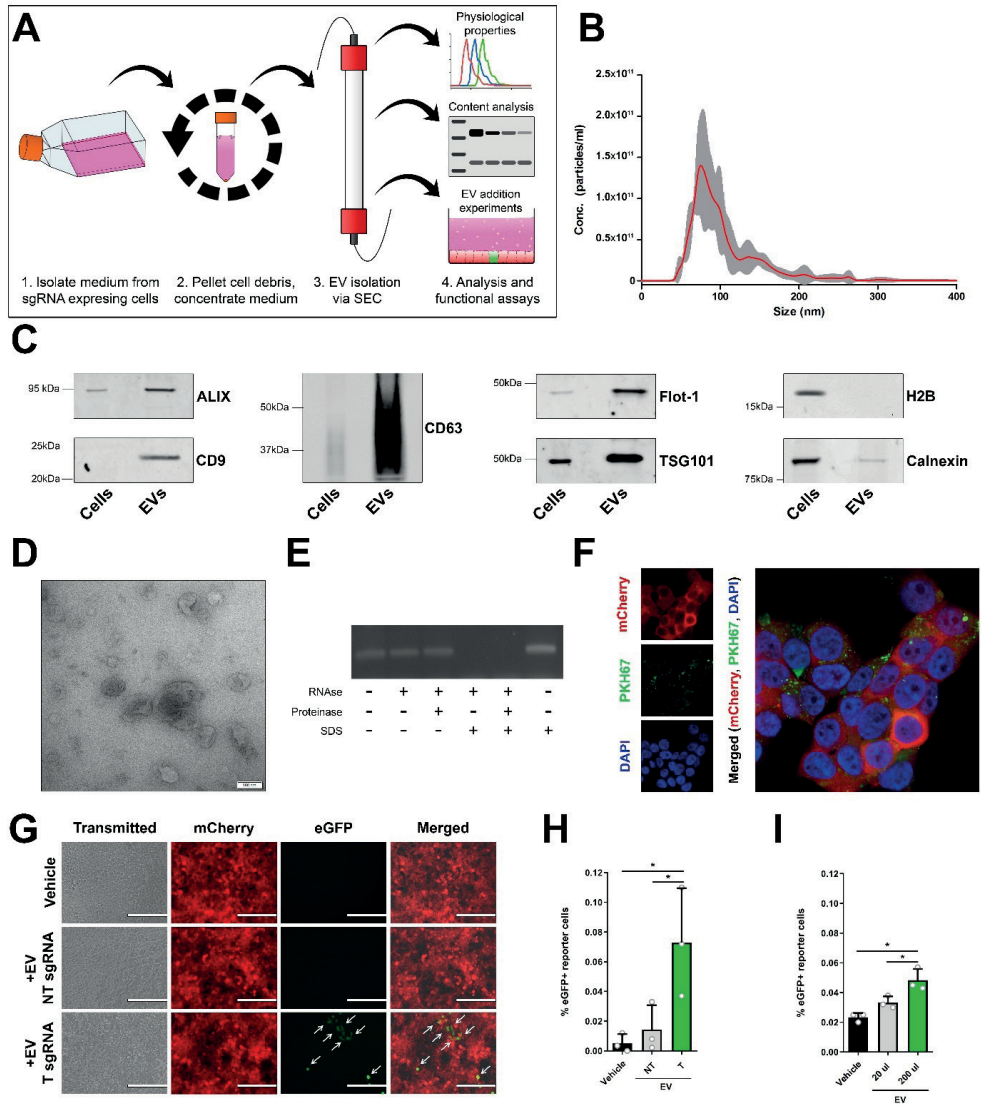
▲Figure 2 | Cell contact is not required for intercellular sgRNA exchange. **a**, A schematic cartoon explaining the use of a transwell co-culture assay using the CROSS-FIRE system. sgRNA⁺ donor cells are cultured in a transwell insert (yellow cells, top), which is suspended in a standard tissue culture well containing Stoplight⁺spCas9⁺ reporter cells, allowing for exchange of secreted factors while avoiding direct cell contact. **b,c** Fluorescence microscopy pictures (**b**) and flow cytometry analysis (**c**) of HEK293T Stoplight⁺spCas9⁺ reporter cells after a 10-day transwell co-culture experiment with MDA-MB-231 sgRNA⁺ donor cells expressing a non-targeting (NT) or a targeting (T) sgRNA. Scale bar represents 200 nm. Means + SD, $n = 3$ independent experiments, Tukey's multiple comparison test. **d**, Flow cytometry analysis of HEK293T Stoplight⁺spCas9⁺ reporter cells after a 10-day transwell co-culture experiment with MDA-MB-231 sgRNA⁺ donor cells expressing a targeting (T) sgRNA with or without the presence of EV release inhibitor GW4869 at a concentration of 1 μ M. Means + SD, $n = 4$ independent experiments, Tukey's multiple comparison test. **e**, Flow cytometry analysis of HEK293T Stoplight⁺spCas9⁺ reporter cells after a five day direct co-culture experiment with MDA-MB-231 sgRNA⁺ donor cells expressing a targeting (T) sgRNA with or without the presence of EV release inhibitor GW4869 at a concentration of 1 μ M. Means + SD, $n = 4$ biologically independent samples, Tukey's multiple comparison test. * = $p < 0.05$, ** = $p < 0.01$, *** = $p < 0.001$.

a seven day co-culture was performed and mCherry⁻eGFP⁻ (donor cells), mCherry⁻eGFP⁻ (unactivated reporter cells), and mCherry⁺eGFP⁺ (activated reporter cells) cells were isolated, as confirmed by fluorescence microscopy (Supplementary Fig. 6C). A luciferase assay on conditioned medium of these cell populations showed strong luciferase activity in the mCherry⁻eGFP⁻ donor cells, but no activity in untreated medium and conditioned medium from both mCherry⁻eGFP⁻ and mCherry⁺eGFP⁺ cells (Supplementary Fig. 6D), excluding transfer of sgRNAs via cell-cell fusion. We were also unable to detect luciferase activity in sgRNA⁺G.Luc⁺ donor cell-derived EVs (Supplementary Fig. 6E, F).

To investigate cell-contact independent transfer of sgRNA, we tested the CROSS-FIRE system in a transwell co-culture assay (Fig. 2A). In concordance with previous observations, co-culture with T sgRNA⁺ resulted in significant reporter activation, whereas transwell co-culture with NT sgRNA⁺ donor cells did not (Fig. 2B, C), demonstrating that direct cell-cell contact is not required for sgRNA transfer. In this assay, we observed a significant but notably lower level of activation as compared to direct co-culture protocols. We hypothesize that this difference is due to the lower number of donor cells as a result of the small transwell membrane surface, as well as limited availability (and potential blockage) of pores that facilitate EV transfer, as also seen in other studies⁸. As an extension of this finding, another transwell co-culture experiment was performed in the presence of GW4869, an nSMase inhibitor which strongly inhibits EV release³⁰. Indeed, the addition of GW4869 resulted in a strong and significant decrease in reporter activation (Fig. 2D). Similarly, presence of GW4869 also resulted in a substantial and significant decrease of reporter activation in a direct co-culture experiment as confirmed by flow cytometry (Fig. 2E) and *in silico* image-based analysis of confocal microscopy images (Supplementary Fig. 3E). Altogether, these data suggest that functional sgRNA transfer is mediated by EVs.

EV-mediated transfer of sgRNAs

To confirm this hypothesis, we tested the direct functionality of isolated EVs in the CROSS-FIRE system. EVs were isolated from sgRNA⁺ MDA-MB-231 donor cell conditioned medium through size exclusion chromatography (SEC) (Fig. 3A, Supplementary Fig. 7A). Isolated EVs were characterized according to the Minimal Information for Studies of Extracellular Vesicles (MISEV) guidelines³¹. Nanoparticle Tracking Analysis (NTA) showed a size-distribution profile in line with EV characteristics (Fig. 3B) (mode = 81±3 nm), and Western Blot analysis showed an enrichment for common EV-markers ALIX, Flot-1, TSG101, and tetraspanins CD9 and CD63, alongside a strong decrease in abundance of nuclear marker histone H2B and organelle marker Calnexin (Fig. 3C). Furthermore,



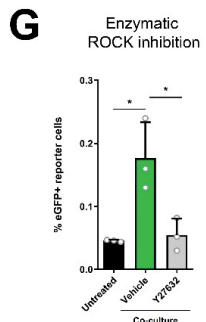
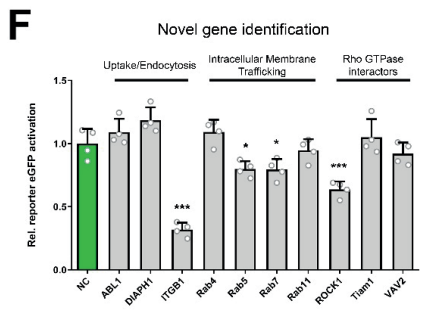
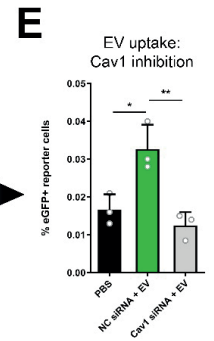
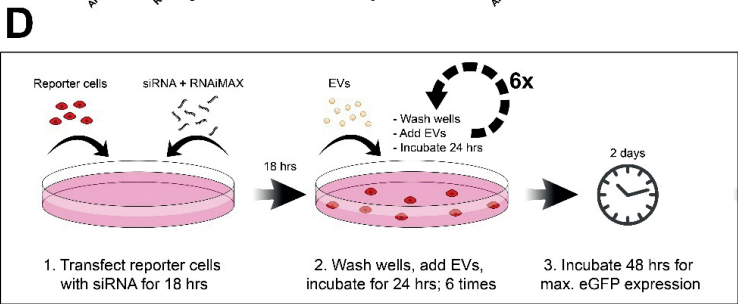
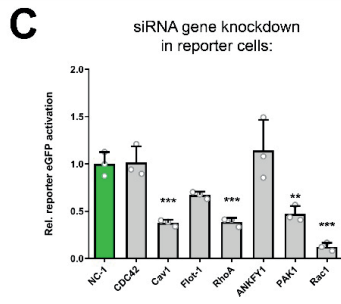
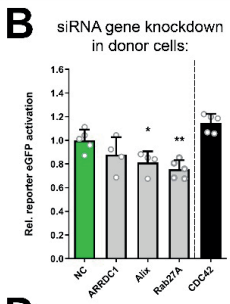
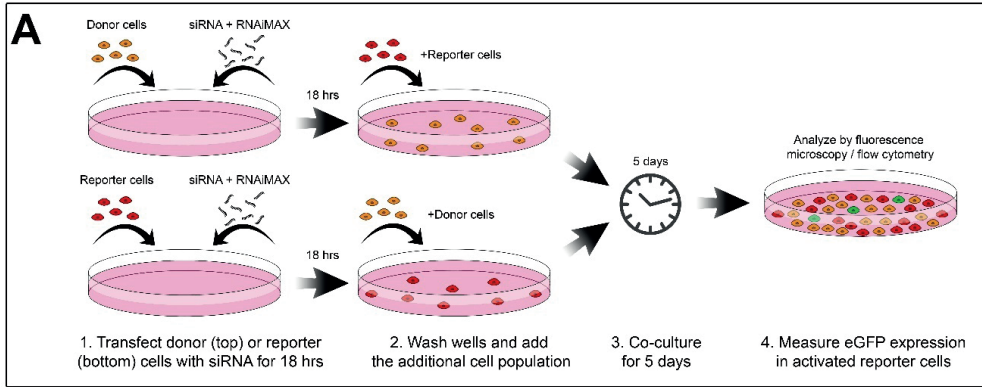
transmission electron microscopy (TEM) of isolated EVs showed lipid bi-layer vesicles displaying common EV morphology, as well as a size-distribution in line with NTA measurements (Fig. 3D). The presence of sgRNA in EVs was confirmed by RT-PCR, and an EV RNase protection assay revealed that sgRNAs were present in the lumen of these EVs, as RNase-mediated degradation of sgRNAs was only observed after SDS-mediated membrane disruption (Fig. 3E). Using a synthetic sgRNA standard curve, we determined an abundance of 1 sgRNA per approx. 4.5×10^5 EVs by qPCR on RNA isolated from sgRNA⁺ MDA-MB-231 donor cells in combination with NTA analysis (Supplementary Fig. 7B, C). To confirm that these isolated EVs were able to be taken up by reporter cells, isolated EVs were fluorescently labelled with PKH67 lipid-dye, and administered to Stoplight⁺ HEK293T cells, followed by confocal microscopy analysis. This experiment revealed that labelled EVs were indeed readily taken up by reporter cells (Fig. 3F). Using isolated EVs, we confirmed significant activation of CROSS-FIRE reporter cells by EV addition when isolating EVs from T sgRNA⁺ donor cells, but not from NT sgRNA⁺ donor cells, as determined by both fluorescence microscopy (Fig. 3G) and flow cytometry (Fig. 3H). EV-mediated reporter activation was also confirmed by *in silico* image-based analysis of confocal microscopy images (Supplementary Fig. 3F) Moreover, EVs dose-dependently activated reporter cells (Fig. 3I). EV-mediated CROSS-FIRE reporter activation was not affected by RNase A treatment of the EVs (Supplementary Fig. 7D). Additionally, we show that addition of the soluble protein-containing fractions isolated alongside these EVs by size exclusion chromatography did not result in the activation of the reporter cells (Supplementary Fig. 7E). These data show that the CROSS-FIRE reporter system is activated by EV-mediated sgRNA transfer.

◀Figure 3 | Intercellular sgRNA exchange is EV-mediated. **a**, Schematic of EV isolation workflow and analysis. Conditioned medium is isolated from sgRNA⁺ MDA-MB-231 donor cells, after which cell debris is pelleted through centrifugation. Conditioned medium is then concentrated by tangential flow filtration, followed by size exclusion chromatography-mediated EV isolation. EVs are then characterized, and used for EV addition experiments in Stoplight⁺spCas9⁺ reporter cells. **b**, Nanosight Nanoparticle Tracking Analysis (NTA) showing the size distribution of the isolated EVs (mode = 81 ± 3 nm). **c**, Western blot analysis of EVs and cell lysates for common EV markers (CD9, CD63, ALIX, Flot-1, and TSG101), and EV-negative markers Calnexin and H2B. Representative images as observed in 3 independent experiments. **d**, Electron microscopy analysis of isolated EVs. Scale bar represents 100 nm. Representative image as observed in 12 separate fields. **e** An EV RNase protection assay, followed by RT-PCR sgRNAs, shows that sgRNAs are only susceptible to RNase-mediated degradation in the presence of the membrane-disrupting anionic surfactant SDS. Representative data as observed in 3 independent experiments. **f**, Confocal microscopy images of HEK293T reporter cells (red) that have taken up MDA-MB-231-derived PKH67-labeled EVs (green). Representative image as observed in 7 randomly selected fields. **g,h**, EV-mediated activation of the CROSS-FIRE platform using EVs isolated from sgRNA⁺ MDA-MB-231 donor cells. EVs were added every 72 hrs for 12 additions with an average dose of $1.1 \times 10^{11} \pm 4.9 \times 10^{10}$ EVs per addition. Cells were analyzed by fluorescence microscopy (**g**) and flow cytometry (**h**). Scale bar represents 200 nm. Means + SD, n = 3 biological replicates, Tukey's multiple comparison test. **i**, EVs from sgRNA⁺ MDA-MB-231 donor cells activate Stoplight⁺ spCas9⁺ HEK293T reporter cells in a dose-dependent manner. EVs were added every 72 hrs for 9 additions with an average concentration of $2.2 \times 10^{10} \pm 1 \times 10^9$ (20 μ l) or $2.2 \times 10^{11} \pm 1 \times 10^{11}$ (200 μ l). Means + SD, n = 3 biological replicates, Tukey's multiple comparison test. * = $p < 0.05$.

Single gene analysis in intercellular RNA transfer

We next established a CROSS-FIRE based workflow to study specific target genes and pathways in EV-mediated RNA transfer by donor- or reporter cell exclusive siRNA-mediated target knockdown (KD), as illustrated in Fig. 4A. As a proof of concept, the effect of knocking down various genes with known involvements in EV biogenesis in MDA-MB-231 donor cells was evaluated (Fig. 4B). Whereas the KD of ARRDC1 (involved in release of a subpopulation of microvesicles) showed no significant effect on RNA transfer, KD of Alix and Rab27A (involved in exosome biogenesis and release, respectively) resulted in a significant decrease of reporter activation, as compared to a non-targeting siRNA negative control (NC)^{32,33}. Recently a potentially novel process for intercellular RNA transfer, exchange through tunneling nanotubes, was described, in which CDC42 plays a pivotal regulatory role³⁴. Interestingly, siRNA-mediated KD of CDC42 in our system showed no effect on intercellular functional RNA exchange. These experiments, alongside a direct co-culture experiment in the presence of EV release inhibitor GW4869 were repeated using Stoplight⁺spCas9⁺ MCF-7 reporter cells, yielding similar results: as observed with HEK293T reporter cells, sgRNA transfer was significantly decreased in the presence of GW4869 (Supplementary Fig. 8A) and by KD of Alix and Rab27A, but not ARRDC1 and CDC42, in donor cells (Supplementary Fig. 8B). These data demonstrate that the CROSS-FIRE system is capable and suitable to study the role of different EV subpopulations in functional RNA transfer.

►Figure 4 | Analysis of cellular pathways to study EV-mediated RNA transfer and uptake. a, Workflow to study the role of specific genetic targets in intercellular RNA transfer using the CROSS-FIRE system. **b,** Flow cytometry analysis of HEK293T Stoplight⁺spCas9⁺ reporter cells after a five day co-culture with sgRNA⁺ MDA-MB-231 donor cells subjected to siRNA-mediated KD of genes as compared to a non-targeting negative control siRNA (NC). Means + SD, n = 5 independent experiments, Dunnett's multiple comparison test. **c,** Flow cytometry analysis of HEK293T Stoplight⁺spCas9⁺ reporter cells after a five day co-culture with sgRNA⁺ MDA-MB-231 donor cells, in which HEK293T reporter cells were subjected to siRNA-mediated KD of various genes as compared to a non-coding control siRNA (NC). Means + SD, n = 4 independent experiments, Dunnett's multiple comparison test. **d,** Schematic of workflow to study the role of genes involved in EV-mediated RNA delivery. **e,** Flow cytometry analysis of Stoplight⁺spCas9⁺ HEK293T reporter cells treated for 6 consecutive days with sgRNA⁺ MDA-MB-231-derived EVs after transfection with a non-coding siRNA (NC), or siRNAs targeting Cav1, as compared to vehicle-treated reporter cells (PBS). EVs were added every 24 hrs for 6 additions with an average concentration of $1.8e11 \pm 1.1e11$ EVs per addition. Means + SD, n = 3 biological replicates, Tukey's multiple comparison test. **f,** Flow cytometry analysis of HEK293T Stoplight⁺spCas9⁺ reporter cells after a five day co-culture with sgRNA⁺ MDA-MB-231 donor cells, in which HEK293T reporter cells were subjected to siRNA-mediated KD of various novel genes as compared to a non-coding control siRNA (NC). Means + SD, n = 4 independent experiments, Dunnett's multiple comparison test. **g,** Flow cytometry analysis of HEK293T reporter cells after a five day direct co-culture experiment with sgRNA⁺MDA-MB-231 donor cells with or without the presence of ROCK-inhibitor Y27632 at a concentration of 1 μ M. Means + SD, n = 3 biologically independent samples, Tukey's multiple comparison test. * = p < 0.05, ** = p < 0.01, *** = p < 0.001.



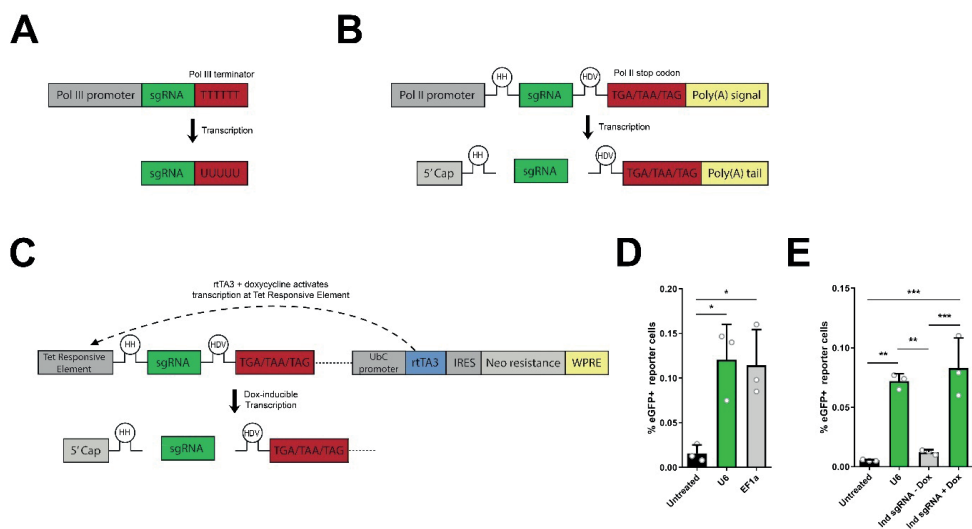
We then employed this CROSS-FIRE based workflow to study EV-mediated RNA delivery and processing, by targeting various regulatory genes of endocytosis and intracellular membrane trafficking in HEK293T recipient reporter cells. Using this method, we uncovered various genes that are pivotal for EV-mediated RNA transfer: Rho GTPases Rac1 and RhoA, the Rho GTPase effector PAK1, and Cav1, involved in endocytosis (Fig. 4C). KD of Rho GTPase CDC42, as well as ANKFY1 (involved in intracellular vesicle transport) and Flot-1 (involved in endocytosis), showed no effect on RNA transfer. In alignment with HEK293T cells, KD of Cav1, Rac1 and RhoA in MCF-7 reporter cells also resulted in significant inhibition of reporter activation, and KD of CDC42 and Flot-1 did not result in significant differences. Interestingly, KD of ANKFY1 and PAK1 in MCF-7 had a different effect than in HEK293T cells: whereas PAK1 KD in MCF-7 cells did not result in a significant decrease in reporter activation, KD of ANKFY1 resulted in a 1.9-fold increase in reporter activation (Supplementary Fig. 8C). These findings underline the importance of confirming such pathways in multiple cell lines, as previous studies have shown that relative roles of various endocytic routes may vary between different cell types^{12,35,36}. Moreover, these findings demonstrate that with the CROSS-FIRE system it is now possible to study the separate roles of relevant pathways in EV-mediated RNA delivery. As a proof of concept, we tested the suitability of the CROSS-FIRE system to study the contribution of specific genes to the RNA delivery process using isolated EVs. To this end, Cav1 was knocked down in reporter cells, which were subsequently treated with 6 doses of sgRNA⁺ EVs, and analyzed by flow cytometry (as illustrated in Fig. 4D). In line with previous observations, reporter cells stimulated with sgRNA⁺ EVs showed significant reporter activation whereas reporter cells treated with a Cav1-targeting siRNA did not (Fig. 4E).

Based on these results, we selected 10 new genetic targets involved in endocytosis (ABL1, DIAPH1), extracellular matrix adhesion (ITGB1), intracellular membrane trafficking (Rab4, Rab5, Rab7, and Rab11), and Rho GTPase interactors (RhoA effector ROCK1, and Rac1 interactors Tiam1 and VAV2) to study their role in functional RNA delivery to recipient reporter cells (Fig. 4F). Of these 10 genetic targets, 4 targets that were not yet previously linked to EV-mediated RNA delivery appeared to play an important role in functional RNA delivery: integrin ITGB1 (also known as CD29), Rab5 and Rab7 (important for early endosome and late endosome trafficking, respectively), and ROCK1 (downstream target protein kinase of RhoA). To further confirm the role of ROCK1 in RNA transfer, the effect of ROCK1 inhibitor Y27632 in a direct 5 day co-culture experiment was assessed (Fig. 4G). Indeed, addition of 1 μ M Y27632 substantially and significantly decreased reporter activation. Altogether, these data show that the CROSS-FIRE system provides a robust

and scalable approach to study and uncover novel regulatory targets and pathways in intercellular RNA exchange in a direct co-culture setting, or using isolated EVs.

Pol II-mediated sgRNA expression

In closing, we modified sgRNA expression constructs to allow for a more adaptable design of CROSS-FIRE based studies. In all experiments described above, sgRNAs were expressed under a Pol III U6 promoter. This is a common strategy for sgRNA expression^{27,28}, as it allows ubiquitous high expression, with minimal post-transcriptional modifications (Fig. 5A)³⁷. However, Pol III promoters provide limited options for transcriptional regulation. In contrast, Pol II promoters allow for more versatile experimental designs for RNA expression³⁸, but result in substantial post-transcriptional modifications that interfere with sgRNA functionality^{39,40}. Recently, a novel technique for sgRNA multiplexing under a single promoter was described using self-cleaving ribozymes⁴¹. We employed this approach to remove Pol II-mediated RNA modifications, allowing Pol II-mediated unmodified sgRNA expression. As a proof of concept, this approach was tested for expression under an EF1a promoter (Fig. 5B), as well as in a doxycycline (dox)-inducible Tet-ON system (Fig. 5C)⁴². Indeed, CROSS-FIRE co-culture experiments confirmed the functionality of both systems (Fig. 5D, E), without a decrease of efficiency as compared to the Pol III U6 promoter. This modification further expands the potential of the CROSS-FIRE system, allowing future use of inducible or tissue-specific regulation of sgRNA expression in donor cells.



▲Figure 5 | Incorporation of self-cleaving RNA ribozymes allows the use of Pol II-mediated donor cell sgRNA expression in the CROSS-FIRE system. a, Standard expression of sgRNAs under a Pol III promoter. Transcription is ended by a Pol III terminator sequence; TTTTT. The expressed sgRNA is not subjected to any additional post-transcriptional modifications under a Pol III promoter. **b**, Incorporation of self-cleaving Hammerhead (HH) and Hepatitis Delta Virus (HDV) RNA ribozymes sequences flanking the sgRNA sequence expressed under a Pol II promoter results in the removal of post-transcriptional Pol II modifications. **c**, A construct for doxycycline-inducible expression of sgRNAs using a Pol II TET-On inducible system, by incorporation of self-cleaving RNA ribozymes. **d**, Flow cytometry analysis of Stoplight⁺spCas9⁺ HEK293T reporter cells after a five day co-culture with sgRNA⁺ MDA-MB-231 donor cells expressing sgRNAs under a U6 Pol III promoter (**a**), or a EF1a Pol II promoter using self-cleaving RNA ribozymes (**b**). Means + SD, n = 3 independent experiments, Tukey's multiple comparison test. **e**, Flow cytometry analysis of Stoplight⁺spCas9⁺ HEK293T reporter cells after a five day co-culture with sgRNA⁺ MDA-MB-231 donor cells expressing sgRNAs under regulation of a U6 Pol III promoter (**a**), and a doxycycline-inducible promoter Pol II promoter (**c**). Means + SD, n = 3 biologically independent samples, Tukey's multiple comparison test. * = p < 0.05, ** = p < 0.01, *** = p < 0.001.

DISCUSSION

Studies over the last decade have shown that there is a natural transport system, extracellular vesicles (EV), which allows cells to transfer proteins, mRNA and microRNA (miRNA) to other cells^{3,43,44}, and by doing so play a role in numerous physiological and pathological processes⁴⁵. EVs have become a topic of great interest as potential therapeutic targets in a variety of pathologies, as well as for designing novel therapeutic drug delivery strategies⁵. Functional EV-mediated transfer of RNA molecules relies on uptake of the target cells, as well as subsequent specific intracellular trafficking and processing. Even though recent studies have shown that EVs are capable of delivery of functional mRNA as well as miRNA to target cells^{16,33}, a significant amount of EVs are transported to lysosomal

compartments after uptake¹⁵. These findings indicate that EVs are suitable vectors for RNA delivery, but also underline that EV uptake and cargo delivery is a highly regulated and intricately complex process. Indeed, to date, much remains unknown about the mechanisms dictating EV targeting, internalization and intracellular trafficking, and the contributing EV components have not yet been characterized. Understanding the biology underlying the EV-based intercellular transfer of RNA is pivotal to gain a better understanding of the role of EVs in both physiological and pathophysiological processes, as potential therapeutic targets, as well as for a more rational development of EVs as drug delivery vehicles or EV-inspired synthetic systems.

In this manuscript, we describe a CRISPR/Cas9-based approach to study EV-mediated functional RNA transfer. This CCRISPR Operated Stoplight System for Functional Intercellular RNA Exchange (CROSS-FIRE) is, to the best of our knowledge, the first system that allows the measurement of small non-coding RNA transfer at single-cell resolution. Such a system is pivotal to unravel the underlying mechanisms of EV-mediated RNA delivery, as currently employed methods either do not demonstrate functional content delivery (e.g. fluorescent dyes), or do not differentiate between RNA and protein delivery (mRNA-based reporter systems)^{12-14,26}. Moreover, sensitivity of measuring EV-mediated transfer of miRNAs on whole cell populations is generally low, as small effects are masked by expression levels in the total cell population. The CROSS-FIRE system addresses all these issues, as reporter activation is based on functional delivery of sgRNAs, which do not rely on protein translation for their functionality²⁷. Furthermore, as the reporter system read-out is high induction of a fluorescent signal, activation can be measured at single-cell resolution.

A previously designed fluorescent reporter system to study EV-mediated cargo transfer is the Cre-LoxP reporter system^{8,16}. Like the CROSS-FIRE system, this reporter system is based on activation of a fluorescent protein in recipient reporter cells upon functional cargo delivery. However, rather than small RNA transfer, the Cre-LoxP reporter system is based on transfer of large Cre mRNA molecules or Cre protein. Therefore, we do not envision the CROSS-FIRE system as a replacement or competing tool of the Cre-LoxP system. Rather, we envision complementary roles for these reporter systems, in which the Cre-LoxP system may be utilized to study the transfer of larger mRNA molecules and Cre protein (as functional transfer of Cre protein currently cannot be ruled out), whereas the CROSS-FIRE system can be used to exclusively study the functional delivery of smaller RNA molecules. Indeed, sgRNAs appear to be a highly suitable RNA molecule to study EV-mediated RNA transfer, as multiple studies have shown that EVs contain higher levels of small RNAs around ~100 nt, whereas only traces amounts of full length mRNA have been detected¹⁷⁻²³. Concordantly, it has been

shown that the majority of mRNAs present in EVs are not present as intact mRNAs^{24,25}. This could explain why we observed a higher sensitivity when comparing the CROSS-FIRE system to the Cre-LoxP reporter system in a 5 day co-culture experiment using the same donor and reporter cell combinations and ratios (Supplementary Fig. 9).

Despite the high sensitivity of the CROSS-FIRE reporter system, reporter activation in our experimental set-up was low (up to 0.2% in HEK293T cells). These data are not due to low levels of efficiency of EV-mediated communication, but rather the result of low amounts of sgRNA loaded into vesicles as no targeted RNA loading or enrichment strategies were employed. As a result, sgRNA abundance is approx. 1 RNA molecule per 4.5e5 EVs, an abundance which is not uncommon for naturally expressed RNA molecules^{46,47}. Moreover, lower percentages of activation can likely be explained by the short time span of the experiments, as both co-culture and addition experiment protocol were designed for timeframes compatible with siRNA target KD protocols. Increasing the ratio of donor- to reporter cells and increasing the dose of sgRNA-containing EVs in addition experiments resulted in a dose-dependent increase of reporter activation, suggesting that indeed the amount of transferred sgRNA is a limiting factor in these experiments. Lastly, inDelphi *in silico* target sequence analysis predicted a frameshift frequency of approx. 80%, meaning that around 20% of all NHEJ-mediated mutations remain undetected²⁹.

Interestingly, sgRNA transfer in co-culture experiments also appears to vary amongst different cell types. This appears to be the case for both reporter cells (Supplementary Fig. 4) and donor cells (Supplementary Fig. 5). These results are in line with observations from Zomer *et al.* using a Cre-LoxP-based reporter system to study EV-mediated cargo transfer from MDA-MB-231 donor cells to various reporter cell lines in co-culture experiments⁸. In line with our results, they observed a higher transfer of EV cargo from MDA-MB-231 cells to MCF-7 and T47D reporter cells than to MDA-MB-231 reporter cells (Supplementary Fig. 4). Moreover, we find that sgRNA transfer to reporter cells is also influenced by donor cell type. Whereas we see functional RNA transfer from MDA-MB-231 (epithelial breast cancer), HMEC-1 (microvascular endothelium), and hTERT-MSC (immortalized mesenchymal stem cell) donor cells within 5 days, no significant transfer was observed from HEK293T donor cells in these conditions (Supplementary Fig. 5). These data indicate that certain cell types may be less prone to exchange RNA with other cells. The latter observation is especially relevant to the field, as HEK293T cells are a commonly used cell source to study strategies for targeted RNA loading and delivery in EVs. It stands out that from these various donor cell lines, the highly metastatic MDA-MB-231 cells appear to show the highest functional transfer of sgRNAs to HEK293T reporter cells as compared

to non-cancerous HEK293T, HMEC-1 and hTERT-MSC donor cells. These observations are in line with previous observations showing high levels of MDA-MB-231 EV-mediated intercellular communication with surrounding cells resulting in increased metastasis and tumor progression^{8,48,49}. Based on these data it is thus tempting to conclude that tumor cells show higher levels of RNA transfer to other cells in general, as a result of increased EV secretion or more efficient uptake. However, based on these results alone we cannot definitively conclude that this applies to tumor cells in general.

In this manuscript, we optimized and demonstrate protocols that allow studying the role of single genetic targets in EV-mediated intercellular RNA transfer, by combining siRNA-mediated single target KD with both CROSS-FIRE co-culture and EV addition experiments. Such experiments are critical to unravel the underlying mechanisms that regulate EV-mediated RNA transfer, and to the best of our knowledge this is the first system that allows such experiments in a robust, scalable manner. Using this approach, we find that knocking down Alix and Rab27a (involved in EV production and release³²) significantly decreases functional RNA transfer, whereas knocking down ARRDC1 (involved in microvesicle release³³) and CDC42 (involved in tunneling nanotube regulation³⁴) does not. These data show that the CROSS-FIRE system can be employed to assess the role of different EV subtypes in functional RNA transfer, a research topic that has recently gained substantial traction in the EV field. Such studies could greatly benefit the design of EV-based delivery systems by uncovering the most potent and suitable EV subpopulations for therapeutic RNA delivery. Additionally, such insights could lead to the discovery of novel ways of specific interfering with EV-mediated RNA transfer, a process involved in the communication between tumor cells and their surrounding tissues, affecting tumor growth and metastasis^{8,48,49}.

Moreover, we studied the effect of knocking down various regulatory genes of endocytosis and intracellular membrane trafficking in reporter cells. We and others have previously observed that these pathways are involved in the regulation of EV uptake^{12,35,36}. Indeed, in line with our previous observations on EV uptake, KD of Pak1 and Rac1, both involved in macropinocytosis, resulted in a significant decrease in reporter activation, whereas KD of ANKFY1 did not¹². KD of Cav1 and RhoA involved in endocytosis, resulted in a substantial decrease of reporter activation, whereas targets CDC42 and Flot-1 showed no significant difference. The latter observation is of interest, as we previously demonstrated that Flot-1 KD does result in a significant decrease in EV uptake¹². It is tempting to speculate that EVs taken up in a Flot-1-dependent manner could play a lesser role in EV-mediated RNA transfer, however additional experiments are required to fully elucidate this observation. Interestingly, knocking down macropinocytosis players PAK1 and ANKFY1 in MCF-7

reporter cells had virtually the opposite effect: whereas the inhibitory effect of PAK1 KD was absent in MCF-7 cells, knocking down ANKFY1 actually resulted in a substantial increase of functional RNA uptake by MCF-7 cells. These data demonstrate that the relative role of varying uptake routes may substantially differ between cell types, and showcases the complexity of such processes.

Lastly, we employed the CROSS-FIRE system to study the role of various novel genetic targets on EV-mediated RNA transfer (Fig. 4F). These experiments uncovered a role of 4 genes for functional sgRNA transfer: ITGB1 (integrin, extracellular matrix interaction), ROCK1 (downstream RhoA effector), and Rab5 and Rab7 (intracellular membrane trafficking). These findings confirm that the CROSS-FIRE system is suitable for uncovering novel genetic targets that are not only involved in EV uptake, but also in intracellular membrane trafficking. This once more underlines the importance of using read-outs that rely on functional RNA transfer to better understand their underlying mechanisms, in order to unravel the post-endocytotic processes that regulate EV-mediated RNA delivery. A better understanding of these mechanisms may greatly aid in the design of EV-mediated RNA-delivery strategies, as EV uptake and EV cargo processing in EV acceptor cells strongly dictate efficiency of RNA delivery⁵⁰.

In summary, the CROSS-FIRE system is a highly sensitive method with broad applicability to study EV-mediated RNA delivery, and will help to increase our understanding of the regulatory pathways that dictate the underlying biological processes. This, in turn, holds the strong potential to provide a better understanding of the role of EV signaling in homeostasis and pathologies, and for uncovering, developing and implementing more efficient EV-mediated therapeutic strategies.

METHODS

Cell culture

HEK293T, HeLa, MCF-7, and MDA-MB-231 cells were cultured in Dulbecco's Modified Eagle Medium (DMEM) with L-Glutamine (Gibco) supplemented with 10% fetal bovine serum (FBS) (Sigma). T47D cells were cultured in DMEM/F12 medium with L-Glutamine supplemented with 10% FBS. hTERT-MSCs were cultured in alpha-MEM supplemented with GlutaMAX and 10% FBS. HMEC-1 cells were cultured in MCDB-131 medium supplemented with GlutaMAX, 10% FBS, 10 ng/ml rhEGF (Peprotech) and 50 nM Hydrocortisone (Sigma) on plates coated with 0.1% gelatin (Sigma). All cell lines were cultured in the presence of 100 µg/ml streptomycin, and 100 u/ml penicillin (Gibco) at 37° C and 5% CO₂.

DNA constructs

The CROSS-FIRE fluorescent Stoplight reporter construct (Supplementary Table 1) was synthesized into a PG9-M2 vector by Gen9Bio. The fluorescent Stoplight reporter construct was subsequently cloned into a pHAGE2 lentiviral plasmid⁵¹; pHAGE2-CMV-IRES-NeoR, using the restriction enzymes NotI and BamHI (New England Biolabs) and a NEB Quick Ligation Kit (New England Biolabs). The fluorescent stoplight reporter construct was fully sequenced to rule out undesirable mutations. For stable spCas9 expression, a lentiCas9-P2A-Blast plasmid⁵² was used (Addgene #52962). For stable sgRNA expression, sgRNA targeting sequences were cloned into the lentiGuide-Puro plasmid⁵² (Addgene #52963), by ligating annealed complementary oligonucleotides into the plasmid after BsmBI digestion (New England Biolabs) using a NEB Quick Ligation Kit. Oligonucleotide sequences used for cloning are listed in Supplementary Table 2. For stable Cre Recombinase expression a pLV-CMV-Cre plasmid was used, and for stable expression of a fluorescent Cre Recombinase Stoplight reporter a pLV-CMV-LoxP-DsRed-LoxP-eGFP plasmid was used^{8,16}. Oligonucleotides were synthesized by Integrated DNA Technologies. Pol II-compatible sgRNA sequences flanked by self-cleaving RNA ribozymes were designed as described by Gao *et al.*⁴¹ (Supplementary Table 3). Sequences were synthesized by Integrated DNA technologies, and cloned into pHAGE2-EF1a-UBC-PuroR or pInducer20⁴² plasmids using NotI and BamHI restriction enzymes, or BsmBI and AscI restriction enzymes, respectively.

Lentiviral production and generation of stable cell lines

For lentiviral transduction of the CROSS-FIRE fluorescent Stoplight reporter construct, spCas9, and expression of sgRNAs, lentivirus was produced in HEK293T cells. HEK293T cells were transfected with lentiviral plasmids containing the gene of interest, pMD2.G plasmid, and PSPAX2 plasmid (Addgene #12259 and #12260, respectively) at a 2:1:1 ratio using 1 μ l Lipofectamine-2000 (Thermo Fisher Scientific) per μ g plasmid DNA. Culture medium was replaced after 18 hours, and lentiviral supernatants were harvested 48 hours later. After harvesting lentiviral supernatant were cleared from cells by a 10 minute centrifugation at 500 x g, followed by filtration using a .45 μ m syringe filter. Cells were transduced with lentiviral stocks overnight in the presence of 8 μ g/ml polybrene (Sigma), after which the lentiviral medium was replaced with standard culture medium. Starting 24 hours after lentiviral transduction, cells were cultured and expanded in the presence of their respective selection antibiotics. Cells lentivirally transduced with CROSS-FIRE and Cre-LoxP fluorescent Stoplight reporter constructs were sorted for eGFP⁺mCherry⁺

or eGFP^{DsRed} fluorescence respectively, 2 weeks after expansion in the presence of selection antibiotics on a BD FACSAria III cell sorter. Stable MDA-MB-231 cell lines expressing Pol II-compatible sgRNA constructs were generated by linearized plasmid transfection using Lipofectamine-2000. pHAGE2-EF1a-sgRNA-UBC-Puro and pInducer20-sgRNA plasmids were linearized using SmaI or FseI restriction enzymes (New England Biolabs) respectively, followed by a DNA clean up using a PCR purification kit (Qiagen). Starting 48 hours after transfection, cells were cultured and expanded in the presence of their respective selection antibiotics. The following concentrations of selection antibiotics were used: 2 µg/ml puromycin, 5 µg/ml blasticidine, or 500 µg/ml G418 for all cell types, with the exception of HEK293T cells being cultured with 1000 µg/ml G418.

Co-cultures and transwell experiments

All co-culture experiments were performed in DMEM containing 10% FBS, L-Glutamine, 100 µg/ml streptomycin, and 100 u/ml penicillin. Unless stated otherwise, direct co-culture experiments were performed for five days at a 1 : 5 ratio of reporter : donor cells. Transwell experiments were performed in 12-well plates for ten days, and after day five of transwell co-culture experiments, reporter cells were passaged to new wells, and new transwell inserts containing donor cells were added to the reporter cells. At the end of a co-culture experiment, cells were directly analyzed by fluorescence microscopy using an EVOS FL Cell Imaging System (Thermo Fisher Scientific), or analyzed by flow cytometry. For flow cytometry analysis cells were trypsinized for 5 minutes using TrypLE Express (Thermo Fisher Scientific), and transferred to 5 ml flow cytometry tubes using a similar volume of DMEM containing 10% FBS. Cells were centrifuged for 5 minutes at 300 x g, washed in 5 ml 1% FBS in PBS, and centrifuged once more for 5 minutes at 300 x g. Cells were then resuspended in 250 µl 1% FBS in PBS, and kept on ice until flow further analysis. Cells were analyzed on an ImageStream Mark II (Amnis), MacsQuant VYB (Miltenyi Biotec), or Fortessa (BD Biosciences) flow cytometer, and further analyzed using FlowJo v10 software.

In silico confocal microscopy image analysis

Cells were seeded in CellStar 96-well cell culture black µClear bottom TC-treated microplates (Greiner-Bio). Prior to imaging, 1 µg/ml Hoechst 33342 (ThermoFisher Scientific) was added to the culture medium for 15 minutes at room temperature. Confocal pictures were then taken using a Yokogawa C7000 confocal microscope with a

live cell stage incubator at 37° C and 5% CO₂. 16 images were taken at 20x magnification per well, at random locations using the following filter settings:

Hoechst: emission = 405 nm, power 30; acquisition =BP445/45. Exposure time = 100. Input level = 2000.

eGFP: emission = 488 nm, power 30; acquisition =BP525/50. Exposure time = 125. Input level = 10000.

mCherry: emission = 561 nm, power;30, acquisition =BP600/37. Exposure time = 125. Input level = 2000.

Per picture, average fluorescence images were generated from z-stacks over a distance of 10 μm (5μm below and 5 μm above nuclear focal point) with a 2 μm slice length. Images were then analyzed using the Columbus Image Data Storage and Analysis System (Perkin-Elmer), using the following settings: Find Nuclei: software analysis method "C". Cytoplasm cell region selection: Region Type = nucleus region, Outer Border = -75%, Inner Border =-5%. mCherry+ selection: Population = all cells, Mean Cytoplasm Intensity BP600/37 > 110. eGFP+ selection: Population = mCherry+ cells, Mean Cytoplasm Intensity BP525/50 > 200.

Luciferase activity assays

Cells were seeded in 96 well plates in 250 μl complete culture medium, 24 hours prior to luciferase activity measurements. After 24 hours, 150 μl conditioned medium was harvested to 1.5 ml Eppendorf tubes, and cleared of cellular debris by 5 minute centrifugation at 300 x g, followed by 15 minute centrifugation at 2,000 x g. 75 μl conditioned medium was then transferred to LumiNunc White 96-well plates (ThermoFisher Scientific), and Gaussia Luciferase activity was analyzed using the Dual-Glo Luciferase Assay System (Promega) according to the manufacturer's protocol, and measured on a SpectraMax L Microplate Reader (Molecular Devices).

EV isolation

For EV isolation, MDA-MB-231 cells expressing sgRNAs were cultured in Celline Adhere 1000 Bioreactors (Integra Biosciences)⁵³⁻⁵⁵, in which MDA-MB-231 cells were maintained in a matrix concentrated cell compartment. This compartment is connected to an outer medium compartment through a 10 kDa pore-size semi-permeable membrane which allows exchange of nutrients, but not extracellular vesicles, between both compartments. The outer medium compartment contained 500 ml complete culture medium with 0.5

$\mu\text{g/ml}$ puromycin, and was changed on a weekly basis. The MDA-MB-231 cells were maintained in the cell compartment in 15 ml serum-free OptiMEM, which was replaced every 48 hours. For EV isolation, the serum-free conditioned medium was isolated from the concentrated cell compartment and cell debris was removed by 5 minute centrifugation at $300 \times g$, followed by 15 minute centrifugation at $2,000 \times g$ ml. Samples were then filtered by $.45 \mu\text{m}$ syringe filtration and further concentrated to a volume of 0.5 – 1.0 ml using a 100 kDa Amicon Ultra-15 Centrifugal filter (Merck). EVs were then isolated by size exclusion chromatography over a Tricorn 10/300 column with Sepharose 4 Fast Flow resin, using the AKTA Start chromatography system (all GE Healthcare Life Sciences). EV-containing fractions were sterilized by $.45 \mu\text{m}$ syringe filtration, and concentrated using a 100 kDa Amicon Ultra-15 Centrifugal filter. Isolated EVs were directly used for functional assays, or stored at -20°C until further analysis. For EV addition experiments on siRNA-treated reporter cells (see below), EVs were isolated from T175 flasks to facilitate high yield EV isolation every 24 hours. For these isolation MDA-MB-231 sgRNA⁺ cells were cultured in T175 flasks in standard culture medium until a confluency of $\sim 80\%$ was reached. Cells were then washed once with OptiMEM, and cultured for 24 hours in OptiMEM containing 100 $\mu\text{g/ml}$ streptomycin, and 100 u/ml penicillin. Conditioned medium was then isolated, and cell debris was removed by 5 minute centrifugation at $300 \times g$, followed by 15 minute centrifugation at $2,000 \times g$. Conditioned medium was then concentrated by tangential flow filtration using a Minimate 100 kDa Omega Membrane (Pall Corporation) to a volume of 15 ml, followed by $.45 \mu\text{m}$ syringe filtration and further concentration to a volume of 0.5 – 1.0 ml using a 100 kDa Amicon Ultra-15 Centrifugal filter (Merck). EVs were then isolated by size exclusion chromatography, sterilized by syringe filtration and concentrated using 100 kDa centrifugal filters as described above. In experiments where soluble protein-containing fractions were isolated from conditioned medium alongside EVs by size exclusion chromatography, we made use of a Minimate 10kDa Omega Membrane and 10 kDa Amicon Ultra-15 Centrifugal filters for sample concentration.

Nanoparticle Tracking Analysis

EV size distribution was determined using a Nanosight S500 nanoparticle analyzer (Malvern Instruments) with a 405 nm laser. Samples were measured in PBS, with the camera setting at level 16. For post-acquisition analysis, all post-acquisition settings were set to 'Auto', with the exception of a fixed detection threshold of level 6. Using a scripted control function, five 60 seconds videos were recorded for each sample, and analyzed using NTA software v3.1.

EV RNase protection assay

50 μ l EVs in PBS were mixed with 250 μ l control (100mM Tris, 5mM EDTA, 200 mM NaCl) or lysis buffer (100mM Tris, 5mM EDTA, 200 mM NaCl, 0.2% SDS). Proteinase K (Thermo Fisher Scientific) was added to the appropriate samples at a final concentration 80 μ g/ml. All samples were then incubated at 37 ° C for 5 minutes, followed by Proteinase K heat inactivation of all samples at 90° C for 5 minutes. After samples had cooled, RNase A (Thermo Fisher Scientific) was added to the relevant samples at a final concentration of 330 μ g/ml, followed by a 20 minute RNase digestion at 37° C. RNase activity was halted by the addition of 900 μ l Trizol LS (Life Technologies) and RNA was isolated according to the manufacturer's protocol using GlycoBlue coprecipitant (Thermo Fisher Scientific). The RNA pellets were resuspended in 10 μ l RNase-free water, followed by cDNA synthesis using a SuperScript 3 kit (Thermo Fisher Scientific), RNasin Ribonuclease inhibitor (Promega) and 2 pmol of Targeting sgRNA reverse primer (See Supplementary Table 6), according to the manufacturer's protocol. The resulting cDNA templates were then diluted 1:4 and PCR was performed by incubation at 95 ° C for 2 minutes followed by 38 cycles of 95 ° C for 30 seconds, 60° C for 30 seconds, and 72 ° C for 60 seconds on a C1000 Touch Thermal Cycler (Bio-Rad). Targeting sgRNA PCR primers are listed in Supplementary Table 6. PCR products were then run on a 1.5% agarose gel containing 1:10,000 GelRed DNA staining dye (Biotium) and imaged in the UGenius gel imaging system (Syngene). Uncropped gel scans have been included in the supplemental Source Data file.

Western Blot

Cells or EVs were lysed in RIPA buffer supplemented with Protease Inhibitor Cocktail (Sigma-Aldrich). Lysates were incubated on ice for 30 minutes and subsequently centrifuged for 15 minutes at 12,000 x g to remove non-soluble materials. Protein concentrations were determined by a MicroBCA Protein Assay, alongside a bovine serum albumin standard according to the manufacturer's protocol (Thermo Fisher Scientific). Samples were mixed with sample loading buffer, where necessary containing 100 μ M DTT, followed by a 10 minute heat-inactivation at 95° C. Samples were then loaded onto 4-12% gradient Bis-Tris polyacrylamide gels (Thermo Fisher Scientific) and subjected to electrophoresis. Proteins were then blotted onto Immobilon-FL polyvinylidene difluoride membranes (Millipore), which were subsequently blocked with in blocking buffer containing 1 part Odyssey Blocking Buffer (LI-COR Biosciences) and 1 part Tris-Buffered Saline (TBS). Membranes were subsequently probed using the following antibodies: Alix 1:1000 (Thermo Fisher Scientific, MA1-83977), Calnexin 1:1000 (GeneTex, GTX101676), CD9 1:1000 (Abcam,

ab92726), CD63 1:1000 (AB8219), Flot-1 1:1000 (Cell Signaling Technology, 3253), TSG101 1:1000 (Abcam, ab30871) and H2B 1:1000 (Abcam, ab52599) in staining buffer consisting of 1 part Odyssey Blocking Buffer and 1 part TBS with 0.1% Tween-20 (TBST). Secondary antibodies consisted of either anti-rabbit IgG conjugated to AlexaFluor 680 (Thermo Fisher Scientific, A-21076) or anti-mouse IgG conjugated to IRDye 800CW and were applied at a 1:10,000 dilution in staining buffer. Proteins were visualized using an Odyssey Infrared Imager (LI-COR Biosciences) at 700 and 800 nm. Uncropped Western Blot scans have been included in the supplemental Source Data file.

Transmission Electron Microscopy

EVs were adsorbed to carbon-coated formvar grids for 15 minutes at room temperature. Unbound EVs were removed by a PBS wash. Grids were then fixed in a 2% paraformaldehyde, 0.2% glutaraldehyde in PBS fixing buffer for 30 minutes at room temperature, followed by counterstaining with uranyl-oxalate. Grids were then embedded in a mixture of 1.8% methyl cellulose and 0.4% uranyl acetate at 4° C. Grids were imaged on a Jeol JEM-1011 TEM microscope (Jeol).

EV staining and uptake

EVs were fluorescently labeled with PKH67 (Sigma-Aldrich) as follows: Diluent C was added to EVs in a 1:1 v/v ratio, which were then labelled with PKH67 by the addition of one half additional volume of PKH67 diluted 1:100 in Diluent C. The mixture was incubated for 5 minutes at room temperature, after which unbound PKH67 dye was removed using the AKTA Start chromatography system (GE Healthcare Life Sciences) and a XK-16/20 column (GE Healthcare) with 30 ml of Sepharose CL-4B resin. After free dye removal, EV containing fractions were concentrated to 250 μ l in 100 kDa Amicon Ultra-15 Centrifugal filter (Merck). 20 μ l labeled EVs were added of HEK293T Stoplight⁺ cells seeded on a gelatin coated glass 2-well chamber slide with removable wells (Thermo Fisher Scientific). After 6 hours of incubation, the cells were fixed by the addition of paraformaldehyde and washed with PBS. Nuclei were stained for 10 minutes in 1 μ g/ml DAPI. After fixation, slides were washed with PBS and mounted using Fluorsave (Calbiochem). Confocal fluorescence imaging was performed using a LSM700 laser scanning confocal microscope (Zeiss). Images were processed using LSM Image Browser.

EV addition experiments

For comparison of EVs containing targeting sgRNAs or non-targeting sgRNAs, and for EV dose response addition experiments, HEK293T Stoplight⁺spCas9⁺ reporter cells were cultured in 24-well plates in 1 ml culture medium, and EVs isolated from MDA-MB-231 cells expressing sgRNAs cultured in Celline Adhere 1000 Bioreactors (Integra Biosciences) were added. For EV addition experiments on siRNA-treated reporter cells, cells were plated in 96-well plate wells in a volume of 200 μ l, and EVs isolated from MDA-MB-231 cells expressing sgRNAs cultured in T175 flasks were added every 24 hours for 6 consecutive days. After EV addition, EVs were incubated with the cells for 24 hours, followed by a culture medium wash. Cell confluences between 40 – 100% were maintained throughout the addition experiment. On average, 1.5×10^{12} EVs per 1×10^5 cells were added in EV addition experiments. For RNase A treatments, EVs were incubated in PBS for 30 minutes at 37° C with 10 μ g/ml RNase A prior to addition to cells. After the last EV addition, reporter cells were incubated for another 48 hours to allow reporter cells activated in the last addition to reach sufficient eGFP levels. Reporter cells were analyzed by fluorescence microscopy and flow cytometry as described above.

siRNA knockdown

Cells were seeded in DMEM containing 10% FBS, L-Glutamine, and no antibiotics, 24 hours prior to siRNA transfection, in 24-well plates. Cells were transfected using Lipofectamine RNAiMax (Life Technologies) according to the manufacturer's protocol. 5 or 1.25 pmol siRNAs previously verified¹², or Dharmacon ON-TARGETplus siRNA smartpools were transfected in 24-well or 96-well plate wells respectively. Annealed siRNA sequences are listed in Supplementary Table 4, Dharmacon ON-TARGETplus siRNA smartpool and non-coding siRNA control product information is listed in Supplementary Table 5. Prior to any functional experiments, target gene knockdown (KD) of all used siRNAs was confirmed by qPCR in the appropriate cell types (Supplementary Fig. 10). After 18 hours, cells were washed once, and subsequently cultured in DMEM containing 10% FCS, L-Glutamine, 100 μ g/ml streptomycin, and 100 u/ml penicillin. In case of co-culture experiments, additional cells were added directly after the culture medium was changed. For qPCR analysis, cells were cultured for an additional 48 hours before RNA isolation.

Cell RNA isolation and qPCR analysis

Total RNA was isolated from cells using TRIzol Reagent (Thermo Fisher Scientific), according to the manufacturer's protocol. Isolated RNA was measured using a DS-11

Spectrophotometer (DeNovix). 1 µg RNA per sample was used for cDNA synthesis using the iScript cDNA Synthesis Kit (Bio-Rad). qPCR was performed using iQ SYBR Green Supermix (Bio-Rad) in a CFX96 Real-Time PCR Detection System (Bio-Rad). Primer sequences were taken from the PrimerBank PCR primer public resource⁵⁶ and synthesized by Integrated DNA Technologies (Supplementary Table 6). Cycle threshold (Ct) values were normalized per experiment and per gene. $\Delta\Delta C_t$ was calculated using housekeeping gene GAPDH. Statistical analysis was performed using a Student's t test.

Quantification of sgRNA abundance in EVs

EVs were isolated from sgRNA⁺ MDA-MB-231 donor cells as described above. EV count was determined using NTA as described above. 250 µl of the EV samples were lysed in 750 µl trizol LS (Thermo Fisher Scientific) and RNA was extracted using glycobluo co-precipitant (Thermo Fisher Scientific) as per manufacturer's instructions. Reverse transcription was then performed using a superscript IV reverse transcriptase kit (Thermo Fisher Scientific) and a targeting RNA specific reverse primer. A standard curve was prepared which contained synthetic targeting sgRNA at known copy numbers in 250 µl PBS. RNA was extracted from these standard curve samples and reverse transcription was performed using an identical method alongside EV samples in order to normalize for RNA extraction and reverse transcription efficiency. A PBS-only blank was also taken along to rule out contamination. qPCR was then performed on the standard curve, targeting EV and blank cDNA samples. The targeting sgRNA copy number in EV samples was then interpolated from the standard curve Ct values using Graphpad Prism 8.0.1 software.

Statistics

All statistical analyses were performed using Graphpad Prism 8.01. Values are expressed as the mean \pm standard deviation (SD), unless indicated otherwise. Two-sided statistical tests were performed in all statistical analyses. Differences were considered statistically significant at $p < 0.05$.

DATA AVAILABILITY STATEMENT

The datasets generated during and/or analyzed during the current study are available from the corresponding author on reasonable request. The source data underlying Figures 1C, 1F-G, 2C-E, 3B-C, 3E, 3H-I, 4B-C, 4E-G, 5D-E, and Supplementary Figures 1B-C, 3C-F, 4B, 4D, 4F, 4H, 4J, 5B, 5D, 5F, 6B, 6D-F, 7B-E, 8A-C, 9B, 9D, 9F, and 10A-C are provided as a Source Data file.

ACKNOWLEDGEMENTS

O.G.d.J. is supported by the Biotechnology and Biological Sciences Research Council (BB/M024393/1), and a VENI Fellowship (VI.Veni.192.174) from the Dutch Research Council (NWO). I.M., D.E.M. and R.M.S. are supported by the B-SMART Consortium, which has received funding from the European Union's Horizon 2020 research and innovation programme under grant agreement No. 721058. E.W. is supported by the John Fell Fund grant 162/044. A.G.G. is supported by "La Caixa" Fellowship Grant for Post-Graduate Studies, "la Caixa" Banking Foundation, and the Oxford University Press John Fell OUP Research Fund. J.v.R. is supported by the European Research Council Grant CANCER-RECURRENCE 648804, and the Doctor Josef Steiner Foundation. S.E.A. is supported by Biological Sciences Research Council (BB/M024393/1), the Swedish Medical Research Council (VR-Med) and the Swedish Foundation for Strategic Research (SSF-IRC). P.V. was supported by a VENI Fellowship (# 13667) from the Dutch Research Council (NWO).

AUTHOR CONTRIBUTIONS

P.V., S.E.A. and M.J.A.W. initiated this project. J.v.R. and R.M.S. helped design and plan the project. O.G.d.J. designed and developed most of the methodology. O.G.d.J., D.E.M., and P.V. designed the experiments. O.G.d.J. and D.E.M. performed and analyzed most of the experiments. I.M., E.W., A.G.G., J.J.G., J.L., D.G., and S.C.S. helped design and perform the experiments. P.V. was responsible for the overall project strategy and management. O.G.d.J. and P.V. wrote the manuscript, which was reviewed by all authors.

COMPETING INTERESTS

S.E.A. is a co-founder of and consultant for Evox Therapeutics, M.J.A.W. is co-founder and non-executive director of and has equity interest in Evox Therapeutics, and P.V. serves on the scientific advisory board of Evox Therapeutics. All other authors declare no conflicts of interest.

REFERENCES

1. Yáñez-Mó, M. *et al.* Biological properties of extracellular vesicles and their physiological functions. *J. Extracell. vesicles* **4**, 27066 (2015) DOI: 10.3402/jev.v4.27066.
2. Camussi, G., Deregibus, M. C. & Tetta, C. Paracrine/endocrine mechanism of stem cells on kidney repair: Role of microvesicle-mediated transfer of genetic information. *Current Opinion in Nephrology and Hypertension* vol. 19 7–12 (2010) DOI: 10.1097/MNH.0b013e328332fb6f.
3. Valadi, H. *et al.* Exosome-mediated transfer of mRNAs and microRNAs is a novel mechanism of genetic exchange between cells. *Nat. Cell Biol.* **9**, 654–659 (2007) DOI: 10.1038/ncb1596.
4. Skog, J. *et al.* Glioblastoma microvesicles transport RNA and proteins that promote tumour growth and provide diagnostic biomarkers. *Nat. Cell Biol.* **10**, 1470–1476 (2008) DOI: 10.1038/ncb1800.
5. Murphy, D. E. *et al.* Extracellular vesicle-based therapeutics: natural versus engineered targeting and trafficking. *Exp. Mol. Med.* **51**, (2019) DOI: 10.1038/s12276-019-0223-5.
6. Stoorvogel, W., Kleijmeer, M. J., Geuze, H. J. & Raposo, G. The biogenesis and functions of exosomes. *Traffic* vol. 3 321–330 (2002) DOI: 10.1034/j.1600-0854.2002.30502.x.
7. Peinado, H. *et al.* Melanoma exosomes educate bone marrow progenitor cells toward a pro-metastatic phenotype through MET. *Nat. Med.* **18**, 883–891 (2012) DOI: 10.1038/nm.2753.
8. Zomer, A. *et al.* In vivo imaging reveals extracellular vesicle-mediated phenocopying of metastatic behavior. *Cell* **161**, 1046–1057 (2015) DOI: 10.1016/j.cell.2015.04.042.
9. Balkom, B. W. M. va. *et al.* Endothelial cells require miR-214 to secrete exosomes that suppress senescence and induce angiogenesis in human and mouse endothelial cells. *Blood* **121**, 3997–4006 (2013) DOI: 10.1182/blood-2013-02-478925.
10. Ciregia, F., Urbani, A. & Palmisano, G. Extracellular Vesicles in Brain Tumors and Neurodegenerative Diseases. *Front. Mol. Neurosci.* **10**, (2017) DOI: 10.3389/fnmol.2017.00276.
11. Ghafarian, F. *et al.* The clinical impact of exosomes in cardiovascular disorders: From basic science to clinical application. *Journal of Cellular Physiology* (2018) doi:10.1002/jcp.27964 DOI: 10.1002/jcp.27964.
12. Costa Verdera, H., Gitz-Francois, J. J., Schiffelers, R. M. & Vader, P. Cellular uptake of extracellular vesicles is mediated by clathrin-independent endocytosis and macropinocytosis. *J. Control. Release* **266**, 100–108 (2017) DOI: 10.1016/j.jconrel.2017.09.019.
13. Tkach, M., Kowal, J. & Théry, C. Why the need and how to approach the functional diversity of extracellular vesicles. *Philos. Trans. R. Soc. B Biol. Sci.* **373**, (2018) DOI: 10.1098/rstb.2016.0479.
14. Mathieu, M., Martin-Jaular, L., Lavieu, G. & Théry, C. Specificities of secretion and uptake of exosomes and other extracellular vesicles for cell-to-cell communication. *Nature Cell Biology* vol. 21 9–17 (2019) DOI: 10.1038/s41556-018-0250-9.
15. Heusermann, W. *et al.* Exosomes surf on filopodia to enter cells at endocytic hot spots, traffic within endosomes, and are targeted to the ER. *J. Cell Biol.* **213**, 173–184 (2016) DOI: 10.1083/jcb.201506084.
16. Zomer, A., Steenbeek, S. C., Maynard, C. & Van Rheenen, J. Studying extracellular vesicle transfer by a Cre-loxP method. *Nat. Protoc.* **11**, 87–101 (2016) DOI: 10.1038/nprot.2015.138.
17. Jenjaroenpun, P. *et al.* Characterization of RNA in exosomes secreted by human breast cancer cell lines using next-generation sequencing. *PeerJ* **2013**, (2013) DOI: 10.7717/peerj.201.
18. Willms, E. *et al.* Cells release subpopulations of exosomes with distinct molecular and biological properties. *Sci. Rep.* **6**, (2016) DOI: 10.1038/srep22519.
19. Rider, M. A., Hurwitz, S. N. & Meckes, D. G. ExtraPEG: A polyethylene glycol-based method for enrichment of extracellular vesicles. *Sci. Rep.* **6**, (2016) DOI: 10.1038/srep23978.

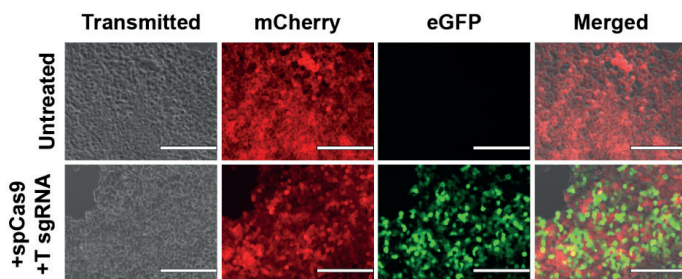
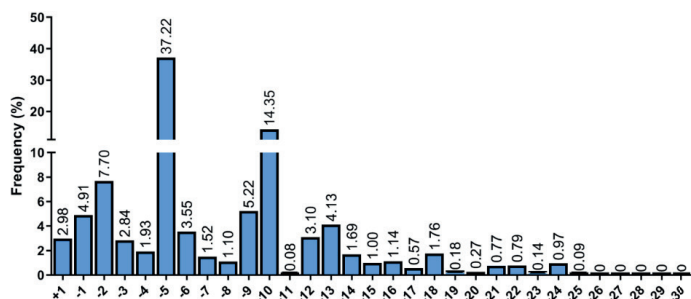
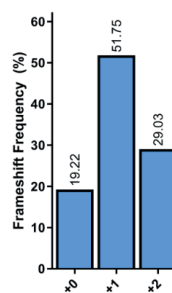
20. Nolte T, Hoen, E. N. M. *et al.* Deep sequencing of RNA from immune cell-derived vesicles uncovers the selective incorporation of small non-coding RNA biotypes with potential regulatory functions. *Nucleic Acids Res.* **40**, 9272–9285 (2012) DOI: 10.1093/nar/gks658.
21. Kagota, S. *et al.* Analysis of extracellular vesicles in gastric juice from gastric cancer patients. *Int. J. Mol. Sci.* **20**, (2019) DOI: 10.3390/ijms20040953.
22. Gai, C. *et al.* Salivary extracellular vesicle-associated miRNAs as potential biomarkers in oral squamous cell carcinoma. *BMC Cancer* **18**, (2018) DOI: 10.1186/s12885-018-4364-z.
23. Enderle, D. *et al.* Characterization of RNA from exosomes and other extracellular vesicles isolated by a novel spin column-based method. *PLoS One* **10**, (2015) DOI: 10.1371/journal.pone.0136133.
24. Hinger, S. A. *et al.* Diverse Long RNAs Are Differentially Sorted into Extracellular Vesicles Secreted by Colorectal Cancer Cells. *Cell Rep.* **25**, 715-725.e4 (2018) DOI: 10.1016/j.celrep.2018.09.054.
25. Wei, Z. *et al.* Coding and noncoding landscape of extracellular RNA released by human glioma stem cells. *Nat. Commun.* **8**, (2017) DOI: 10.1038/s41467-017-01196-x.
26. Mateescu, B. *et al.* Obstacles and opportunities in the functional analysis of extracellular vesicle RNA - An ISEV position paper. *J. Extracell. Vesicles* **6**, (2017) DOI: 10.1080/20013078.2017.1286095.
27. Cong, L. *et al.* Multiplex genome engineering using CRISPR/Cas systems. *Science (80-.)*. **339**, 819–823 (2013) DOI: 10.1126/science.1231143.
28. Xu, T., Li, Y., Van Nostrand, J. D., He, Z. & Zhou, J. Cas9-based tools for targeted genome editing and transcriptional control. *Applied and Environmental Microbiology* vol. 80 1544–1552 (2014) DOI: 10.1128/AEM.03786-13.
29. Shen, M. W. *et al.* Predictable and precise template-free CRISPR editing of pathogenic variants. *Nature* **563**, 646–651 (2018) DOI: 10.1038/s41586-018-0686-x.
30. Kosaka, N. *et al.* Secretory mechanisms and intercellular transfer of microRNAs in living cells. *J. Biol. Chem.* **285**, 17442–17452 (2010) DOI: 10.1074/jbc.M110.107821.
31. Théry, C. *et al.* Minimal information for studies of extracellular vesicles 2018 (MISEV2018): a position statement of the International Society for Extracellular Vesicles and update of the MISEV2014 guidelines. *J. Extracell. Vesicles* **7**, (2018) DOI: 10.1080/20013078.2018.1535750.
32. Villarroya-Beltri, C., Baixauli, F., Gutiérrez-Vázquez, C., Sánchez-Madrid, F. & Mittelbrunn, M. Sorting it out: Regulation of exosome loading. *Seminars in Cancer Biology* vol. 28 3–13 (2014) DOI: 10.1016/j.semcancer.2014.04.009.
33. Wang, Q. *et al.* ARMMs as a versatile platform for intracellular delivery of macromolecules. *Nat. Commun.* **9**, (2018) DOI: 10.1038/s41467-018-03390-x.
34. Haimovich, G. *et al.* Intercellular mRNA trafficking via membrane nanotube-like extensions in mammalian cells. *Proc. Natl. Acad. Sci. U. S. A.* **114**, E9873–E9882 (2017) DOI: 10.1073/pnas.1706365114.
35. Svensson, K. J. *et al.* Exosome uptake depends on ERK1/2-heat shock protein 27 signaling and lipid raft-mediated endocytosis negatively regulated by caveolin-1. *J. Biol. Chem.* **288**, 17713–17724 (2013) DOI: 10.1074/jbc.M112.445403.
36. Fitzner, D. *et al.* Selective transfer of exosomes from oligodendrocytes to microglia by macropinocytosis. *J. Cell Sci.* **124**, 447–458 (2011) DOI: 10.1242/jcs.074088.
37. Arimbasseri, A. G. & Maraia, R. J. RNA Polymerase III Advances: Structural and tRNA Functional Views. *Trends Biochem. Sci.* **41**, 546–559 (2016) DOI: 10.1016/j.tibs.2016.03.003.
38. Haberle, V. & Stark, A. Eukaryotic core promoters and the functional basis of transcription initiation. *Nature Reviews Molecular Cell Biology* vol. 19 621–637 (2018) DOI: 10.1038/s41580-018-0028-8.

39. Nachtergaele, S. & He, C. The emerging biology of RNA post-transcriptional modifications. *RNA Biology* vol. 14 156–163 (2017) DOI: 10.1080/15476286.2016.1267096.
40. Xie, C. *et al.* SgRNA Expression of CRISPR-Cas9 System Based on MiRNA Polycistrons as a Versatile Tool to Manipulate Multiple and Tissue-Specific Genome Editing. *Sci. Rep.* **7**, (2017) DOI: 10.1038/s41598-017-06216-w.
41. Gao, Y. & Zhao, Y. Self-processing of ribozyme-flanked RNAs into guide RNAs in vitro and in vivo for CRISPR-mediated genome editing. *J. Integr. Plant Biol.* **56**, 343–349 (2014) DOI: 10.1111/jipb.12152.
42. Meerbrey, K. L. *et al.* The pINDUCER lentiviral toolkit for inducible RNA interference in vitro and in vivo. *Proc Natl Acad Sci U S A* **108**, 3665–3670 (2011) DOI:
43. Pegtel, D. M. *et al.* Functional delivery of viral miRNAs via exosomes. *Proc. Natl. Acad. Sci.* **107**, 6328–6333 (2010) DOI: 10.1073/pnas.0914843107.
44. Théry, C., Zitvogel, L. & Amigorena, S. Exosomes: composition, biogenesis and function. *Nat. Rev. Immunol.* **2**, 569–579 (2002) DOI: 10.1038/nri855.
45. De Jong, O. G., Van Balkom, B. W. M., Schiffelers, R. M., Bouten, C. V. C. & Verhaar, M. C. Extracellular Vesicles: Potential Roles in Regenerative Medicine. *Front. Immunol.* **5**, (2014) DOI: 10.3389/fimmu.2014.00608.
46. Wei, Z. *et al.* Coding and noncoding landscape of extracellular RNA released by human glioma stem cells. *Nat. Commun.* **8**, (2017) DOI: 10.1038/s41467-017-01196-x.
47. Chevillet, J. R. *et al.* Quantitative and stoichiometric analysis of the microRNA content of exosomes. *Proc. Natl. Acad. Sci. U. S. A.* **111**, 14888–14893 (2014) DOI: 10.1073/pnas.1408301111.
48. Tominaga, N. *et al.* Brain metastatic cancer cells release microRNA-181c-containing extracellular vesicles capable of destructing blood-brain barrier. *Nat. Commun.* **6**, (2015) DOI: 10.1038/ncomms7716.
49. Fong, M. Y. *et al.* Breast-cancer-secreted miR-122 reprograms glucose metabolism in premetastatic niche to promote metastasis. *Nat. Cell Biol.* **17**, 183–194 (2015) DOI: 10.1038/ncb3094.
50. Hung, M. E. & Leonard, J. N. A platform for actively loading cargo RNA to elucidate limiting steps in EV-mediated delivery. *J. Extracell. Vesicles* **5**, (2016) DOI: 10.3402/jev.v5.31027.
51. Wilson, A. A. *et al.* Sustained expression of alpha1-antitrypsin after transplantation of manipulated hematopoietic stem cells. *Am. J. Respir. Cell Mol. Biol.* **39**, 133–141 (2008) DOI: <http://dx.doi.org/10.1165/rcmb.2007-0133OC>.
52. Sanjana, N. E., Shalem, O. & Zhang, F. Improved vectors and genome-wide libraries for CRISPR screening. *Nat. Methods* **11**, 783–784 (2014) DOI: 10.1038/nmeth.3047.
53. Jeppesen, D. K. *et al.* Reassessment of Exosome Composition In Brief Article Reassessment of Exosome Composition. *Cell* **177**, 428–445 (2019) DOI: 10.1016/j.cell.2019.02.029.
54. Mitchell, J. P., Court, J., Mason, M. D., Tabi, Z. & Clayton, A. Increased exosome production from tumour cell cultures using the Integra CELLLine Culture System. *J. Immunol. Methods* **335**, 98–105 (2008) DOI: 10.1016/j.jim.2008.03.001.
55. Jeppesen, D. K. *et al.* Quantitative proteomics of fractionated membrane and lumen exosome proteins from isogenic metastatic and nonmetastatic bladder cancer cells reveal differential expression of EMT factors. *Proteomics* **14**, 699–712 (2014) DOI: 10.1002/pmic.201300452.
56. Wang, X. A PCR primer bank for quantitative gene expression analysis. *Nucleic Acids Res.* **31**, 154e – 154 (2003) DOI: 10.1093/nar/gng154.

A CRISPR-CAS9-BASED REPORTER SYSTEM FOR SINGLE-CELL DETECTION OF EXTRACELLULAR VESICLE-MEDIATED FUNCTIONAL TRANSFER OF RNA

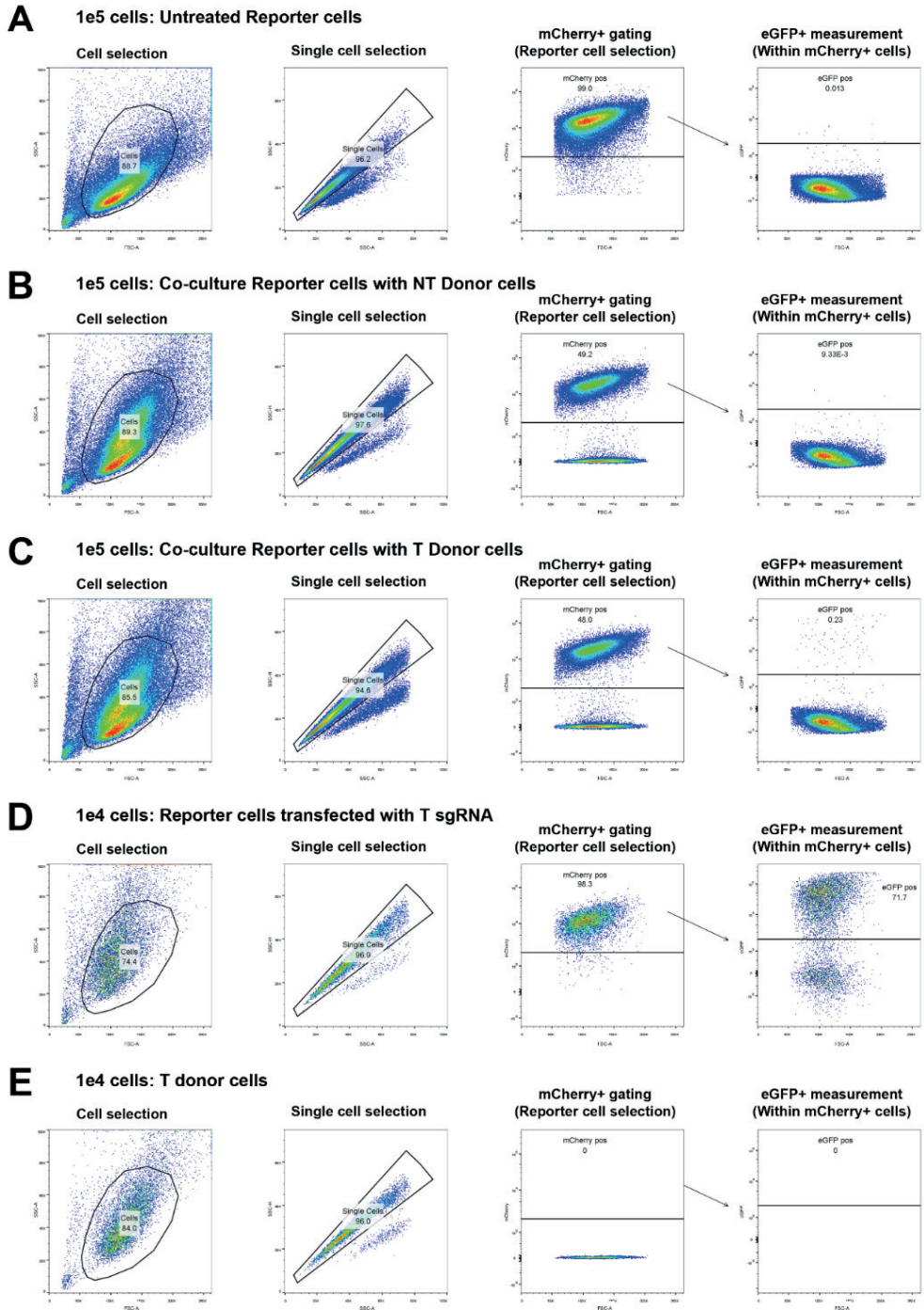
Olivier G. de Jong, Daniel E. Murphy, Imre Mäger, Eduard Willms, Antonio Garcia Guerra, Jerney J. Gitz-Francois, Juliet Lefferts, Dhanu Gupta, Sander C. Steenbeek, Jacco van Rheenen, Samir El Andaloussi, Raymond M. Schiffelers, Matthew J.A. Wood, Pieter Vader

Supplementary Figures, Tables, and References

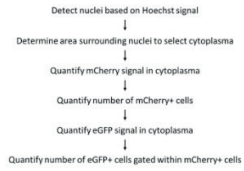
A**B****C**

▲Supplementary Figure 1 | Characterization of the Cas9 Non-Homologous End Joining (NHEJ) Fluorescent Stoplight reporter. a, Fluorescent microscopy images of stable HEK293T Stoplight+ cells left untreated (top row), or 72 hrs after transfection with plasmids encoding for spCas9 and a sgRNA targeting the stoplight construct. Scale bar represents 200 μ m. Representative images as observed in 3 biologically independent samples. b, c, inDelphi in silico CRISPR editing prediction¹ of spCas9 in HEK293 cells using a 5'-ACTCCGATCGGAGACAGTACTCCGCTCG-Cut Site-AGTCGGCTAGCGGGCCCGGGTTC-3' prediction sequence showing predictions for indel frequency (b) and frameshift frequency (c). Both +1nt and +2nt frameshifts result in permanent activation of eGFP expression.

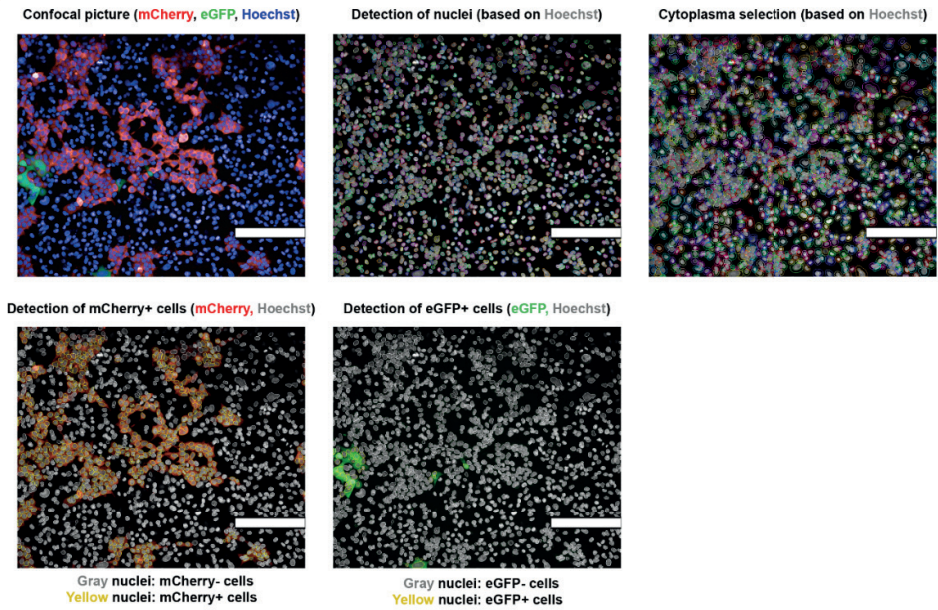
▶Supplementary Figure 2 | Flow cytometry gating strategy employed to analyze expression and activation of the Fluorescent Stoplight reporter construct. First, cells are gated using forward scatter area (FSC-A) and sideward scatter area (SSC-A). Then, single cells are selected based on SSC-A and sideward scatter height (SSC-H) signals. Thirdly, Stoplight+ reporter cells are measured and gated using FSC-A and mCherry signals. Lastly, eGFP+ cells are measured within mCherry+ cells FSC-A and eGFP signals. Representative flow cytometry plots are shown for untreated HEK293T Stoplight+ spCas9+ reporter cells (a), A five day co-culture of HEK293T Stoplight+spCas9+ reporter cells with sgRNA+ MDA-MB-231 donor cells expressing a non-targeting sgRNA (b), and a non-targeting sgRNA (c), HEK293T Stoplight+ spCas9+ reporter cells 3 days after transfection with a plasmid encoding a targeting sgRNA (d), and untreated sgRNA+ MDA-MB-231 donor cells (e), all from within the same experiment. Representative data as observed in 17 independent experiments.



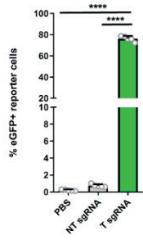
A



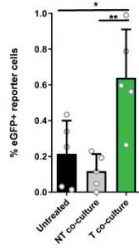
B



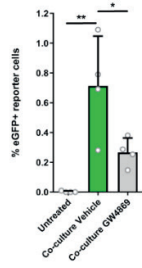
C



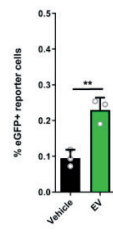
D



E

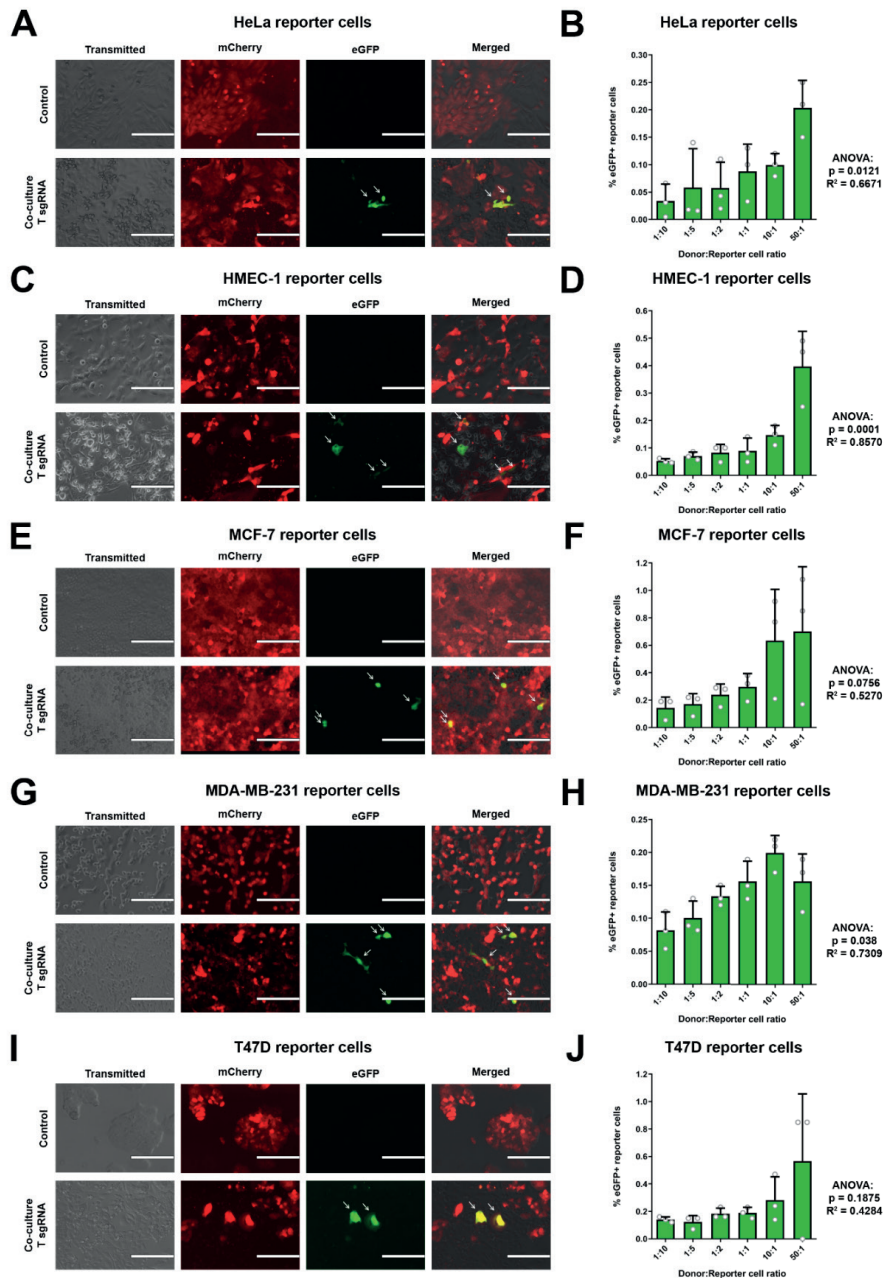


F

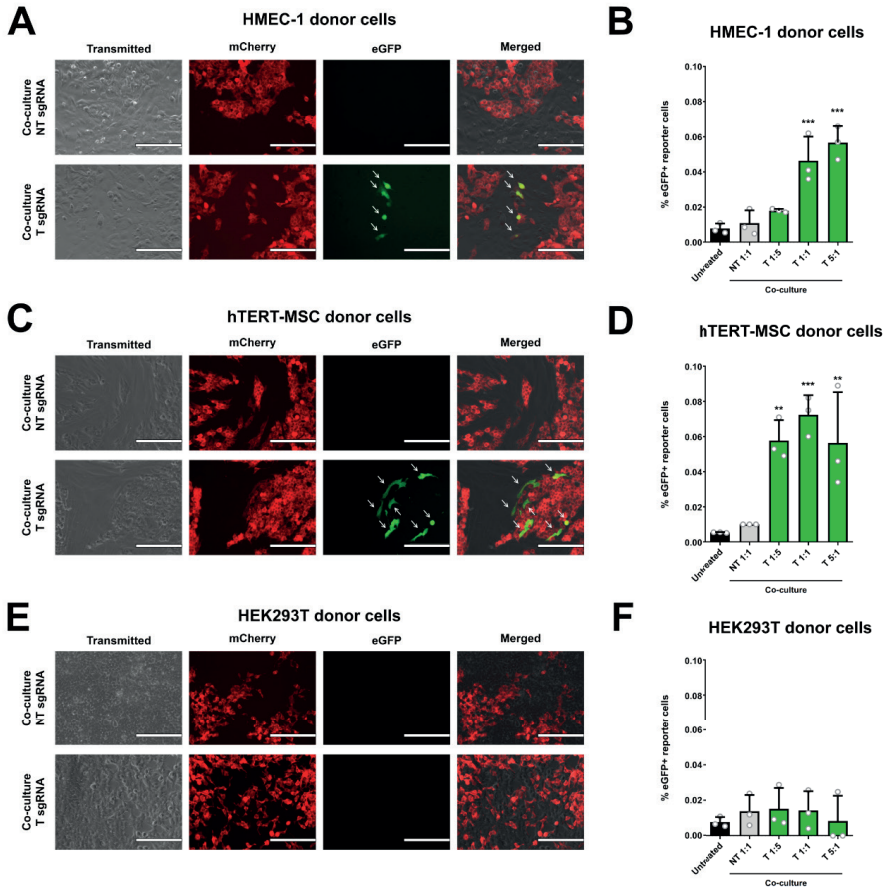


◀Supplementary Figure 3 | In silico confocal microscopy image analysis of the CROSS-FIRE system.

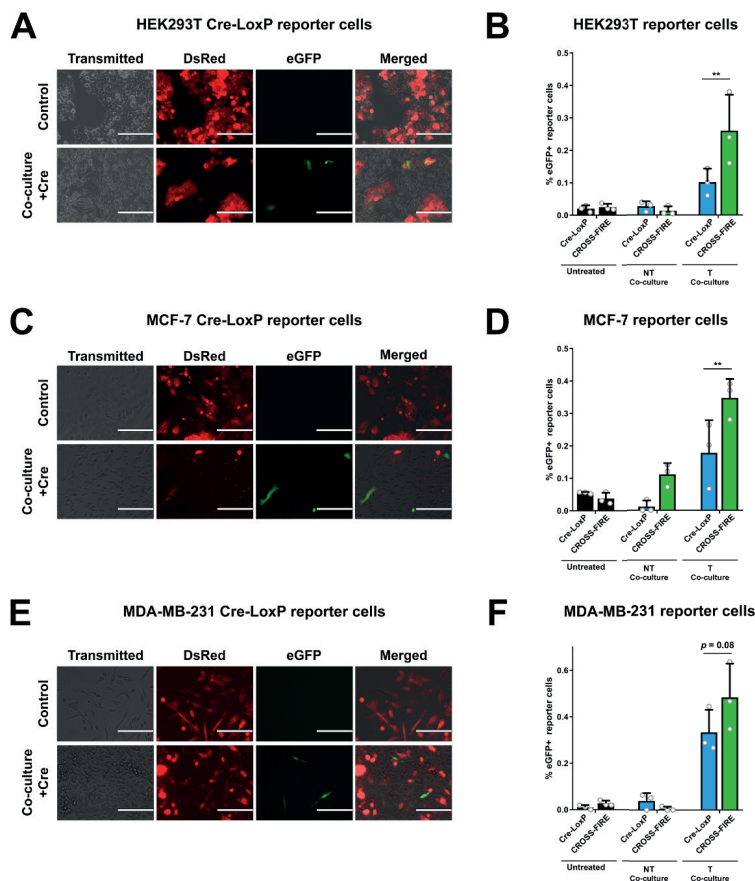
Confocal images were analyzed using the Columbus Image Data Storage and Analysis System. A workflow of the analysis is shown in (a). b, Representative images of a five day co-culture of HEK293T Stoplight+spCas9+ reporter cells with sgRNA+ MDA-MB-231 donor cells are shown to demonstrate the in silico analysis. From left to right, top to bottom, the following analyses are presented: 1, a merged confocal microscopy picture showing mCherry (red), eGFP (green) and Hoechst (blue); 2, detection of nuclei based on nuclear staining (Hoechst, gray); 3, selection of the areas directly surrounding the detected nuclei (Hoechst, gray) serves as a cytoplasm selection tool; 4, detection of nuclei (Hoechst, gray) positive for mCherry (red) in their respective cytoplasm region. Nuclei of mCherry-positive cytoplasm regions are marked in yellow; 5, detection of nuclei (Hoechst, gray) positive for eGFP (green) in their respective cytoplasm region. Nuclei of eGFP-positive cytoplasm regions are marked in yellow. Scale bar = 200 μ m. c Confocal microscopy image analysis of HEK293T Stoplight+ spCas9+ cells after transfection of a plasmid encoding a sgRNA targeting the Stoplight construct (+T sgRNA) or a non-targeting sgRNA (NT sgRNA) 3 days after transfection. Means + SD, n = 5 independent experiments, Tukey's multiple comparison test. d, Confocal microscopy image analysis of a five day co-culture of HEK293T Stoplight+ spCas9+ reporter cells with MDA-MB-231 sgRNA+ donor cells expressing a targeting sgRNA (T), and a non-targeting sgRNA (NT). Means + SD, n = 5 independent experiments, Tukey's multiple comparison test. e, Confocal microscopy image analysis of a five day direct co-culture experiment with MDA-MB-231 sgRNA+ donor cells with or without the presence of EV release inhibitor GW4869 at a concentration of 1 μ M. Means + SD n = 4 independent experiments, Tukey's multiple comparison test. f, Confocal microscopy image analysis of EV-mediated activation of the CROSS-FIRE platform using EVs isolated from sgRNA+ MDA-MB-231 donor cells, as compared to vehicle-treated reporter cells (PBS). EVs were added every 24 hrs for 6 additions with an average concentration of $2.2 \times 10^{11} \pm 6.1 \times 10^{10}$ EVs per addition. Means + SD, n = 3 biological replicates, treated with EVs from parallel isolations, Tukey's multiple comparison test. * = p < 0.05, ** = p < 0.01, **** = p < 0.01, *** = p < 0.01, **** = p < 0.05, ** = p < 0.01, *** = p < 0.01.



▲Supplementary Figure 4 | Functional intercellular sgRNA transfer to multiple additional reporter cell lines. sgRNA⁺ MDA-MB-231 donor cells were cultured in various donor : reporter cell ratios with multiple additional Stoplight⁺ spCas9⁺ reporter cell lines for five days: HeLa (a,b), HMEC-1 (c,d), MCF-7 (e,f), MDAMB-231 (g,h) and T47D (i,j). Co-cultures were analyzed by fluorescence microscopy (a,c,e,g,i) and flow cytometry (b,d,f,h,j). Scale bar represents 200 μ m. Means + SD, n =3 independent experiments, ANOVA.

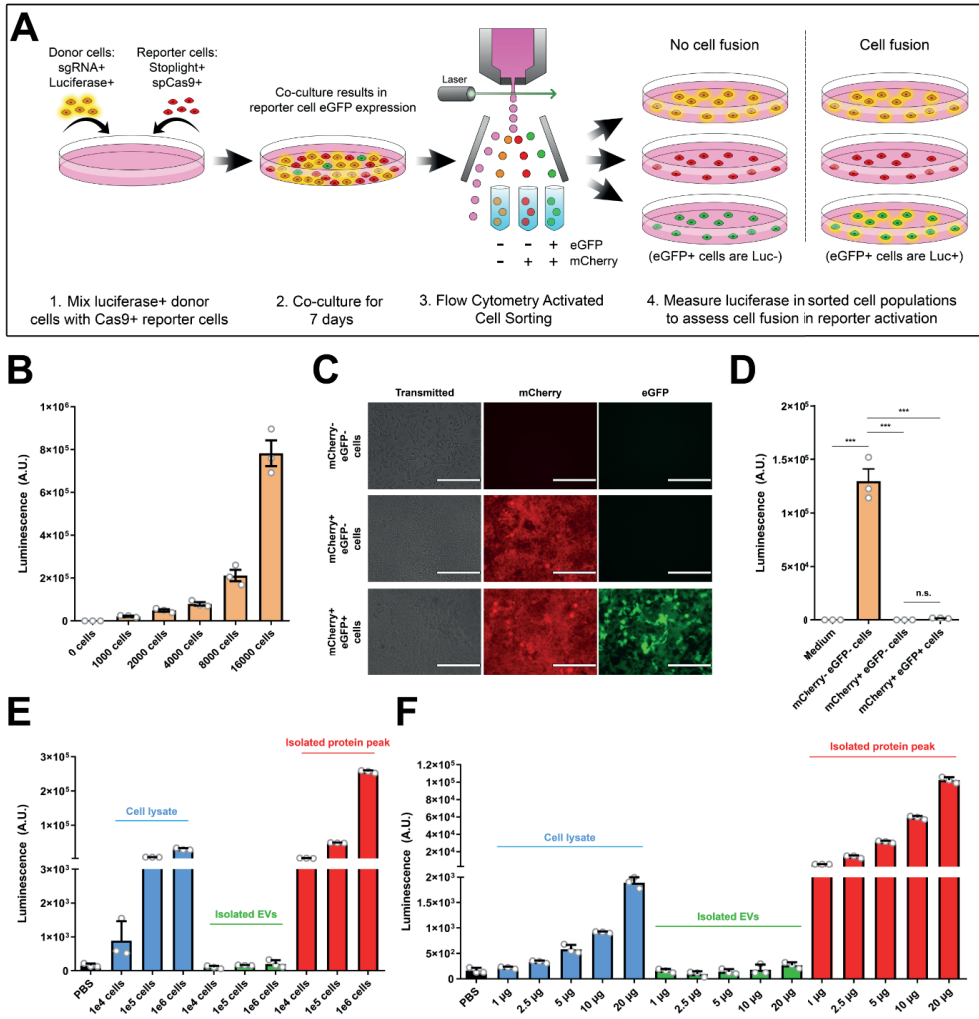


▲Supplementary Figure 5 | Functional intercellular sgRNA transfer by multiple additional donor cell lines. Stoplight+ spCas9+ HEK293T reporter cells were cultured with various sgRNA+ donor cell lines in a multiple ratios expressing targeting or non-targeting sgRNAs for five days: HMEC-1 (a,b), hTERT-MSC (c,d), and HEK293T (e,f). Co-cultures were analyzed by fluorescence microscopy (a,c,e) and flow cytometry (b,d,f). Scale bar represents 200 μ m. Means + SD, n = 3 independent biological samples, Dunnett's multiple comparison test. ** = p < 0.01, *** = p < 0.001.

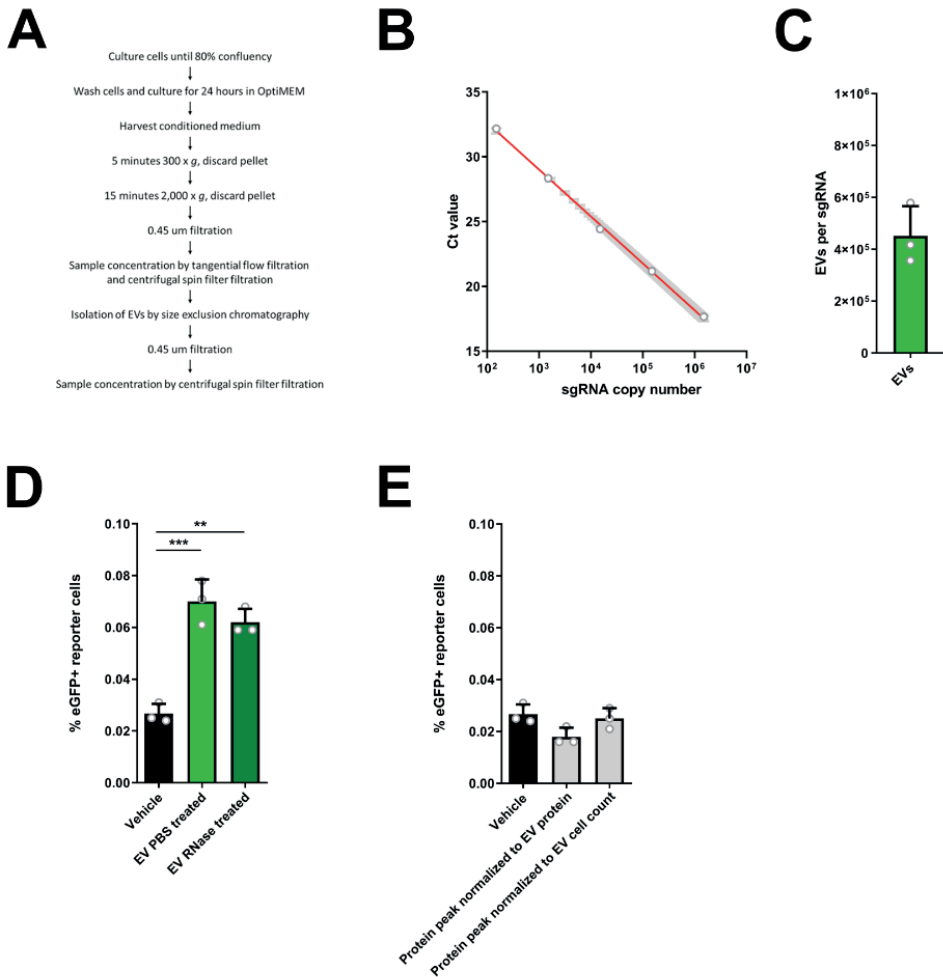


▲Supplementary Figure 6 | CROSS-FIRE reporter activation is not mediated by cellular fusion.

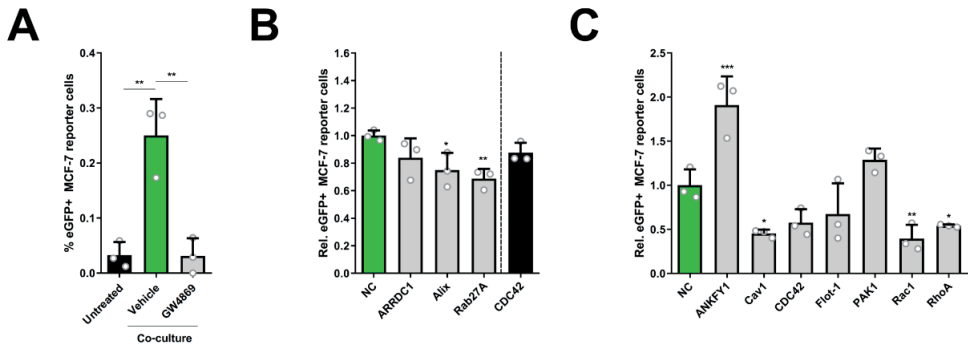
a, Schematic of the experimental set up to study the potential role of cellular fusion in reporter activation. Gaussia Luciferase+ sgRNA+ MDA-MB-231 donor cells and Stoplight+ spCas9+ reporter cells are cultured in standard co-culture conditions for 7 days, resulting in reporter cells activation (eGFP expression). Cells are then harvested and subjected to fluorescence activated cell sorting in which 3 cell populations will be collected: donor cells (eGFPmCherry⁻), non-activated reporter cells (eGFPmCherry⁺), and activated reporter cells (eGFP+ mCherry⁺). These 3 populations are then analyzed for luciferase activity. If reporter activation is not the result of cellular fusion, only the eGFPmCherry⁻ population will display luciferase activity (section 4, left), whereas cellular fusion would also result in luciferase activity in the eGFP+ mCherry⁺ population (section 4, right). **b,** Confirmation of luciferase activity in the supernatant of Gaussia Luciferase+ sgRNA+ stable MDA-MB-231 donor cells. Means + SD, n = 3 technical replicates, data representative of 2 independent experiments. **c,** Fluorescence microscopy pictures of plated eGFPmCherry⁻, eGFPmCherry⁺, and eGFP+ mCherry⁺ cell populations isolated by fluorescence activated cell sorting after a 7-day co-culture. Scale bar represents 200 μ m. **d,** A luciferase activity assay on conditioned medium of 10,000 plated eGFPmCherry⁻, eGFPmCherry⁺, and eGFP+ mCherry⁺ cells after a seven day co-culture only shows luciferase activity in eGFPmCherry⁻ cells. Means + SD, n = 3 biological replicates, Tukey's multiple comparison test. **e, f,** A luciferase activity assay on Gaussia Luciferase+ sgRNA+ MDA-MB-231 donor cell lysates, alongside EVs and proteins isolated simultaneously from conditioned medium by size exclusion chromatography using 10 kDa tangential flow filtration and kDa Amicon Ultra-15 Centrifugal filters, as normalized for producing cell count (e) or BCA protein measurement (f). Means + SD, n = 3 technical replicates. *** = p



▲ Supplementary Figure 7 | Characterization of EV-associated sgRNA. a, Overview of the applied workflow for EV isolation. b, qPCR of a concentration curve of synthetic CROSS-FIRE targeting sgRNAs after having undergone TRIzol RNA isolation and cDNA synthesis equal to, and alongside, RNA isolation and cDNA synthesis from sgRNA+ MDA-MB-231-derived EVs. c, Quantification of the amount of sgRNA per sgRNA+ MDA-MB-231-derived EV, based on qPCR alongside the sgRNA concentration curve (b) and NTA Nanosight Nanoparticle Tracking Analysis (NTA). Means + SD, n = 3 independent biological samples. d,e, Flow cytometry analysis of activation of the CROSS-FIRE platform using EVs (d) or the soluble protein-containing fractions (e) isolated from sgRNA+ MDA-MB-231 donor cells by size exclusion chromatography using 10 kDa tangential flow filtration and 10 kDa Amicon Ultra-15 Centrifugal filters, as compared to vehicle-treated reporter cells (PBS). EVs were incubated for 30 minutes at 37°C in PBS with or without 10 µg/ml RNase A, and were added every 24 hrs for 6 additions with an average concentration of $2.2 \times 10^{11} + 6.1 \times 10^5$ EVs per addition. Added protein was either normalized for EV protein content based on BCA protein measurement, or for producing cell count. Means + SD, n = 3 biological replicates, treated with EVs from parallel isolations, Tukey's multiple comparison test. ** = $p < 0.01$, *** = $p < 0.001$.

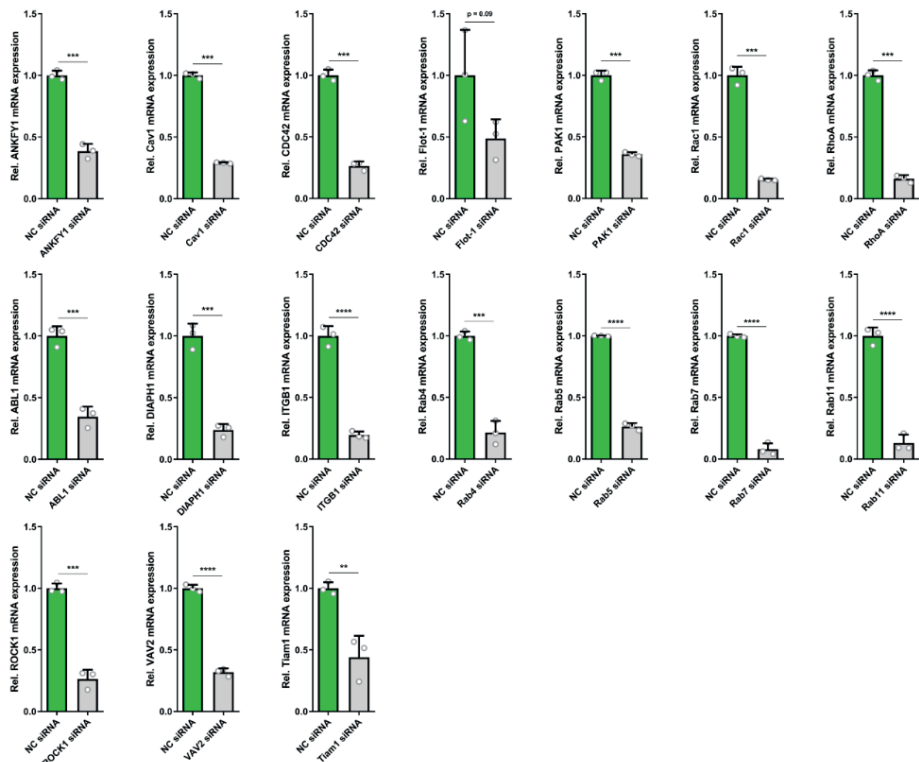


▲Supplementary Figure 8 | Confirmation of EV-mediated sgRNA transfer in Stoplight+ spCas9+ MCF-7 reporter cells. a, Flow cytometry analysis of a five day direct co-culture experiment with EV release inhibitor GW4869 at a concentration of 1 μM. Means + SD, n = 3 independent experiments, Tukey's multiple comparison test. b, Flow cytometry analysis of HEK293T Stoplight+ spCas9+ reporter cells after a five day co-culture with sgRNA+ MDA-MB-231 donor cells subjected to siRNA-mediated KD of ARDC1, Alix, Rab27A, and CDC42, alongside a non-coding control siRNA (NC). Means + SD, n = 3 independent experiments, Dunnett's multiple comparison test. c, Flow cytometry analysis of MCF-7 reporter cells after a 5-day co-culture with sgRNA+ MDA-MB-231 donor cells, in which the reporter cells were subjected to siRNA-mediated KD of ANKFY1, Cav1, CDC42, Flot-1, PAK1, Rac1, and RhoA alongside a noncoding control siRNA (NC). Means + SD, n = 3 independent experiments, Dunnett's multiple comparison test. * = p < 0.05, ** = p < 0.01, *** = p

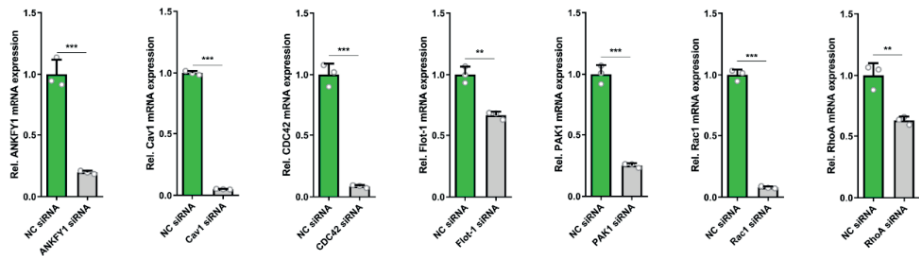


▲Supplementary Figure 9 | Analysis of the Cre-LoxP reporter system for EV cargo transfer. a,c,e, Fluorescence microscopy pictures of HEK293T (a), MCF-7 (c), or MDA-MB-231 (e) Cre-LoxP reporter cells (CMV-DsRed-LoxP-eGFP-LoxP) cultured for 5 days without (Control) or co-cultured with Cre+ MDA-MB-231 donor cells. Scale bar = 200 μ m. b,d,f, Flow cytometry analysis of HEK293T (b), MCF-7 (d), or MDA-MB-231 (f) Stoplight+ spCas9+ reporter cells (CROSS-FIRE) or Cre-LoxP reporter cells after a five day direct co-culture experiment with their respective MDA-MB-231 non-targeting (NT) or targeting (T) donor cells. CROSS-FIRE and Cre-LoxP donor cells were used as NT donor cells for the opposite reporter system, respectively. Means + SD, n =3 biologically independent samples, Sidak's multiple comparisons test. ** = $p < 0.01$.

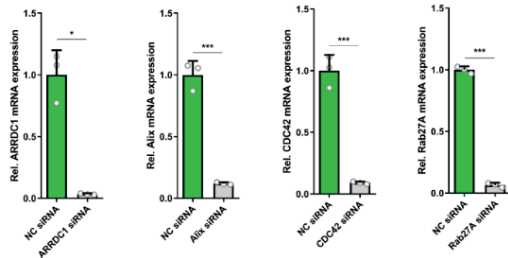
A



B



C



◀**Supplementary Figure 10 | Confirmation of siRNA-mediated gene knockdown by qPCR.** a, qPCR analysis of Stoplight+ Cas9+ HEK293T cells transfected with siRNAs targeting genes involved in the regulation of EV uptake, 72 hours after siRNA transfection. Gene expression levels were normalized to GAPDH housekeeping levels. Means + SD, n = 3 biologically independent samples, Student's t-test. b, qPCR analysis of Stoplight+ Cas9+ MCF-7 cells transfected with siRNAs genes involved in the regulation of EV uptake, 72 hours after siRNA transfection. Gene expression levels were normalized to GAPDH housekeeping levels. Means + SD, n = 3 biologically independent samples, Student's t-test. c, qPCR analysis of sgRNA+ MDA-MB-231 cells transfected with siRNAs targeting genes involved in EV release and tunneling nanotube formation, 72 hours after siRNA transfection. Gene expression levels were normalized to GAPDH housekeeping levels. Means + SD, n = 3 biologically independent samples, Student's t-test. * = p < 0.05, ** = p < 0.01, *** = p

Supplementary Table 1: Stoplight reporter construct:

Stoplight reporter construct	<p>atggtgagcaaggcgaggaggataacatggccatcatcaaggagttcatgctgctcaagggtgcacatggagggctccgtgaacggccacgagttcgagatcgaggcgaggcgaggcgccctacgagggcacccagaccgccaagctgaaggtgaccaagggtggccccctgcccttcgctgggacatcctgtccctcagttcatgtacggtccaaggcctacgtgaagcaccccgccgacatcccgactacttgaagctgtccttcccgagggtcctcaagtgggagcgctgatgaacttcgaggacggcggtggtgacctgacccaggactcctcctgaggacggcgagttcatctacaagtgaaagctgcgaggcaccaacttccctccgacggccccgtaatgcagaagaagacgatgggtggaggcctcctccgagcggatgtacccgaggacggcgccctgaaggcgagatcaagcagaggctgaagctgaaggacggcgccactacgacgtgaggtcaagaccctacaaggccaagaagcccgctgagctgcccgcgctacaacgtcaacatcaagttggacatcacctcccacaaggactacacatcgtggaacagtagcaacgcgccgaggggccactccaccggcgcatggacgagctgtacaagtgaaagcagaccctgaacttgc atctgctgaagctggccggcgatgtggagagcaaccgggcccgtagccgactcgagcggagtagtctctcctcgatcggagtagtctcctcgcgaattccggagtagtctcctcgaagacgctgcagtagtgagcaagg gcgaggagctgttaccgggggtggtcccatcctggtcagctggacggcgacgtaaacggccacaagttcagctgtccggcgaggggcgaggcgatgccactacggcaagctgacctcagctgaccaccggcga agctgccctgacctgcccaccctctgaccaccctgacctacggcgtgagtgcttcagccgctacccggac cacatgaagcagcacgacttctcaagtccgcatgccgaaggctacgtccaggagcgcacatcttctcaaggacgacgcaactacaagaccgctgcgaggtgaagttcgaggggcgacacctggtgaaccgcatcga gctgaaggcatcgacttcaaggaggacggcaacatcctggggcacaagctggagtacaactacaacagcc acaactctatatcatggccgacaagcagaagaacggcatcaagtgaaactcaagatccgccacaacatc gaggacggcagcgtgcagctgcgaccactaccagcagaacacccccatcgcgacggccccgtgctgctg cccgacaaccactactgagcaccagctccgctgagcaagaccccaacgagaagcgcgatcacatggt cctgctggagttcgtgaccgccgggatcactctcggcatggacgagctgtacaagtgtgaagcagaccct gaacttcca tctgctgaagctggccggcgatgtggagagcaaccgggcccattgtagtaaggcgaggga gcttccacggggtcgtgctatactggtgaaactgacgtgacgtgaaacggacacaacttctgtgagcggagaagg agagggtgatgccacttacggaaaactgacctgaagttatgtaccacggaaaagttgccgttccatggcc cactctgtgacgacctgacctatggggtccaatgcttcagccgctatcccgatcatgaaacaacag acttctcaaaagtgccatgccagaggatattgagcaggagcggaccatctttaaagacgatggaattac aaaaacgagcagaagtttaagttgaggggatacgttggtgaataggatagaacttaaaggtattgatttaa agaagatggcaatatttgggacacaagctggagtaacaattacaattctcaaatgtttatcatggcggaaca aaaaaagaatggcattaaggtgaaacttaagattagacataatcagggacggaagcgtccaacttccgac cactatcaacagaatacggcctcggcaggtcctctcctcctcggacaaccattactgtccactcagtc cgacttgcacaagatccaatgagaaaagatcatatggtcctgctggagttcgtcactgcggcggcgata acactcgggatgatgagctttataataa</p>
------------------------------	---

Legend: mCherry F2A domain Linker sgRNA PAM site sgRNA targeting sequence Stop codon eGFP1 eGFP2

Supplementary Table 5: Commercial siRNAs

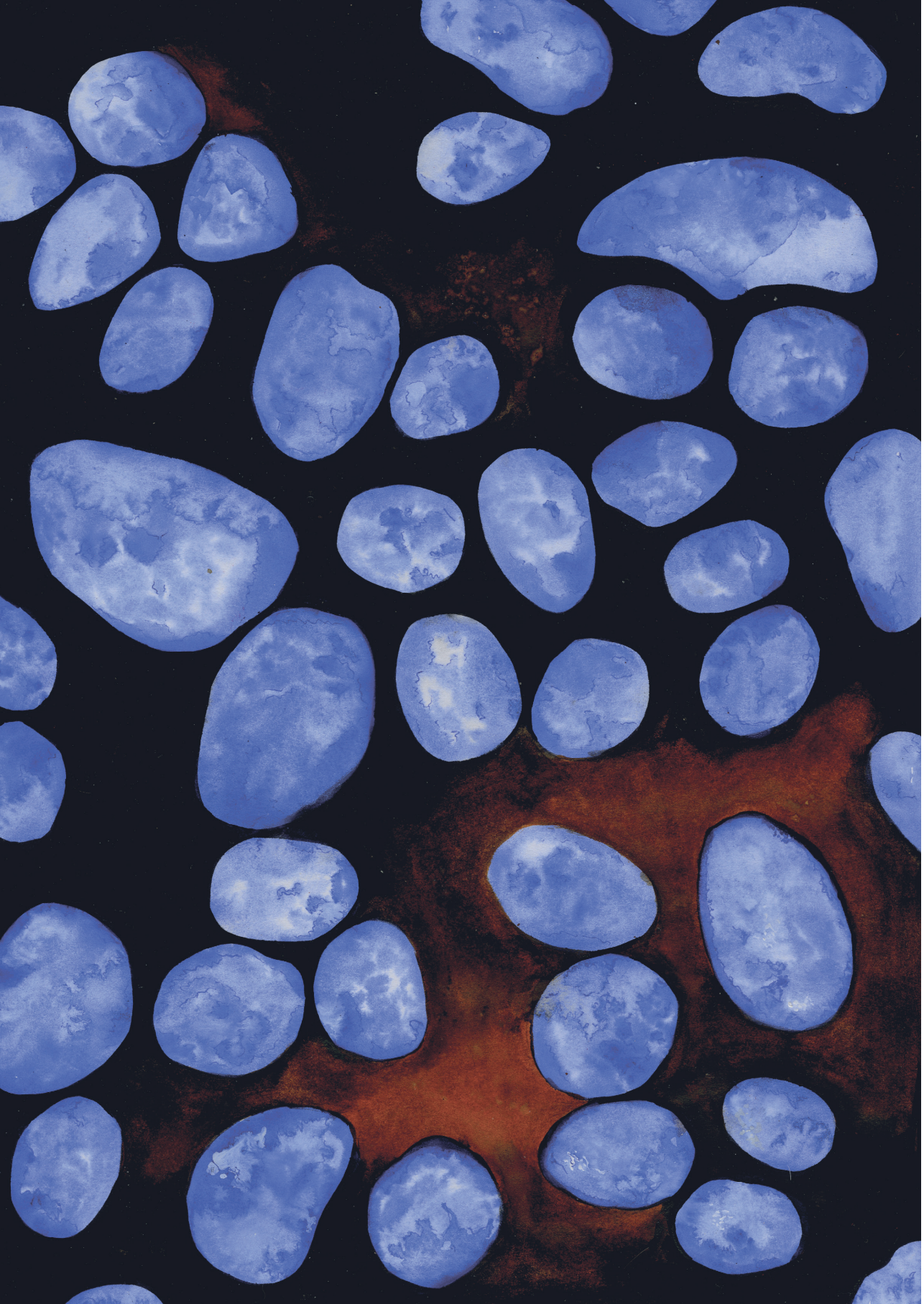
Target Non Coding	Product type siRNA	Product nr. 51-01-14-04	Company Integrated DNA Technologies
ABL1	ON-TARGETplus Smartpool	L-003100-00-0005	Horizon Discovery LTD
Alix	ON-TARGETplus Smartpool	L-004233-00-0005	Horizon Discovery LTD
ANKFY1	ON-TARGETplus Smartpool	L-013161-00-0005	Horizon Discovery LTD
ARRDC1	ON-TARGETplus Smartpool	L-015918-02-0005	Horizon Discovery LTD
DIAPH1	ON-TARGETplus Smartpool	L-010347-00-0005	Horizon Discovery LTD
ITGB1	ON-TARGETplus Smartpool	L-004506-00-0005	Horizon Discovery LTD
PAK1	ON-TARGETplus Smartpool	L-003521-00-0005	Horizon Discovery LTD
Rab4	ON-TARGETplus Smartpool	L-008539-00-0005	Horizon Discovery LTD
Rab5	ON-TARGETplus Smartpool	L-004009-00-0005	Horizon Discovery LTD
Rab7	ON-TARGETplus Smartpool	L-010388-00-0005	Horizon Discovery LTD
Rab11	ON-TARGETplus Smartpool	L-004726-00-0005	Horizon Discovery LTD
Rab27a	ON-TARGETplus Smartpool	L-004667-00-0005	Horizon Discovery LTD
ROCK1	ON-TARGETplus Smartpool	L-003536-00-0005	Horizon Discovery LTD
Tiam1	ON-TARGETplus Smartpool	L-003932-00-0005	Horizon Discovery LTD
VAV2	ON-TARGETplus Smartpool	L-005199-00-0005	Horizon Discovery LTD

Supplementary Table 6: qPCR primers

Target	Orientation	Sequence
ABL1	Forward	5'-TGAAAAGCTCCGGTCTTAGG-3'
	Reverse	5'-TTGACTGGCGTGATGTAGTTG-3'
Alix	Forward	5'-ATCGCTGCTAAACATTACCAAGT-3'
	Reverse	5'-AGGGTCCCAACAGTATCTGGA-3'
ANKFY1	Forward	5'-CCATCGTGGCAGACCTCTAC-3'
	Reverse	5'-AGTGGAAGACAAGTTAGCCAGA-3'
ARRDC1	Forward	5'-TAGTGGAGGAGGGTTACTTCAAC-3'
	Reverse	5'-TCTGGGATGCTGTTCAAGTTC-3'
Cav1	Forward	5'-CATCCCGATGGCACTCATCTG-3'
	Reverse	5'-TGCACTGAATCTCAATCAGGAAG-3'
DIAPH1	Forward	5'-CAGTTGGGTGCAAACATTTGG-3'
	Reverse	5'-TCCGGCTATCGTAACTCCCAG-3'
CDC42	Forward	5'-CCATCGGAATATGTACCGACTG-3'
	Reverse	5'-CTCAGCGGTCGTAATCTGTCA-3'
Flot-1	Forward	5'-GCCCTGCATCCAACAGATCC-3'
	Reverse	5'-AATGCCAGTGACTGAGATGGG-3'
GAPDH	Forward	5'-ACAGTCAGCCGCATCTTC-3'
	Reverse	5'-GCCCAATACGACCAAATCC-3'
ITGB1	Forward	5'- CCTACTTCTGCACGATGTGATG-3'
	Reverse	5'- CCTTTGCTACGGTTGGTTACATT-3'
PAK1	Forward	5'-AGGGGAGTTTACGGGAATGC-3'
	Reverse	5'-TCTTCTGCTCCGACTTAGTGATA-3'
Rab27a	Forward	5'-GCTTTGGGAGACTCTGGTGTA-3'
	Reverse	5'-TCAATGCCCACTGTTGTGATAAA-3'
Rab4	Forward	5'-GTCCGTGACGAGAAGTTATTACC-3'
	Reverse	5'-TGAGCGCACTGTTTCCAAA-3'
Rab5	Forward	5'-CAAGGCCACCTAGCAAATAA-3'
	Reverse	5'-GATGTTTTAGCGGATGTCTCCAT-3'
Rab7	Forward	5'-TACAAAGCCACAATAGGAGCTG-3'
	Reverse	5'-GCAGTCTGCACCTCTGTAGAAG-3'
Rab11	Forward	5'-CAACAAGAAGCATCCAGGTTGA-3'
	Reverse	5'-GCACCTACAGCTCCACGATAAT-3'
Rac1	Forward	5'-ATGTCCGTGCAAAGTGGTATC-3'
	Reverse	5'-CTCGGATCGCTTCGTCAAAACA-3'
RhoA	Forward	5'-GGAAAGCAGGTAGAGTTGGCT-3'
	Reverse	5'-GGCTGTCGATGGAAAAACAT-3'
ROCK1	Forward	5'-AACATGCTGCTGGATAAATCTGG-3'
	Reverse	5'-TGTATCACATCGTACCATGCCT-3'
Tiam1	Forward	5'-GATCCACAGGAAGTCCGAAGT-3'
	Reverse	5'-GCTCCGAAGTCTTCTAGGGT-3'
VAV2	Forward	5'-CTGTTTGACCCCTTTGACCTC-3'
	Reverse	5'-GACGCAGTCGTAGATGTCCTC-3'
Targeting sgRNA	Forward	5'-CAGTACTCCGCTCGAGTGTT-3'
	Reverse	5'-GACTCGGTGCCACTTTTTCAA-3'

SUPPLEMENTARY REFERENCES

1. Shen, M. W. et al. Predictable and precise template-free CRISPR editing of pathogenic variants. *Nature* **563**, 646–651 (2018) DOI: 10.1038/s41586-018-0686-x.
2. Costa Verdera, H., Gitz-Francois, J. J., Schiffelers, R. M. & Vader, P. Cellular uptake of extracellular vesicles is mediated by clathrin-independent endocytosis and macropinocytosis. *J. Control. Release* **266**, 100–108 (2017) DOI: 10.1016/j.jconrel.2017.09.019.



NATURAL OR SYNTHETIC RNA DELIVERY: A STOICHIOMETRIC COMPARISON OF EXTRA-CELLULAR VESICLES AND SYNTHETIC NANOPARTICLES

Daniel E. Murphy^a, Olivier G. de Jong^a, Martijn J. W. Evers^a,
Maratussholikhah Nurazizah^a, Raymond M. Schiffelers^a,
Pieter Vader^{a,b}

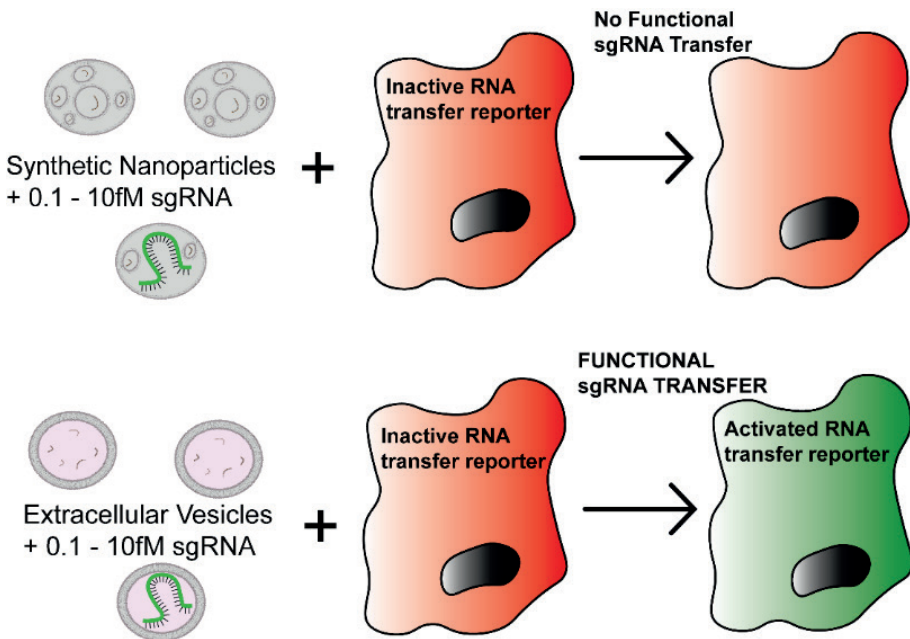
a: CDL Research, University Medical Center Utrecht, Utrecht, the
Netherlands

b: Department of Experimental Cardiology, University Medical
Center Utrecht, Utrecht, the Netherlands

**ACS Nano Letters. 2021, 21, 4, 1888–1895,
Publication Date: February 11, 2021**

ABSTRACT

RNA therapeutics have high potential which is yet to be fully realized, largely due to challenges involved in the appropriate delivery to target cells. Extracellular vesicles (EVs) are lipid bound nanoparticles released by cells of all types and possess numerous features that may help overcome this hurdle and have emerged as a promising RNA delivery vehicle candidate. Despite extensive research into the engineering of EVs for RNA delivery, it remains unclear how the intrinsic RNA delivery efficiency of EVs compares to currently used synthetic RNA delivery vehicles. Using a novel CRISPR/Cas9-based RNA transfer reporter system, we compared the delivery efficiency of EVs to clinically approved state-of-the-art DLin-MC3-DMA lipid nanoparticles and several *in vitro* transfection reagents. We found that EVs delivered RNA several orders of magnitude more efficiently than these synthetic systems. This finding supports the continued research into EVs as potential RNA delivery vehicles.



RNA therapeutics possess great therapeutic potential as they target disease at its genetic source in a highly selective manner¹. In order to function, RNA therapeutics must reach therapeutic concentrations within the cytosol of specific target cells. However, numerous obstacles prevent therapeutic RNA from reaching its site of action. For example, free circulating RNA is subject to renal clearance while extracellular RNases degrade unprotected RNA². Even if an RNA molecule is able to reach its target cell it remains unable to cross the plasma membrane due to its large size and charge³.

To bypass these barriers therapeutic RNA cargo can be delivered inside synthetic nanoparticle (NP) carriers such as lipid nanoparticles (LNPs) which protect the delicate RNA from degradation and facilitate uptake into recipient cells⁴. However, synthetic systems are hindered by their own set of challenges. They can be highly immunogenic⁵ and are subject to uptake and clearance by Kupffer cells of the liver⁶. Furthermore, upon cellular uptake, most NPs are destined for lysosomal degradation⁷.

Extracellular vesicles (EVs) are lipid bound NPs of biological origin. They are released from all cell types, range from 30-2000 nm in diameter⁸ and are involved in intercellular transfer of biological cargo, including RNA⁹. Potentially, EVs could avoid the toxicity and immunogenicity which hamper the use and development of clinically effective synthetic NPs¹⁰. In addition, EVs have been shown to be capable of crossing biological barriers and possess endogenous targeting ability¹¹. These features make EVs an interesting candidate for an RNA delivery vehicle. The concept of hijacking this endogenous RNA transfer system to deliver therapeutic RNAs is an attractive one but despite their advantages, EVs – like synthetic NPs – must bypass cellular barriers in order to release their cargo to the cytosol.

There are numerous examples of EVs functionally delivering RNA in (patho)physiology. A striking example is that of hsa-miR-21, which is relatively highly abundant in EV preparations. The EV-mediated transfer of hsa-miR-21 is strongly implicated in tumor growth and progression^{12,13,16}. It has been speculated that to achieve this functional delivery, EVs must be highly efficient at bypassing cellular barriers¹⁴ as RNA loading of even the most abundant miRNAs is as low as 1 copy per 100 EVs with other miRNAs present in quantities several orders of magnitude lower¹⁵. For example, despite the suggested pathophysiological function of EV-associated hsa-miR-21, the loading of this RNA into the relevant EVs has been found to be far lower than 1 copy per particle¹⁶. Such analyses of the stoichiometry of functional RNA in EVs are rare meaning the efficiency of EV-mediated RNA transfer remains unclear.

This lack of clarity is partly due to the absence of a suitable assay to allow for the appropriate stoichiometric study of EV-mediated RNA delivery with sufficient sensitivity¹⁷. siRNA or miRNA-mediated gene knockdown as a read-out for RNA delivery is insensitive as it relies on the bulk measurement of cell populations. The Cre recombinase reporter assay used to demonstrate the EV-mediated transfer of mRNA both *in vitro* and *in vivo*¹⁸ is able to detect the transfer of mRNA with single-cell resolution. However, it can also be activated by the transfer of miniscule quantities of Cre protein derived from donor cell translation of Cre mRNA¹⁷, the presence of which has been confirmed in Cre mRNA⁺ EVs¹⁹. In addition, experiments assessing the functional transfer of RNA by EVs based on phenotypical changes or expression of endogenous genes can be confounded by the fact that the simple addition of nanoparticles alters cellular behavior²⁰. To further study the efficiency of EVs, a highly sensitive reporter system with single-cell resolution which can only be activated by RNA transfer is required.

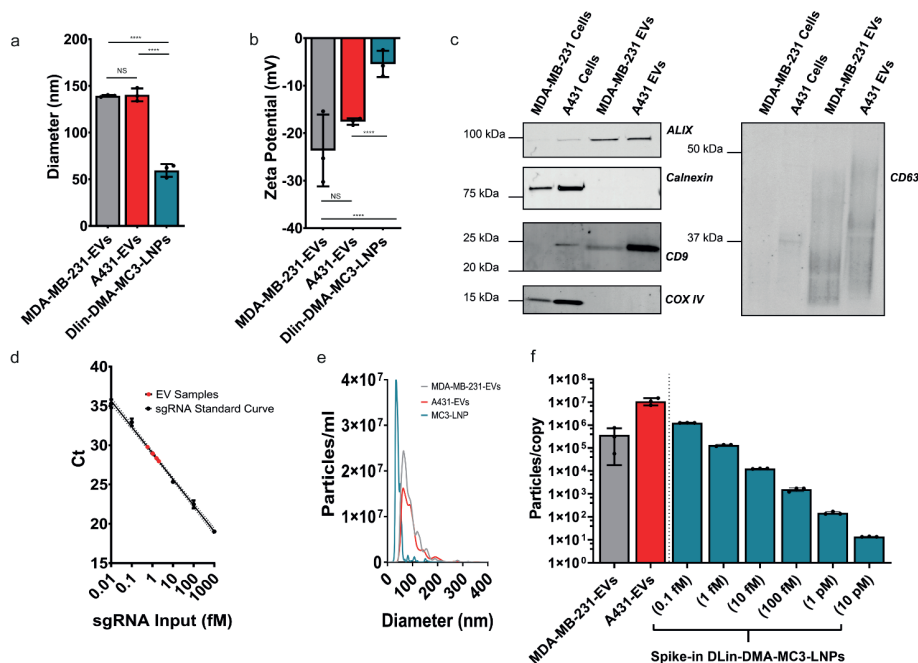
To address this need, we developed the highly sensitive and specific CRISPR Operated Stoplight System for Functional Intercellular RNA Exchange (CROSS-FIRE) reporter system. This system is only activated by the functional transfer of a specific sgRNA and allows the detection of EV-mediated RNA delivery at the single cell level (Figure S1)²¹. Here we use the CROSS-FIRE system to compare the delivery efficiency of EVs isolated from MDA-MB-231 and A431 cells to *in vitro* transfection reagents and state-of-the-art DLin-MC3-DMA-LNPs, which are the most advanced therapeutic RNA delivery system available and are used for clinical delivery of siRNAs targeting transthyretin under the name Onpatro® (Patisiran)²².

Firstly, EVs were isolated from both MDA-MB-231 and A431 cells using size exclusion chromatography. DLin-MC3-DMA LNPs were produced by microfluidic mixing. The sizes of these NPs were then determined using dynamic light scattering (DLS) (Fig 1a). MDA-MB-231-EVs and A431-EVs possessed mean diameters of 139±1nm and 140±7nm respectively. DLin-MC3-DMA-LNPs were smaller at 59±7 nm, which is comparable to Onpatro® which possesses a size of less than 100nm²³. This may be of significance as endocytosis of nanoparticles can be influenced by particle size, however also by other factors such as shape, rigidity and the presence of surface ligands²⁴.

To assess the surface charge of particles, zeta-potential analysis was performed (Fig 1b). As is typical of EVs, MDA-MB-231-EVs and A431-EVs possessed negative surface charges of -24±8 mV and -18±1mV respectively. In line with previously reported data²³, DLin-MC3-DMA-LNPs were close to neutral charge with a zeta-potential of -5±3mV. It should be noted that a positive charge is considered important for the endosomal fusion of LNPs and that while DLin-MC3-DMA-LNPs are neutrally charged at physiological pH,

they are known to be positively charged at endosomal pH. The mechanisms by which the negatively charged EVs fuse with endosomal membranes remains unclear, but may involve fusogenic proteins or lipids²⁵.

According to MISEV guidelines²⁶, Western blot analysis (Fig 1c) was used to confirm positive enrichment of EV markers CD9, CD63 and ALIX as compared to cell lysates. The organelle markers calnexin and COX IV were negatively enriched in EVs confirming an absence of cellular contamination.



▲Figure 1. Physical characterisation of NPs. DLS analysis of EVs and synthetic nanoparticles (a). Zeta-potentials of EVs and synthetic nanoparticles (b). Western blot analysis of MDA-MB-231 and A431 cell lysates alongside A431-EVs and MDA-MB-231-EVs for EV markers (ALIX, CD9, CD63) and EV-negative markers (Calnexin and Cox IV)(c). An RT-qPCR interpolation of sgRNA concentration in MDA-MB-231-EV samples from known sgRNA input standard measurements (d). Nanoparticle Tracking Analysis (NTA) size distributions of MDA-MB-231-EVs, A431-EVs and DLin-MC3-DMA-LNPs (e). Using RT-qPCR and NTA data, the number of EVs per single sgRNA was determined and plotted next to a similar number of particles per single sgRNA of spike-in DLin-DMA-MC3-LNPs used in comparative experiments (f). Means \pm SD are displayed, $n=3$ biological replicates, Tukey's multiple comparison test, $*=p<0.05$, $**=p<0.01$, $***=p<0.0001$.

To determine the concentration of sgRNA in EV samples, RT-qPCR was performed on sgRNA⁺ MDA-MB-231-EVs and A431-EVs alongside an extraction efficiency-corrected sgRNA standard curve. After RT-qPCR analysis, the sgRNA concentrations of EV samples were interpolated (Fig 1d). It should be also noted that we have previously demonstrated

that EV associated sgRNA is located within the EV lumen²¹. sgRNA was also confirmed to be stable inside all NPs using RT-qPCR as no reduction in sgRNA signal was observed after 24 hours of incubation at 4°C for any NP. After 24 hours of incubation at 37°C no reduction in sgRNA signal was observed in A431-EVs and DLin-DMA-MC3-LNPs while a slight but significant drop was observed in MDA-MB-231-EVs (Fig S2).

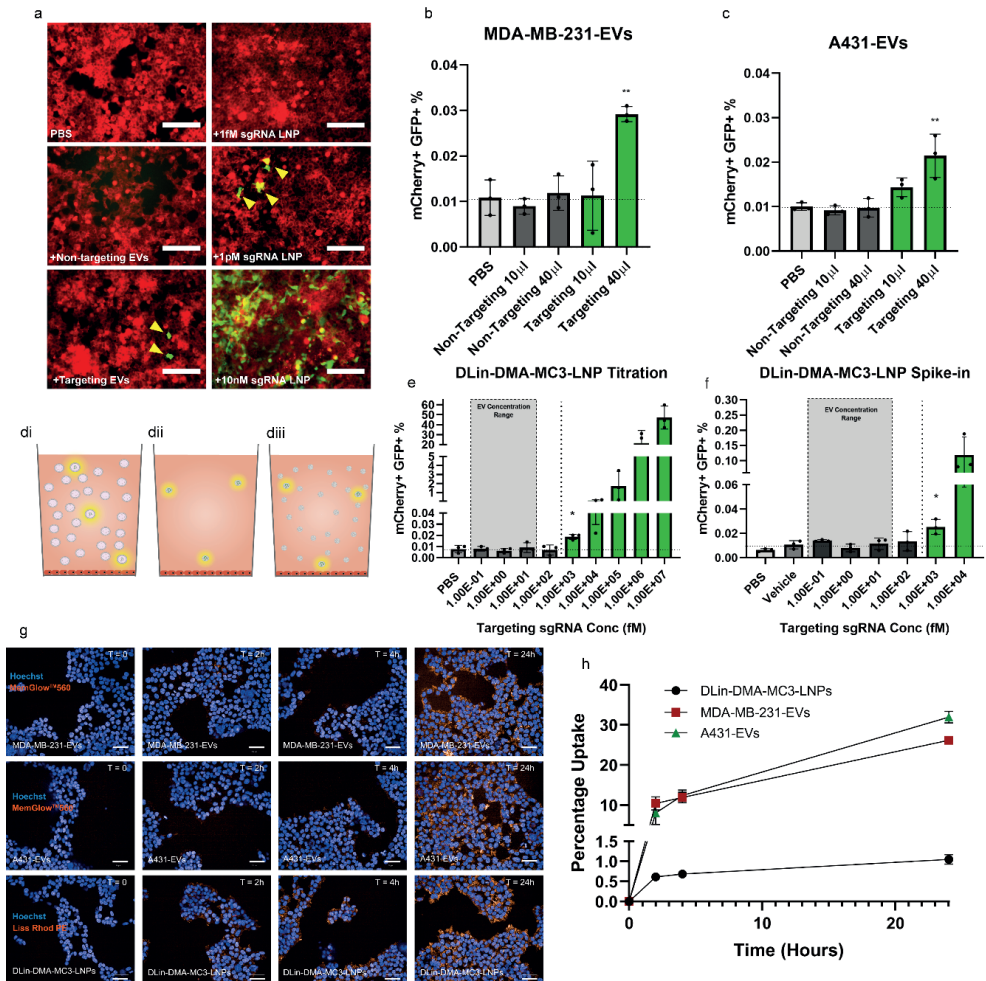
Using the sgRNA concentration values determined by RT-qPCR and particle concentrations measured by NTA (Fig 1e), the quantity of sgRNA per EV could be calculated. This showed that loading was extremely low with 1 sgRNA/ $3.6 \times 10^5 \pm 3.3 \times 10^5$ MDA-MB-231-EVs. sgRNA loading into A431 EVs was approximately 30-fold lower, with 1 sgRNA/ $1.1 \times 10^7 \pm 3.9 \times 10^6$ EVs (Fig 1f).

We then tested the ability of EVs to functionally deliver sgRNA. Despite low EV loading, we were able to observe GFP expression in HEK293T CROSS-FIRE reporter cells indicating activation upon 6 daily EV additions (Fig 2a). To demonstrate dose dependence, EVs were applied at two doses. Only the high dose of both EV types was sufficient to induce significant activation as compared to the vehicle control. To rule out non-specific activation, an equal dose of EVs containing a non-targeting sgRNA was also applied. These non-targeting controls showed no reporter cell activation (Fig 2b and c). In these experiments the average sgRNA high concentration for MDA-MB-231-EV additions was 2.3 ± 2.9 fM while the average A431-EV high concentration was considerably lower at 0.1 ± 0.04 fM. Additional parameters of this experiment can be seen in table 1.

The fact that EVs caused reporter activation at such low sgRNA concentrations suggests highly efficient delivery. We therefore compared EVs to a state-of-the-art RNA delivery vehicle, the DLin-MC3-DMA-LNP (Onpattro®).

DLin-MC3-DMA-LNPs containing targeting sgRNA were produced and a 10-fold serial dilution series from 10nM to 0.1fM sgRNA was prepared. This covered the average sgRNA concentration delivered per daily dose by both A431-EVs and MDA-MB-231-EVs which allowed for comparison of CROSS-FIRE activation between EVs and DLin-MC3-DMA-LNPs.

Although this approach allowed the direct comparison of absolute sgRNA concentration between EVs and LNPs, the LNP particle dose was considerably lower at the sgRNA concentrations functionally delivered by EVs. In order to achieve a more comparable sgRNA stoichiometry, DLin-MC3-DMA-LNPs batches were prepared in which the majority of the RNA cargo was composed of an inert scaffold while the sgRNA was spiked in to achieve final targeting sgRNA concentrations ranging from 10pM to 0.1fM. This allowed the sgRNA concentration to be titrated while particle dose remained comparable to EV particle doses (Table 1).



▲ Figure 2. EVs functionally deliver RNA at a concentration orders of magnitude lower than those required for synthetic NPs. Fluorescent microscopy images of Stoptlight⁺ spCas9⁺ HEK293T reporter cells after 6 consecutive daily additions of PBS, non-targeting sgRNA⁺, targeting sgRNA⁺ A431-EVs or 1fM, 1pM or 10nM sgRNA DLin-DMA-MC3-LNPs. Scale bars represent 150 μ m. Flow cytometry analysis of Stoptlight⁺ spCas9⁺ HEK293T reporter cells after 6 consecutive days of targeting sgRNA⁺ or non-targeting sgRNA⁺ MDA-MB-231-EV addition, (b) and 6 consecutive days of targeting sgRNA⁺ or non-targeting sgRNA⁺ A431-EV addition (c), n=3 biological replicates. A graphical representation of the sgRNA composition of samples used for comparative analysis (d): Low abundance of sgRNA copies in a large number of EVs (di), DLin-MC3-DMA-LNPs containing targeting sgRNA only at EV concentration levels (dii) and DLin-MC3-DMA-LNPs containing mainly inert scaffold with targeting sgRNA spiked in to mimic the sgRNA stoichiometry of EV samples (diii). Flow cytometry analysis of Stoptlight⁺ spCas9⁺ HEK293T reporter cells after 6 consecutive daily doses of DLin-MC3-DMA-LNPs containing targeting sgRNA at a range of 1E+07 fM to 1E-01 fM, n=3 biological replicates (e). Flow cytometry analysis of Stoptlight⁺ spCas9⁺ HEK293T reporter cells after 6 consecutive daily doses of LNP preparations containing a similar total particle dose to EV samples but with targeting sgRNA spiked in to achieve a targeting sgRNA concentration range of 1E+04 to 1E-01 fM, n=3 biological replicates (f). Confocal microscopy images of HEK293T cells at 0, 2, 4 and 24 hours after the addition of MemGlow[™] labelled MDA-MB-231-EVs, MemGlow[™] labelled A431-EVs or Lissamine-Rhodamine PE labelled DLin-DMA-MC3-LNPs (g). Percentage uptake of NPs determined using a fluorescent plate reader and interpolation from a background corrected standard curve, n=3 technical replicates (h). Means plus SD are displayed, Tukey's multiple comparison test was used for statistical analysis of both EV addition experiments and titrations, *p<0.05, **p<0.01 versus vehicle.

This is visualized in a simplified schematic (Fig 2d) in which sgRNA is delivered by a few highlighted EVs in a background of EVs containing no sgRNA (Fig 2di). An equal amount of sgRNA to that found in EV is preparations is delivered by a few highlighted LNP particles delivered from a highly diluted stock LNP preparation (Fig dii). To provide a more representative comparison between EVs and LNPs, an equal amount of sgRNA is delivered within a background of empty LNPs (Fig 2diii).

DLin-MC3-DMA-LNPs containing only sgRNA (Fig 2dii) produced a dose dependent response from 10nM to 1pM (Fig 2a,e). At 1pM, activation was 2.5 fold higher than background levels, which is a similar level of activation induced by EVs (Fig 2b,c). Below 1pM no activation was observed. This is in contrast to EVs, which were able to functionally deliver RNA at these lower concentrations.

When sgRNA was delivered via spike-in DLin-MC3-DMA-LNPs mimicking EV stoichiometry (Fig 2diii) significant activation was observed at 1pM sgRNA at a similar level to that seen in the direct titration. Again, at concentrations below this, no significant activation was observed (Fig 2f). Taken together, these results indicate that EV-mediated RNA delivery is at least two orders of magnitude more efficient than DLin-MC3-DMA-LNP-mediated RNA delivery.

Lastly, in order to allow comparison to commonly used *in vitro* transfection reagents, we also performed sgRNA titrations using the transfection reagents lipofectamine RNAiMax, 25 kDa linear polyethylenimine (PEI) and TransIT-2020. The minimal effective dose for lipofectamine RNAiMax and TransIT-2020 was 1pM and 10pM respectively. PEI induced a clear increase in reporter activation at 100pM, but a statistically significant minimal effective dose was not reached until 10nM due to large variation between experiments with this reagent (Fig S3).

These results show that EV-mediated RNA delivery is considerably more efficient than that of synthetic systems. This is demonstrated by the fact that the minimal effective DLin-MC3-DMA-LNP dose (1pM) was more than two orders of magnitude higher than the sgRNA dose required for significant reporter activation when sgRNA was delivered by MDA-MB-231-EVs (2.3fM). Furthermore, the sgRNA dose delivered by A431-EVs (0.1fM) was around four orders of magnitude lower than the DLin-MC3-DMA-LNP minimal effective dose, but was nevertheless capable of inducing significant activation.

There are multiple steps in the uptake and endosomal trafficking process at which EVs could achieve this efficiency. The first step in nanoparticle-mediated RNA delivery is

uptake into recipient cells and there is evidence that EVs may be more efficient at this process than synthetic NPs. For instance, doxorubicin loaded HEK293-EVs have been found to be taken up

Table 1: Parameters of synthetic nanoparticles and EV samples used for comparative experiments.

Sample	Daily sgRNA Concentration (fM)	Daily sgRNA Copy Number	Daily Particle Concentration (Particles/ml)	Daily Particle Dose	Particles/sgRNA
MDA-MB-231-EVs (High Dose)	2.3E00 (2.9E00)	3.3E05 (4.2E05)	1.04E11 (1.3E10)	2.6E10 (3.2E09)	3.6E05 (3.3E05)
A431-EVs (High Dose)	1.0E-01 (4E-02)	1.0E04 (5.4E03)	3.36E11 (9.00E10)	8.4E10 (2.3E10)	1.1E07 (3.9E06)
sgRNA only- DLin-MC3-DMA-LNPs	1.0E+07 – 1.0E-01	1.51 E12 - 1.51E04	2.16E11 (5.4E10) – 2.16E03 (5.4E02)	5.14E10 (1.3E10) - 5.14E02 (1.3E02)	3.0E-02
sgRNA spike-in-DLin-MC3-DMA-LNPs (10,000 fM)	1.0E+04	1.5E+09	8.0E10 (2.4E09)	2.0E10 (6.0E08)	1.4E01 (4.0E-01)
sgRNA spike-in-DLin-MC3-DMA-LNPs (1000 fM)	1.0E+03	1.5E+08	9.2E10 (1.5E09)	2.3E10 (3.7E08)	1.5E02 (2.4E01)
sgRNA spike-in-DLin-MC3-DMA-LNPs (100 fM)	1.0E+02	1.5E+07	8.8E10 (2.1E09)	2.2E10 (5.3E08)	1.5E03 (3.5E02)
sgRNA spike-in-DLin-MC3-DMA-LNPs (10 fM)	1.0E+01	1.5E+06	7.6E10 (2.5E09)	1.9E10 (6.2E08)	1.3E04 (4.1E02)
sgRNA spike-in-DLin-MC3-DMA-LNPs (1 fM)	1.0E+00	1.5E+05	8.0E10 (8.4E08)	2.0E10 (2.1E09)	1.3E05 (1.4E04)
sgRNA spike-in-DLin-MC3-DMA-LNPs (0.1 fM)	1.0E-01	1.5E+04	7.6E10 (6.4E08)	1.9E10 (1.6E08)	1.3E06 (1.1E04)
Scaffold RNA only- DLin-MC3-DMA-LNPs	0.0E+00	0.0E+00	7.2E10 (1.64E09)	1.8E10 (4.1E08)	N.A

Standard deviations are shown in brackets where applicable.

more rapidly by HEK293 cells and deliver more doxorubicin to the cytosol than a liposome-loaded doxorubicin formulation²⁷. Furthermore, EV-mimicking liposomes which possessed a lipid composition resembling that of EVs show threefold higher rates of cellular uptake as compared to conventional PC-Chol liposomes²⁸. Therefore, to determine the extent to which uptake efficiency contributed to the differences in RNA delivery efficiency between EVs and DLin-DMA-MC3-LNPs, we compared the uptake of these particles.

To allow visualization and quantification of uptake, MDA-MB-231-EVs and A431-EVs were

labelled with MemGlow™ 560 and DLin-DMA-MC3-LNPs were produced containing 0.2% Lissamine Rhodamine PE. HEK293T cells were then seeded at the same density used in the aforementioned addition experiments. These cells were then treated with a similar particle dose of NPs as used in these experiments. Fluorescent signal was observed inside cells for all NPs after 2 hours and this signal further increased in intensity after 4 and 24 hours (Fig 2g), confirming uptake.

To compare the uptake efficiency between these NPs, HEK293T cells were dosed using the same setup used for the confocal microscopy experiment at 24, 4 and 2 hours prior to measurement. The percentage of particles taken up was then determined by comparing the fluorescent intensity in lysed cells to a background corrected standard curve (Fig 2h). It was determined that roughly 10% of both the total MDA-MB-231-EV and A431-EV dose had been taken up after 2 hours and after 24 hours this had increased to 26% and 32% respectively. In contrast, after 2 hours only 0.6% of the total DLin-DMA-MC3-LNP dose had been taken up rising to 1% after 24 hours. It should be noted that the confocal microscopy images show similar signal in cells between EVs and DLin-DMA-MC3-LNPs, due to a higher labelling efficiency of DLin-DMA-MC3-LNPs. These data clearly demonstrate that in this setup, EV uptake is highly more efficient than that of DLin-DMA-MC3-LNPs which may in part explain the observed differences in RNA delivery efficiency.

The physical routes by which EVs are taken up and trafficked post-uptake could also differ between EVs and LNPs. Interestingly, in a comparison of EV and LNP uptake, EVs were shown to be rapidly taken up at filopodia active regions while LNPs collected in islands at the cell surface and were taken up slowly²⁹. If the way in which EVs and LNPs are taken up differs, then it is plausible that post-uptake trafficking also differs which may explain their differing delivery efficiencies. The intracellular routes taken by LNPs to deliver RNA to the cytosol are well studied and endosomes have been identified as the site of escape. This is the rate-limiting step for RNA delivery and occurs at a low efficiency with only 1-2% of LNP cargo escaping into the cytosol³⁰. In comparison, less is known about the trafficking and endosomal escape efficiency of EVs. Therefore, a study to elucidate the routes EVs and LNPs follow post-uptake could help to explain the increased efficiency of EVs observed here.

EVs may also possess features which allow them to fuse with plasma membranes thereby allowing endolysosomal escape. Evidence to support this is provided by Bonsergent *et al* who observed that EVs fuse with plasma membranes and release their cargo in conditions resembling the endolysosome. In an *in vitro* assay designed to mimic conditions within the endolysosome, they demonstrated that incubation of EVs in a cell-free extract containing

purified plasma membrane induced the release of protein cargo. This process is protein dependent as cargo release was abrogated after proteinase pretreatment of either the plasma membrane sheets or EVs³¹. In addition, Bhagyashree *et al* demonstrated that a proportion of EVs taken up by HEK93T cells fused with the membranes of late endosomes and lysosomes. This process was also dependent on low pH as inhibition of endosome acidification blocked fusion³². These observations highlight the potential fusogenic properties of EVs which could contribute to their high delivery efficiency.

Furthermore, the results obtained here are in line with those obtained by Reshke *et al* who demonstrated that EVs were able to achieve siRNA-mediated target gene knockdown in the liver, intestine and kidney glomeruli *in vivo* at a dose at least tenfold lower than those required for InvivoFectamine 3.0 or C12-200 LNP-mediated knockdown³³.

Conversely, Stremersch *et al* found that anionic liposomes were able to functionally deliver siRNA while EVs coated with cholesterol anchored siRNA were not³⁴. This difference could be explained by the way in which EVs were loaded with RNA. In contrast to the cholesterol anchored siRNA used by Stremersch *et al*, the sgRNA used here is located within the EV lumen²¹. Similarly, the siRNA used by Reshke *et al* was loaded by insertion into a pre-miR-451 backbone, which is abundant in the EV lumen³³. It is possible that siRNA anchoring prevented escape of the siRNA post-uptake, meaning that it was unable to function. This may explain the difference in results between Stremersch *et al* and those presented here and by Reshke *et al*.

It is also possible that EVs of different origins could possess inherently different delivery efficiencies. Although A431-EVs and MDA-MB-231-EVs appear capable of efficient delivery, it is possible that EVs from different sources are not. Furthermore, EV-delivery efficiency may also differ depending on the recipient cell.

Although these results suggest EVs are a highly efficient delivery vehicle, they also demonstrate that passively loaded EVs are unlikely to be utilized as therapeutics for RNA delivery. To induce reporter activation, multiple doses of EVs were isolated and concentrated from a large volume of donor-cell conditioned medium. Even with this EV enrichment, reporter activation was only induced in a small percentage of cells, albeit at concentrations much lower than those required for similar activation levels by DLin-MC3-DMA-LNPs. This minimal response is most likely the result of low sgRNA loading. Therefore, to fully harness the delivery efficiency of EVs, a suitable RNA loading strategy must be found.

In conclusion, this analysis demonstrates that EVs possess a higher RNA delivery efficiency than the synthetic RNA delivery systems tested here. Further research is required to determine the features of EVs that confer this efficiency in order to utilize EVs as RNA delivery vehicles.

CORRESPONDING AUTHOR

Pieter Vader - CDL Research, University Medical Center Utrecht, Utrecht, the Netherlands.
Email: pvader@umcutrecht.nl

ACKNOWLEDGMENTS

We thank Dr. Emilia Nagyova, Jerney Gitz Francois and Omnia M. Elsharkasy for their technical assistance. In addition we thank Dr. Maria Laura Tognoli for her critical reading of the manuscript and Dr. Sander van der Laan for his assistance with statistical analysis. The work of D.E.M, M.J.W.E, R.M.S and P.V is supported by the European Union's Horizon 2020 Research and Innovation program in the project B-SMART (to P.V. and R.M.S.) under grant agreement No. 721058. O.G.d.J. is supported by a VENI Fellowship (VI.Veni.192.174) from the Dutch Research Council (NWO).

DECLARATION OF COMPETING INTEREST

P.V. serves on the scientific advisory board of Evox Therapeutics.

REFERENCES

1. Dowdy, S. F. Overcoming Cellular Barriers for RNA Therapeutics. *Nat. Biotechnol.* **2017**, *35* (3), 222–229.
2. Huang, Y.; Hong, J.; Zheng, S.; Ding, Y.; Guo, S. Elimination Pathways of Systemically Delivered SiRNA. *Mol. Ther.* **2009**, *19* (2), 381–385.
3. Springer, A. D.; Dowdy, S. F. GalNAc-SiRNA Conjugates: Leading the Way for Delivery of RNAi Therapeutics. *Nucleic Acid Ther.* **2018**, *28* (3), 109–118.
4. Evers, M. J. W.; Kulkarni, J. A.; Meel, R. Van Der; Cullis, P. R.; Vader, P.; Schiffelers, R. M. State-of-the-Art Design and Rapid-Mixing Production Techniques of Lipid Nanoparticles for Nucleic Acid Delivery. *Small Methods* **2018**, *1700375*, 1–20.
5. Engin, A. B.; Hayes, A. W. The Impact of Immunotoxicity in Evaluation of the Nanomaterials Safety. *Toxicol. Res. Appl.* **2018**, *2*, 1–9.
6. Sadauskas, E.; Wallin, H.; Stoltenberg, M.; Vogel, U.; Doering, P.; Larsen, A.; Danscher, G. Kupffer Cells Are Central in the Removal of Nanoparticles from the Organism. *Part. Fibre Toxicol.* **2007**, *7* (3), 1–7.
7. Sahay, G.; Alakhova, D. Y.; Kabanov, A. V. Endocytosis of Nanomedicines. *J. Control. Release* **2010**, *145* (3), 182–195.
8. El Andaloussi, S.; Mäger, I.; Breakefield, X. O.; Wood, M. J. A. Extracellular Vesicles: Biology and Emerging Therapeutic Opportunities. *Nat. Rev. Drug Discov.* **2013**, *12* (5), 347–357.
9. Yáñez-mó, M.; Siljander, P. R.; Andreu, Z.; Bedina, A.; Borràs, F. E.; Buzas, E. I.; Buzas, K.; Casal, E.; Cappello, F.; Carvalho, J.; Colás, E.; Cordeiro-da, A.; Fais, S.; Falcon-perez, J. M.; Ghobrial, I. M.; Giebel, B.; Gimona, M.; Graner, M.; Gursel, I.; Gursel, M.; Niels, H. H.; Hendrix, A.; Kierulf, P.; Kokubun, K.; Kosanovic, M.; Kralj-iglic, V.; Laitinen, S.; Lässer, C.; Lener, T.; Ligeti, E.; Linē, A.; Lipps, G.; Llorente, A.; Manček-keber, M.; Marcilla, A.; Mittelbrunn, M.; Hoen, E. N. M. N.; Nyman, T. A.; Driscoll, L. O.; Oliván, M.; Oliveira, C.; Pällinger, É.; Portillo, H. A.; Rigau, M.; Rohde, E.; Sammar, M.; Sánchez, F.; Santarém, N.; Schallmoser, K.; Ostefeld, M. S.; Stoorvogel, W.; Stukelj, R.; Grein, S. G. Van Der; Helena, M.; Wauben, M. H. M.; Wever, O. De. Biological Properties of Extracellular Vesicles and Their Physiological Functions. *J. Extracell. Vesicles* **2015**, *3078* (May).
10. Vader, P.; Mol, E. A.; Pasterkamp, G.; Schiffelers, R. M. Extracellular Vesicles for Drug Delivery. *Adv. Drug Deliv. Rev.* **2016**, *106*, 148–156.
11. Murphy, D. E.; Jong, O. G. De; Brouwer, M.; Wood, M. J.; Lavie, G.; Schiffelers, R. M.; Vader, P. Extracellular Vesicle-Based Therapeutics : Natural versus Engineered Targeting and Traf Ficking. *Exp. Mol. Med.* **2019**.
12. Abels, E. R.; Maas, S. L. N.; Nieland, L.; Krichevsky, A. M.; Breakefield, X. O.; Abels, E. R.; Maas, S. L. N.; Nieland, L.; Wei, Z.; Cheah, P. S.; Tai, E.; Kolsteeg, C. Glioblastoma-Associated Microglia Reprogramming Is Mediated by Functional Transfer of Extracellular Article Glioblastoma-Associated Microglia Reprogramming Is Mediated by Functional Transfer of Extracellular MiR-21. *Cell Reports* **2019**, *28* (12), 3105–3119.e7.
13. Liao, J.; Liu, R. A. N.; Shi, Y.; Yin, L.; Pu, Y. Exosome-Shuttling MicroRNA-21 Promotes Cell Migration and Invasion-Targeting PDCD4 in Esophageal Cancer. *Int J Oncol* **2016**, No. 87, 2567–2579.
14. Leonid, M.; Sadovsky, Y. The Biology of Extracellular Vesicles : The Known Unknowns. *PLoS Biol.* **2019**, *17* (7), 1–12.
15. Chevillet, J. R.; Kang, Q.; Ruf, I. K.; Briggs, H. A.; Vojtech, L. N.; Hughes, S. M.; Cheng, H. H.; Arroyo, J. D.; Meredith, E. K.; Gallichotte, E. N.; Pogosova-agadjanyan, E. L. Quantitative and Stoichiometric Analysis of the MicroRNA Content of Exosomes. *PNAS* **2014**, *111* (41), 14888–14893.

16. He, D.; Wang, H.; Ho, S.; Chan, H.; Hai, L.; He, X.; Wang, K. Total Internal Reflection-Based Single-Vesicle in Situ Quantitative and Stoichiometric Analysis of Tumor-Derived Exosomal MicroRNAs for Diagnosis and Treatment Monitoring. *Theranostics* **2019**, *9* (15), 4494–4507.
17. Somiya, M. Where Does the Cargo Go?: Solutions to Provide Experimental Support for the “Extracellular Vesicle Cargo Transfer Hypothesis.” *J. Cell Commun. Signal.* **2020**, *14* (2), 135–146.
18. Zomer, A.; Maynard, C.; Verweij, F. J.; Kamermaans, A.; Schäfer, R.; Beerling, E.; Schiffelers, R. M.; De Wit, E.; Berenguer, J.; Ellenbroek, S. I. J.; Wurdinger, T.; Pegtel, D. M.; Van Rheenen, J. In Vivo Imaging Reveals Extracellular Vesicle-Mediated Phenocopying of Metastatic Behavior. *Cell* **2015**, *161* (5), 1046–1057.
19. Pucci, F.; Garris, C.; Lai, C. P.; Newton, A.; Pfirschke, C.; Engblom, C.; Alvarez, D.; Sprachman, M.; Evavold, C.; Magnuson, A.; von Andrian, U. H.; Glatz, K.; Breakefield, X. O.; Mempel, T. R.; Weissleder, R.; Pittet, M. J. SCS Macrophages Suppress Melanoma by Restricting Tumor-Derived Vesicle-B Cell Interactions. *Science* **2016**, *352* (6282), 242–246.
20. Fujita, K.; Somiya, M.; Hinuma, S. Biochemical and Biophysical Research Communications Induction of Lipid Droplets in Non-Macrophage Cells as Well as Macrophages by Liposomes and Exosomes. *Biochem. Biophys. Res. Commun.* **2019**, *510* (1), 184–190.
21. de Jong, O. G.; Murphy, D. E.; Mäger, I.; Willms, E.; Garcia-Guerra, A.; Gitz-Francois, J. J.; Lefferts, J.; Gupta, D.; Steenbeek, S. C.; van Rheenen, J.; El Andaloussi, S.; Schiffelers, R. M.; Wood, M. J. A.; Vader, P. A CRISPR-Cas9-Based Reporter System for Single-Cell Detection of Extracellular Vesicle-Mediated Functional Transfer of RNA. *Nat. Commun.* **2020**, *11* (1), 1113.
22. Hoy, S. M. Patisiran: First Global Approval. *Drugs* **2018**, *78* (15), 1625–1631.
23. Akinc, A.; Maier, M. A.; Manoharan, M.; Fitzgerald, K.; Jayaraman, M.; Barros, S.; Ansell, S.; Du, X.; Hope, M. J.; Madden, T. D.; Mui, B. L.; Semple, S. C.; Tam, Y. K.; Ciufolini, M.; Witzigmann, D.; Kulkarni, J. A.; van der Meel, R.; Cullis, P. R. The Onpattro Story and the Clinical Translation of Nanomedicines Containing Nucleic Acid-Based Drugs. *Nat. Nanotechnol.* **2019**, *14* (12), 1084–1087.
24. Manzanares Darío, C. V. Endocytosis: The Nanoparticle and Submicron Nanocompounds Gateway into the Cell. *Pharmaceutics* **2020**, *12* (371), 1–22.
25. Maugeri, M.; Nawaz, M.; Papadimitriou, A.; Angerfors, A.; Camponeschi, A.; Na, M.; Hölttä, M.; Skantze, P.; Johansson, S.; Sundqvist, M.; Lindquist, J.; Kjellman, T.; Mårtensson, I.-L.; Jin, T.; Sunnerhagen, P.; Östman, S.; Lindfors, L.; Valadi, H. Linkage between Endosomal Escape of LNP-mRNA and Loading into EVs for Transport to Other Cells. *Nat. Commun.* **2019**, *10* (1), 4333.
26. Théry, C.; Witwer, K. W.; Aikawa, E.; Alcaraz, M. J.; Anderson, J. D.; Andriantsitohaina, R.; Antoniou, A.; Arab, T.; Archer, F.; Atkin-Smith, G. K.; Ayre, D. C.; Bach, J.-M.; Bachurski, D.; Baharvand, H.; Balaj, L.; Baldacchino, S.; Bauer, N. N.; Baxter, A. A.; Bebawy, M.; Beckham, C.; Bedina Zavec, A.; Benmoussa, A.; Berardi, A. C.; Bergese, P.; Bielska, E.; Blenkiron, C.; Bobis-Wozowicz, S.; Boilard, E.; Boireau, W.; Bongiovanni, A.; Borràs, F. E.; Bosch, S.; Boulanger, C. M.; Breakefield, X.; Breglio, A. M.; Brennan, M. Á.; Brigstock, D. R.; Brisson, A.; Broekman, M. L. D.; Bromberg, J. F.; Bryl-Górecka, P.; Buch, S.; Buck, A. H.; Burger, D.; Busatto, S.; Buschmann, D.; Bussolati, B.; Buzás, E. I.; Byrd, J. B.; Camussi, G.; Carter, D. R. F.; Caruso, S.; Chamley, L. W.; Chang, Y.-T.; Chen, C.; Chen, S.; Cheng, L.; Chin, A. R.; Clayton, A.; Clerici, S. P.; Cocks, A.; Cocucci, E.; Coffey, R. J.; Cordeiro-da-Silva, A.; Couch, Y.; Coumans, F. A. W.; Coyle, B.; Crescitelli, R.; Criado, M. F.; D’Souza-Schorey, C.; Das, S.; Datta Chaudhuri, A.; de Candia, P.; De Santana, E. F.; De Wever, O.; del Portillo, H. A.; Demaret, T.; Deville, S.; Devitt, A.; Dhondt, B.; Di Vizio, D.; Dieterich, L. C.; Dolo, V.; Dominguez Rubio, A. P.; Dominici, M.; Dourado, M. R.; Driedonks, T. A. P.; Duarte, F. V.; Duncan, H. M.; Eichenberger, R. M.; Ekström, K.; EL Andaloussi, S.; Elie-Caille, C.; Erdbrügger, U.; Falcón-Pérez, J. M.; Fatima, F.; Fish, J. E.; Flores-Bellver, M.; Försönits, A.; Fretet-Barrand, A.; Fricke, F.; Fuhrmann,

- G.; Gabrielsson, S.; Gámez-Valero, A.; Gardiner, C.; Gärtner, K.; Gaudin, R.; Gho, Y. S.; Giebel, B.; Gilbert, C.; Gimona, M.; Giusti, I.; Goberdhan, D. C. I.; Görgens, A.; Gorski, S. M.; Greening, D. W.; Gross, J. C.; Gualerzi, A.; Gupta, G. N.; Gustafson, D.; Handberg, A.; Haraszti, R. A.; Harrison, P.; Hegyesi, H.; Hendrix, A.; Hill, A. F.; Hochberg, F. H.; Hoffmann, K. F.; Holder, B.; Holthofer, H.; Hosseinkhani, B.; Hu, G.; Huang, Y.; Huber, V.; Hunt, S.; Ibrahim, A. G.-E.; Ikezu, T.; Inal, J. M.; Isin, M.; Ivanova, A.; Jackson, H. K.; Jacobsen, S.; Jay, S. M.; Jayachandran, M.; Jenster, G.; Jiang, L.; Johnson, S. M.; Jones, J. C.; Jong, A.; Jovanovic-Talisman, T.; Jung, S.; Kalluri, R.; Kano, S.; Kaur, S.; Kawamura, Y.; Keller, E. T.; Khamari, D.; Khomyakova, E.; Khvorova, A.; Kierulf, P.; Kim, K. P.; Kislinger, T.; Klingeborn, M.; Klinke, D. J.; Kornek, M.; Kosanović, M. M.; Kovács, Á. F.; Krämer-Albers, E.-M.; Krasemann, S.; Krause, M.; Kurochkin, I. V.; Kusuma, G. D.; Kuypers, S.; Laitinen, S.; Langevin, S. M.; Languino, L. R.; Lannigan, J.; Lässer, C.; Laurent, L. C.; Lavieu, G.; Lázaro-Ibáñez, E.; Le Lay, S.; Lee, M.-S.; Lee, Y. X. F.; Lemos, D. S.; Lenassi, M.; Leszczynska, A.; Li, I. T. S.; Liao, K.; Libregts, S. F.; Ligeti, E.; Lim, R.; Lim, S. K.; Liné, A.; Linnemannstöns, K.; Llorente, A.; Lombard, C. A.; Lorenowicz, M. J.; Lörcincz, Á. M.; Lötvall, J.; Lovett, J.; Lowry, M. C.; Loyer, X.; Lu, Q.; Lukomska, B.; Lunavat, T. R.; Maas, S. L. N.; Malhi, H.; Marcilla, A.; Mariani, J.; Mariscal, J.; Martens-Uzunova, E. S.; Martin-Jaular, L.; Martinez, M. C.; Martins, V. R.; Mathieu, M.; Mathivanan, S.; Maugeri, M.; McGinnis, L. K.; McVey, M. J.; Meckes, D. G.; Meehan, K. L.; Mertens, I.; Minciocchi, V. R.; Möller, A.; Møller Jørgensen, M.; Morales-Kastresana, A.; Morhayim, J.; Mullier, F.; Muraca, M.; Musante, L.; Mussack, V.; Muth, D. C.; Myburgh, K. H.; Najrana, T.; Nawaz, M.; Nazarenko, I.; Nejsum, P.; Neri, C.; Neri, T.; Nieuwland, R.; Nimrichter, L.; Nolan, J. P.; Nolte-’t Hoen, E. N. M.; Noren Hooten, N.; O’Driscoll, L.; O’Grady, T.; O’Loghlen, A.; Ochiya, T.; Olivier, M.; Ortiz, A.; Ortiz, L. A.; Osteikoetxea, X.; Østergaard, O.; Ostrowski, M.; Park, J.; Pegtel, D. M.; Peinado, H.; Perut, F.; Pfaffl, M. W.; Phinney, D. G.; Pieters, B. C. H.; Pink, R. C.; Pisetsky, D. S.; Pogge von Strandmann, E.; Polakovicova, I.; Poon, I. K. H.; Powell, B. H.; Prada, I.; Pulliam, L.; Quesenberry, P.; Radeghieri, A.; Raffai, R. L.; Raimondo, S.; Rak, J.; Ramirez, M. I.; Raposo, G.; Rayyan, M. S.; Regev-Rudzki, N.; Ricklefs, F. L.; Robbins, P. D.; Roberts, D. D.; Rodrigues, S. C.; Rohde, E.; Rome, S.; Rouschop, K. M. A.; Rughetti, A.; Russell, A. E.; Saá, P.; Sahoo, S.; Salas-Huenuleo, E.; Sánchez, C.; Saugstad, J. A.; Saul, M. J.; Schiffelers, R. M.; Schneider, R.; Schøyen, T. H.; Scott, A.; Shahaj, E.; Sharma, S.; Shatnyeva, O.; Shekari, F.; Shelke, G. V.; Shetty, A. K.; Shiba, K.; Siljander, P. R.-M.; Silva, A. M.; Skowronek, A.; Snyder, O. L.; Soares, R. P.; Sódar, B. W.; Soekmadji, C.; Sotillo, J.; Stahl, P. D.; Stoorvogel, W.; Stott, S. L.; Strasser, E. F.; Swift, S.; Tahara, H.; Tewari, M.; Timms, K.; Tiwari, S.; Tixeira, R.; Tkach, M.; Toh, W. S.; Tomasini, R.; Torrecilhas, A. C.; Tosar, J. P.; Toxavidis, V.; Urbanelli, L.; Vader, P.; van Balkom, B. W. M.; van der Grein, S. G.; Van Deun, J.; van Herwijnen, M. J. C.; Van Keuren-Jensen, K.; van Niel, G.; van Royen, M. E.; van Wijnen, A. J.; Vasconcelos, M. H.; Vechetti, I. J.; Veit, T. D.; Vella, L. J.; Velot, É.; Verweij, F. J.; Vestad, B.; Viñas, J. L.; Visnovitz, T.; Vukman, K. V.; Wahlgren, J.; Watson, D. C.; Wauben, M. H. M.; Weaver, A.; Webber, J. P.; Weber, V.; Wehman, A. M.; Weiss, D. J.; Welsh, J. A.; Wendt, S.; Wheelock, A. M.; Wiener, Z.; Witte, L.; Wolfram, J.; Xagorari, A.; Xander, P.; Xu, J.; Yan, X.; Yáñez-Mó, M.; Yin, H.; Yuana, Y.; Zappulli, V.; Zarubova, J.; Žekas, V.; Zhang, J.; Zhao, Z.; Zheng, L.; Zheutlin, A. R.; Zickler, A. M.; Zimmermann, P.; Zivkovic, A. M.; Zocco, D.; Zuba-Surma, E. K. Minimal Information for Studies of Extracellular Vesicles 2018 (MISEV2018): A Position Statement of the International Society for Extracellular Vesicles and Update of the MISEV2014 Guidelines. *J. Extracell. Vesicles* **2018**, *7* (1), 1535750.
27. Christina, S.; Collinson, A.; Matthews, C.; Pointon, A.; Jenkinson, L.; Minter, R. R.; Vaughan, T. J.; Tigue, N. J. Exosomal Delivery of Doxorubicin Enables Rapid Cell Entry and Enhanced in Vitro Potency. *PLoS One* **2019**, *14* (3), 1–19.
 28. Lu, M.; Zhao, X.; Xing, H.; Xun, Z.; Zhu, S.; Lang, L.; Yang, T.; Cai, C.; Wang, D.; Ding, P. Comparison of Exosome-Mimicking Liposomes with Conventional Liposomes for Intracellular Delivery of siRNA. *Int. J. Pharm.* **2018**, *550* (1–2), 100–113.

29. Heusermann, W.; Hean, J.; Trojer, D.; Steib, E.; von Bueren, S.; Graff-Meyer, A.; Genoud, C.; Martin, K.; Pizzato, N.; Voshol, J.; Morrissey, D. V.; Andaloussi, S. E. L.; Wood, M. J.; Meisner-Kober, N. C. Exosomes Surf on Filopodia to Enter Cells at Endocytic Hot Spots, Traffic within Endosomes, and Are Targeted to the ER. *J. Cell Biol.* **2016**, *213* (2), 173–184.
30. Gilleron, J.; Querbes, W.; Zeigerer, A.; Borodovsky, A.; Marsico, G.; Schubert, U.; Manygoats, K.; Seifert, S.; Andree, C.; Stöter, M.; Epstein-Barash, H.; Zhang, L.; Koteliansky, V.; Fitzgerald, K.; Fava, E.; Bickle, M.; Kalaidzidis, Y.; Akinc, A.; Maier, M.; Zerial, M. Image-Based Analysis of Lipid Nanoparticle-Mediated siRNA Delivery, Intracellular Trafficking and Endosomal Escape. *Nat. Biotechnol.* **2013**, *31* (7), 638–646.
31. Bonsergent, E.; Lavieu, G. Content Release of Extracellular Vesicles in a Cell-Free Extract. *FEBS Lett.* **2019**, *593* (15), 1983–1992.
32. Joshi, B. S.; de Beer, M. A.; Giepmans, B. N. G.; Zuhorn, I. S. Endocytosis of Extracellular Vesicles and Release of Their Cargo from Endosomes. *ACS Nano* **2020**, *14* (4), 4444–4455.
33. Reshke, R.; Taylor, J. A.; Savard, A.; Guo, H.; Rhym, L. H.; Kowalski, P. S.; Trung, M. T.; Campbell, C.; Little, W.; Anderson, D. G.; Gibbings, D. Reduction of the Therapeutic Dose of Silencing RNA by Packaging It in Extracellular Vesicles via a Pre-MicroRNA Backbone. *Nat. Biomed. Eng.* **2020**, *4* (1), 52–68.
34. Stremersch, S.; Vandenbroucke, R. E.; Wouterghem, E. Van; Hendrix, A.; Smedt, S. C. De; Raemdonck, K. Comparing Exosome-like Vesicles with Liposomes for the Functional Cellular Delivery of Small RNAs. *J. Control. Release* **2016**, *232*, 51–61.

NATURAL OR SYNTHETIC RNA DELIVERY: A STOICHIOMETRIC COMPARISON OF EXTRACELLULAR VESICLES AND SYNTHETIC NANOPARTICLES

Daniel E. Murphy^a, Olivier G. de Jong^a, Martijn J. W. Evers^a, Maratussholikhah Nurazizah^a,
Raymond M. Schiffelers^a, Pieter Vader^{a,b}

a: CDL Research, University Medical Center Utrecht, Utrecht, the Netherlands

b: Department of Experimental Cardiology, University Medical Center Utrecht, Utrecht,
the Netherlands

Supporting Information

METHODS

Cell Culture

HEK293T, MDA-MB-231 and A431 cells were cultured in Dulbecco's Modified Eagle Medium (DMEM) with L-Glutamine (Gibco) supplemented with 10% fetal bovine serum (FBS). Streptomycin and penicillin was added to all cell culture medium at 100 µg/ml and 100 u/ml (Gibco) respectively. Stable HEK293T reporter cell lines expressing the CROSS-FIRE reporter construct and Cas9 and sgRNA expressing donor MDA-MB-231 and A431 lines were prepared and cultured with selection antibiotics as previously described¹.

EV Isolation

Targeting-sgRNA or non-targeting control sgRNA expressing MDA-MB-231 and A431 cells were cultured in T175 flasks. Cells were seeded in 6 batches of 20 flasks at varying densities so that each batch would reach approximately 90% confluency on 6 consecutive days in order to isolate EVs on 6 consecutive days for addition experiments. At 90% confluency, the FBS containing culture medium was aspirated and cells were washed with 10ml PBS. 20ml of serum free OptiMEM (Gibco) was then added and cells were cultured for a further 24 hours. The conditioned OptiMEM was then spun for 5 minutes at 4°C at 300 x g to remove detached cells followed by 2000 x g for 15 minutes at 4°C to remove dead cells and cell debris. Conditioned medium was then filtered using a 0.45µm bottle top filter and concentrated to approximately 10ml using tangential flow filtration with a peristaltic pump attached to a Minimate 100 kDa Omega Membrane cassette (Pall Corporation). This medium was further concentrated to 1ml using a a 100 kDa Amicon Ultra-15 Centrifugal filter (Merck). EVs were then isolated using size exclusion chromatography using a Tricorn 10/300 column with Sepharose 4 Fast Flow resin attached to an AKTA Start or AKTA Pure chromatography system (all GE Healthcare Life Sciences). Fractions containing the EV peak were then pooled, 0.45µm syringe filtered for sterility and concentrated to approximately 180µl using a 100 kDa Amicon Ultra-15 Centrifugal filter.

LNP Production

DLin-MC3-DMA containing LNPs were composed of DLin-MC3-DMA/Cholesterol/DSPC/PEG-DMG at a molar ratio of 50/38.5/10/1.5. LNPs were produced by microfluidic mixing in a NanoAssemblr Benchtop device (Precision Nanosystems, Vancouver, BC, Canada). Prior to production, lipids were diluted to a total lipid concentration of 5mM in pure ethanol while RNA was diluted in a 25mM acetate buffer (pH4). LNPs were produced with

an N/P ratio of 12 at a flow of 6ml/minute with a flow rate ratio of 3:1 aqueous to lipid phase. LNPs were then dialysed into PBS overnight using 20kDa G2 dialysis cassettes (ThermoFisher). After dialysis, LNPs were sterilized by membrane filtration using 0.45µm syringe membrane filters. Final encapsulated RNA concentration was determined using a Quant-iT Ribogreen assay (ThermoFisher) according to manufacturer's instructions which confirmed that encapsulation efficiency was close to 100%.

Size and Zeta potential measurement

Dynamic Light Scattering (DLS) was performed to measure the hydrodynamic radius of EVs and DLin-MC3-DMA-LNPs using a Nano S Zetasizer instrument (Malvern). Samples were diluted in DPBS and light scattering was measured at an angle of 173 at 25°C for 10s and repeated at least 10 times. Zeta potential measurement was performed on samples using a Nano Z Zetasizer device on samples diluted in 0.1x PBS.

Western Blotting

Cells and EV samples were lysed in RIPA buffer containing a protease inhibitor cocktail (Sigma-Aldrich). Cell lysates were spun at max speed at 4°C for 5 minutes to pellet precipitates. Protein concentrations were determined using a MicroBCA protein assay according to Manufacturer's protocol (ThermoFisher Scientific). Sample input was normalised by loading an equal weight of total protein per sample. Samples were mixed with sample loading buffer with 100µM DTT, or without DTT when blotting for tetraspanins. Samples were run on a 4-12% gradient Bis-Tris polyacrylamide gel (Thermo Fisher Scientific) before blotting onto Immobilon-FL polyvinylidene difluoride membranes (Millipore). Membranes were then blocked overnight at 4°C by incubation in blocking buffer composed of Odyssey Blocking Buffer (LI-COR Biosciences) mixed 1:1 with Tris-Buffered Saline, 0.1% tween (TBS-T). Membranes were then probed overnight at 4°C using primary antibodies diluted 1:500 in blocking buffer. These antibodies were ALIX 1:500 (ThermoFisher Scientific, MA1-83977), Calnexin 1:500 (GeneTex, GTX101676), CD9 1:500 (Abcam, ab92726), CD63 1:500 (Abcam, ab8219) and COX IV (Abcam, ab33985). After primary antibody incubation, the blots were washed 3 times for 10 minutes at room temperature in TBS-T. Secondary antibodies were applied overnight at 4°C at a 1:7500 dilution in blocking buffer. The secondary antibodies used were anti-rabbit IgG conjugated to AlexaFluor680 (ThermoFisher Scientific, A-21076) or anti-mouse IgG conjugated to IR dye 800CW. Blots were then washed 3 times for 10 minutes at room temperature in TBS-T and scanned using an Odyssey Infrared Imager (LI-COR Biosciences) at 700nm and 800nm.

Nanoparticle tracking analysis

EV and LNP particle concentrations were determined using a Nanosight S500 nanoparticle analyzer (Malvern Instruments) equipped with a 405nm laser. Samples were diluted in PBS to a concentration that gave between 30 to 100 tracks per frame. Videos were acquired with a camera level of 16. EVs were analyzed with a detection threshold of 6 while LNPs were analyzed with a detection threshold of 4, due to their smaller size. NTA Software version 3.3 was used for video analysis.

RT-qPCR

Firstly, EV samples of unknown targeting-sgRNA concentration were diluted to 250ul in PBS. Standard curve samples of known targeting-sgRNA concentration were prepared in 250ul of PBS and were treated identically to EV samples throughout the entire process. Then, 750ul of Trizol LS (Life Technologies) was added to all samples. To allow normalisation for extraction efficiency, an equal quantity of non-targeting spike-in sgRNA was applied to all samples at this point. RNA was then isolated according to the manufacturer's protocol using GlycoBlue coprecipitant (Thermo Fisher Scientific). RNA pellets were resuspended in 20ul of nuclease free water and cDNA synthesis was performed on 10ul RNA suspension using a SuperScript 4 kit (Thermo Fisher Scientific), RNasin Ribonuclease inhibitor (Promega) and 2 pmol of sgRNA reverse primer which was specific for both targeting sgRNA and the non-targeting spike-in sgRNA. The resulting cDNA was diluted 1:5 in nuclease free water before qPCR analysis using iQ SYBR Green Supermix (Bio-Rad) in a CFX96 Real-Time PCR Detection System (Bio-Rad). To normalise for extraction efficiency, spike-in RNA Ct values were subtracted from targeting-RNA values. Using these normalised Ct values and starting dilution factor, the sgRNA concentration of EV samples was interpolated from the normalised standard curve Ct values using Graphpad Prism 8.0.1 software.

EV Addition experiments

HEK293T CROSS-FIRE reporter cells were seeded in a volume of 200µl in a 96-well plate. EVs were then isolated from targeting-sgRNA or non-targeting control sgRNA expressing MDA-MB-231 and A431 cells. Particle concentration was determined using NTA after each isolation and the particle concentrations of targeting and non-targeting EVs were normalised before addition. EVs were applied on 6 consecutive days in a high dose volume of 40µl or a low dose volume of 10µl. Medium was replaced before each addition and cell confluency was maintained between 30-100% throughout the experiment. After the last

EV addition reporter cells were incubated for a further 24 hours to allow GFP expression. Reporter cells were then analysed using an EVOS FL Cell Imaging System (Thermo Fisher Scientific) and measured using a Fortessa (BD Biosciences) flow cytometer.

DLin-MC3-DMA-LNP Titration

DLin-MC3-DMA LNPs were produced as described using targeting-sgRNA as cargo. After production, dialysis and filtration, final RNA concentration was determined using a Quant-iT Ribogreen assay (ThermoFisher) according to manufacturer's instructions. LNPs were diluted to so that upon addition to 200 μ l culture volume, the final concentration would be 10nM. A 1:10 dilution series of this LNP stock was prepared so that LNPs could be titrated onto HEK293T CROSS-FIRE reporter cells at a wide range of sgRNA concentrations. Cells were dosed with LNPs and treated in an identical manner to that of EV addition experiments.

Spike-in LNP Titration

DLin-MC3-DMA LNPs were produced as described using scaffold-sgRNA as cargo. 6 different batches were produced with targeting sgRNA spiked in to achieve targeting to scaffold sgRNA ratios ranging from 1:325 to 1:32500000. After production, dialysis and filtration, final total RNA concentration was determined using a Quant-iT Ribogreen assay (ThermoFisher) according to manufacturer's instructions. LNPs were diluted to a 16.25nM stock so that upon addition of 50 μ l stock to 200 μ l culture volume, the final total RNA concentration would be 3.25nM. This gave final targeting-sgRNA concentrations ranging from 0.1fM to 10,000 fM. Cells were dosed with LNPs and treated in an identical manner to that of EV addition experiments.

In vitro transfection reagent titration

HEK293T CROSS-FIRE reporter cells were transfected with targeting sgRNA at a concentration of 10nM using Lipofectamine RNAiMax and TransIT-2020 according to manufacturer's instructions. Reporter cells were transfected with 25 kDa linear polyethylenimine (PEI) by diluting 3 μ l of 1mg/ml 25kDa PEI stock in 50 μ l of OptiMEM. Targeting sgRNA was diluted in a separate tube of 50 μ l of OptiMEM and mixed with the PEI dilution and incubated for 30 minutes at room temperature to allow polyplex formation. The transfection mixes used to achieve a concentration of 10nM were serially diluted 1:10 in order to achieve the same final targeting sgRNA concentrations used in DLin-MC3-DMA-LNP titrations. Cells were transfected according to the same schedule as EV addition experiments.

Quantification of NP uptake

MDA-MB-231-EVs and A431-EVs were labelled with MemGlow™560 according to manufacturer's instructions. DLin-DMA-MC3-LNPs were produced as described with the addition of 0.2% 18:1 Liss Rhod PE (Avanti Polar Lipids). HEK293T cells were seeded at the same density used in EV addition experiments and spike-in LNP titrations in CellStar 96-well cell culture black µClear bottom TC-treated microplates (Greiner-Bio). Cells were treated for 2, 4 or 24 hours with a similar dose of fluorescent particles as used in EV addition experiments and spike-in LNP titrations. Prior to measurement, medium was aspirated and cells were washed in PBS. Cells which had been treated with NPs were then lysed in 1x RIPA buffer. A standard curve was produced by lysing a series of wells containing cells which had not been treated with NPs in 1x RIPA. A 1:1 dilution series standard curve starting at 100% of the dose applied to the cells at the 2, 4 and 24 hour time points was then added to this lysed cell mixture. Fluorescent signal was then measured at excitation = 561, emission = 601 on a Spectramax™ plate reader. The percentage of total dose that had been taken up by cells could then be interpolated from the standard curve.

Confocal Microscopy

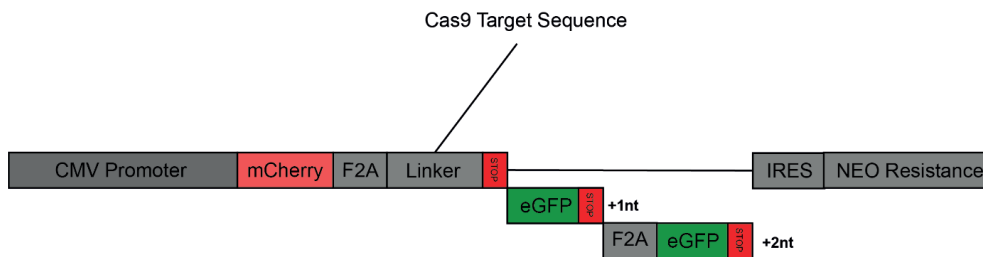
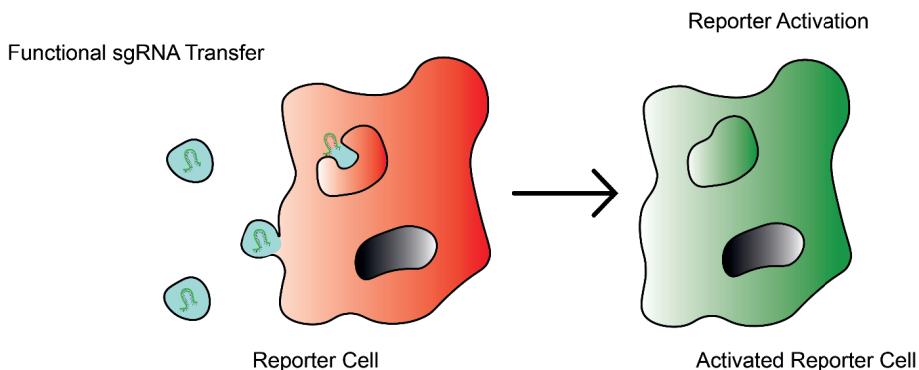
MDA-MB-231-EVs and A431-EVs were labelled with MemGlow™560 according to manufacturer's instructions. DLin-DMA-MC3-LNPs were produced as described with the addition of 0.2% 18:1 Liss Rhod PE (Avanti Polar Lipids). HEK293T cells were seeded at the same density used in EV addition experiments and spike-in LNP titrations in CellStar 96-well cell culture black µClear bottom TC-treated microplates (Greiner-Bio). Cells were treated for 2, 4 or 24 hours with a similar dose of fluorescent particles as used in EV addition experiments and spike-in LNP titrations. 1 µg/ml Hoechst 33342 (ThermoFisher Scientific) was then added to the culture medium and a Yokogawa C7000 confocal microscope was used to produce confocal images at 40x magnification using the following filter settings: Hoechst: emission = 405 nm, power 30; acquisition =BP445/45, Exposure time = 200 ms. MemGlow™560 and Liss Rhod: emission = 561 nm, power 30; acquisition =BP600/37, Exposure time = 200ms.

FACS Analysis

After treatment with EVs or synthetic transfection reagents, CROSS-FIRE reporter cells were trypsinised and resuspended in DMEM, 10% FBS. Cells were then transferred to a round bottom 96 well plate and pelleted by spinning at 300g for 5 minutes at 4°C. Cells were then resuspended in 200µl FACS buffer consisting of PBS, 1% FBS including 1µg/ml DAPI as a live dead stain. Cells were then analysed using a Fortessa or Canto (BD Biosciences) flow cytometer. FACS analysis was performed using FlowJo v10 software and gating was performed as shown in Figure S2.

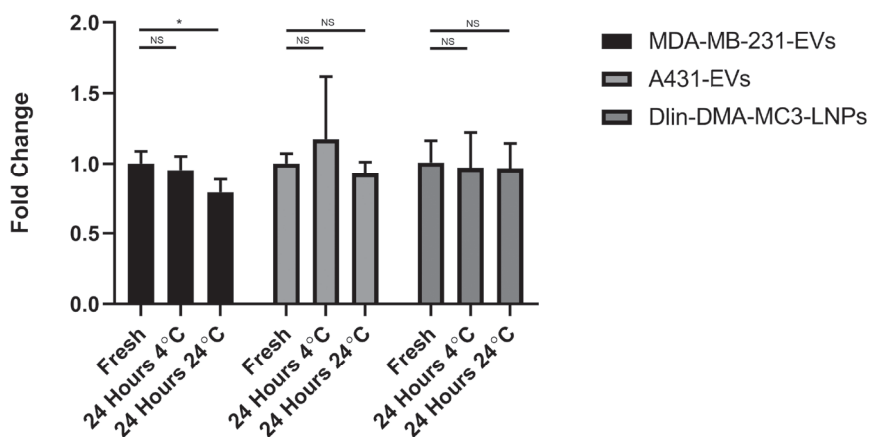
Statistical Analysis

All statistical analysis was performed using Graphpad prism software V8.01. EV addition experiments were analysed using ANOVA with a post-hoc Tukey's test. The minimal effective dose of DLin-MC3-DMA-LNPs, Spike-in DLin-MC3-DMA-LNPs and *in vitro* transfection reagents was determined in the same way using ANOVA with a post-hoc Tukey's test.

A**B**

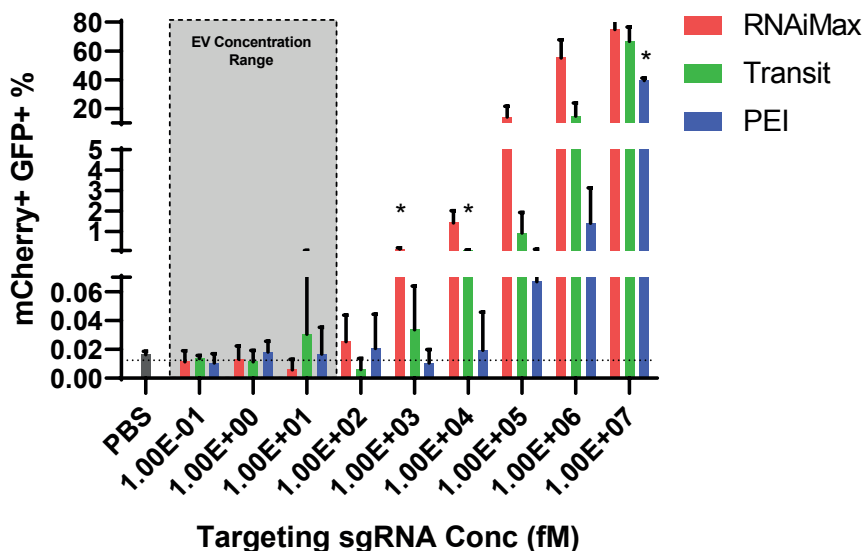
▲Figure S1 – The CROSS-FIRE reporter system.

The reporter construct is expressed under a CMV promoter. The first component is mCherry which allows identification of reporter cells. This is followed by a linker sequence which is specifically targeted by sgRNA bound to Cas9. Upon Cas9-mediated cleavage of the linker sequence, the cut is repaired through a process of non-homologous end joining. This process can introduce frameshift mutations which cause readthrough of the downstream stop codon and brings eGFP open reading frames, which are either 1 or 2 nucleotides out of frame, into frame. This results in the permanent expression of eGFP. F2A self-cleaving domains are placed between each fluorescent protein (A). This system allows the detection of functional sgRNA transfer to reporter cells which express the reporter construct and Cas9. In the absence of sgRNA, reporter cells express only mCherry. Upon functional delivery of sgRNA, Cas9 is guided to the reporter linker sequence and GFP expression is induced (B)⁽¹⁾.

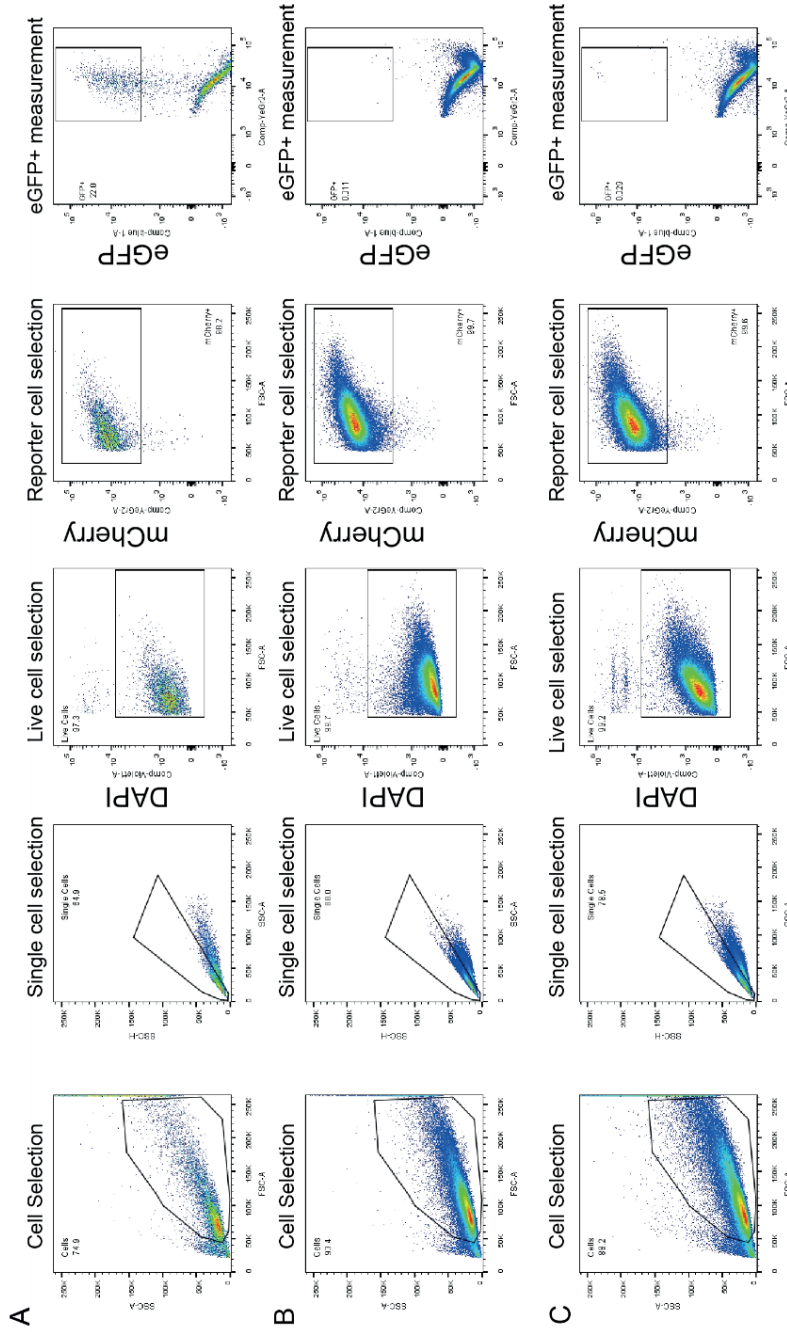


▲Figure S2 – MDA-MB-231-EV, A431-EV and DLin-DMA-MC3-LNP associated sgRNA is stable. RT-qPCR analysis of targeting sgRNA in MDA-MB-231-EV, A431-EV and DLin-DMA-MC3-LNP samples freshly after isolation, after incubation at 24 hours of incubation at 4°C and 24 hours of incubation at 37°C. Fold changes were calculated relative to the average Ct value of the fresh condition of each NP type. N=4 technical replicates, Tukey’s multiple comparison test, **p*<0.05.

In Vitro Transfection Reagent Titration



▲Figure S3 - in vitro transfection reagent titration. Flow cytometry analysis of Stoptight+ spCas9+ HEK293T reporter cells after 6 consecutive daily transfections of targeting sgRNA using the typical in vitro transfection reagents RNAiMax, TransitIT-2020 and 25 kDa linear PEI at a range of 1E+07 fM to 1E-01 fM. Tukey’s multiple comparison test, **p*<0.05, ***p*<0.01 versus vehicle.



▲ **Figure S4 - Flow cytometry gating strategy used to measure CROSS-FIRE reporter cell activation.** Firstly, cells are selected by gating using forward scatter area (FSC-A) and sideward scatter area (SSC-A). Singlets are then selected from a SSC-A vs sideward scatter height (SSC-H) plot. Dead cells which can contribute to background signal are removed from the analysis by selecting DAPI negative live cells using their FSC-A and DAPI signals. Reporter cells are then selected using their FSC-A and mCherry signals. From this population, reporter activation is determined by measuring eGFP signal on a mCherry vs eGFP plot. Gates for eGFP+mCherry+ cells were determined using targeting sgRNA transfected positive control cells. (A). For comparison, the same plots are shown for a PBS treated negative control (B). A representative flow cytometry plot of CROSS-FIRE reporter cells treated with targeting sgRNA+ A431-EVs on 6 consecutive days is shown (C).

Table S1- RNA Sequences

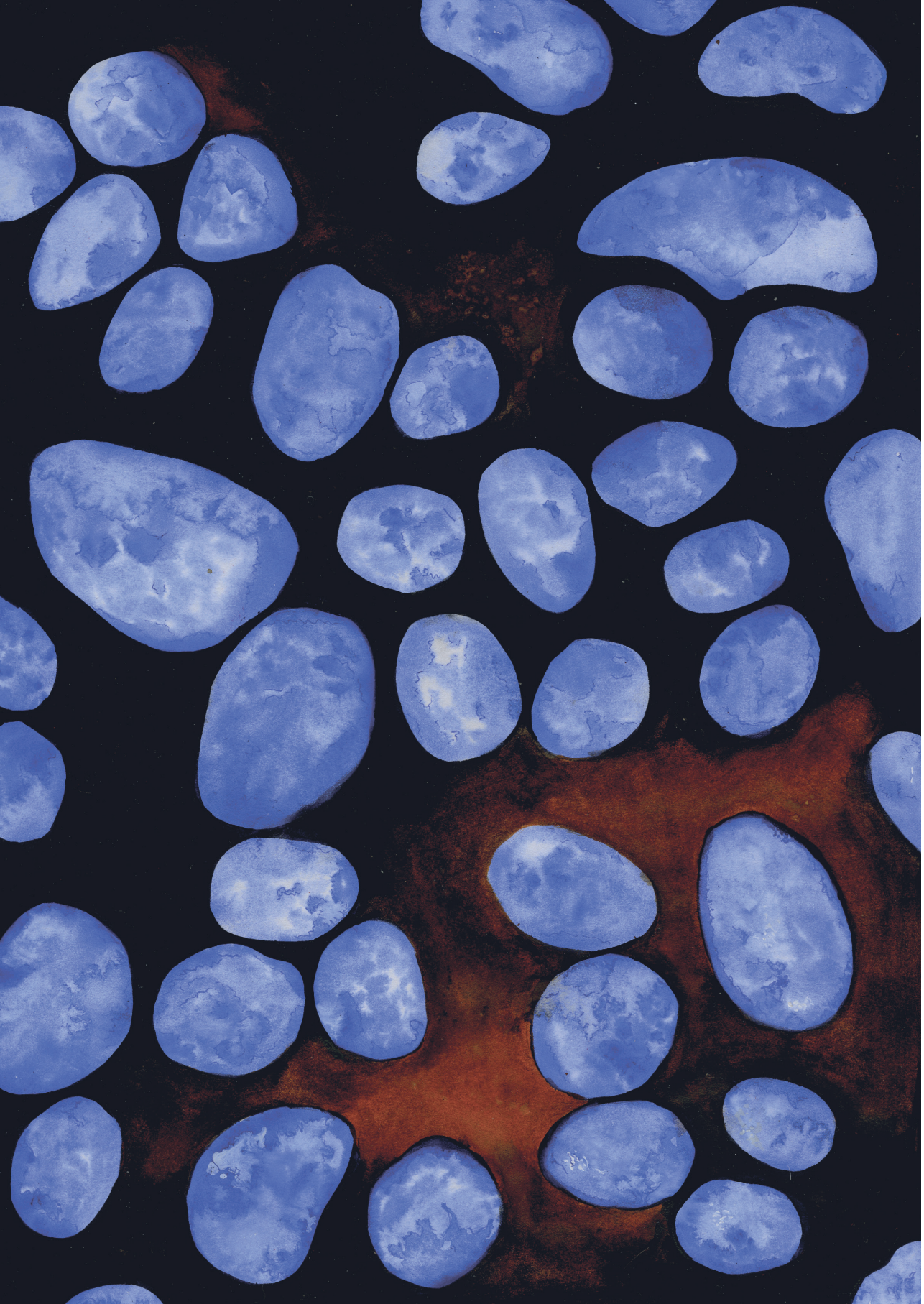
Targeting sgRNA	GGACAGTACTCCGCTCGAGTGTTTTAGAGCTAG AAATAGCAAGTTAAAATAAGGCTAGTCCGTTATCA ACTTGAAAAAGTGGCACCGAGTCGGTGCTTTTTT
Non-targeting sgRNA	TCTCTACTACTGATAGGGAGGTTTTAGAGCTAGA AATAGCAAGTTAAAATAAGGCTAGTCCGTTATCAA CTTGAAAAAGTGGCACCGAGTCGGTGCTTTTTT
Scaffold sgRNA	UCUCUACCAGGGCUAUGGGCGUUUUAGAGCU AGAAAUAGCAUGUUAAAAUAAUUCUAGUAAGU UAUCAACUUGAAAAAGUGGCACCGAGUCG GUGCUUUUUU

Table S2- qPCR Primer Sequences

Targeting sgRNA forward	CAGTACTCCGCTCGAGTGTT
Non-targeting sgRNA spike-in forward	TCACTGATAGGGAGGTTTTAGAGC
Targeting and non-targeting sgRNA reverse	GACTCGGTGCCACTTTTTCAA

References

1. de Jong OG, Murphy DE, Mäger I, et al. A CRISPR-Cas9-based reporter system for single-cell detection of extracellular vesicle-mediated functional transfer of RNA. *Nat Commun.* 2020;11(1):1113. doi:10.1038/s41467-020-14977-8



A COMPARISON OF EXTRACELLULAR VESICLE AND LIPID NANOPARTICLE CELLULAR UPTAKE AND INTRA- CELLULAR TRAFFICKING

Daniel E. Murphy^a, Willemijn S. de Voogt^a, Marieke Roefs^b,
Raymond M. Schiffelers^a, Pieter Vader^{a,b}

a: CDL Research, University Medical Center Utrecht, Utrecht, the
Netherlands

b: Department of Experimental Cardiology, University Medical
Center Utrecht, Utrecht, the Netherlands

ABSTRACT

Extracellular vesicles (EVs) possess numerous advantageous features which make them a promising RNA therapeutic delivery vehicle candidate. Amongst these features is an RNA delivery efficiency several orders of magnitude higher than that of synthetic RNA delivery systems. However, the mechanisms by which EVs achieve this high delivery efficiency remain unknown. In order to study whether this high delivery efficiency could be related to features of uptake and post-uptake trafficking of EVs, live cell confocal microscopy and confocal colocalisation analysis was performed to compare the uptake and trafficking of cardiac progenitor cell EVs (CPC-EVs) to DLin-DMA-MC3-LNPs. This analysis revealed no clear difference in uptake kinetics or colocalisation with endosomal compartment markers, suggesting that other mechanisms are responsible for the high RNA delivery efficiency of EVs.

INTRODUCTION

In recent years, the field of RNA therapeutics has experienced great growth and progress, from the first clinical approval of an RNA therapeutic in the form of Onpattro¹ to the successful development and widespread use of Moderna's mRNA1273 and Pfizer-BioNTech's BNT162b2 vaccines to combat the COVID19 pandemic^{2,3}.

Despite this success, the full potential of RNA therapeutics is yet to be achieved as appropriate delivery is generally limited. This is due to the fact that the body possesses numerous defence mechanisms to prevent the entry of exogenous RNA. For example, unprotected RNA is unable to cross cell membranes and is rapidly degraded in the circulation by RNases⁴. To bypass these barriers and facilitate cellular uptake, therapeutic RNA is conventionally encapsulated within a nanoparticle (NP) delivery vehicle, of which the most clinically advanced are the lipid nanoparticles (LNPs)⁵.

Unfortunately, LNPs possess their own set of obstacles. They can be highly immunogenic and are subject to uptake and removal from the circulation by Kupffer cells of the liver⁶. Even upon LNP uptake by target cells, the successful delivery and escape of the therapeutic RNA payload to its cytosolic site of action occurs at low efficiency. The majority of LNP cargo is destined for lysosomal degradation⁷ with only an estimated 1%-2% of LNP cargo reaching the cytosol⁸.

A potential alternative RNA delivery vehicle is the extracellular vesicle (EV). These are lipid bilayer bound particles of between 30 to 2000nm in size and are involved in intercellular communication via the cell to cell transfer of messenger molecules, including RNAs⁹. This feature of EVs could be utilised to produce improved therapeutic RNA delivery vehicles as EVs possess numerous favourable features such as reduced immunogenicity¹⁰, an ability to cross biological barriers, and endogenous targeting capabilities¹¹. EVs also appear to be more efficient at delivering their cargo, with a recent estimate concluding that in contrast to the 1-2% delivered by LNPs, 30% of EV cargo taken up by HEK293T cells reaches the cytosol^{12,13}. In addition, our lab has recently produced evidence to suggest that EVs functionally deliver their cargo to recipient cells with an efficiency orders of magnitude greater than that of state-of-the-art DLin-DMA-MC3-LNPs¹⁴.

This difference in delivery efficiency may be explained by EVs and LNPs following differing physical routes post-uptake. Indeed, EVs have been shown to be rapidly taken up at filopodia active regions while LNPs were taken up more slowly at islands on the cell surface¹⁵. If the routes by which EVs and LNPs are taken up differs, then it is also possible

that the routes followed by EVs and LNPs post uptake also differ, which may explain the differences observed in functional delivery of cargo to the cytosol between these NPs. An improved understanding of EV and LNP trafficking may provide insights which could potentially help to improve the efficiency of therapeutic RNA delivery.

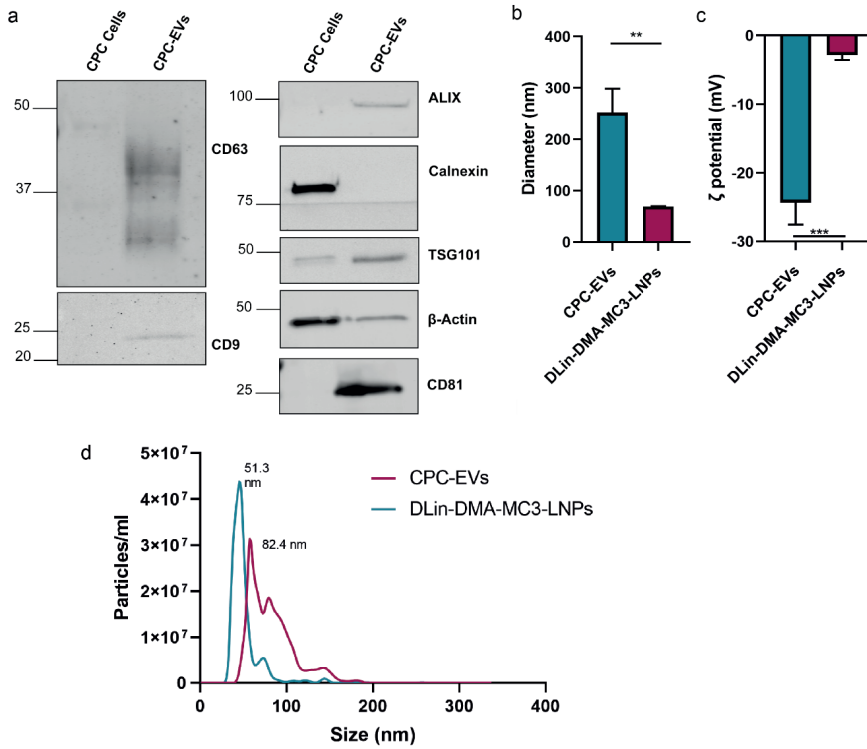
This study therefore aimed to compare the uptake and trafficking of cardiac progenitor cell-EVs (CPC-EVs) to state-of-the-art DLin-DMA-MC3-LNPs using high-content confocal microscopy live cell imaging and colocalisation analysis.

RESULTS

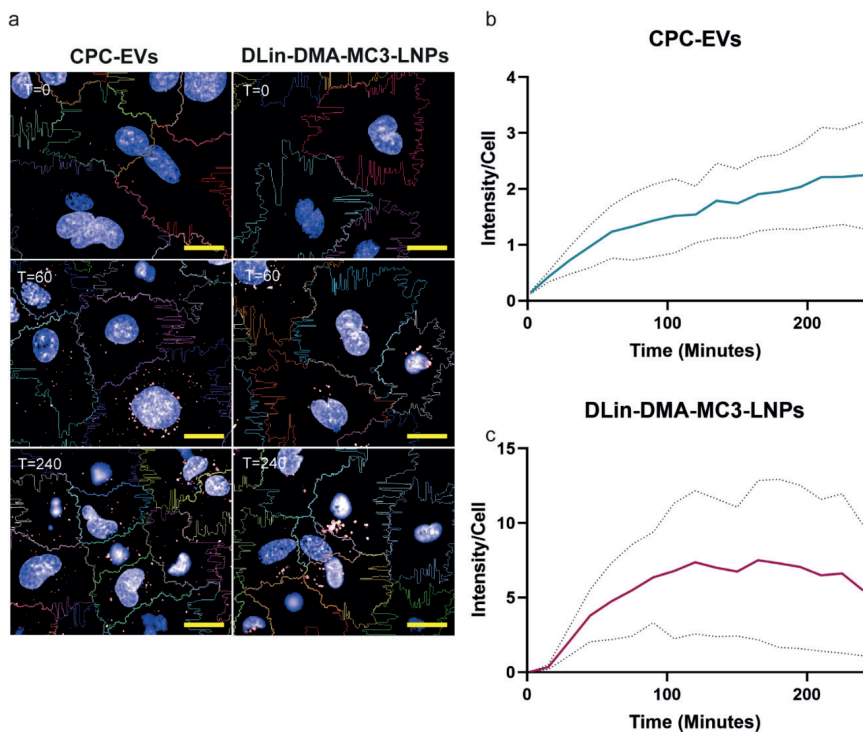
Firstly, EVs were isolated from CPC cells stably expressing palmTdT_oTomato. This fluorescent protein is attached to membranes of the cell via a palmitoylation (palm) anchor which results in the production of fluorescently labelled EVs which would allow tracking post-uptake¹⁶. To produce fluorescently labelled DLin-DMA-MC3-LNPs, 0.2% Liss-Rhodamine PE was included in the formulation.

Western blot analysis was performed to confirm the purity of EV preparations, adhering to MISEV guidelines¹⁷. This confirmed the positive enrichment of EV markers CD63, ALIX, Tsg101 and CD81 in CPC-EVs while negative enrichment of the ER marker calnexin and cytoskeletal β -Actin confirmed an absence of cellular contamination (Fig 1a).

It is possible that the size and charge of particles could influence uptake, so firstly, these properties were assessed. To measure the size of particles, dynamic light scattering (DLS) was performed. CPC-EVs possessed an average size of 252 \pm 46nm while DLin-DMA-MC3-LNPs were considerably smaller at 69 \pm 1nm (Fig 1b), which is in line with values recorded for the clinically approved formulation Onpattro¹. The surface charge of the NPs was measured using zeta potential analysis. CPC-EVs possessed a negative surface charge of -24 \pm 3 mV while DLin-DMA-MC3-LNPs possessed a neutral charge of -2 \pm 1 mV (Fig 1c). Nanoparticle tracking analysis (NTA) was also performed and produced typical size distributions for EVs and DLin-DMA-MC3-LNPs. DLin-DMA-MC3-LNPs possessed a mode size of 51.3nm while CPC-EVs possessed a mode size of 82.4nm. The discrepancy in size estimates between DLS and NTA can be explained by the sensitivity of DLS to high light scattering larger particles which can result in inflated size estimates.

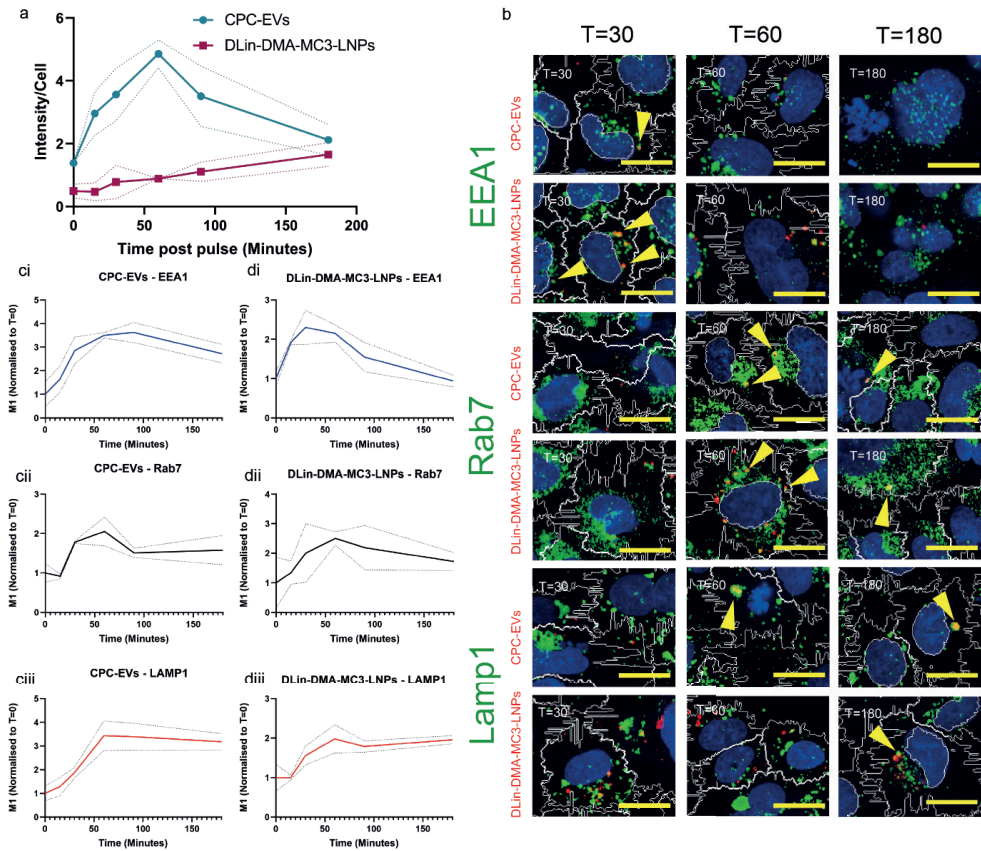


▲ Figure 1. Physical characterisation of NPs. Western blot analysis of CPC cell lysates and CPC-EVs for EV markers (CD63, ALIX, TSG101 and CD81) and EV negative markers (Calnexin and β -Actin) (a). DLS analysis of CPC-EVs and DLin-DMA-MC3-LNPs (b). ζ potential analysis of CPC-EVs and DLin-DMA-MC3-LNPs (c). Nanoparticle Tracking Analysis (NTA) size distributions of CPC-EVs and DLin-DMA-MC3-LNPs (d). n=3 technical replicates, means and S.D. are displayed, Student's T test was used for statistical analysis, ** = $p < 0.005$, *** = $p < 0.0005$.



▲ **Figure 2.** Uptake kinetics of NPs in HMEC-1 cells. Live cell confocal imagery of HMEC-1 cells treated with CPC-EVs and DLin-DMA-MC3-LNPs at 0, 60 and 240 minutes post addition of NPs (a). tdTomato (CPC-EV) (b) and rhodamine (DLin-DMA-MC3-LNPs) (c) signal intensity per cell over time post addition of NPs as determined by Columbus image analysis software, $n=3$ technical replicates, means \pm S.D. are displayed.

It is known that endocytosis is the major route by which EVs and LNPs are taken up by cells^{7,18}. To assess and compare this process, DLin-DMA-MC3-LNPs and CPC-EVs were applied to HMEC-1 cells and the uptake of particles was assessed over time by calculating fluorescence intensity per cell. Fluorescent signal was then observed inside HMEC-1 cells for both CPC-EVs and DLin-DMA-MC3-LNPs (Fig 2a). This signal was detected immediately after CPC-EV addition and steadily increased over the 4 hour time course of the experiment (Fig 2b). In comparison to CPC-EVs, DLin-DMA-MC3-LNP took longer to be detected, with detectable signal appearing after 15 minutes. This signal steadily increased in intensity for two hours until levelling off (Fig 2c).



▲Figure 3. Endosomal marker pulse-chase colocalisation analysis. tdTomato (CPC-EV) and rhodamine (DLin-DMA-MC3-LNPs) signal intensity per cell at each time point used in pulse-chase experiments as determined by Columbus image analysis software (a). Confocal microscopy images obtained 30 minutes, 60 minutes and 180 minutes post pulse addition of CPC-EVs and DLin-DMA-MC3-LNPs. Early endosomal (EEA1), late endosomal (Rab7) and lysosomal markers (Lamp1) are shown in green, NPs are shown in red and nuclei in blue. White lines indicate cell area. Areas of colocalisation are indicated with yellow arrows, scale bars represent 20 μ m (b). M1 localisation coefficients normalised to T=0 value of CPC-EVs and EEA1 (ci), Rab7 (cii) and Lamp1 (ciii) over time. M1 localisation coefficients normalised to T=0 value of DLin-DMA-MC3-LNPs and EEA1 (di), Rab7 (dii) and Lamp1 (diii) over time. n=3 technical replicates, means \pm S.D. are displayed.

To investigate and compare post-uptake trafficking of EVs and LNPs, a pulse-chase experiment was then performed. Prior to addition to cells, nanoparticles were first preincubated in 10% FCS in order to allow PEG dissociation from the surface of DLin-DMA-MC3-LNPs, which is a critical step in their uptake¹⁹. HMEC-1 cells were then pulsed with NPs by incubation at 4°C to allow binding while inhibiting uptake. HMEC-1 cells were then washed and the cells were incubated at 37°C to allow uptake and post-uptake trafficking.

The chase phase of the experiment involved fixation at various time points followed by visualisation of endosomal markers using immunofluorescence and colocalisation analysis to determine the proportion of overlap with endosomal markers at different time points. The experiment was performed with a single pulse of nanoparticles at 4°C rather than a period of uninhibited uptake followed by colocalisation analysis as a shorter and more condensed pulse of particles would allow for better resolution of the order through which particles travelled through endosomal compartments.

The endosomal markers chosen were EEA1, Rab7 and Lamp1. EEA1 is an early endosome marker and is involved in the trafficking and fusion of endosomal membranes²⁰. Rab7 is a late endosome marker which belongs to the small Rab GTPases and is involved with the trafficking of early to late endosomes²¹, while Lamp1 is a lysosomal membrane protein²². By assessing the timing and magnitude of colocalisation with these early, middle and late endocytic markers, the routes of NP post-uptake trafficking was assessed.

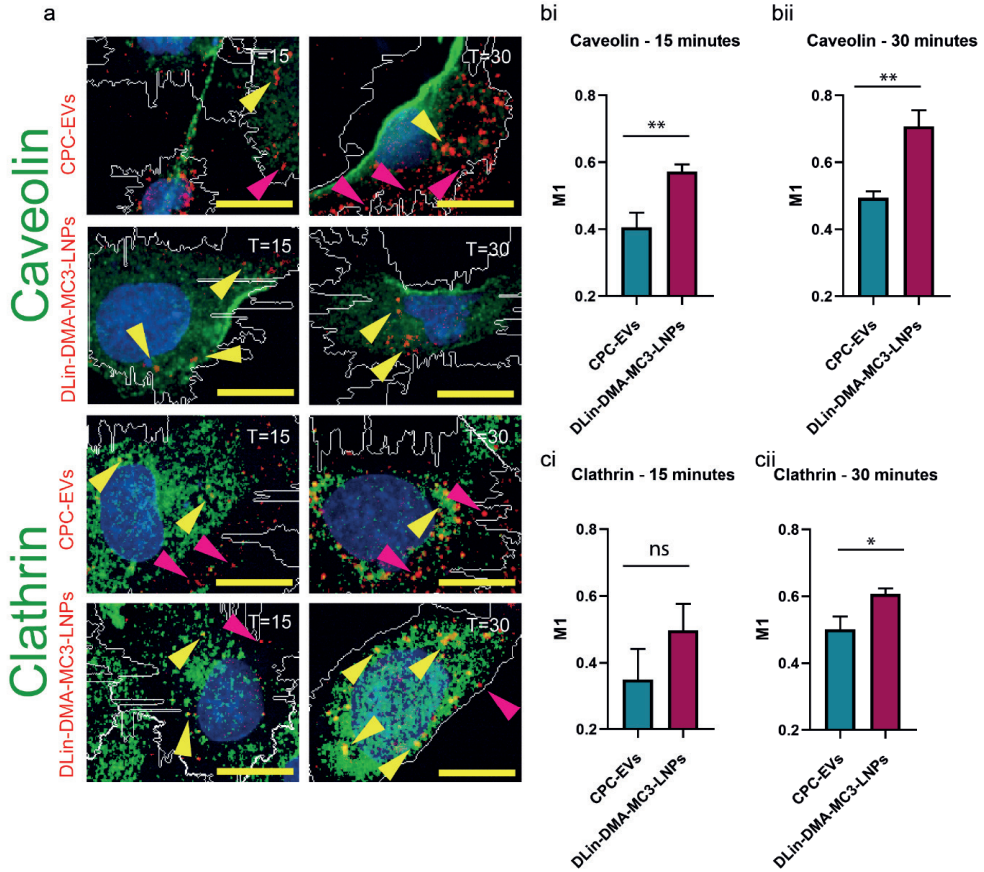
Interestingly, during this analysis it became apparent that signal intensity did not remain stable during the chase phase of the experiment. tdTomato signal derived from CPC-EVs increased at each time point before peaking at 60 minutes and reducing at following time points. Rhodamine intensity derived from DLin-DMA-MC3-LNPs produced a less distinct pattern and increased slightly at each time point (Fig 3a).

The initial increase in signal may be explained by concentration of EVs in intracellular compartments, thereby increasing the level of signal above the threshold of detection. At earlier time points, EVs could be more dispersed throughout the cell, resulting in less regions at which signal intensity is above the threshold detection. The reduction in signal at later time points could be explained similarly, or alternatively by lysosomal degradation of EVs resulting in loss of signal.

The endosomal markers produced distinct cellular distribution patterns while NP signal could be observed in a punctuate pattern. Spots of colocalisation could be observed between the different endosomal markers and NP signal (Fig 3b). Endosomal staining was also confirmed to be specific as dual staining with different endosomal markers did not demonstrate colocalisation between different markers (Sup Fig 1).

Colocalisation of CPC-EVs and EEA1 steadily increased with time, plateauing at 60 minutes before slightly reducing by 180 minutes (Fig 3b,ci). Rab7 displayed a similar pattern, with colocalisation peaking at 60 minutes before dropping off at later timepoints (Fig 3cii). LAMP1 colocalisation also peaked at 60 minutes and did not drop at later time points

(Fig 3cii). This is not unexpected as LAMP1 is a lysosomal marker, which is the terminal endocytic compartment reached by NPs post-uptake.



▲Figure 4. Endocytosis pathway component pulse-chase colocalisation analysis. Confocal microscopy images obtained 15 and 30 minutes post pulse addition of CPC-EVs and DLin-DMA-MC3-LNPs. Caveolin and Clathrin are shown in green, NPs are shown in red and nuclei in blue. Areas of colocalisation are indicated with yellow arrows, areas of no colocalisation are indicated in pink scale bars represent 20 μ m (1). M1 colocalisation coefficients of CPC-EVs and DLin-DMA-MC3-LNPs with Caveolin at 15 minutes (bi) and 30 minutes (bii) post pulse addition. M1 colocalisation coefficients of CPC-EVs and DLin-DMA-MC3-LNPs with Clathrin at 15 minutes (ci) and 30 minutes (cii) post pulse addition. n=3 technical replicates, means plus S.D are displayed. Student's T test was used for statistical analysis, * = $p < 0.05$, ** = $p < 0.005$.

DLin-DMA-MC3-LNP colocalisation with EEA1, Rab7 and LAMP1 displayed similar patterns, however, interestingly the timing of colocalisation with EEA1 was different. In contrast to CPC-EVs, DLin-DMA-MC3-LNPs colocalisation with EEA1 peaked earlier after 30 minutes before dropping to baseline by 180 minutes (Fig 3di). Similar to CPC-EVs,

colocalisation with Rab7 peaked at 60 minutes before dropping slightly at later timepoints (Fig 3dii) while colocalisation with LAMP1 also peaked at 60 minutes (Fig 3diii).

In order to compare routes of NP uptake, the pulse-chase experiment was repeated using the markers caveolin and clathrin. Caveolin lines caveolae on the cell surface and is a mediator of caveolae-mediated, clathrin-independent endocytosis⁷, while clathrin, which is found on cells of all types is involved in the classical clathrin-mediated route of endocytosis⁷. Both proteins have been investigated for their roles in EV uptake¹⁸. Colocalisation with these markers at early time points could therefore provide information regarding routes of endocytosis.

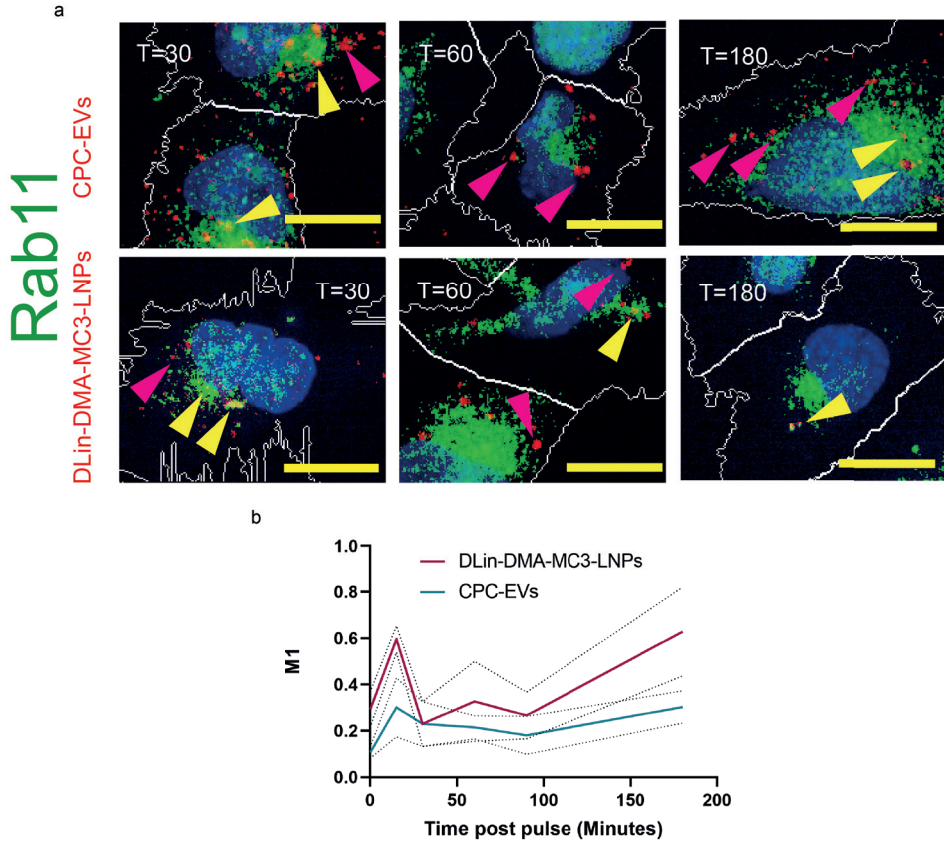
As with the previous pulse-chase experiment, these markers again produced distinct staining patterns while NP signal was observed in a punctate pattern with varying degrees of colocalisation with endocytic markers at different time points (Fig 4a). To investigate the extent to which clathrin or caveolin mediated uptake was involved in the uptake of CPC-EVs and DLin-DMA-MC3-LNPs, the raw M1 colocalisation coefficients rather than the normalised coefficients normalised to background T=0 levels were determined (Fig 4b, c).

Colocalisation of CPC-EVs with caveolin was lower than that of DLin-DMA-MC3-LNPs with M1 values of 0.4 ± 0.04 versus 0.57 ± 0.02 15 minutes post-pulse (Fig 4bi) and 0.49 ± 0.02 versus 0.7 ± 0.05 30 minutes post-pulse (Fig 4bii). This points towards a greater involvement of caveolin in the uptake of DLin-DMA-MC3-LNPs as compared to CPC-EVs.

Similarly to caveolin, the colocalisation of CPC-EVs with clathrin was also lower than that of DLin-DMA-MC3-LNPs. M1 values for Clathrin 15 minutes post-pulse addition of nanoparticles were 0.34 ± 0.09 versus 0.49 ± 0.07 for CPC-EVs and DLin-DMA-MC3-LNPs respectively. At 30 minutes these values rose to 0.5 ± 0.01 and 0.6 ± 0.02 for CPC-EVs and DLin-DMA-MC3-LNPs respectively. This suggests that clathrin, as well as caveolin play a greater role in the uptake of DLin-DMA-MC3-LNPs as compared to CPC-EVs in HMEC-1 cells.

The final marker to be investigated in pulse-chase colocalisation experiments was Rab11. Rather than being directly involved in the early endosome to lysosome pathway this protein is a regulator of recycling endosomes²³ and may be of relevance as colocalisation with this marker has been shown to affect functional delivery²⁴. As with all other markers investigated here, Rab11 staining produced a distinct pattern (Fig 5a). Interestingly, and in contrast to other markers investigated here, both CPC-EVs and DLin-DMA-MC3-LNPs displayed two peaks of colocalisation with Rab11, the first at 15 minutes and the second after 180 minutes (Fig 5b).

Interestingly, despite CPC-EVs and DLin-DMA-MC3-LNPs displaying the same patterns, overall levels of colocalisation were higher for DLin-DMA-MC3-LNPs at both the 15 minute and 180 minute peaks.



▲**Figure 5** – Rab11 pulse-chase colocalisation analysis. Confocal microscopy images obtained 30 minutes, 60 minutes and 180 minutes post pulse addition of CPC-EVs and DLin-DMA-MC3-LNPs. Rab11 is shown in green, NPs are shown in red and nuclei in blue. Areas of colocalisation are indicated with yellow arrows, scale bars represent 20µm (b). M1 colocalisation coefficients normalised to T=0 value of Rab 11 and CPC-EVs (b) and DLin-DMA-MC3-LNPs (c) over time. n=3 technical replicates, means plus S.D. are displayed.

DISCUSSION

It has recently been demonstrated that EVs functionally deliver RNA to cells with an efficiency orders of magnitude greater than that of DLin-DMA-MC3-LNPs¹⁴. However, the mechanisms by which EVs achieve this greater efficiency remain unclear but could involve differential trafficking post-uptake. Therefore, this study aimed to investigate the intracellular routes of trafficking of CPC-EVs and DLin-DMA-MC3-LNPs post-uptake.

The results presented here demonstrate that CPC-EVs and DLin-DMA-MC3-LNPs colocalise with the endocytic compartments EEA1, Rab7 and Lamp1 to similar extents with similar timing. Peaks of colocalisation with DLin-DMA-MC3-LNPs and the endocytic markers displayed an ordered and expected pattern with early endosome marker EEA1 peaking first after 30 minutes, followed by the late endosome marker Rab7 and lysosomal marker Lamp1 which both peaked at 60 minutes. CPC-EVs displayed a similar pattern with colocalisation of all three markers peaking at 60 minutes.

A further point of consideration regarding the experiments performed here is the location of fluorescent label within the studied nanoparticles. As the likely mechanism of EV cargo release is membrane fusion in acidic late endosomes^{12,25} and the palmTdTTomato label found on CPC-EVs is membrane anchored, endosomal escape and cytosolic localisation of EV cargo would not be visualised. If membrane fusion and cargo release occurs, the membrane anchored label would remain in the membrane of endosomal compartment. Similarly, the rhodamine label on DLin-DMA-MC3-LNPs was membrane anchored. It should therefore be noted that the study of colocalisation performed here investigated the localisation of delivery vehicle rather than cargo and that studies investigating labelled cargo rather than membrane would also be of interest.

It is of interest that colocalisation of DLin-DMA-MC3-LNPs with EEA1 occurred at an earlier time point than was observed for CPC-EVs. This could suggest that CPC-EVs pass through an intermediate compartment before reaching early endosomal compartments while DLin-DMA-MC3-LNPs do not. The fact that DLin-DMA-MC3-LNPs displayed higher colocalisation signal with both caveolin and clathrin as compared to CPC-EVs at early time points is indicative of differential routes of endocytosis.

The trafficking rates of CPC-EVs and DLin-DMA-MC3-LNPs is of great interest as the rate of nanoparticle trafficking has been linked to delivery efficiency. In a study of various cancer cell lines, Sayers *et al* demonstrated that the speed of trafficking post-uptake was correlated with the functional delivery of an mRNA LNP cargo²⁷. However, the fact that

DLin-DMA-MC3-LNPs and CPC-EVs both appear to have accumulated in the lysosome at similar rates suggests that the trafficking rates of the two nanoparticles is not an explanation for the higher functional delivery efficiency of EVs.

DLin-DMA-MC3-LNPs were observed to colocalise with Rab11 to a greater extent than CPC-EVs. Rab11 positive compartments are recycling endosomes. The fact that DLin-DMA-MC3-LNPs were more highly colocalised with Rab11 suggests that they could have been sequestered within these compartments to a greater extent than CPC-EVs, which may help to explain the higher functional efficiency of EVs. Furthermore, acidic endolysosomes have been identified as the site of EV cargo release^{13,12}, meaning that EV accumulation in recycling endosomes could diminish functional delivery. Interestingly however, a recent report has implicated Rab11 positive recycling endosomes in the functional delivery of RNA to cells. Paramasivam *et al* demonstrated that colocalisation of a panel of LNPs with Rab11 correlated with an increased functional delivery of mRNA²⁴. This suggests that different intracellular sites may be important for the delivery of different NPs.

In this study, subtle differences between the trafficking of CPC-EVs and DLin-DMA-MC3-LNPs were observed. It is unclear what properties of the two nanoparticles may be responsible for dictating the manner in which they were trafficked. However, there are numerous features of nanoparticles which may influence trafficking. For instance, the size of a nanoparticle was shown to play a role by Aoyama *et al* who demonstrated that smaller particles of 30-100nm in diameter were trafficked faster than larger submicron sized particles²⁸.

In addition, the strength of interaction between a nanoparticle and the cell membrane has been shown to influence intracellular trafficking. Vasir *et al* employed atomic force microscopy to demonstrate that poly-(D,L-lactide-co-glycolide) particles functionalised with a poly-L-lysine coating to increase the force of cell surface membrane binding were more rapidly internalised and functionally delivered more of their cargo to the cytosol as compared to non-functionalised particles²⁹. This is of interest as EVs possess many surface proteins such as integrins which may increase the strength of cell surface binding¹¹.

In a similar manner to Vasir *et al* functionalised nanoparticles were used by Al Hajaj *et al* to study uptake and trafficking. In this case, quantum dots were coated with the surface ligands mercaptopropionic acid, dihydrolipoic acid, L-cysteine, or cysteamine in order to investigate how the surface chemistry of particles influences uptake and trafficking. It was found that although cysteamine coated particles were taken up the most efficiently, the majority of these particles were trafficked out of recipient cells via p-glycoprotein

mediated efflux³⁰. This demonstrates that the surface composition of particles can influence the endocytic routes taken post-uptake, which may explain the differences observed between DLin-DMA-MC3-LNPs and CPC-EVs as these particles possess highly different surface compositions.

The results of Al Hajaj *et al* also point towards an involvement of particle surface charge in trafficking as the cysteamine coating gave the quantum dots a cationic charge while the other tested particles were anionic. In addition, Yue *et al* demonstrated that anionic and cationic chitosan-based nanoparticles were trafficked differently in multiple cell lines with positively charged particles colocalising preferentially with the perinuclear region, while negatively charged particles colocalised more strongly with the lysosome³¹.

It should be noted that the results presented here are specific for a specific combination of recipient cell type, type of synthetic NP and EV-donor cell type. Although these results provide a useful insight into the post-uptake trafficking of CPC-EVs and DLin-DMA-MC3-LNPs in HMEC cells, these results cannot be extrapolated to explain observations in other cell types.

In conclusion, this study successfully compared the uptake and trafficking of CPC-EVs and DLin-DMA-MC3-LNPs. While some subtle differences were observed, CPC-EVs and DLin-DMA-MC3-LNPs displayed similar general uptake kinetic and post-uptake colocalisation patterns. This suggests that other features of EVs may confer them with high RNA delivery efficiency.

MATERIALS AND METHODS

Uptake Kinetics

24 hours prior to the experiment, HMEC-1 recipient cells were seeded at a density of 10,000 cells in CellStar 96-well cell culture black μ Clear bottom TC-treated microplates (Greiner-Bio). Before the addition of DLin-DMA-MC3-LNPs, the fluorescent dose was normalised by measuring the fluorescent signal of CPC-EVs and DLin-DMA-MC3-LNPs using a fluorescent plate reader at 561nm excitation, 601nm emission. The DLin-DMA-MC3-LNP stock was then diluted accordingly to normalise the fluorescent dose between the two particles. DLin-DMA-MC3-LNPs were then incubated for 1 hour at 37°C in 10% FBS to allow for the removal of PEG, which must happen before uptake can occur. For fair comparison, CPC-EVs were also incubated for 1 hour at 37°C in 10% FBS. HMEC-1 culture medium was then replaced with 100 μ l of fresh medium with 1 μ g/ml Hoechst 33342

(ThermoFisher Scientific). 50µl of nanoparticle suspension was added to the appropriate well in triplicate and the plate was immediately placed into a Yokogawa CV7000 confocal microscope with the incubator set at 37°C and 5% CO₂. Confocal images were produced immediately and every following 15 minutes at 60x magnification using the following filter settings: Hoechst: emission = 405 nm, power 30; acquisition =BP445/45, Exposure time = 200ms. PalmTdTomato and Liss Rhod: emission = 561 nm, power 30; acquisition =BP600/37, Exposure time = 200ms. To determine uptake at each time point, Columbus image analysis software was used (Perkin-Elmer).

Pulse-Chase Colocalisation

24 hours prior to the experiment, HMEC-1 recipient cells were seeded at a density of 10,000 cells in CellStar 96-well cell culture black µClear bottom TC-treated microplates (Greiner-Bio). In order to promote loss of PEG from the surface of DLin-DMA-MC3-LNPs, these particles were incubated for 1 hour in 10% FCS. For a fair comparison, the same treatment was applied to CPC-EVs. Prior to the addition of nanoparticles, plates were incubated at 4°C for 15 minutes. For the pulse phase of the experiment, nanoparticles were then added and plates were returned to incubation at 4°C for 1.5 hours to allow binding to the cell surface. After this 4°C incubation, the plates were placed on parafilm covered ice and cell culture medium was aspirated. Cells were then washed using PBS and plates were either fixed immediately in 2% PFA for 15 minutes to provide a T=0 timepoint or returned to incubation at 37°C. Plates were then fixed in 2% PFA after 15, 30, 60, 90 or 180 minutes of incubation. Cells were then permeabilised and labelled using the method described and a Yokogawa CV7000 confocal microscope was used to image cells using the following filter settings: Hoechst: emission = 405 nm, power 30; acquisition =BP445/45, Exposure time = 300ms. PalmTdTomato and Liss Rhod: emission = 561 nm, power 30; acquisition =BP600/37, Exposure time = 300ms. AF488: emission = 488 nm, power 30; acquisition =BP525/30, Exposure time = 300ms. To determine colocalisation, Columbus image analysis software was used.

Immunofluorescence

Prior to staining, cell culture medium was aspirated and cells were washed in PBS, then fixed for 15 minutes in 2% PFA. Nuclei were then labelled by incubation with 1 µg/ml Hoechst 33342 (ThermoFisher Scientific) for 10 minutes. Cells were then blocked and permeabilised by incubation in blocking buffer (5% FBS, 0.1% Saponin in PBS) for 1 hour at room temperature or overnight at 4°C. Primary antibodies were then added to cells

in antibody dilution buffer (1% BSA, 0.1% saponin in PBS) overnight at 4°C. The primary antibodies used were: Caveolin-1 1:200 (Cell signalling, (D46G3) XP Rabbit mAb 3267), Clathrin Heavy Chain 1:100 (Cell signalling, (D3C6) XP Rabbit mAb 4796), EEA1 1:100 (Cell signalling (C45B10) Rabbit mAb 3288), Rab7 1:100 (Cell signalling, (D95F2) XP Rabbit mAb 9367), Rab11 1:100 (Rab11 (D4F5) XP Rabbit mAb 5589) and Lamp1/CD107a (Thermo Fisher Scientific, (H4A3) 1:150). After 1 hour of primary antibody incubation or overnight incubation at 4°C, cells were washed 3 times using PBS containing 0.1% Saponin. Primary antibodies were detected using the addition of AF488 conjugated anti-rabbit 1:200 and FITC conjugated anti-mouse 1:200 secondary antibodies. After 2 hours of secondary antibody incubation at room temperature or overnight incubation at 4°C, cells were again washed 3 times using PBS containing 0.1% saponin and left in PBS before confocal imaging.

Image Analysis

Image analysis was performed using Columbus image analysis software (Perkin Elmer) as follows. Firstly, nuclei were identified using method B with a common threshold of 0.40. Cytoplasm region of interest was identified for each nucleus using the 445/45 channel with a common threshold of 0.0. All colocalisation coefficients were derived from analysis within this cytoplasmic region of interest. PalmTdTomato and Rhodamine signal was thresholding any signal >160 to 0. Endosomal marker signal was thresholded according to the intensity of each specific endosomal label. Signal intensity per cell was determined using the Calculate Intensity Properties feature. Mander's colocalisation coefficient for the two thresholded channels was determined using an ABB Calculate Correlation Properties plugin.

Cell Culture

HMEC-1 cells were cultured in MCDB-131 medium 10% FBS with GlutaMAX, 10 ng/ml rhEGF (Peprotech), 50 nM Hydrocortisone (Sigma) and 100 U/mL Penicillin-Streptomycin (Gibco) on plates coated with 0.1% gelatin (Sigma). Stable CPC lines were produced using lentiviral transduction using plasmids kindly provided by Prof. Xandra Breakefield¹⁶. CPC cells expressing the palmTdTomato construct were cultured in a 3:1 mix of M199 medium (Gibco) and EGM2/ Endothelial Cell Growth Medium 2 (Lonza) supplemented with Endothelial cell growth medium 2 supplement mix (CC-3162 or CC-4176, LONZA), NEAA/ MEM Non-Essential Amino Acids Solution (Gibco) and 100 U/mL Penicillin-Streptomycin (Gibco).

EV Isolation

palmTdToma cells were seeded in T175 flasks. Upon reaching 60-90% confluency, the supernatant was removed and cells were washed in PBS. The medium was then replaced with 20ml OptiMEM (Gibco). After 24h of incubation, the conditioned supernatant was removed and spun at 300 x g for 5 minutes at 4°C to remove floating cells and then again at 2000 x g for 15 minutes at 4°C to remove debris and dead cells. This conditioned supernatant was then filtered through 0.45µm bottle top filters and concentrated to approximately 10ml using tangential filter flow filtration with a peristaltic pump attached to a Minimate 100 kDa Omega Membrane cassette (Pall Corporation). A 100 kDa Amicon Ultra-15 Centrifugal filter (Merck) was then used to concentrate this medium further down to 1 ml. EVs were then isolated using size exclusion chromatography using a Tricorn 10/300 column with Sepharose 4 Fast Flow resin on an AKTA Start chromatography system (all GE Healthcare Life Sciences). Fractions containing the EVs were then pooled and concentrated to the required volume using a 100 kDa Amicon Ultra-15 Centrifugal filter.

DLin-DMA-MC3-LNP Production

Rhodamine labelled DLin-MC3-DMA containing LNPs were composed of DLin-MC3 DMA/Cholesterol/DSPC/PEG-DMG/Liss Rhodamine PE at a molar ratio of 50/38.3/10/1.5/0.2. LNPs were produced by microfluidic mixing in a NanoAssemblr Benchtop device (Precision Nanosystems, Vancouver, BC, Canada). Prior to production, lipids were diluted to a total lipid concentration of 5mM in pure ethanol while RNA was diluted in a 25mM acetate buffer (pH4). LNPs were produced with an N/P ratio of 12 at a flow of 6ml/minute with a flow rate ratio of 3:1 aqueous to lipid phase. LNPs were then dialysed into PBS overnight using 20kDa G2 dialysis cassettes (ThermoFisher). After dialysis, LNPs were sterilized by membrane filtration using 0.45µm syringe membrane filters.

Western Blotting

CPC cells and EV samples were lysed in RIPA buffer containing a protease inhibitor cocktail. Cell lysates were spun at max speed for 5 minutes at 4°C in order to pellet non-soluble debris. In order to determine protein concentrations and load equal quantities of protein on SDS-PAGE gels, a microBCA protein assay kit (ThermoFisher) was used according to manufacturer's protocol. Samples were mixed with sample loading buffer with 100µM DTT, or without DTT when blotting for tetraspanins. Samples were run on a 4-12% gradient Bis-Tris polyacrylamide gel (Thermo Fisher Scientific) before blotting

onto Immobilon-FL polyvinylidene difluoride membranes (Millipore). Membranes were then blocked using blocking buffer composed of Odyssey Blocking Buffer (LI-COR Biosciences) mixed 1:1 with Tris-Buffered Saline, 0.1% tween-20 (TBS-T). Membranes were then probed using primary antibodies diluted 1:100 in blocking buffer. These antibodies were ALIX 1:1000 (ThermoFisher Scientific, MA1-83977), Calnexin 1:1000 (GeneTex, GTX101676), CD9 1:1000 (Abcam, ab92726), TSG101 1:1000 (Abcam, ab30871) and CD63 1:1000 (Abcam, ab8219). The blots were then washed 3 times for 10 minutes at room temperature in TBS-T before Secondary antibodies were applied overnight at 4°C at a 1:7500 dilution in blocking buffer. The secondary antibodies used were anti-rabbit IgG conjugated to AlexaFluor680 (ThermoFisher Scientific, A-21076) or anti-mouse IgG conjugated to IR dye 800CW. Blots were then washed 3 times for 10 minutes at room temperature in TBS-T and scanned using an Odyssey Infrared Imager (LI-COR Biosciences) at 700nm and 800nm.

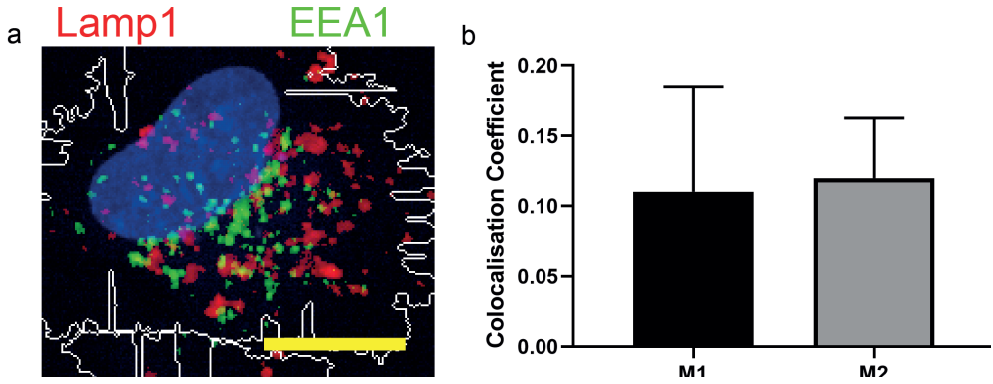
Nanoparticle Tracking Analysis

EV and LNP particle size distributions were produced using a Nanosight S500 nanoparticle analyzer (Malvern Instruments) equipped with a 405nm laser. Samples were diluted in PBS to a concentration that gave between 30 to 100 tracks per frame. Videos were acquired with a camera level of 16. EVs were analyzed with a detection threshold of 6 while LNPs were analyzed with a detection threshold of 4, due to their smaller size. NTA Software version 3.4 was used for video analysis

Size and Zeta potential measurement

Dynamic Light Scattering (DLS) was performed to measure the hydrodynamic radius of EVs and DLin-MC3-DMA-LNPs using a Nano S Zetasizer instrument (Malvern). Samples were diluted in DPBS and light scattering was measured at an angle of 173 at 25°C for 10s and repeated at least 10 times. Zeta potential measurement was performed on samples using a Nano Z Zetasizer device on samples diluted in 0.1x PBS.

SUPPLEMENTARY INFORMATION



▲**Supplementary Figure 1:** Dual staining colocalisation analysis. Confocal microscopy images obtained after staining with both EEA1 and LAMP1 (b). Scale bar represents 20 μm . Mander's M1 and M2 colocalisation coefficient determined from dual staining. M1 = proportion of red pixels (Lamp1) that are also green (EEA1), M2 = proportion of green pixels (EEA1) that are also red (Lamp1).

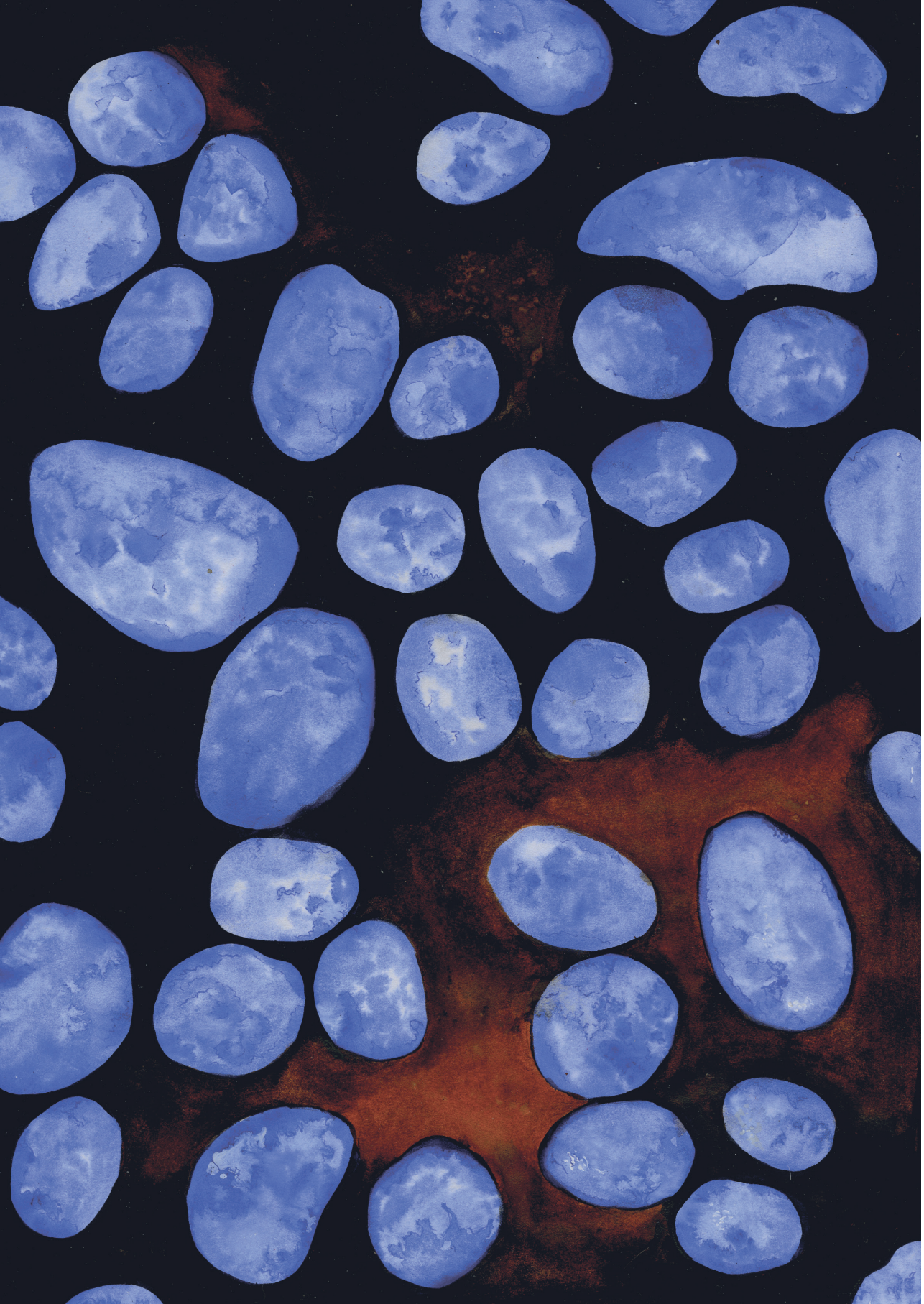
REFERENCES

- (1) Akinc, A.; Maier, M. A.; Manoharan, M.; Fitzgerald, K.; Jayaraman, M.; Barros, S.; Ansell, S.; Du, X.; Hope, M. J.; Madden, T. D.; Mui, B. L.; Semple, S. C.; Tam, Y. K.; Ciufolini, M.; Witzigmann, D.; Kulkarni, J. A.; van der Meel, R.; Cullis, P. R. The Onpattro Story and the Clinical Translation of Nanomedicines Containing Nucleic Acid-Based Drugs. *Nat. Nanotechnol.* **2019**, *14* (12), 1084–1087. <https://doi.org/10.1038/s41565-019-0591-y>.
- (2) Baden, L. R.; El Sahly, H. M.; Essink, B.; Kotloff, K.; Frey, S.; Novak, R.; Diemert, D.; Spector, S. A.; Roupheal, N.; Creech, C. B.; McGettigan, J.; Khetan, S.; Segall, N.; Solis, J.; Brosz, A.; Fierro, C.; Schwartz, H.; Neuzil, K.; Corey, L.; Gilbert, P.; Janes, H.; Follmann, D.; Marovich, M.; Mascola, J.; Polakowski, L.; Ledgerwood, J.; Graham, B. S.; Bennett, H.; Pajon, R.; Knightly, C.; Leav, B.; Deng, W.; Zhou, H.; Han, S.; Ivarsson, M.; Miller, J.; Zaks, T. Efficacy and Safety of the mRNA-1273 SARS-CoV-2 Vaccine. *N. Engl. J. Med.* **2020**, *384* (5), 403–416. <https://doi.org/10.1056/NEJMoa2035389>.
- (3) Polack, F. P.; Thomas, S. J.; Kitchin, N.; Absalon, J.; Gurtman, A.; Lockhart, S.; Perez, J. L.; Pérez Marc, G.; Moreira, E. D.; Zerbini, C.; Bailey, R.; Swanson, K. A.; Roychoudhury, S.; Koury, K.; Li, P.; Kalina, W. V.; Cooper, D.; Frenck, R. W.; Hammitt, L. L.; Türeci, Ö.; Nell, H.; Schaefer, A.; Ünal, S.; Tresnan, D. B.; Mather, S.; Dormitzer, P. R.; Şahin, U.; Jansen, K. U.; Gruber, W. C. Safety and Efficacy of the BNT162b2 mRNA Covid-19 Vaccine. *N. Engl. J. Med.* **2020**, *383* (27), 2603–2615. <https://doi.org/10.1056/NEJMoa2034577>.
- (4) Huang, Y.; Hong, J.; Zheng, S.; Ding, Y.; Guo, S. Elimination Pathways of Systemically Delivered siRNA. *Mol. Ther.* **2009**, *19* (2), 381–385. <https://doi.org/10.1038/mt.2010.266>.
- (5) Evers, M. J. W.; Kulkarni, J. A.; Meel, R. Van Der; Cullis, P. R.; Vader, P.; Schiffelers, R. M. State-of-the-Art Design and Rapid-Mixing Production Techniques of Lipid Nanoparticles for Nucleic Acid Delivery. *Small Methods* **2018**, *1700375*, 1–20. <https://doi.org/10.1002/smt.201700375>.
- (6) Sadauskas, E.; Wallin, H.; Stoltenberg, M.; Vogel, U.; Doering, P.; Larsen, A.; Danscher, G. Kupffer Cells Are Central in the Removal of Nanoparticles from the Organism. *Part. Fibre Toxicol.* **2007**, *7* (3), 1–7. <https://doi.org/10.1186/1743-8977-4-10>.
- (7) Sahay, G.; Alakhova, D. Y.; Kabanov, A. V. Endocytosis of Nanomedicines. *J. Control. Release* **2010**, *145* (3), 182–195. <https://doi.org/10.1016/j.jconrel.2010.01.036>.
- (8) Gilleron, J.; Querbes, W.; Zeigerer, A.; Borodovsky, A.; Marsico, G.; Schubert, U.; Manygoats, K.; Seifert, S.; Andree, C.; Stöter, M.; Epstein-Barash, H.; Zhang, L.; Kotliansky, V.; Fitzgerald, K.; Fava, E.; Bickle, M.; Kalaidzidis, Y.; Akinc, A.; Maier, M.; Zerial, M. Image-Based Analysis of Lipid Nanoparticle-Mediated siRNA Delivery, Intracellular Trafficking and Endosomal Escape. *Nat. Biotechnol.* **2013**, *31* (7), 638–646. <https://doi.org/10.1038/nbt.2612>.
- (9) El Andaloussi, S.; Mäger, I.; Breakefield, X. O.; Wood, M. J. A. Extracellular Vesicles: Biology and Emerging Therapeutic Opportunities. *Nat. Rev. Drug Discov.* **2013**, *12* (5), 347–357. <https://doi.org/10.1038/nrd3978>.
- (10) Vader, P.; Mol, E. A.; Pasterkamp, G.; Schiffelers, R. M. Extracellular Vesicles for Drug Delivery. *Adv. Drug Deliv. Rev.* **2016**, *106*, 148–156. <https://doi.org/10.1016/j.addr.2016.02.006>.
- (11) Murphy, D. E.; Jong, O. G. De; Brouwer, M.; Wood, M. J.; Lavie, G.; Schiffelers, R. M.; Vader, P. Extracellular Vesicle-Based Therapeutics : Natural versus Engineered Targeting and Trafficking. *Exp. Mol. Med.* **2019**. <https://doi.org/10.1038/s12276-019-0223-5>.
- (12) Bonsergent, E.; Grisard, E.; Buchrieser, J.; Lavie, G. Quantitative Characterization of Extracellular Vesicle Uptake and Content Delivery within Mammalian Cells. *Nat. Commun.* No. 2021, 1–11. <https://doi.org/10.1038/s41467-021-22126-y>.

- (13) Joshi, B. S.; de Beer, M. A.; Giepmans, B. N. G.; Zuhorn, I. S. Endocytosis of Extracellular Vesicles and Release of Their Cargo from Endosomes. *ACS Nano* **2020**, *14* (4), 4444–4455. <https://doi.org/10.1021/acsnano.9b10033>.
- (14) Murphy, D. E.; de Jong, O. G.; Evers, M. J. W.; Nurazizah, M.; Schiffelers, R. M.; Vader, P. Natural or Synthetic RNA Delivery: A Stoichiometric Comparison of Extracellular Vesicles and Synthetic Nanoparticles. *Nano Lett.* **2021**, *21* (4), 1888–1895. <https://doi.org/10.1021/acs.nanolett.1c00094>.
- (15) Heusermann, W.; Hean, J.; Trojer, D.; Steib, E.; von Bueren, S.; Graff-Meyer, A.; Genoud, C.; Martin, K.; Pizzato, N.; Voshol, J.; Morrissey, D. V.; Andaloussi, S. E. L.; Wood, M. J.; Meisner-Kober, N. C. Exosomes Surf on Filopodia to Enter Cells at Endocytic Hot Spots, Traffic within Endosomes, and Are Targeted to the ER. *J. Cell Biol.* **2016**, *213* (2), 173–184. <https://doi.org/10.1083/jcb.201506084>.
- (16) Lai, C. P.; Kim, E. Y.; Badr, C. E.; Weissleder, R.; Mempel, T. R.; Tannous, B. A.; Breakefield, X. O. Visualization and Tracking of Tumour Extracellular Vesicle Delivery and RNA Translation Using Multiplexed Reporters. *Nat. Commun.* **2015**, *6* (May), 1–12. <https://doi.org/10.1038/ncomms8029>.
- (17) Théry, C.; Witwer, K. W.; Aikawa, E.; Alcaraz, M. J.; Anderson, J. D.; Andriantsitohaina, R.; Antoniou, A.; Arab, T.; Archer, F.; Atkin-Smith, G. K.; Ayre, D. C.; Bach, J.-M.; Bachurski, D.; Baharvand, H.; Balaj, L.; Baldacchino, S.; Bauer, N. N.; Baxter, A. A.; Bebawy, M.; Beckham, C.; Bedina Zavec, A.; Benmoussa, A.; Berardi, A. C.; Bergese, P.; Bielska, E.; Blenkiron, C.; Bobis-Wozowicz, S.; Boilard, E.; Boireau, W.; Bongiovanni, A.; Borràs, F. E.; Bosch, S.; Boulanger, C. M.; Breakefield, X.; Breglio, A. M.; Brennan, M. Á.; Brigstock, D. R.; Brisson, A.; Broekman, M. L. D.; Bromberg, J. F.; Bryl-Górecka, P.; Buch, S.; Buck, A. H.; Burger, D.; Busatto, S.; Buschmann, D.; Bussolati, B.; Buzás, E. I.; Byrd, J. B.; Camussi, G.; Carter, D. R. F.; Caruso, S.; Chamley, L. W.; Chang, Y.-T.; Chen, C.; Chen, S.; Cheng, L.; Chin, A. R.; Clayton, A.; Clerici, S. P.; Cocks, A.; Cocucci, E.; Coffey, R. J.; Cordeiro-da-Silva, A.; Couch, Y.; Coumans, F. A. W.; Coyle, B.; Crescitelli, R.; Criado, M. F.; D'Souza-Schorey, C.; Das, S.; Datta Chaudhuri, A.; de Candia, P.; De Santana, E. F.; De Wever, O.; del Portillo, H. A.; Demaret, T.; Deville, S.; Devitt, A.; Dhondt, B.; Di Vizio, D.; Dieterich, L. C.; Dolo, V.; Dominguez Rubio, A. P.; Dominici, M.; Dourado, M. R.; Driedonks, T. A. P.; Duarte, F. V.; Duncan, H. M.; Eichenberger, R. M.; Ekström, K.; EL Andaloussi, S.; Elie-Caille, C.; Erdbrügger, U.; Falcón-Pérez, J. M.; Fatima, F.; Fish, J. E.; Flores-Bellver, M.; Försönits, A.; Frelet-Barrand, A.; Fricke, F.; Fuhrmann, G.; Gabrielsson, S.; Gámez-Valero, A.; Gardiner, C.; Gärtner, K.; Gaudin, R.; Gho, Y. S.; Giesel, B.; Gilbert, C.; Gimona, M.; Giusti, I.; Goberdhan, D. C. I.; Görgens, A.; Gorski, S. M.; Greening, D. W.; Gross, J. C.; Gualerzi, A.; Gupta, G. N.; Gustafson, D.; Handberg, A.; Haraszti, R. A.; Harrison, P.; Hegyesi, H.; Hendrix, A.; Hill, A. F.; Hochberg, F. H.; Hoffmann, K. F.; Holder, B.; Holthofer, H.; Hosseinkhani, B.; Hu, G.; Huang, Y.; Huber, V.; Hunt, S.; Ibrahim, A. G.-E.; Ikezu, T.; Inal, J. M.; Isin, M.; Ivanova, A.; Jackson, H. K.; Jacobsen, S.; Jay, S. M.; Jayachandran, M.; Jenster, G.; Jiang, L.; Johnson, S. M.; Jones, J. C.; Jong, A.; Jovanovic-Talisman, T.; Jung, S.; Kalluri, R.; Kano, S.; Kaur, S.; Kawamura, Y.; Keller, E. T.; Khamari, D.; Khomyakova, E.; Khvorova, A.; Kierulf, P.; Kim, K. P.; Kislinger, T.; Klingeborn, M.; Klinke, D. J.; Kornek, M.; Kosanović, M. M.; Kovács, Á. F.; Krämer-Albers, E.-M.; Krasemann, S.; Krause, M.; Kurochkin, I. V.; Kusuma, G. D.; Kuypers, S.; Laitinen, S.; Langevin, S. M.; Languino, L. R.; Lannigan, J.; Lässer, C.; Laurent, L. C.; Lavieu, G.; Lázaro-Ibáñez, E.; Le Lay, S.; Lee, M.-S.; Lee, Y. X. F.; Lemos, D. S.; Lenassi, M.; Leszczynska, A.; Li, I. T. S.; Liao, K.; Libregts, S. F.; Ligeti, E.; Lim, R.; Lim, S. K.; Linē, A.; Linnemannstöns, K.; Llorente, A.; Lombard, C. A.; Lorenovic, M. J.; Lörlincz, Á. M.; Lötvall, J.; Lovett, J.; Lowry, M. C.; Loyer, X.; Lu, Q.; Lukomska, B.; Lunavat, T. R.; Maas, S. L. N.; Malhi, H.; Marcilla, A.; Mariani, J.; Mariscal, J.; Martens-Uzunova, E. S.; Martin-Jaular, L.; Martinez, M. C.; Martins, V. R.; Mathieu, M.; Mathivanan, S.; Mauger, M.; McGinnis, L. K.; McVey, M. J.; Meckes, D. G.; Meehan, K. L.; Mertens, I.; Minciacchi, V. R.; Möller, A.; Møller Jørgensen, M.; Morales-Kastresana, A.; Morhayim, J.; Mullier, F.; Muraca, M.; Musante, L.; Mussack, V.; Muth, D. C.; Myburgh, K. H.; Najrana, T.; Nawaz, M.; Nazarenko, I.; Nejsun,

- P.; Neri, C.; Neri, T.; Nieuwland, R.; Nimrichter, L.; Nolan, J. P.; Nolte-’t Hoen, E. N. M.; Noren Hooten, N.; O’Driscoll, L.; O’Grady, T.; O’Loughlen, A.; Ochiya, T.; Olivier, M.; Ortiz, A.; Ortiz, L. A.; Osteikoetxea, X.; Østergaard, O.; Ostrowski, M.; Park, J.; Pegtel, D. M.; Peinado, H.; Perut, F.; Pfaffl, M. W.; Phinney, D. G.; Pieters, B. C. H.; Pink, R. C.; Pisetsky, D. S.; Pogge von Strandmann, E.; Polakovícova, I.; Poon, I. K. H.; Powell, B. H.; Prada, I.; Pulliam, L.; Quesenberry, P.; Radeghieri, A.; Raffai, R. L.; Raimondo, S.; Rak, J.; Ramirez, M. I.; Raposo, G.; Rayyan, M. S.; Regev-Rudzki, N.; Ricklefs, F. L.; Robbins, P. D.; Roberts, D. D.; Rodrigues, S. C.; Rohde, E.; Rome, S.; Rouschop, K. M. A.; Rughetti, A.; Russell, A. E.; Saá, P.; Sahoo, S.; Salas-Huenuleo, E.; Sánchez, C.; Saugstad, J. A.; Saul, M. J.; Schiffelers, R. M.; Schneider, R.; Schøyen, T. H.; Scott, A.; Shahaj, E.; Sharma, S.; Shatnyeva, O.; Shekari, F.; Shelke, G. V.; Shetty, A. K.; Shiba, K.; Siljander, P. R.-M.; Silva, A. M.; Skowronek, A.; Snyder, O. L.; Soares, R. P.; Sódar, B. W.; Soekmadji, C.; Sotillo, J.; Stahl, P. D.; Stoorvogel, W.; Stott, S. L.; Strasser, E. F.; Swift, S.; Tahara, H.; Tewari, M.; Timms, K.; Tiwari, S.; Tixeira, R.; Tkach, M.; Toh, W. S.; Tomasini, R.; Torrecilhas, A. C.; Tosar, J. P.; Toxavidis, V.; Urbanelli, L.; Vader, P.; van Balkom, B. W. M.; van der Grein, S. G.; Van Deun, J.; van Herwijnen, M. J. C.; Van Keuren-Jensen, K.; van Niel, G.; van Royen, M. E.; van Wijnen, A. J.; Vasconcelos, M. H.; Vechetti, I. J.; Veit, T. D.; Vella, L. J.; Velot, É.; Verweij, F. J.; Vestad, B.; Viñas, J. L.; Visnovitz, T.; Vukman, K. V.; Wahlgren, J.; Watson, D. C.; Wauben, M. H. M.; Weaver, A.; Webber, J. P.; Weber, V.; Wehman, A. M.; Weiss, D. J.; Welsh, J. A.; Wendt, S.; Wheelock, A. M.; Wiener, Z.; Witte, L.; Wolfram, J.; Xagorari, A.; Xander, P.; Xu, J.; Yan, X.; Yáñez-Mó, M.; Yin, H.; Yuana, Y.; Zappulli, V.; Zarubova, J.; Žekas, V.; Zhang, J.; Zhao, Z.; Zheng, L.; Zheutlin, A. R.; Zickler, A. M.; Zimmermann, P.; Zivkovic, A. M.; Zocco, D.; Zuba-Surma, E. K. Minimal Information for Studies of Extracellular Vesicles 2018 (MISEV2018): A Position Statement of the International Society for Extracellular Vesicles and Update of the MISEV2014 Guidelines. *J. Extracell. Vesicles* **2018**, 7 (1), 1535750. <https://doi.org/10.1080/20013078.2018.1535750>.
- (18) Costa Verdera, H.; Gitz-Francois, J. J.; Schiffelers, R. M.; Vader, P. Cellular Uptake of Extracellular Vesicles Is Mediated by Clathrin-Independent Endocytosis and Macropinocytosis. *J. Control. Release* **2017**, 266 (July), 100–108. <https://doi.org/10.1016/j.jconrel.2017.09.019>.
- (19) Mui, B. L.; Tam, Y. K.; Jayaraman, M.; Ansell, S. M.; Du, X.; Tam, Y. Y. C.; Lin, P. J.; Chen, S.; Narayanannair, J. K.; Rajeev, K. G.; Manoharan, M.; Akinc, A.; Maier, M. A.; Cullis, P.; Madden, T. D.; Hope, M. J. Influence of Polyethylene Glycol Lipid Desorption Rates on Pharmacokinetics and Pharmacodynamics of siRNA Lipid Nanoparticles. *Mol. Ther. Nucleic Acids* **2013**, 2 (12), e139–e139. <https://doi.org/10.1038/mtna.2013.66>.
- (20) Christoforidis, S.; McBride, H. M.; Burgoyne, R. D.; Zerial, M. The Rab5 Effector EEA1 Is a Core Component of Endosome Docking. *Nature* **1999**, 397 (6720), 621–625. <https://doi.org/10.1038/17618>.
- (21) Feng, Y.; Press, B.; Wandinger-Ness, A. Rab7: An Important Regulator of Late Endocytic Membrane Traffic. *J. Cell Biol.* **1995**, 131 (6 Pt 1), 1435–1452. <https://doi.org/10.1083/jcb.131.6.1435>.
- (22) Fukuda, M. Lysosomal Membrane Glycoproteins. Structure, Biosynthesis, and Intracellular Trafficking. *J. Biol. Chem.* **1991**, 266 (32), 21327–21330.
- (23) Ullrich, O.; Reinsch, S.; Urbé, S.; Zerial, M.; Parton, R. G. Rab11 Regulates Recycling through the Pericentriolar Recycling Endosome. *J. Cell Biol.* **1996**, 135 (4), 913–924. <https://doi.org/10.1083/jcb.135.4.913>.
- (24) Paramasivam, P.; Franke, C.; Stöter, M.; Höijer, A.; Bartesaghi, S.; Sabirsh, A.; Lindfors, L.; Arteta, M. Y.; Dahlén, A.; Bak, A.; Andersson, S.; Kalaidzidis, Y.; Bickle, M.; Zerial, M. Endosomal Escape of Delivered mRNA from Endosomal Recycling Tubules Visualized at the Nanoscale. *bioRxiv* **2021**, 2020.12.18.423541. <https://doi.org/10.1101/2020.12.18.423541>.

- (25) Joshi, B. S.; Beer, M. A. De; Giepmans, B. N. G.; Zuhorn, I. S. Endocytosis of Extracellular Vesicles And. **2020**. <https://doi.org/10.1021/acsnano.9b10033>.
- (26) Kumari, S.; MG, S.; Mayor, S. Endocytosis Unplugged: Multiple Ways to Enter the Cell. *Cell Res.* **2010**, *20* (3), 256–275. <https://doi.org/10.1038/cr.2010.19>.
- (27) Sayers, E. J.; Peel, S. E.; Schantz, A.; England, R. M.; Beano, M.; Bates, S. M.; Desai, A. S.; Puri, S.; Ashford, M. B.; Jones, A. T. Endocytic Profiling of Cancer Cell Models Reveals Critical Factors Influencing LNP- Mediated mRNA Delivery and Protein Expression. *Mol. Ther.* **2019**, *27* (11), 1950–1962. <https://doi.org/10.1016/j.ymthe.2019.07.018>.
- (28) Aoyama, M.; Yoshioka, Y.; Arai, Y.; Hirai, H.; Ishimoto, R. Intracellular Trafficking of Particles inside Endosomal Vesicles Is Regulated by Particle Size. *J. Control. Release* **2017**, *260* (June), 183–193. <https://doi.org/10.1016/j.jconrel.2017.06.007>.
- (29) Vasir, J. K.; Labhassetwar, V. Biomaterials Quantification of the Force of Nanoparticle-Cell Membrane Interactions and Its Influence on Intracellular Trafficking of Nanoparticles. **2008**, *29*, 4244–4252. <https://doi.org/10.1016/j.biomaterials.2008.07.020>.
- (30) Al-Hajaj, N. A.; Moquin, A.; Neibert, K. D.; Soliman, G. M.; Winnik, F. M.; Maysinger, D. Short Ligands Affect Modes of QD Uptake and Elimination in Human Cells. *ACS Nano* **2011**, *5* (6), 4909–4918. <https://doi.org/10.1021/nn201009w>.
- (31) Yue, Z.-G.; Wei, W.; Lv, P.-P.; Yue, H.; Wang, L.-Y.; Su, Z.-G.; Ma, G.-H. Surface Charge Affects Cellular Uptake and Intracellular Trafficking of Chitosan-Based Nanoparticles. *Biomacromolecules* **2011**, *12* (7), 2440–2446. <https://doi.org/10.1021/bm101482r>.



DEVELOPMENT AND OPTIMISATION OF A CELL MEMBRANE SHEET-BASED RNA RELEASE ASSAY TO ASSESS EXTRA- CELLULAR VESICLE CONTENT RELEASE

Daniel E. Murphy^a, Chela Loeters^a, Grégory Lavieuc,
Raymond M. Schiffelers^a, Pieter Vader^{a,b}

- a: CDL Research, University Medical Center Utrecht, Utrecht, the Netherlands
- b: Department of Experimental Cardiology, University Medical Center Utrecht, Utrecht, the Netherlands
- c: Université de Paris, INSERM, CNRS UMR 7057, Paris, France

ABSTRACT

In recent years, extracellular vesicles (EVs) have received great interest as potential vehicles for the delivery of RNA therapeutics. This interest has led to research which has revealed several advantageous features of EVs as drug delivery vehicles. Despite this extensive research, little is known about the mechanisms by which EVs deliver their cargo to recipient cells. In order to utilise EVs for the delivery of therapeutics, a better understanding is required which necessitates the development of assays that can be used to study EV-mediated RNA delivery. An important step in functional RNA delivery to cells is fusion of membranes. Here, we adapt an existing protocol for the detection of protein cargo release to develop an assay capable of detecting EV-membrane fusion and subsequent RNA release. We use this assay to demonstrate that RNA release is pH-dependent which suggests that the acidic late endosome and lysosome are the sites of RNA release to the cytosol. This assay could be used to further extend our understanding of EV-mediated RNA delivery.

INTRODUCTION

Extracellular vesicles (EVs) are lipid bound particles of 30 to 2000nm in size, are released from cells of all types and have been identified as mediators of intercellular communication via the cell to cell transfer of nucleic acid, lipid and protein cargo¹. In recent years, the EV-mediated transfer of RNA has received particular study and has been implicated in numerous (patho)physiological processes such as tumour growth^{2,3}, metastasis⁴, angiogenesis⁵ and atherosclerosis⁶.

The mechanisms by which RNA is functionally transferred from within the EV lumen to its site of action, the cytosol of recipient cells, are poorly understood. Despite this paucity of knowledge, there is both indirect and direct evidence to suggest that this process is highly efficient. Firstly, the relative abundance of active RNA in EV preparations is extremely low with even the most abundant RNAs being present at less than 1 copy per 100 particles⁷. For example, EV-mediated hsa-miR-21 transfer has been linked to tumour growth and progression³, yet it is present at far less than 1 copy per particle⁸. The functional transfer of RNA at such low abundance is suggestive of highly efficient delivery. Furthermore, in a direct comparison of RNA transfer efficiency recently performed at our lab, it was revealed that A431-EVs and MDA-MB-231-EVs were at least an order of magnitude more efficient in RNA delivery than state-of-the-art DLin-DMA-MC3 lipid nanoparticles⁹, while a recent *in vivo* study found a 10 fold higher delivery efficiency of EVs as compared to synthetic delivery.¹⁰

An understanding of how EVs are able to achieve this efficient delivery would be greatly advantageous for the development of RNA therapeutics. RNA therapeutics possess huge potential but their use in certain contexts is hindered by inefficient delivery to their site of action¹¹. Improved knowledge of EV-mediated RNA delivery mechanisms may provide insights to help overcome this hurdle.

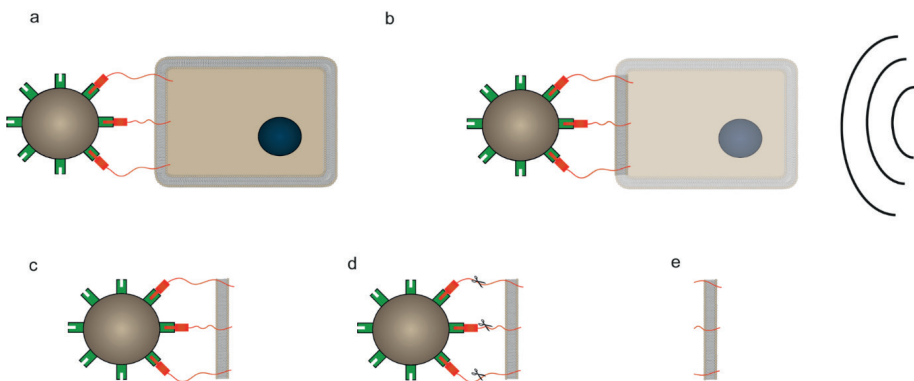
EV-mediated cargo delivery has been hypothesised to occur via multiple routes. Direct fusion of EVs with the cell plasma membrane has been reported¹² but the most likely route of delivery is via endocytic uptake followed by membrane fusion within endo/lysosomes¹³. An important breakthrough was provided by Bonsergent and Lavieau who developed a cell free assay to study EV cargo delivery. This assay was based on well-established proteinase protection assays and involved the isolation of cell membrane sheets (CMS). At acidic pH, these sheets were capable of fusion with EVs resulting in the release of luminal protein cargo. In contrast, at neutral pH this behaviour was not observed¹⁴. The authors drew a comparison between EVs and the Semliki forest virus

which displays similar behaviour and suggested that the acidic endolysosome is the site of EV fusion and protein cargo delivery¹⁴.

To identify key components and to elucidate mechanisms of EV-mediated cargo delivery, the development of such rigorous cell free assays are crucial. To provide such an assay for the study of EV-mediated RNA transfer, we here aim to modify the CMS release assay developed by Bonsergent and Lavieu in order to investigate EV-CMS fusion and subsequent RNA release.

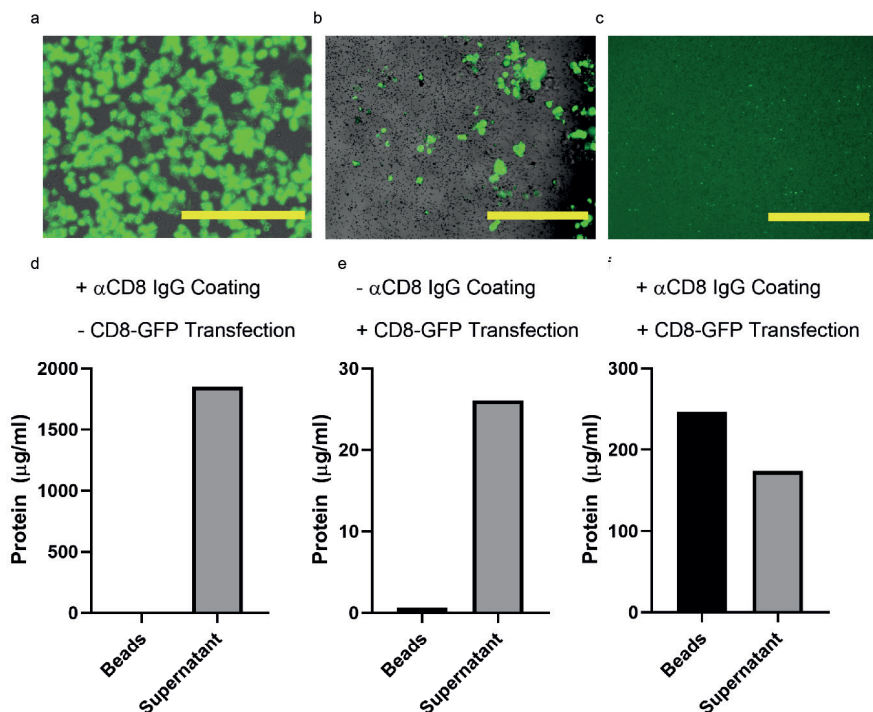
RESULTS

The first crucial step of the assay is the isolation of purified cell membrane sheets using the same method developed and validated by Bonsergent and Lavieu¹⁴. This process is based on the expression of a transmembrane CD8-GFP protein which can be bound to magnetic beads coated with an anti-CD8 antibody, thereby anchoring the cell membrane to the bead (Fig 1a). To separate the membrane from the rest of the cell, the attached cells are sonicated (Fig 1b). CMS can then be purified from cellular debris by pelleting the magnetic beads and aspirating supernatant (Fig 1c). In order to separate the CMS from the beads the CD8-GFP construct is treated with TEV protease which specifically cleaves at a TEV cleavage site in the transmembrane domain (Fig 1d). Beads can then be pelleted and removed leaving isolated CMS in suspension (Fig 1e).



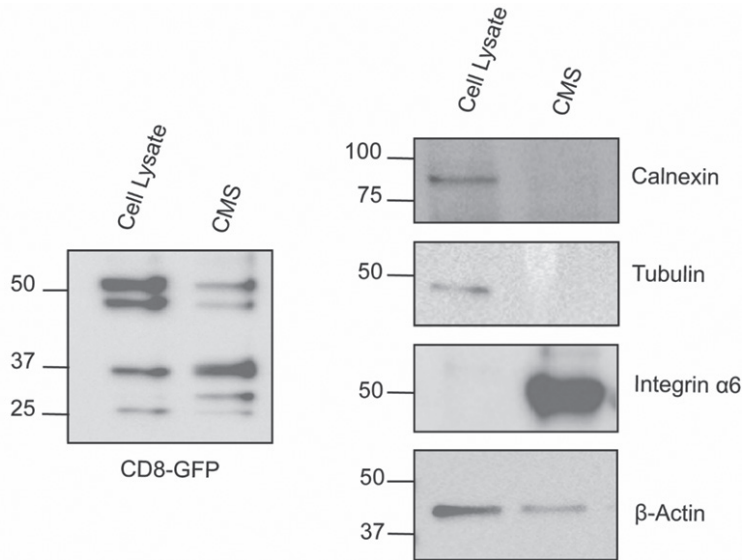
▲Figure 1. CMS isolation procedure. Cells expressing a transmembrane CD8-GFP protein are bound to anti-CD8 antibody coated beads (a). Sonication is used to lyse cells (b) and beads associated with membrane sheets are isolated with a magnet (c). TEV protease is used to cleave the CD8-GFP construct (d) and magnetic beads are removed using a magnet to leave purified sheets (e).

Firstly, to confirm that each step of the sheet isolation protocol was fully functional in our hands, several steps of quality control were performed. Fluorescent microscopy confirmed efficient transfection of HEK293T cells with the CD8-GFP construct (Fig 2a). After incubation with anti-CD8 coated magnetic beads, CD8-GFP transfected cells were then seen to be associated with the coated beads (Fig 2b). Following sonication and removal of cellular debris, anti-CD8 antibody coated magnetic beads were associated with GFP+ material, confirming binding of sheets to the beads (Fig 2c). To confirm that this binding was specific, anti-CD8 antibody coated magnetic beads were incubated with HEK293T cells which had not been transfected with the CD8-GFP construct. microBCA analysis of both the beads and supernatant demonstrated that the majority of protein remained in the supernatant, indicating that the CD8-GFP construct is required for specific binding to the beads (Fig 2d). A similar result was obtained when magnetic beads lacking the anti-CD8 coating were incubated with CD8-GFP+ HEK293T cells (Fig 2e), which again suggested that a-specific binding did not occur and that both CD8-GFP expression and anti-CD8 antibody coating was required for cell to bead binding. Only when cells expressed CD8-GFP and beads were coated with anti-CD8 antibody was protein found to be present on the beads (Fig 2f). In this case, the quantity of protein bound to the beads and present in the supernatant was similar, indicating that cell to bead binding was roughly 50% efficient.



▲ Figure 2. Quality control of sheet production protocol. Fluorescent microscopy images of HEK293T cells transfected with CD8-GFP (a). Fluorescent microscopy images of HEK293T cells transfected with CD8-GFP bound to anti-CD8 coated magnetic beads (b). Fluorescent microscopy images of anti-CD8 coated magnetic beads coated with CMS (c). Scale bars represent 400μm. microBCA analysis of supernatant obtained from anti-CD8 coated magnetic beads incubated with HEK293T cells without CD8-GFP transfection (d). microBCA analysis of supernatant obtained from magnetic beads incubated with HEK293T transfected with CD8-GFP (e). microBCA analysis of supernatant obtained from anti-CD8 coated magnetic beads incubated with HEK293T transfected with CD8-GFP (f).

CMS samples isolated using the CMS isolation protocol were then characterised using Western blotting. In cell lysates of HEK293T cells transfected with CD8-GFP, the intact uncleaved CD8-GFP construct could be observed at around 50 kDa as well as a weak signal derived from the cleaved product at 37 kDa which could be present as a result of construct instability. In contrast, in the CMS sample, the majority of signal is seen in the 37 kDa cleaved CD8-GFP band while a weak signal is seen at 50 kDa. This demonstrates successful, albeit incomplete, TEV digestion of the CD8-GFP construct (Fig 3a). In addition, the HEK293T CD8-GFP+ cell lysate samples were highly enriched for the ER protein Calnexin, cytosolic Tubulin and cytoskeletal β-Actin as compared to CMS samples, demonstrating a lack of contamination with cellular debris. In contrast, the cell membrane Integrin α6 was highly enriched in the CMS sample indicating an enrichment of cell membrane associated material (Fig 3).



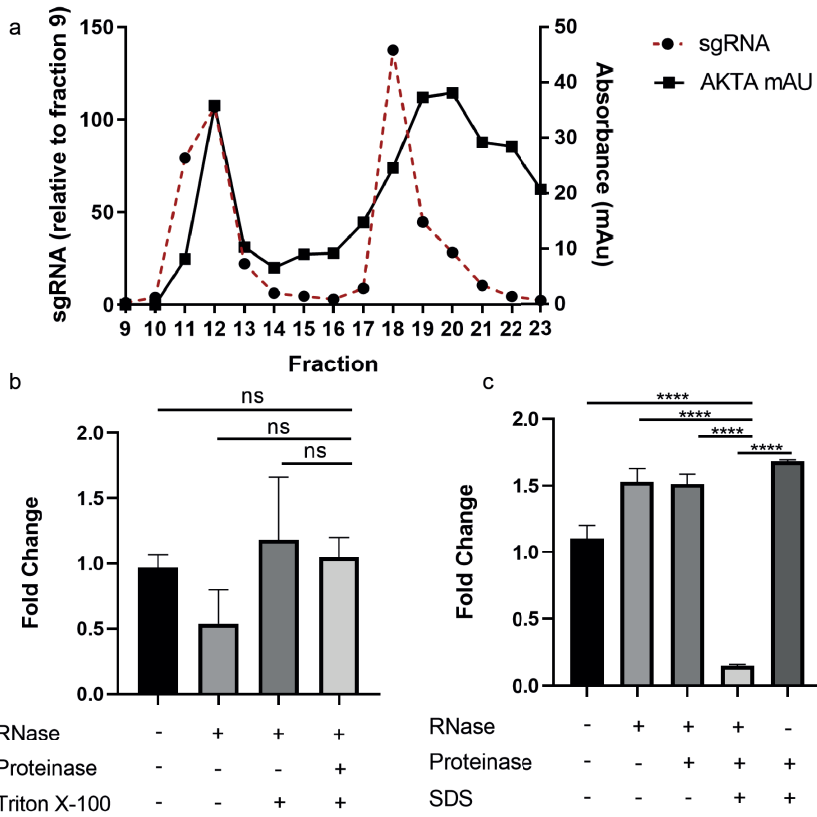
▲**Figure 3.** Western blot analysis of HEK293T CD8-GFP+ cell lysates and CMS for GFP (a), Calnexin, Tubulin, Integrin α6 and β-Actin (b). An equal amount of protein was loaded for both samples.

Once we had confirmed successful isolation of CMS we next needed to identify a suitable cargo RNA, the degradation of which could be used as a readout of RNA release in an RNase protection assay. Such a cargo RNA must be EV-associated and located fully within the EV lumen. The sgRNA for Cas9 produced by donor cells as part of the CROSS-FIRE system developed in our lab¹⁵ was identified as a possible candidate as we have extensive experience with the isolation of sgRNA+ EVs from MDA-MB-231 cells and possess established and robust RT-qPCR protocols for sgRNA detection^{9,15}. To determine the location of extracellular sgRNA, conditioned supernatant was prepared from sgRNA+ MDA-MB-231 cells followed by concentration and fractionation using size exclusion chromatography. This produced a distinctive two peak chromatogram (Figure 4a) in which EVs eluted in the first peak (fractions 10 to 13) followed by proteins in the second peak (fractions 17 to 23). To determine the location of sgRNA, RT-qPCR was performed on each fraction. This also produced two distinct peaks of approximately equal size, one associated with the EV peak, the other with the protein peak. This confirmed that EV-associated sgRNA could be separated from non EV-associated sgRNA for use in RNase protection assays. Next, a simple RNase protection assay was performed. EVs were treated with combinations of RNase, Triton x-100 detergent and proteinase followed by RNase inactivation with Trizol, RNA isolation and RT-qPCR analysis. Upon treatment of sgRNA+ MDA-MB-231-EVs with RNase alone, no significant reduction in signal was observed, indicating that sgRNA was encapsulated and protected within EVs. Neither

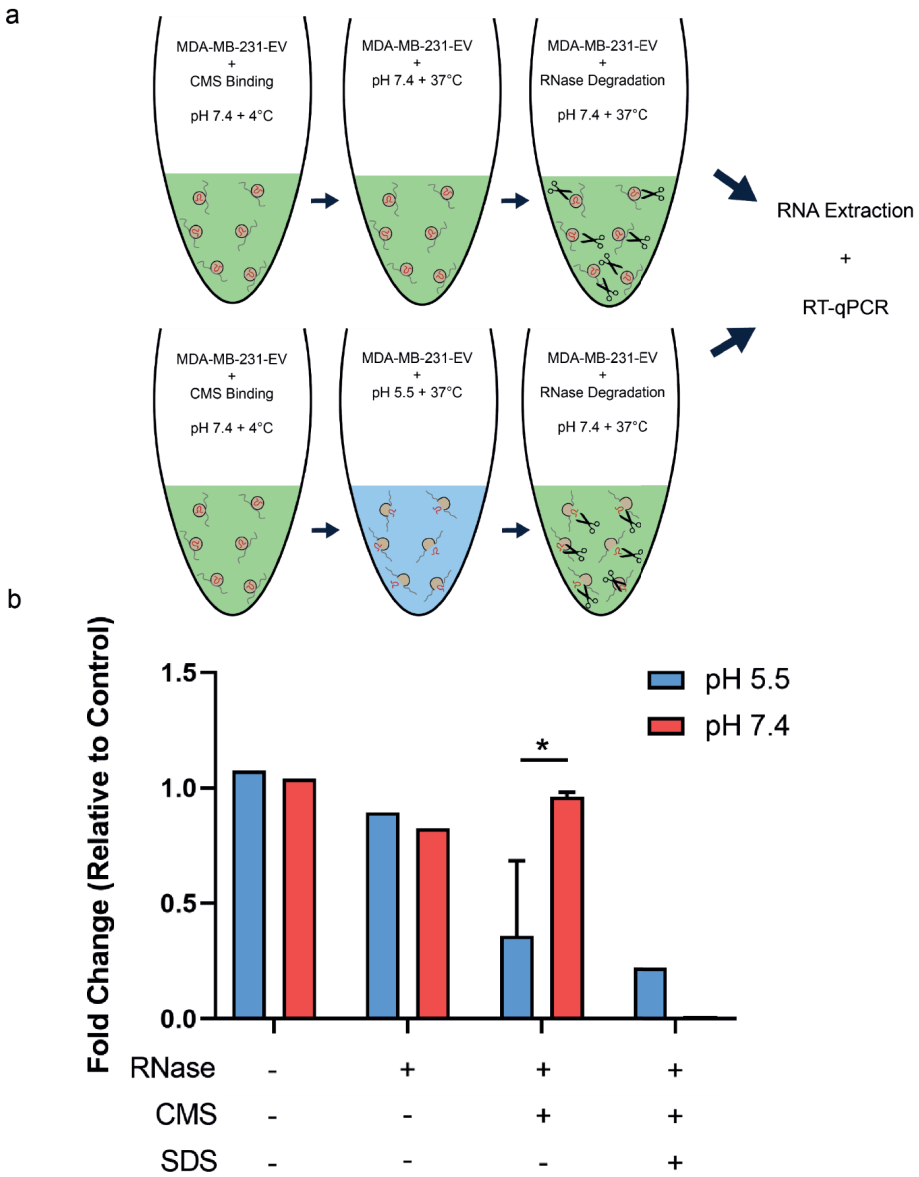
the addition of Triton X-100 or Proteinase K in addition to RNase induced a significant reduction in signal. This demonstrates that sgRNA was not protein associated and suggests Triton X-100 detergent was incapable of lysing EV membranes (Fig 4b). The experiment was repeated using SDS as a lysis agent. Again, upon the addition of RNase alone, no significant reduction in sgRNA signal was observed. This did not change upon the addition of proteinase K to the RNase. However, upon the addition of SDS to RNase and proteinase K, a roughly 6-fold reduction in sgRNA signal was observed. No such reduction was observed in the presence of proteinase and SDS alone (Fig 4d). These results confirm that sgRNA is located within the lumen of MDA-MB-231-EVs and that this RNase protection assay is capable of detecting the release of RNA from MDA-MB-231-EVs when a sufficiently strong detergent is used.

The RNase protection assay shown in figure 4c was then adapted to investigate fusion of MDA-MB-231-EVs with CMS. Firstly, MDA-MB-231-EVs were bound to CMS by incubation on ice for 1 hour. In order to investigate the effect of pH on fusion post CMS binding, the pH was then dropped to 5.5 by the addition of an acidification buffer. A pH 7.4 buffer was added to neutral pH samples to maintain equal volumes. These samples were then incubated at 37°C for 45 minutes to allow fusion to take place. Following this step, the pH was returned to neutral to allow RNase to function by applying a basic buffer and RNase was added to digest released RNA for 30 minutes at 37°C. In order to inactivate RNase to halt digestion and to prepare samples for RNA isolation, Trizol was added followed by RNA extraction and RT-qPCR analysis (Fig 5a).

As seen in Fig 4b and Fig 4c, the addition of RNase alone did not induce a reduction in sgRNA signal, indicating that sgRNA was located within the MDA-MB-231-EV lumen. This was the case for samples incubated at both pH 5.5 and pH 7.4, indicating that low pH did not alter MDA-MB-231-EV membrane integrity. Interestingly, pH-dependent release was observed, as sgRNA signal dropped 3-fold for MDA-MB-231-EV samples incubated with CMS at pH 5.5 while no such reduction was observed for samples incubated at pH 7.4. Again, upon addition of SDS before RNase treatment, a large reduction in sgRNA signal was observed in both acidic and neutral conditions, although this drop was greater at neutral pH which may suggest insufficient neutralisation of acidic pH and impaired RNase function. Altogether, these data suggest that the sheet release assay developed by Bonsergent *et al* has here been successfully adapted to study the release of RNA from EVs.



▲Figure 4. Determination of sgRNA localisation. UV absorbance of 1ml fractions obtained after size exclusion chromatography of MDA-MB-231 conditioned supernatant alongside the quantity of sgRNA relative to fraction 9 as determined by RT-qPCR (a). RT-qPCR analysis of targeting sgRNA samples from RNase protection assays using either Triton X-100 (b) or SDS (c) as a detergent. n=3 technical replicates, means + S.D are displayed. ANOVA with post-hoc Tukey's test was used for statistical analysis, * = $p < 0.00005$.



▲Figure 5. CMS release assay. Schematic representation of the CMS release assay (a). RT-qPCR analysis of targeting sgRNA from CMS release assay samples. $n=3$ technical replicates for CMS conditions (b) (3 separate sheet preparations), $n=1$ technical replicate for all other samples. Means and S.D. are displayed, Student's *T* test was used for statistical analysis, * = $p < 0.05$.

DISCUSSION

This study aimed to produce an assay capable of studying EV – RNA content release which could allow us to study mechanisms by which EVs deliver their RNA cargo. Here, we successfully demonstrated the adaptation of the CMS release assay developed by Bonsergent and Lavieu to detect the release of RNA rather than protein cargo. We then used this assay to demonstrate pH-dependent fusion and release of RNA.

The CMS isolation procedure was confirmed to be capable of isolating highly purified membrane sheets as the absence of either CD8-GFP transfection or anti-CD8 coating of magnetic beads resulted in an almost complete reduction in isolation of protein from the beads in the final step of isolation. Furthermore, the absence of cellular contaminants in CMS preparations confirms their high purity and suitability for use in fusion experiments. The sgRNA readout of the CMS release assay was also confirmed to be highly suitable as size exclusion experiments and RNase protection assays confirmed that the sgRNA is EV-associated and located within the EV lumen. Interestingly, only the anionic detergent SDS but not the non-ionic Triton X-100 was capable of sufficiently lysing EV membranes for RNase-mediated degradation. This is in contrast to previous research which has found both SDS and Triton X-100 to be capable of lysing EV membranes at the concentrations tested in this study¹⁶.

The pH-dependent CMS fusion and subsequent RNA release points towards the acidic compartments of the endolysosomal system as the site of EV cargo release. This is consistent with the results of Joshi *et al* who found that the EV cargo delivery to the cytosol occurred in late endosomes and lysosomes. In line with the data presented here, this process was pH-dependent as blocking of endosome acidification prevented this delivery to the cytosol¹⁷. Furthermore, this phenomenon was further demonstrated by Bonsergent *et al* who demonstrated that EV content release to the cytosol was strongly inhibited by the blocking of endosome acidification with Bafilomycin A1 while EV uptake was not¹⁸. This behaviour is analogous to many viruses and interestingly the authors were able to demonstrate that the proteins IFITM1 and 3, which block the fusion of viruses with membranes, were able to fully inhibit the pH-dependent fusogenic properties of EVs in a sheet release assay¹⁸.

The variation in sheet release efficiency between different sheet batches used here was large. This may be due to differing quality and purity of sheet batches. Indeed, personal correspondence with the Lavieu lab confirmed that purity, in terms of negative enrichment of cellular contaminants, and quality of sheets in terms of the efficiency

of TEV digestion is a critical factor in determining the efficiency of sheet release. For improved consistency in future experiments consistent high quality sheet batches in which efficient TEV digestion and strong negative enrichment of cellular contaminants is observed should be used between experiments.

An interesting experiment to further characterise the mechanisms of EV-mediated RNA delivery would be the protease treatment of EVs before their use in the RNA release assay. Bonsergent and Lavieu demonstrated that the pH-dependent fusion and release of protein cargo from EVs was abrogated by proteinase treatment of the EVs prior to use in the assay¹⁸. This suggests that the fusogenic properties of EVs may be conferred by a protein factor on their surface and it would be of interest to use the assay developed here to identify the specific proteins responsible for pH-dependent fusion.

The development of this assay provides opportunities for the study of nanoparticle mediated RNA delivery. For example, previous work from our lab has demonstrated that A431-EVs and MDA-MB-231-EVs functionally delivered RNA with an efficiency orders of magnitude higher than that of state-of-the-art DLin-DMA-MC3 lipid nanoparticles⁹. It would be of interest to perform a comparison of these EVs and LNPs using the RNA release assay to investigate whether this difference in efficiency could be partially explained by differences in pH-dependent fusion efficiency.

In conclusion the work presented here successfully adapted the CMS fusion assay developed by Bonsergent and Lavieu in order to detect EV fusion and RNA cargo rather than protein cargo release. This assay has the potential to improve our understanding of the mechanisms underlying EV-mediated RNA delivery.

MATERIALS AND METHODS

Cell Culture

HEK293T and MDA-MB-231 cells were cultured in Dulbecco's Modified Eagle Medium (DMEM) with L-Glutamine (Gibco) supplemented with 10% heat-inactivated fetal bovine serum and Streptomycin and penicillin at 100 µg/ml and 100 u/ml (Gibco) respectively. MDA-MB-231 cells expressing Gal4-1sgRNA were generated in a previous study¹⁵ and were cultured with 2ug/ml puromycin selection antibiotics to maintain expression of the Gal4-1 sgRNA construct.

SHEET ISOLATION

50% confluent 10cm petri dishes of HEK293T cells were transfected with 50µg of plasmid encoding the CD8-GFP construct (Gift from Dr. Gregory Lavieu) using lipofectamine 2000 (Thermo Fisher) according to manufacturer's protocol. Two days after transfection, the cells were washed two times in ice cold PBS then gently removed from the dish using a cell scraper. The cells were resuspended in 500µl PBS. 40µl of ProtG magnetic dynabeads (ThermoFisher) coated with anti-CD8 monoclonal antibody (RPA-T8) (ThermoFisher) were resuspended in 500µl PBS and mixed with the cell suspension. This mix was incubated on a slowly rotating mixer for at least 4 hours at 4°C. Unbound cells were then removed and the bound cells were sonicated using two 5 second pulses at 60% amplitude using an Eppendorf probe sonicator. Free cytoplasm and cell debris was discarded using a pipette and sheet coated beads were resuspended in 100µl PBS. Sheets were released from the beads using 0.1 u/µl of TEV protease (Sigma Aldrich) and overnight incubation on a rotator at 4°C.

6

CMS RELEASE ASSAY

To allow binding, 10µl of EVs in PBS and 10µl CMS or PBS control were incubated for 1 hour on ice. To lower the pH, 180µl of 100 mM Tris, 5mM EDTA, 0.2M NaCl at pH 5.1 was added and the sheet/EV mixture was incubated for 45 minutes at 37°C. To return the pH to neutral, 31µl of basic buffer consisting of 100 mM Tris, 5mM EDTA, 0.2M NaCl at pH 8.6 was added. To act as a positive control, 0.2% SDS was added to positive control samples. To degrade released RNA, RNase A (ThermoFisher) was then added at a final concentration of 0.14ug/ml and samples were incubated for 30 minutes at 37°C. RNase was inactivated by the addition of 750µl Trizol LS before RNA extraction and RT-qPCR analysis.

EV Isolation

sgRNA expressing MDA-MB-231 cells were seeded in T175 flasks. Upon reaching 60-90% confluency, the supernatant was removed and cells were washed in PBS. The medium was then replaced with 20ml OptiMEM (Gibco). After 24h of incubation, the conditioned supernatant was removed and spun at 300 x g for 5 minutes at 4°C to remove floating cells and then again at 2000 x g for 15 minutes at 4°C to remove cell debris. This conditioned supernatant was then filtered through 0.45µm bottle top filters and concentrated to approximately 10ml using tangential filter flow filtration with a peristaltic pump attached

to a Minimate 100 kDa Omega Membrane cassette (Pall Corporation). A 100 kDa Amicon Ultra-15 Centrifugal filter (Merck) was then used to concentrate this medium further down to 1ml. EVs were then isolated using size exclusion chromatography using a Tricorn 10/300 column with Sepharose 4 Fast Flow resin using an AKTA Start chromatography system (all GE Healthcare Life Sciences). Fractions containing the EVs were then pooled and concentrated to the required volume using a 100 kDa Amicon Ultra-15 Centrifugal filter.

RNA Extraction and RT-qPCR

RNA was isolated using Trizol LS and glycoblue according to manufacturer's protocol (Thermo Fisher Scientific). RNA pellets were resuspended in 20 μ l of nuclease free water and cDNA synthesis was performed on 10 μ l RNA suspension using a SuperScript 4 kit (Thermo Fisher Scientific), RNasin Ribonuclease inhibitor (Promega) and 2 pmol of sgRNA reverse primer which was specific for the sgRNA. The resulting cDNA was diluted 1:5 in nuclease free water before qPCR analysis using iQ SYBR Green Supermix (Bio-Rad) in a CFX96 Real-Time PCR Detection System (Bio-Rad). Forward primer sequence: CAGTACTCCGCTCGAGTGTT. Reverse primer sequence: GACTCGGTGCCACTTTTTCAA.

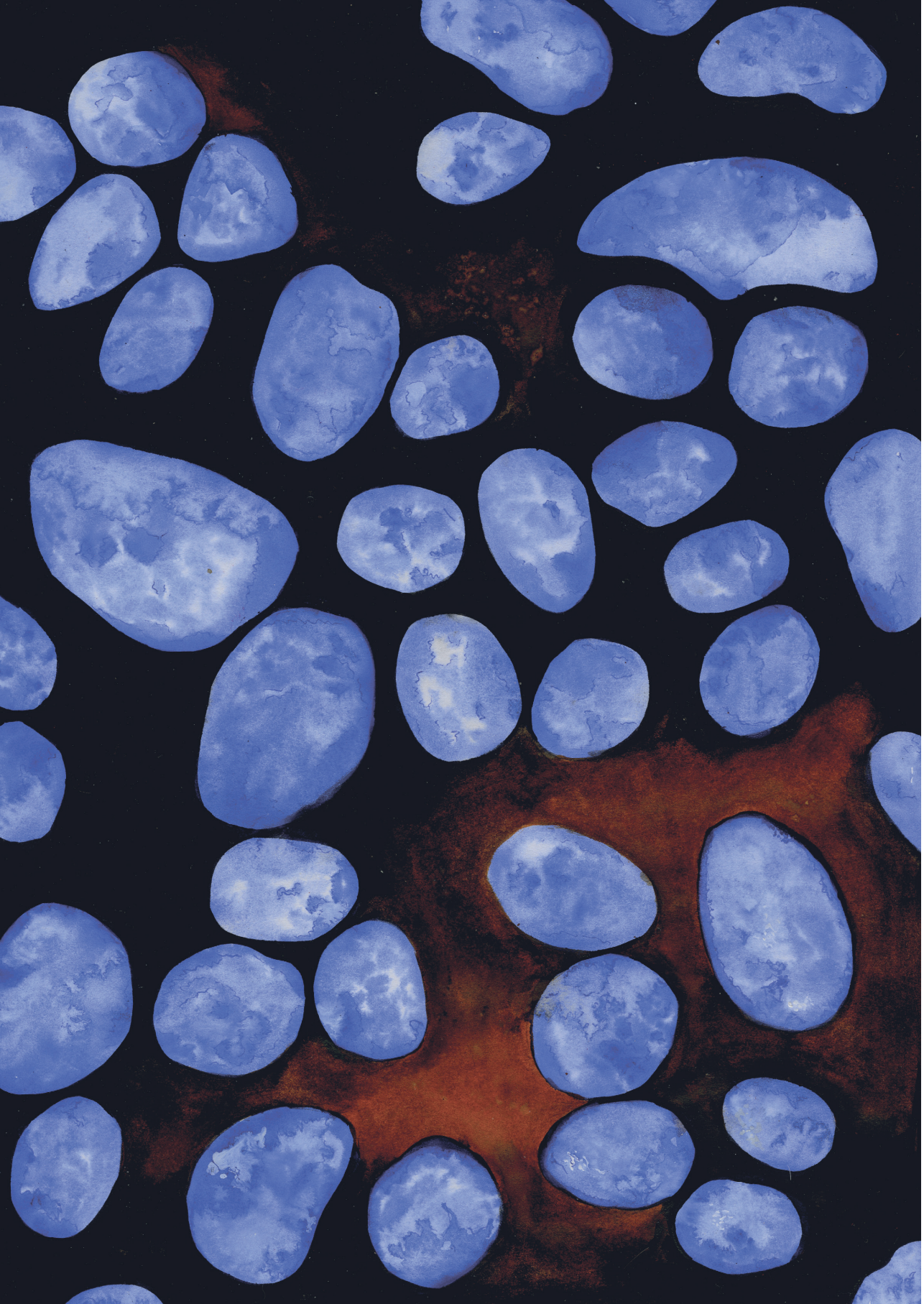
Western Blotting

In order to determine protein concentrations and load equal quantities of protein on SDS-PAGE gels, a microBCA protein assay kit (ThermoFisher) was used according to manufacturer's protocol. Samples were boiled for 5 minutes and then run on 4–15% miniprotean-TGX stain-free gels (Biorad) in the presence of 5% β -mercaptoethanol and then transferred onto PVDF membranes (Biorad). Membranes were then blocked using 5% fat free milk in PBS 0.5% tween before incubation in primary antibody dilutions. Primary antibodies were detected using HRP-conjugated secondary antibodies and a Chemidoc Touch Imaging system (Biorad) to detect chemiluminescence. Primary antibodies used are as follows, mouse anti-GFP (GF28R, ThermoFisher scientific), rabbit anti-calnexin (ab133615, Abcam), mouse anti-integrin α 6 (#3750, Cell Signalling) and mouse anti-actin (C4, Millipore).

REFERENCES

1. El Andaloussi, S.; Mäger, I.; Breakefield, X. O.; Wood, M. J. A. Extracellular Vesicles: Biology and Emerging Therapeutic Opportunities. *Nat. Rev. Drug Discov.* **2013**, *12* (5), 347–357. <https://doi.org/10.1038/nrd3978>.
2. Skog, J.; Würdinger, T.; Rijn, S. Van; Meijer, D. H.; Gainche, L.; Sena-esteves, M.; Curry, W. T.; Carter, B. S.; Krichevsky, A. M.; Breakefield, X. O. Glioblastoma Microvesicles Transport RNA and Proteins That Promote Tumour Growth and Provide Diagnostic Biomarkers. **2008**, *10* (12). <https://doi.org/10.1038/ncb1800>.
3. Abels, E. R.; Maas, S. L. N.; Nieland, L.; Krichevsky, A. M.; Breakefield, X. O.; Abels, E. R.; Maas, S. L. N.; Nieland, L.; Wei, Z.; Cheah, P. S.; Tai, E.; Kolsteeg, C. Glioblastoma-Associated Microglia Reprogramming Is Mediated by Functional Transfer of Extracellular Article Glioblastoma-Associated Microglia Reprogramming Is Mediated by Functional Transfer of Extracellular MiR-21. *CellReports* **2019**, *28* (12), 3105–3119.e7. <https://doi.org/10.1016/j.celrep.2019.08.036>.
4. Zomer, A.; Maynard, C.; Verweij, F. J.; Kamermans, A.; Schäfer, R.; Beerling, E.; Schiffelers, R. M.; De Wit, E.; Berenguer, J.; Ellenbroek, S. I. J.; Würdinger, T.; Pegtel, D. M.; Van Rheenen, J. In Vivo Imaging Reveals Extracellular Vesicle-Mediated Phenocopying of Metastatic Behavior. *Cell* **2015**, *161* (5), 1046–1057. <https://doi.org/10.1016/j.cell.2015.04.042>.
5. van Balkom, B. W. M.; de Jong, O. G.; Smits, M.; Brummelman, J.; den Ouden, K.; de Bree, P. M.; van Eijndhoven, M. A. J.; Pegtel, D. M.; Stoorvogel, W.; Würdinger, T.; Verhaar, M. C. Endothelial Cells Require MiR-214 to Secrete Exosomes That Suppress Senescence and Induce Angiogenesis in Human and Mouse Endothelial Cells. *Blood* **2013**, *121* (19), 3997–4006, S1-15. <https://doi.org/10.1182/blood-2013-02-478925>.
6. Zheng, B.; Yin, W.-N.; Suzuki, T.; Zhang, X.-H.; Zhang, Y.; Song, L.-L.; Jin, L.-S.; Zhan, H.; Zhang, H.; Li, J.-S.; Wen, J.-K. Exosome-Mediated MiR-155 Transfer from Smooth Muscle Cells to Endothelial Cells Induces Endothelial Injury and Promotes Atherosclerosis. *Mol. Ther.* **2017**, *25* (6), 1279–1294. <https://doi.org/10.1016/j.ymthe.2017.03.031>.
7. Chevillet, J. R.; Kang, Q.; Ruf, I. K.; Briggs, H. A.; Vojtech, L. N.; Hughes, S. M.; Cheng, H. H.; Arroyo, J. D.; Meredith, E. K.; Gallichotte, E. N.; Pogosova-agadjanyan, E. L. Quantitative and Stoichiometric Analysis of the MicroRNA Content of Exosomes. *PNAS* **2014**, *111* (41), 14888–14893. <https://doi.org/10.1073/pnas.1408301111>.
8. He, D.; Wang, H.; Ho, S.; Chan, H.; Hai, L.; He, X.; Wang, K. Total Internal Reflection-Based Single-Vesicle in Situ Quantitative and Stoichiometric Analysis of Tumor-Derived Exosomal MicroRNAs for Diagnosis and Treatment Monitoring. *Theranostics* **2019**, *9* (15), 4494–4507. <https://doi.org/10.7150/thno.33683>.
9. Murphy, D. E.; de Jong, O. G.; Evers, M. J. W.; Nurazizah, M.; Schiffelers, R. M.; Vader, P. Natural or Synthetic RNA Delivery: A Stoichiometric Comparison of Extracellular Vesicles and Synthetic Nanoparticles. *Nano Lett.* **2021**, *21* (4), 1888–1895. <https://doi.org/10.1021/acs.nanolett.1c00094>.
10. Reshke, R.; Taylor, J. A.; Savard, A.; Guo, H.; Rhym, L. H.; Kowalski, P. S.; Trung, M. T.; Campbell, C.; Little, W.; Anderson, D. G.; Gibbings, D. Reduction of the Therapeutic Dose of Silencing RNA by Packaging It in Extracellular Vesicles via a Pre-MicroRNA Backbone. *Nat. Biomed. Eng.* **2020**, *4* (1), 52–68. <https://doi.org/10.1038/s41551-019-0502-4>.
11. Dowdy, S. F. Overcoming Cellular Barriers for RNA Therapeutics. *Nat. Biotechnol.* **2017**, *35* (3), 222–229. <https://doi.org/10.1038/nbt.3802>.

12. Montecalvo, A.; Larregina, A. T.; Shufesky, W. J.; Stolz, D. B.; Sullivan, M. L. G.; Karlsson, J. M.; Baty, C. J.; Gibson, G. A.; Erdos, G.; Wang, Z.; Milosevic, J.; Tkacheva, O. A.; Divito, S. J.; Jordan, R.; Lyons-Weiler, J.; Watkins, S. C.; Morelli, A. E. Mechanism of Transfer of Functional MicroRNAs between Mouse Dendritic Cells via Exosomes. *Blood* **2012**, *119* (3), 756–766. <https://doi.org/10.1182/blood-2011-02-338004>.
13. Mulcahy, L. A.; Pink, R. C.; Carter, D. R. F. Routes and Mechanisms of Extracellular Vesicle Uptake. *J. Extracell. Vesicles* **2014**, *3* (1). <https://doi.org/10.3402/jev.v3.24641>.
14. Bonsergent, E.; Lavieu, G. Content Release of Extracellular Vesicles in a Cell-Free Extract. *FEBS Lett.* **2019**, *593* (15), 1983–1992. <https://doi.org/10.1002/1873-3468.13472>.
15. de Jong, O. G.; Murphy, D. E.; Mäger, I.; Willms, E.; Garcia-Guerra, A.; Gitz-Francois, J. J.; Lefferts, J.; Gupta, D.; Steenbeek, S. C.; van Rheenen, J.; El Andaloussi, S.; Schiffelers, R. M.; Wood, M. J. A.; Vader, P. A CRISPR-Cas9-Based Reporter System for Single-Cell Detection of Extracellular Vesicle-Mediated Functional Transfer of RNA. *Nat. Commun.* **2020**, *11* (1), 1113. <https://doi.org/10.1038/s41467-020-14977-8>.
16. Osteikoetxea, X.; Sódar, B.; Németh, A.; Szabó-Taylor, K.; Pálóczi, K.; Vukman, K. V.; Tamási, V.; Balogh, A.; Kittel, Á.; Pállinger, É.; Buzás, E. I. Differential Detergent Sensitivity of Extracellular Vesicle Subpopulations. *Org. Biomol. Chem.* **2015**, *13* (38), 9775–9782. <https://doi.org/10.1039/C5OB01451D>.
17. Joshi, B. S.; de Beer, M. A.; Giepmans, B. N. G.; Zuhorn, I. S. Endocytosis of Extracellular Vesicles and Release of Their Cargo from Endosomes. *ACS Nano* **2020**, *14* (4), 4444–4455. <https://doi.org/10.1021/acsnano.9b10033>.
18. Bonsergent, E.; Grisard, E.; Buchrieser, J.; Lavieu, G. Quantitative Characterization of Extracellular Vesicle Uptake and Content Delivery within Mammalian Cells. *Nat. Commun.* No. 2021, 1–11. <https://doi.org/10.1038/s41467-021-22126-y>.



SUMMARY AND PERSPECTIVES

CHAPTER 7

SUMMARY AND PERSPECTIVES

At the start of this PhD project in May 2017 the use of nanoparticle delivered RNA therapeutics in the clinic was still out of reach. However, a major milestone was attained in 2018 with the approval Onpattro¹, to treat hereditary transthyretin-mediated amyloidosis. This growth was further accelerated in 2020 by the emergence of the SARS-Cov2 virus and the ensuing COVID19 pandemic which was soon followed by the rapid development and approval of the Pfizer/BioNTech and Moderna mRNA vaccines. It is poignant to think that upon the initiation of this PhD project, RNA therapeutics were still clinically unapproved, while at the time of writing in May 2021, the author is sitting with a sore arm and plaster after the injection of 500µl of Moderna's mRNA-1273 vaccine suspension into his left deltoid muscle.

The rapid and (so far) successful harnessing of RNA technology to combat the COVID19 pandemic displays its enormous potential. This demonstration that the widespread and successful use of RNA therapeutics is possible provides regulatory routes to approval and opens up a plethora of opportunities for the treatment of diseases which were previously thought 'undruggable'.

A good example is that of Alzheimer's disease. The pathogenesis of this disease is well understood and involves the formation of amyloid beta plaques in the brain². Despite abundant knowledge regarding the underlying pathogenesis, the development of conventional therapeutics to prevent this process has been so far unsuccessful. siRNA therapeutics could overcome this problem by treating this disease at its genetic source. Instead of attempting to prevent the formation of amyloid beta plaques after expression of the amyloid protein, siRNA-mediated knockdown of amyloid beta mRNA would prevent the expression of amyloid beta, thereby preventing the formation of plaques².

There are numerous further examples of diseases for which RNA therapeutics could dramatically improve our current treatment options. However, this optimism is dampened by several unfortunate features of the RNA molecule. RNA is large and polar and will not passively diffuse across membranes. Furthermore, it is delicate and is rapidly degraded by circulating RNases upon introduction to the body³. In order to successfully utilise RNA as a drug a delivery vehicle which encapsulates RNA, thereby protecting the cargo from degradation and facilitating entry into cells, is required.

The current conventional approach to RNA therapeutic delivery is to complex anionic RNA with a cationic/ionizable lipid to form a lipid nanoparticle (LNP)⁴. This approach

protects the RNA from degradation and allows uptake and entry into cells. However, these particles are largely limited to use in the liver as circulating LNPs are rapidly cleared from the circulation by hepatic Kupfer cells³.

For RNA therapeutics to truly achieve their potential, appropriate delivery to cells and tissues is required. For this reason, attention has turned to Extracellular Vesicles (EVs) as potential RNA delivery vehicles. These are lipid bound particles of between 30-2000nm in size and are released from cells of all types⁵. Interestingly, these particles perform a similar function to LNPs and act as natural RNA delivery vehicles inside the body as they have been shown to functionally transfer RNA between cells⁶. These features are the source of great excitement as the opportunity to learn from or utilise nature's own RNA delivery system could allow us to move one step closer to a full realisation of RNA's therapeutic potential.

In **Chapter 2** the features of EVs which make them highly attractive RNA delivery vehicles are discussed, along with ways in which EVs can be used as therapeutics directly. We discuss how EVs display lower immunogenicity and could avoid the dose limiting toxicity displayed by LNPs. In addition, we review features and aspects of EV biology that must be considered in order to successfully utilise EVs in a therapeutic context. The natural cell targeting characteristics of certain EV types along with their circulation kinetics and biodistribution profiles are covered. We also cover how EVs can be modified in order to improve their clinical characteristics.

As described in Chapter 2, EVs possess many attractive clinical characteristics as a therapeutic RNA delivery vehicle. However, EV-mediated RNA transfer is a relatively recently described phenomenon and therefore, many of the tools required to appropriately study the mechanisms involved have been lacking. For this reason, we performed the work described in **Chapter 3**. This chapter describes the development of the CROSS-FIRE system, a highly sensitive reporter system capable of detecting EV-mediated functional RNA transfer at the single cell level⁷. It also describes how the system was used to identify novel genes involved in this process. Briefly described, this system is based on the EV-mediated transfer of sgRNA from donor cells to reporter cells. This sgRNA directs the Cas9 nuclease to a target sequence on the CROSS-FIRE reporter construct which results in a double strand break. Through a process of non-homologous end joining, the double strand break is repaired and a frameshift mutation is induced, which induces eGFP expression, which can be used as a readout for functional sgRNA transfer.

Prior to the development of the CROSS-FIRE system, EV-mediated RNA transfer was studied using EV-associated siRNA or miRNA transfer and subsequent knockdown of target genes in reporter systems⁸. However, these systems lack the single-cell sensitivity required to appropriately study this phenomenon. mRNA based systems such as the Cre recombinase-based system described by Zomer *et al*⁹ are indeed able to detect EV-mediated RNA transfer with single-cell resolution but are hindered by the fact the system can also be activated by the transfer of Cre recombinase protein expressed in the donor cell rather than transfer of Cre recombinase mRNA. A further major advantage of the CROSS-FIRE system is its sensitivity to a single specific sgRNA only.

It is interesting to note that the overall levels of activation observed when using the protocols described for the CROSS-FIRE reporter system are low. In coculture experiments using a combination of MDA-MB-231 sgRNA+ donor cells and HEK293T reporter cells for 5 days, reporter activation is typically around 0.2% while in EV addition experiments reporter activation is only 0.03%. These low activation levels do not suggest a low level of EV-mediated RNA transfer as the loading of EVs with sgRNA is extremely low, with only $3.6 \times 10^5 \pm 3.3 \times 10^5$ MDA-MB-231-EVs containing a sgRNA copy.

Furthermore, the difference in activation levels observed between coculture and EV addition experiments is of interest. In coculture experiments, reporter cells and donor cells are present in similar ratios. However, in EV addition experiments, there were orders of magnitude fewer reporter cells than the number of cells from which EVs were purified. One may expect that this enrichment of EVs would lead to higher reporter activation. The fact that this is not the case could be explained in several ways. Firstly, the dynamics of EV exposure may be of importance. In coculture experiments reporter cells were constantly exposed to EVs over the 5 day incubation. In contrast, in addition experiments, reporter cells were pulsed with high doses of EVs on 6 consecutive days. It is perhaps possible that a constant exposure of EVs leads to higher functional delivery than separate large pulses. Secondly, the EVs used in addition experiments were purified from the extracellular milieu into which they were released. In contrast, in coculture experiments cells were exposed to EVs directly after release. This may explain the difference in delivery efficiency as components which enhance functional delivery by EVs could have been lost during the isolation process.

In chapter 3 we demonstrated that the CROSS-FIRE system can be used to study EV-mediated RNA transfer by showing that knockdown of specific genes involved in endocytosis influence functional RNA transfer levels. For instance, the knockdown of

Pak1 and Rac1 which are mediators of macropinocytosis lead to a significant reduction in reporter activation. In contrast, the knockdown of Flot-1 and CDC42 which are involved in clathrin-independent endocytosis and have been demonstrated to play a role in EV-uptake by our lab in other cell types¹⁰, did not lead to a decrease in reporter activation. This provides a hint to differences among cell types, or to the fact that certain routes of endocytosis result in functional delivery while others do not and demonstrates how the CROSS-FIRE system can be used to elucidate mechanisms involved in functional RNA delivery.

Our initial work performed with the CROSS-FIRE system also highlights the complexity of EV-mediated RNA delivery as results were not consistent between different reporter cell lines. For instance, in contrast to HEK293T reporters, the knockdown of the macropinocytosis components Pak1 and ANKFY1 lead to an increased reporter activation in MCF-7 cells. This observation demonstrates our lack of clarity regarding the mechanisms involved in EV-mediated functional RNA transfer and highlights the need for a system such as CROSS-FIRE to help us elucidate the components involved. In this regard, we envision the CROSS-FIRE system being employed in large scale screens which may help us uncover as yet unknown key mediators of these processes.

With the development, validation and demonstration that the CROSS-FIRE system can be used to study EV-mediated RNA transfer, we had the tools in place to study and test the exciting claim that EVs functionally deliver RNA in a highly efficient manner. In **Chapter 4** we isolated and characterised EVs from A431 and MDA-MB-231 sgRNA+ donor cells. We determined that sgRNA loading into these EVs was extremely low, with only one copy of sgRNA being present per $3.6 \times 10^5 \pm 3.3 \times 10^5$ MDA-MB-231-EVs and $1.1 \times 10^7 \pm 3.9 \times 10^6$ A431-EVs. Nevertheless, both EV types were capable of inducing reporter activation. In contrast, when a similar quantity of sgRNA was applied to cells via state-of-the-art DLin-DMA-MC3-LNPs, reporter activation was not detected. In fact, several orders of magnitude higher sgRNA quantities were required for significant functional delivery. This demonstrates that in addition to the many clinically advantageous features of EVs described in chapter 2, EVs also possess an intrinsic high delivery efficiency.

This finding is of great significance to the field and supports the continued research of EV-mediated RNA delivery for the purposes of improving therapeutic RNA delivery. However, it must be noted that the levels of reporter activation induced by EVs were minimal with functional sgRNA delivery induced GFP expression being observed in only roughly 3 out of 10,000 reporter cells after 6 consecutive daily doses of EVs. Although the

primary finding of this chapter was that EVs deliver RNA with high efficiency, this low level of absolute activation indicates that unmodified EVs containing passively loaded RNA are unlikely to ever find clinical use.

In addition, the amount of sgRNA loaded into MDA-MB-231-EVs and A431-EVs differed greatly, while levels of activation in addition experiments did not. Furthermore, the levels of reporter cell activation in coculture experiments performed in chapter 3 were greatly influenced by the combination of cell types used. For example, when HEK293T reporters were cultured with MDA-MB-231 donors for 5 days, an activation level of around 0.2% was reached. In contrast, when HEK293T donors were used, no significant activation could be observed. These observations suggest that EV-mediated RNA transfer is cell type specific, however the extent to which cell types differ remains to be elucidated.

In order to utilise EVs as RNA delivery vehicles, a suitable method by which EVs can be loaded with RNA must be developed. Historically, electroporation has been used, however this method is unsuitable as it results in aggregation and degradation of RNA¹¹. A suitable loading method must result in RNA being loaded into the EV lumen as RNA loaded onto the surface of EVs has been shown to be delivered with poor efficiency¹². In order to achieve this goal, our lab is currently working on EV loading methods which link specific RNA sequences to the EV luminal side of proteins which are highly abundant on EV membranes. In this way, RNA molecules can be pulled from the cytosol into the EV lumen, thereby increasing loading. However, preliminary results from our lab suggest that in order to function, the interaction between RNA cargo and EV membrane protein must be broken as too strong of an interaction likely results in the retention of EV cargo within the endolysosomal system post-membrane fusion, as has been observed by others¹³.

Instead of the direct use of EVs as RNA delivery vehicles, the features of EVs which confer their high RNA delivery efficiency could be utilised by their incorporation into existing synthetic delivery vehicles. For example, the fusion of RNA loaded LNPs with EVs could produce hybrids which are loaded with RNA through the fusion process while being simultaneously conferred with improved delivery efficiency via the incorporation of EV components. Furthermore, the incorporation of EV components onto the surface of polymer based transfection reagents such as polyethylenimine could also improve their efficiency.

A recent non-peer reviewed preprint by Albanese *et al* presents conflicting conclusions to those drawn in Chapter 4⁸. Similarly to our results in which loading of EVs with sgRNA was extremely low, Albanese *et al* demonstrated that only a small fraction of EVs contained miRNA. In contrast to our findings, the authors concluded that EVs derived from HEK293T and B cells do not functionally deliver their miRNA cargo to recipient cells. An explanation for this discrepancy can be provided by the fact that the dual luciferase reporter system used by Albanese *et al* does not possess single cell sensitivity and relies on a bulk measurement of all cells. Our results using the CROSS-FIRE system which possesses single cell sensitivity demonstrate that the size of effect induced by EVs loaded with low amounts of RNA is miniscule (0.03% GFP+ cells). A dual luciferase system would be incapable of detecting such low levels of RNA transfer events which may explain the discrepancy in conclusions between our studies. Furthermore, it should be noted that HEK293T cells contain an unusually low amount of small RNAs, containing mainly ribosomal RNA¹⁴, which may explain the inability of these EVs to transfer miRNA.

After the demonstration that EVs deliver RNA with high efficiency, the next obvious question is which features of EVs confer this high ability. Therefore, in **Chapter 5** we investigated whether the routes by which EVs and LNPs are trafficked post-uptake differs as this may potentially help to explain the different efficiencies as EVs may follow a route which allows higher access of their cargo to the cytosol. In this chapter we demonstrated that CPC-EVs and DLin-DMA-MC3-LNPs followed largely similar trafficking routes post-uptake, which suggests that the features which confer EVs with high delivery efficiency are not likely to be related to differing trafficking routes post-uptake.

However, important differences in trafficking and cellular localisation post-uptake between EVs and LNPs may be subtle and hard to detect. The light microscopy based confocal microscopy analysis of colocalisation method employed in Chapter 5 may not possess the required resolution to appropriately analyse post-uptake trafficking at sufficient detail. Moreover, the membrane labelling of EVs may not be representative of actual cargo delivery to cells. Future studies to investigate this process could make use of single-molecule imaging techniques. This would allow us to study this process at a considerably higher resolution, which may help to identify the specific sites at which EVs deliver their cargo. In order to perform such studies, our lab has recently acquired an ONI Nanoimager capable of such analysis which will hopefully lead to further elucidation of the trafficking routes followed by EVs and LNPs post-uptake.

To investigate other features of EVs which may confer them with high delivery efficiency we collaborated with Dr. Gregory Lavieu who developed a method for isolating highly purified cell membrane sheets (CMS) which were capable of inducing EV fusion at low pH¹⁵. In **Chapter 6** we utilised this method to demonstrate that in a manner analogous to certain viruses, EVs fuse with membranes and release their RNA cargo. This finding may help to explain the high functional delivery efficiency displayed by EVs in Chapter 4.

This pH dependent fusion of EVs is in line with a growing body of evidence which points to acidic late endosomes and lysosomes as the site of EV cargo release. This is in agreement with results presented by Joshi *et al* and Bonsergent *et al* who both demonstrated that late endosomes and lysosomes are the sites of EV content release and that this process is dependent on the acidification of endosomes^{16,17}.

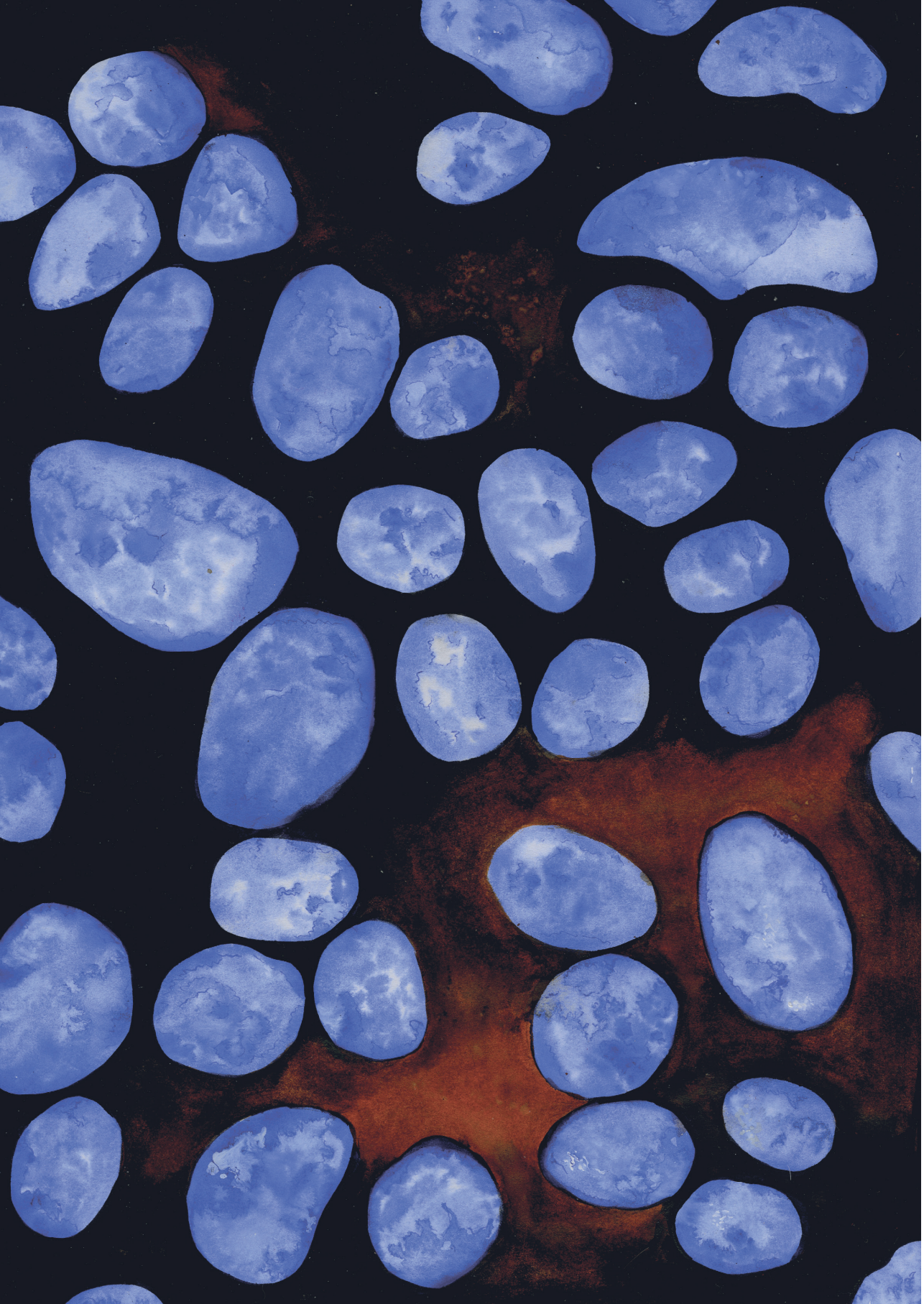
In addition to providing interesting evidence to support the identification of the site of EV cargo release, this assay could also be used to further investigate potential components of EVs involved in RNA transfer. We envision the use of the CMS release assay as an ideal companion to large scale screens using the CROSS-FIRE system. Potentially, key proteins identified in donor cells using the CROSS-FIRE screen could be tested in a cell free environment to determine whether they play a role in EV fusion. Such a combination of techniques could play a role in elucidating the unknown mechanisms used by EVs to deliver their cargo.

In conclusion, the ability to hijack nature's own RNA delivery system for the purposes of RNA therapeutic delivery is an extremely attractive proposition. However, before this proposition can become a reality, the underlying mechanisms by which EVs carry out their functions requires extensive future study. In this thesis we have provided tools to enhance the study of EV-mediated RNA delivery, and used these tools to demonstrate their extremely high efficiency. Through this work, we have been able to bring the utilisation of EVs in a therapeutic context one step closer to fruition.

REFERENCES

- (1) Akinc, A.; Maier, M. A.; Manoharan, M.; Fitzgerald, K.; Jayaraman, M.; Barros, S.; Ansell, S.; Du, X.; Hope, M. J.; Madden, T. D.; Mui, B. L.; Semple, S. C.; Tam, Y. K.; Ciufolini, M.; Witzigmann, D.; Kulkarni, J. A.; van der Meel, R.; Cullis, P. R. The Onpattro Story and the Clinical Translation of Nanomedicines Containing Nucleic Acid-Based Drugs. *Nat. Nanotechnol.* **2019**, *14* (12), 1084–1087. <https://doi.org/10.1038/s41565-019-0591-y>.
- (2) Chen, S.; Ge, X.; Chen, Y.; Lv, N.; Liu, Z.; Yuan, W. Advances with RNA Interference in Alzheimer's Disease Research. *Drug Des. Devel. Ther.* **2013**, *7*, 117–125. <https://doi.org/10.2147/DDDT.S40229>.
- (3) Dowdy, S. F. Overcoming Cellular Barriers for RNA Therapeutics. *Nat. Biotechnol.* **2017**, *35* (3), 222–229. <https://doi.org/10.1038/nbt.3802>.
- (4) Evers, M. J. W.; Kulkarni, J. A.; Meel, R. Van Der; Cullis, P. R.; Vader, P.; Schiffelers, R. M. State-of-the-Art Design and Rapid-Mixing Production Techniques of Lipid Nanoparticles for Nucleic Acid Delivery. *Small Methods* **2018**, *1700375*, 1–20. <https://doi.org/10.1002/smt.201700375>.
- (5) El Andaloussi, S.; Mäger, I.; Breakefield, X. O.; Wood, M. J. A. Extracellular Vesicles: Biology and Emerging Therapeutic Opportunities. *Nat. Rev. Drug Discov.* **2013**, *12* (5), 347–357. <https://doi.org/10.1038/nrd3978>.
- (6) Yáñez-mó, M.; Siljander, P. R.; Andreu, Z.; Bedina, A.; Borràs, F. E.; Buzas, E. I.; Buzas, K.; Casal, E.; Cappello, F.; Carvalho, J.; Colás, E.; Cordeiro-da, A.; Fais, S.; Falcon-perez, J. M.; Ghobrial, I. M.; Giebel, B.; Gimona, M.; Graner, M.; Gursel, I.; Gursel, M.; Niels, H. H.; Hendrix, A.; Kierulf, P.; Kokubun, K.; Kosanovic, M.; Kralj-iglic, V.; Laitinen, S.; Lässer, C.; Lener, T.; Ligeti, E.; Linē, A.; Lipps, G.; Llorente, A.; Manček-keber, M.; Marcilla, A.; Mittelbrunn, M.; Hoen, E. N. M. N.; Nyman, T. A.; Driscoll, L. O.; Oliván, M.; Oliveira, C.; Pállinger, É.; Portillo, H. A.; Rigau, M.; Rohde, E.; Sammar, M.; Sánchez, F.; Santarém, N.; Schallmoser, K.; Ostendorf, M. S.; Stoorvogel, W.; Stukelj, R.; Grein, S. G. Van Der; Helena, M.; Wauben, M. H. M.; Wever, O. De. Biological Properties of Extracellular Vesicles and Their Physiological Functions. *J. Extracell. Vesicles* **2015**, *3078* (May). <https://doi.org/10.3402/jev.v4.27066>.
- (7) de Jong, O. G.; Murphy, D. E.; Mäger, I.; Willms, E.; Garcia-Guerra, A.; Gitz-Francois, J. J.; Lefferts, J.; Gupta, D.; Steenbeek, S. C.; van Rheenen, J.; El Andaloussi, S.; Schiffelers, R. M.; Wood, M. J. A.; Vader, P. A CRISPR-Cas9-Based Reporter System for Single-Cell Detection of Extracellular Vesicle-Mediated Functional Transfer of RNA. *Nat. Commun.* **2020**, *11* (1), 1113. <https://doi.org/10.1038/s41467-020-14977-8>.
- (8) Albanese, M.; Chen, Y.-F. A.; Hüls, C.; Gärtner, K.; Tagawa, T.; Mejias-Perez, E.; Keppler, O.; Göbel, C.; Zeidler, R.; Shein, M.; Schütz, A.; Hammerschmidt, W. Micro RNAs Are Minor Constituents of Extracellular Vesicles and Are Hardly Delivered to Target Cells. *bioRxiv* 2020. <https://doi.org/10.1101/2020.05.20.106393>.
- (9) Zomer, A.; Maynard, C.; Verweij, F. J.; Kamermans, A.; Schäfer, R.; Beerling, E.; Schiffelers, R. M.; De Wit, E.; Berenguer, J.; Ellenbroek, S. I. J.; Wurdinger, T.; Pegtel, D. M.; Van Rheenen, J. In Vivo Imaging Reveals Extracellular Vesicle-Mediated Phenocopying of Metastatic Behavior. *Cell* **2015**, *161* (5), 1046–1057. <https://doi.org/10.1016/j.cell.2015.04.042>.
- (10) Costa Verdura, H.; Gitz-Francois, J. J.; Schiffelers, R. M.; Vader, P. Cellular Uptake of Extracellular Vesicles Is Mediated by Clathrin-Independent Endocytosis and Macropinocytosis. *J. Control. Release* **2017**, *266* (July), 100–108. <https://doi.org/10.1016/j.jconrel.2017.09.019>.

- (11) Kooijmans, S. A. A.; Stremersch, S.; Braeckmans, K.; De Smedt, S. C.; Hendrix, A.; Wood, M. J. A.; Schiffelers, R. M.; Raemdonck, K.; Vader, P. Electroporation-Induced siRNA Precipitation Obscures the Efficiency of siRNA Loading into Extracellular Vesicles. *J. Control. Release* **2013**, *172* (1), 229–238. <https://doi.org/10.1016/j.jconrel.2013.08.014>.
- (12) Stremersch, S.; Vandenbroucke, R. E.; Wouterghem, E. Van; Hendrix, A.; Smedt, S. C. De; Raemdonck, K. Comparing Exosome-like Vesicles with Liposomes for the Functional Cellular Delivery of Small RNAs. *J. Control. Release* **2016**, *232*, 51–61. <https://doi.org/10.1016/j.jconrel.2016.04.005>.
- (13) Hung, M. E.; Leonard, J. N. A Platform for Actively Loading Cargo RNA to Elucidate Limiting Steps in EV-Mediated Delivery. *J. Extracell. vesicles* **2016**, *5*, 31027. <https://doi.org/10.3402/jev.v5.31027>.
- (14) Sork, H.; Corso, G.; Krjutskov, K.; Johansson, H. J.; Nordin, J. Z.; Wiklander, O. P. B.; Lee, Y. X. F.; Westholm, J. O.; Lehtiö, J.; Wood, M. J. A.; Mäger, I.; El Andaloussi, S. Heterogeneity and Interplay of the Extracellular Vesicle Small RNA Transcriptome and Proteome. *Sci. Rep.* **2018**, *8* (1), 10813. <https://doi.org/10.1038/s41598-018-28485-9>.
- (15) Bonsergent, E.; Lavieu, G. Content Release of Extracellular Vesicles in a Cell-Free Extract. *FEBS Lett.* **2019**, *593* (15), 1983–1992. <https://doi.org/10.1002/1873-3468.13472>.
- (16) Joshi, B. S.; de Beer, M. A.; Giepmans, B. N. G.; Zuhorn, I. S. Endocytosis of Extracellular Vesicles and Release of Their Cargo from Endosomes. *ACS Nano* **2020**, *14* (4), 4444–4455. <https://doi.org/10.1021/acsnano.9b10033>.
- (17) Bonsergent, E.; Grisard, E.; Buchrieser, J.; Lavieu, G. Quantitative Characterization of Extracellular Vesicle Uptake and Content Delivery within Mammalian Cells. *Nat. Commun.* No. 2021, 1–11. <https://doi.org/10.1038/s41467-021-22126-y>.



APPENDICES

SAMENVATTING

In recente decennia heeft het veld van geneeskunde veel vooruitgang geboekt. We verwachten nu een veel langer en gezonder leven dan vijftig jaar geleden ondanks ontwikkeling in het behandeling en diagnoses van ziekte. Wij hebben veel voortgang gemaakt, maar sommige ziekten blijven ongeneesbaar met conventionele geneesmiddelen, want veel ziektes hebben een genetische oorsprong die conventionele medicijnen niet beïnvloeden kan.

RNA medicijnen zijn een nieuwe groep van medicijnen die wellicht dit kan veranderen. RNA functioneert als een boodschapper molecule in ons lichaam en biedt een brug tussen onze genen en de functie van onze lichaam. Dit klinkt veelbelovend, maar de succesvolle levering van RNA naar de binnenkant van cellen waar het functioneert is heel uitdagend.

Om dit doel te bereiken, is therapeutische RNA verpakt binnen een beschermend nanodeeltje zoals een liposome of een lipid nanoparticle. Deze synthetische deeltjes zorgen voor levering van therapeutische RNA en heeft succesvol gebruik gevonden met de Moderna en Pfizer/BioNTech COVID19 vaccinaties. Maar, deze deeltjes hebben een paar nadelen. Het lichaam ziet ze als vreemd en verwijderd meeste van hen door de werking van de lever. Sterker nog, de meerderheid van deze deeltjes die de binnenkant van de cel bereiken zijn gedegradert voordat zij functioneren kunnen.

Voor deze reden hebben extracellular vesicles (EVs) in recente jaren veel aandacht gekregen. Deze zijn natuurlijke deeltjes die uitgescheiden zijn van cellen in ons eigen lichaam en bevatten RNA en nog veel andere biologische moleculen. De mogelijkheid om deze natuurlijke deeltjes te gebruiken als RNA leveringsmiddelen is echt aantrekkelijk, want ze zijn van natuurlijke oorsprong. Dit betekent dat ze minder giftig zijn bij een hoge dosis en het is ook mogelijk dat ze efficiënter zijn en leveren een grote fractie van de bevatten RNA naar cellen dan kunstmatige deeltjes.

Om EVs te gebruiken als RNA leveringsmiddelen is meer onderzoek nodig. We hebben niet alle gereedschappen die nodig zijn om dit proces goed te bestuderen. Daardoor weten we nog niet precies hoe efficiënt EVs zijn in vergelijking met kunstmatige deeltjes. We weten ook niet de mechanismes en routes waardoor EVs zijn bevatten RNA naar de binnenkant van cellen sturen. Het doel van dit proefschrift is om dit te onderzoeken.

In hoofdstuk een geven we een introductie naar EVs en de manieren dat ze gebruikt kunnen worden om RNA te leveren. In hoofdstuk twee geven we een overzicht van de manieren hoe EVs gebruikt kunnen worden in een therapeutische manier. We praten

over de routes die EVs nemen om zijn cargo te leveren bij een cel en de invloed die deze route kan hebben op de hoeveelheid van de cargo dat is geleverd. We praten ook over de manieren hoe EVs gemodificeerd kunnen worden om zijn therapeutische eigenschappen te verbeteren.

In hoofdstuk drie stellen we een nieuw systeem voor om RNA overdracht tussen cellen binnen EVs te bestuderen genoemd CROSS-FIRE. Dit systeem is gebaseerd op CRISPR/Cas9 en wij hebben dit systeem gebruikt om genen te ontdekken die betrokken zijn in cel naar cel RNA overdracht binnen EVs.

In hoofdstuk vier bestuderen we en vergelijken we de efficiëntie van RNA levering tussen EVs en de meest moderne LNP formulatie, de DLin-DMA-MC3-LNP. We gebruiken het CROSS-FIRE systeem om te laten zien dat EVs RNA leveren met een veel grotere efficiëntie dan DLin-DMA-MC3-LNPs.

In hoofdstuk vijf onderzoeken we of de route van EVs in de cellen verantwoordelijk is voor hun hoge boodschap efficiëntie. Wij hebben gezien dat EVs en LNPs vergelijkbare routes volgen door de cel. Dit suggereert dat de hoge leveringsefficiëntie van EVs komt door andere eigenschappen van het nanodeeltje.

Een andere eigenschap van EVs die dit proces wellicht kan beïnvloeden is fusie van EV membranen bij laag pH. In hoofdstuk 6 hebben we een RNA uitgave assay ontwikkelt en deze assay gebruikt om te laten zien dat bij een laag pH de RNA cargo van EVs is uitgegeven.

Tot slot, in hoofdstuk zeven hebben we een overzicht van het onderzoek bewaard in dit proefschrift. We geven ook perspectieven voor toekomstig werk die uitgevoerd kunnen worden die de therapeutische potentie van EVs verbeteren.

CURRICULUM VITAE

Daniel Murphy was born on the 26th May, 1992 in Bristol (UK). He completed his primary education at Bishop Road Primary School and his secondary education at Bristol Cathedral School, both in Bristol (UK). He undertook his Bachelor's in Biomedical Science at the University of Warwick (UK) during which he performed a year in industry at Crucell, Leiden. He obtained his Bachelor's in 2014 and started his Master's in Drug Innovation at Utrecht University in the same year. During this Master's program, he first became interested in EVs during a 9-month internship at the Faculty of Veterinary Medicine which focused on the role of mast cell-EVs in innate immunity. This was followed by a 6-month internship at Harvard Medical School which focused on EV-mediated RNA transfer in glioblastoma. He obtained his Master's in 2016 and briefly worked as a conference organization consultant for Select Biosciences in Berlin. He started his PhD project in Utrecht under the supervision of Prof. Raymond Schiffelers and Dr. Pieter Vader in 2017. This PhD focused on the use of EVs as therapeutic RNA delivery vehicles and compared these natural nanoparticles to synthetic RNA delivery vehicles. Following his PhD work, he moved into industry and now works as a scientist for Nanocell Therapeutics who aim to develop cell directed nanoparticles to improve the application of CAR-T therapies.

LIST OF PUBLICATIONS

Murphy, D. E.; de Jong, O. G.; Evers, M. J. W.; Nurazizah, M.; Schiffelers, R. M.; Vader, P. Natural or Synthetic RNA Delivery: A Stoichiometric Comparison of Extracellular Vesicles and Synthetic Nanoparticles. *Nano Lett.* **2021**, 21 (4), 1888–1895. <https://doi.org/10.1021/acs.nanolett.1c00094>.

de Jong, O. G.; **Murphy, D. E.;** Mäger, I.; Willms, E.; Garcia-Guerra, A.; Gitz-Francois, J. J.; Lefferts, J.; Gupta, D.; Steenbeek, S. C.; van Rheenen, J.; El Andaloussi, S.; Schiffelers, R. M.; Wood, M. J. A.; Vader, P. A CRISPR-Cas9-Based Reporter System for Single-Cell Detection of Extracellular Vesicle-Mediated Functional Transfer of RNA. *Nat. Commun.* **2020**, 11 (1), 1113. <https://doi.org/10.1038/s41467-020-14977-8>.

Jong, O. G. De; Kooijmans S. A. A., **Murphy, D. E.;** Jiang L., Evers, M. J. W.; Sluijter J.P.G.; R. M.; Vader, and M.; Schiffelers, R. M. Drug Delivery with Extracellular Vesicles: From Imagination to Innovation, *Accounts of Chemical Research* **2019** 52 (7), 1761-1770, DOI: 10.1021/acs.accounts.9b00109

Murphy, D. E.; Jong, O. G. De; Brouwer, M.; Wood, M. J.; Lavieu, G.; Schiffelers, R. M.; Vader, P. Extracellular Vesicle-Based Therapeutics : Natural versus Engineered Targeting and Trafficking. *Exp. Mol. Med.* **2019**. 51, 1–12,

ACKNOWLEDGEMENTS

To my promotor **Prof. Dr. Raymond Schiffelers** First of all, thank you for providing me with the opportunity to work within your lab all those years ago. I had no idea what I was embarking on at the time, but I knew that working within a group led by someone who immediately impressed me with his intellect and jovial nature was a good idea. I think it is very impressive how you remain so down-to-earth and in touch with the everyday goings on at the lab despite being so important! I am also really glad that we can continue to work together at Nanocell. Thank you for all the help!

Thank you to **Dr. Pieter Vader**, my patient and attentive supervisor. You were always on hand to answer and guide me. Nothing did more for my scientific development than our weekly data discussions. You have an incredible ability to see patterns and meaning in data and I am very lucky as I like to think a little bit of that ability has rubbed off onto me. You knew when to push me which challenged me to work at a level I didn't think I was capable of achieving. In addition to all of this, you were always extremely supportive and you have built a friendly and open environment within your lab that was crucial for my success, as well as the success of others. I will always remember having Christmas dinner with you and your family. That kind gesture towards me at a difficult moment was very much appreciated and is a sign of your good character. Thank you for your years of support, I can say that I am now a more content, fulfilled and confident person because of it.

Dr. Olivier de Jong. You are an absolute lab colossus. Your tireless work set the foundations for my PhD and it is clear that there is no way I would have got to this point without you. You never hesitated to sacrifice your time and energy to help me set up or think through an experiment. You were really a foundation of the lab during my time there and you kept the place running through thick and thin (and my occasional addition experiment induced chaos). I was just one of the many lucky PhD and Master's students who you help and support on a daily basis. So much success around the CDL and Pharmaceuticals department is connected directly or indirectly to you. I am very happy that we still get to work close to each other. Thank you for all the help, I am very grateful.

Dr. Greg Lavieu Thank you for hosting me in your lab and giving me the opportunity to briefly live and work in Paris. You were very kind and supportive and I was able to learn a huge amount in the short time I was there. I was immediately impressed by your clear analytical thinking. I hope the Vader and Lavieu labs continue to collaborate in future!

Prof. Dr Enrico Mastrobattista. Thank you for the useful guidance and during our nucleic acid delivery meetings. You provided some very useful input during these meetings in the early phase of my PhD and I am very happy we can continue to collaborate via Nanocell.

Martijn, working alongside you for so many years has been an absolute privilege. You are one of the most competent and hardworking people I have ever come across. These qualities combined with your sharp ability to critically analyse information make you a very impressive scientist. Despite these skills you are also one of the most humble people I know. You were the perfect PhD companion and I am extremely lucky that our careers have followed such similar trajectories. It has been great getting to know you over the years and I count you as a true friend.

Omnia, you are a person who radiates good energy and it is impossible to be in a bad mood around you. Even when you are stuck in the dark midst of a particularly challenging addition experiment, you keep smiling and laughing and make everyone else feel happy. This ability kept me sane during those lonely EV culturing weekends when we were the only two people in the CDL. You are also extremely intelligent and my only advice is to remember that most people aren't as smart as you when explaining your highly complex data! I have really enjoyed watching you follow on and add to my PhD project. After all our addition experiments we share an unbreakable bond. Thank you for all your help during the PhD, both as a scientist and as a friend.

To **Dr. Sander Kooijmans** you were on hand to fix my lab issues on countless occasions. You were also always willing to cast a critical eye over my data and we're always enthusiastic and encouraging. Thank you for the help and see you around during our Nanocell PBMC isolations!

To **Ana.** You are someone who has been by my side for the whole PhD experience. Everyone knows about your incredible energy levels, but what I value most in you is your equally impressive level of wisdom. You were there to give me advice at really critical moments and I value your friendship immensely. We had so much fun together during the last year's and shared many adventures around Utrecht, Spain and Italy.

Linglei, You are truly a CDL legend. You made such an impression on this place and we still often speak about all the fun and laughter you brought to the lab. Your diligence and hard work was a very good example for me early in my PhD and I am very proud to have been your paranymph. It is great to see you being so successful across the lab.

Dear **Khalid**. The year and a half you were in the lab was probably the period of my PhD I enjoyed the most and that is likely no coincidence. You are really one of a kind. You have an excellent sense of humour and your kindness and easy going nature was of great value in the lab. Your dedication to your work was impressive and was exemplified by some obscenely long days behind the Fortessa. I am really happy, but not surprised, that we have stayed such good friends since you left the CDL and I look forward to many future misadventures together with you.

Dear **Maria Laura and Greg**, I am so happy to have found you in the last years of my PhD. You helped me through difficult times inside and outside of the lab and for that I am specifically grateful. Your approach to life is something I greatly admire and you both possess a brilliant combination of humour, intelligence and charm. I look forward to spending lots more time with the both of you (and Stefano) in the future.

Dear **Ayik**. You really went above and beyond what was expected of you during your internship and the help you gave me was absolutely crucial in attaining our excellent results. You sacrificed so many weekends and never grumbled. You were a great presence in the lab and kept my spirits up during difficult moments. I am sure if you take this attitude forward and apply it to whatever you try next, you will be able to achieve a huge amount. Thank you for everything and well done.

To **Jeff**. Thank you for the regular and dependable support during my PhD. You have become one of my closest friends and someone I know I can rely on. Your commitment and dedication to your own PhD is truly impressive and I know that your hard work is going to pay off. I am very grateful to have known you for so long. We have both helped each other during difficult moments and that means our friendship is of great value to me. I'm looking forward to seeing you finish your own PhD soon!

To **Jerney**. You are really an unsung hero of the lab and so much of the work that gets done is supported by you. You are always willing to step in and help and every time you do I know that the work will be done to the best possible standard with only minimal input required. Your excellent Western blotting and assistance during the setup of addition experiments was extremely helpful and I couldn't have performed so many of them without your assistance. Thank you very much!

To **Arnold**, your ability to keep the entire CDL research lab ticking over and operating properly with minimum visible stress while keeping a smile on your face is extremely impressive. You clearly do your job very well and it shows. Also, thank you for being the

proprietor of the CDL's very own Cafe Koekman. Many of my best PhD memories were made there. I am very happy that we can continue to work together via Nanocell's work at the UMC.

Elma. How lucky I am to have had you as a housemate (and Dutch editor). Your happiness and relentless cheekiness was always great to come back home to after a long day in the lab. You really helped to keep me going during the last weeks of writing this thesis. I am very impressed by your devotion to your patients which is genuinely inspiring. You do so much good and almost never complain. Thank you for lots of great memories over the past months!

Willemijn it was an absolute privilege to work so closely with you on the last experiments of my PhD. I think we made a great team and we were able to be very productive when we combined forces. You came up with some very good ideas and were very helpful in keeping me on track and motivated. My PhD would have taken much longer without your assistance for which I am very grateful.

To **Leonie.** When I think back of people that supported and helped me during my PhD you are one of the first people who come to mind. You were always there to listen to me when I came home after a long failed experiment and gave me a lot of strength to continue. You are someone who taught me a lot and helped me get to this point. I am very happy that we remain friends and I wish you the best of luck with your own PhD.

Esmee and August I am sad that our time together in the Biltstraat was so short. You are both great people and probably possess the highest combined I.Q of any couple I have ever met. I wish you the best of luck in Sweden and Switzerland and I hope to see you next time you're in Utrecht.

To **Rowan,** you very smartly turned down the opportunity to do an internship with me, thereby losing the opportunity to prepare stacks upon stacks of T175 flasks. You are a great presence in the lab, your calm and helpful demeanour is a real blessing to everyone you work with. Good luck with your own PhD!

Diego, thank you for helping to make the last months of my PhD so fun. You are always up for a good chat and I am very glad to have shared so many Biltstraat adventures with you.

Vania thanks for all the happy lunches and coffee breaks. Your office was always a sanctuary to escape to for a bit of calm on busy days. Good luck with the end of your PhD and the start of your new job!

To **Demian**. I really enjoyed our brief collaboration in the last months of our PhD and it would have been great if we could have worked together more. Good luck finishing your thesis. You will go on to great things after it is finished I am sure.

Mariona, you work hard and are very successful while at the same time create a very relaxed atmosphere in your surroundings. You are one of the funniest people in the lab and I always experienced the highest laugh per minute rates in your presence.

Emma, Jason and Natasha. Thank you for all the fun we had. Our barbecue sessions at the snake lake were always a great occasion!

Simon, Nazma and Marieke. I think the three of you appreciate the pains of an EV based PhD better than most. You both gave me extremely valuable advice and assistance (Simon is the NTA master) on many occasions for which I am very grateful. I wish you the best of luck with your own PhDs.

To the cardiology PhDs **Michele, Qiangbing, Juntao, Yao Bin, Lotte, Margarida and Clara**. Thank you for creating such a welcoming and friendly environment at cardiology. It was always a treat to come downstairs to use your RT-qPCR facilities thanks to the good vibes you guys produce.

To the DDW PhDs **Johanna, Danny, Boning, Blessing, Barbara, Jerry and many others**. Thank you for bringing such a happy environment to the DDW. You all made me feel very welcome during my occasional trips over the road. I am very happy that I can now share my workspace with you guys!

Dear **Minke**. Sharing an office with you and Martijn was really a privilege. I remember many excellent and motivating chats during the early years of my PhD. Your commitment to your project was really inspiring and you produced one of the most impressive theses the CDL has ever seen.

To **Else, Astrid, Salas** and all the Biltstraat employees, thank you for creating such a happy and comfortable environment at the Biltstraat. It was a real privilege to both start and finish my PhD while living in that wonderful place. Your hard work and friendly attitude created the perfect environment in which many many UMC international students have been able to greatly enjoy.

To **Pol**. It was great to share the lab with you during my last year of my PhD. You are extremely motivated and work very hard but you always remain extremely calm! Thanks for all the good moments and I look forward to watching your own PhD progress.

Hinde, I will remember you as the lab's foremost conversationalist. You are a real intellect and some of the most interesting conversations of my PhD have been with you. Our very interesting chats about a wide range of topics (politics, cats, phage display, philosophy) broke up the occasional monotony of lab life and were very much appreciated!

Marcel na 5 jaren ben jij nog degene mens op werk die alleen in het nederlands met mij praat en voor dat ben ik heel dankbaar! Jij brengt altijd een goede sfeer en jij was zeer behulpzaam met alle van mijn wetenschappelijke vragen. Ik ben blij dat we elkaar nog ziet in het DDW gebouw.

To **Wariya, Tessa, Marc, Luuk, Minka, Virginia, Aida, Birgit, Stephanie, Rick** and all the other great CDL PhDs that I have crossed paths with over the years, thank you for being part of such a great community at the lab and for helping me to have such an enjoyable time during my time there.

To **Anil(etje) and the Deshantri family**. Thank you for bringing a lot of happiness to the lab in the early days of my PhD. We were always a very good influence on each other's Dutch language skills! I will never forget the amazing experience you helped me have in India and I am very grateful for how you introduced me to your extended family. That trip was a great turning point in my PhD and helped turn my focus towards the last year.

Zhiyong. You possess an incredible wealth of information which you very helpfully share with all your colleagues. Within minutes of our very first conversation you solved the RT-qPCR issues I had been having and the result is figure 2d of chapter 4. Thanks a lot for your help!

Arjan, Gabi and the rest of the football group. Our Thursday football sessions were one of the highlights of my week! We had a great group of players and I really enjoyed letting off steam after work playing football with you guys. You were also great to be around in the lab!

To **Marcos, Clara, Maria, Pancho, Ele, Vero, Helena, Irati and all the other penguins**. I started my Utrecht experience with you and I am very happy that we are still going strong after all these years. Our annual reunions were some of the best times of my PhD years!

To **Shu**. Thank you for being such an entertaining presence at the UMC. We had a lot of fun together at many borrels and events in and outside the UMC. Good luck with your own PhD!

To **Grane**. I am very lucky to have such an energetic and inquisitive grandmother. You have always stayed up to date with the progress of my PhD and were always very interested in how my exosomes were getting on. Thank you for being such a unique person and for shaping my view of the world from early childhood to the present day.

To **Grandpa**. I think it is clear that I am in the position I am today due to your influence. You talked to me about exciting scientific concepts and discoveries from my very early childhood which motivated me to pursue a scientific career from an early age. You were a great role model to me and I would not be in the position I am today without you.

To **Grandma and Grandad**. Thank you for your unconditional support and strong interest in my PhD research. I promise to explain this whole thesis to you in detail next time I am in Bristol.

To my **Parents**. No one deserves more gratitude than you. Your unwavering support, love, care and encouragement got me to where I am today. Thank you.

To my fantastic siblings. **Anna**, you are probably the smartest of the Murphys. Your drive and motivation in recent years has been quite inspiring. Thank you for all the great times we shared while growing up. **Will**, no one can make me laugh like you do. Your sense of humour and wit was very refreshing during my trips back home to Bristol. **Evie**, it has been great to see you grow up so much in recent years. You are turning into a very impressive super nanny and I am very proud. Thank you so much for the beautiful cover art of this thesis!